METHODS IN MOLECULAR BIOLOGY™

Volume 279

Nitric Oxide Protocols

Second Edition

Edited by

Aviv Hassid

Humana Press

1

Measurement of Nitric Oxide by Reconversion of Nitrate/Nitrite to NO

Reinhard Berkels, Svenja Purol-Schnabel, and Renate Roesen

Summary

A simple and sensitive method is presented to measure the unstable molecule nitric oxide (NO) by reconversion of nitrate/nitrite to NO. Nitrate and nitrite are the stable degradation products of NO that accumulate in supernatants of biological samples that release nitric oxide. First, nitrate is enzymatically converted to nitrite using nitrate reductase. In a second step, nitrite is reduced to equimolar NO concentrations by an acidic iodide solution and quantified with an amperometric Clark-type electrode. This method provides the ability to assess basal- and agonist-stimulated cumulative NO formation in different biological models and is a sensitive alternative to the widely used Griess assay.

Key Words: Nitric oxide; endothelium; nitrite.

1. Introduction

Over the past two decades, it was found that the small messenger molecule nitric oxide (NO) plays a pivotal role in a multitude of physiological processes ***(1–5)***. NO is a small diffusible radical with a short half-life, which causes difficulties in measuring it. Different techniques to measure NO directly or indirectly are described in detail elsewhere ***(6)***. Briefly, NO may be measured by bioassay ***(7)***, an oxy-hemoglobin assay ***(8)***; electron paramagnetic resonance (EPR) ***(9)***, chemiluminescence ***(10)***, high-performance liquid chromatography (HPLC) ***(11)***, the Griess reaction ***(12)***, microchip capillary electrophoresis ***(13)***, or different electrochemical electrodes ***(14–16)***. Moreover, it is possible to measure NO via its second messenger, cGMP. NO degrades rapidly in biological samples to the stable products nitrite and nitrate. Therefore, different assays have been developed to determine nitrate/nitrite concentrations as an indirect method to quantify NO formation. In this chapter, we will describe a very sensitive technique to measure NO in aqueous solutions by reconversion of nitrite

From: *Methods in Molecular Biology, vol. 279: Nitric Oxide Protocols: Second Edition*
Edited by: A. Hassid © Humana Press Inc., Totowa, NJ

to nitric oxide in an acidic iodide solution. First, nitrate is enzymatically converted to nitrite to gage the total NO produced, because the redox potential of the acidic iodide solution is not strong enough to reduce nitrate to NO. Nitrite is then converted in a stoichiometric manner to NO, which is determined using a highly sensitive and selective amperometric electrode. Therefore, this method provides a significantly higher sensitivity compared to the Griess assay ***(17)***. It offers the possibility to measure the total (cumulative) NO release of cells in culture because the stable degradation products of NO (nitrate/nitrite) accumulate in the incubation buffer. This refers to basal NO release as well as an agonist-induced NO release. The method is not suitable to determine real-time NO concentrations.

2. Materials

1. ISO-NO electrode (WPI, Sarasota).
2. Magnetic stirrer with heating functions.
3. Segments or pieces of vessels with intact and functioning endothelium.
4. Attached monolayers of endothelial cell cultures.
5. Cell culture equipment.
6. Calibration solution for the electrode: 0.1*M* H_2SO_4, 0.1*M* KI, 0.14*M* K_2SO_4.
7. HEPES-buffered physiological solution: 5 m*M* HEPES, 140 m*M* NaCl, 5 m*M* KCl, 2 m*M* $CaCl_2$, 1 m*M* $MgCl_2$, 5 m*M* glucose, adjusted to a pH of 7.4.
8. KNO_2.
9. NADPH/FAD mixture [1.5:0.3 mg/mL] (Sigma) buffered at pH 7.4 in 50 m*M* sodium–potassium phosphate.
10. Nitrate reductase (10 U/mL) solution (Roche).
11. L-Arginine (Merck).
12. Carbachol (Alexis Corp.).

3. Methods

The methods describe in detail how to calibrate the electrode and how to measure endothelial NO by reconversion of nitrite.

3.1. Calibration of the NO Electrode

To determine NO, we used the commercially available NO sensor (∅ 2 mm) of WPI (ISO-NO electrode; WPI, Sarasota) ***(14,15,17,18)***. In principal, it measures NO by oxidizing it at the working electrode and the resulting current is displayed in picoamperes and is directly proportional to actual NO concentrations (*see* **Note 1**). The electrode is covered with a sleeve that has a specialized membrane at its top that prevents nitrate and nitrite from interfering with the electrode. Other diffusable gases such as CO are not measured because of the potential at the electrode. A manual describing the calibration procedure is provided with the electrode. It is essential to perform a calibration every couple

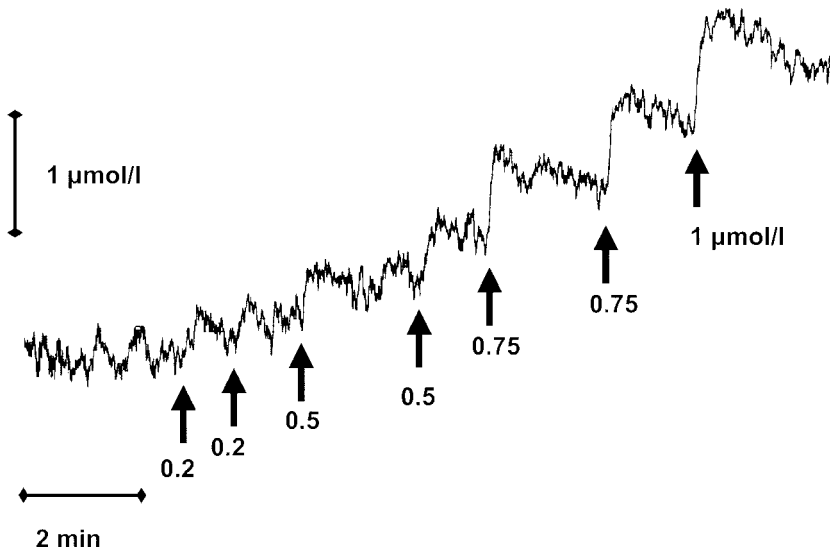

Fig. 1. A typical original recording of a calibration curve in which KNO_2 (50 µL) in increasing concentrations was added to a 10-mL solution (placed above magnetic stirrer set at 100 rpm) in which the electrode was placed.

of days or at least every time the sleeve of the electrode has been replaced, because of potential damage to the membrane.

1. First, the tip of the electrode is placed approx 0.2 cm in the calibration solution (10 mL), which is constantly stirred (100 rpm) at room temperature. Afterward, it is necessary to wait until a stable baseline has been established.
2. A chemical titration calibration is then performed using the acidic iodide calibration solution. Equal volumes (50 µL) of the standard KNO_2 solutions are added (*see* **Fig. 1**). Instantly, NO is formed from the nitrite in a stoichiometrical manner and directly measured. Larger volumes (up to 500 µL) may be used in calibrating to increase the sensitivity of the analysis (*see* **Note 2**).
3. The increase in signal amplitude upon addition of the standard solutions is plotted against the concentration of the standard solutions (*see* **Fig. 2**). From the appropriate calibration curves, the unknown concentration of a probe may be read.
4. In a second set, it is possible to perform a calibration with increasing volumes (5–100 µL) of a KNO_2 solution with a definite concentration (5 µ*M*) ***(17)***. Plotting the change in signal amplitude upon the addition of the different volumes against the NO content in these volumes (25 pmol to 2 nmol), you get calibration curves for the amount of NO released during the incubation time.
5. Using either calibration, you will find out that the lower detection limit of the electrode is approx 2 n*M* NO ***(15,19)*** in aqueous solution. This is the final concentration in the acidic iodide calibration solution. This means that a minimum of

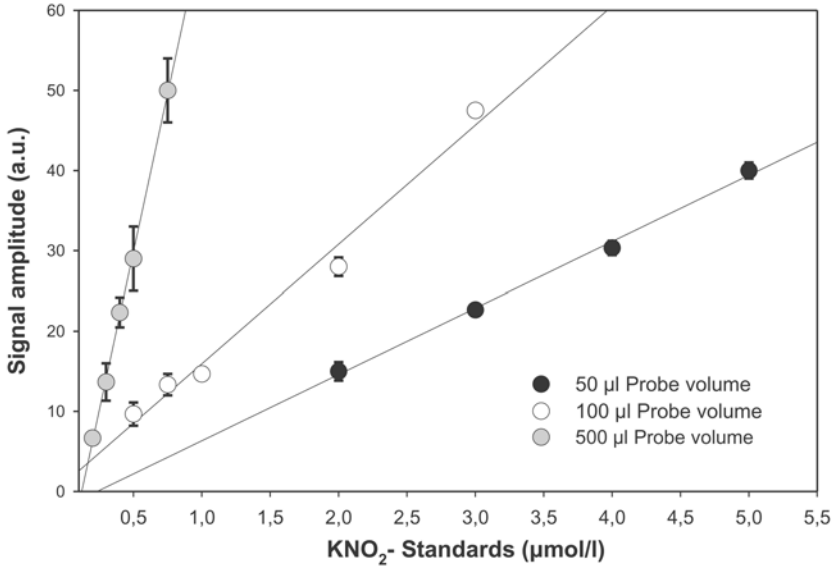

Fig. 2. Calibration curves of KNO_2 for different probe volumes. The regression line of four experiments has been calculated. For the 50-µL probe volume, slope = 7.45 and $r^2 = 0.9958$; for the 100-µL probe volume: slope = 14.56 and $r^2 = 0.9968$; for the 500-µL probe volume: slope = 72.7 and $r^2 = 0.99755$.

50 µL of a 0.4-µ*M* nitrite solution must be added to the 10-mL bath in order to be detectable. Therefore, you must take into account that the added nitrite sample is diluted according to its volume in relation to the 10-mL bath. Following the first procedure, this has already been done. Thus, the sample volume must be adjusted to reach detection limit.

6. As mentioned earlier, it is possible to add a volume of up to 500 µL (single addition) to the 10-mL solution to still achieve a valid measurement. Still, volumes smaller than 500 µL per injection are preferable and bring better results. You should not add more than 1 mL (total sum of serial injections) into one 10-mL bath, because, then, results become inconsistent as a consequence of pH change and insufficient redox capacity. In this case, replace the acidic iodide solution by a fresh solution to perform further experiments. To quantify our values, we always measured peak currents.

3.2. Measurement of Endothelial NO From Vessels by Reconversion of Nitrite

We used a model of porcine coronary arteries ***(17)*** to measure NO that is released from the functional endothelium (*see* **Note 3**). This model should be easily adapted to other vessels or vessel segments (*see* **Note 4**).

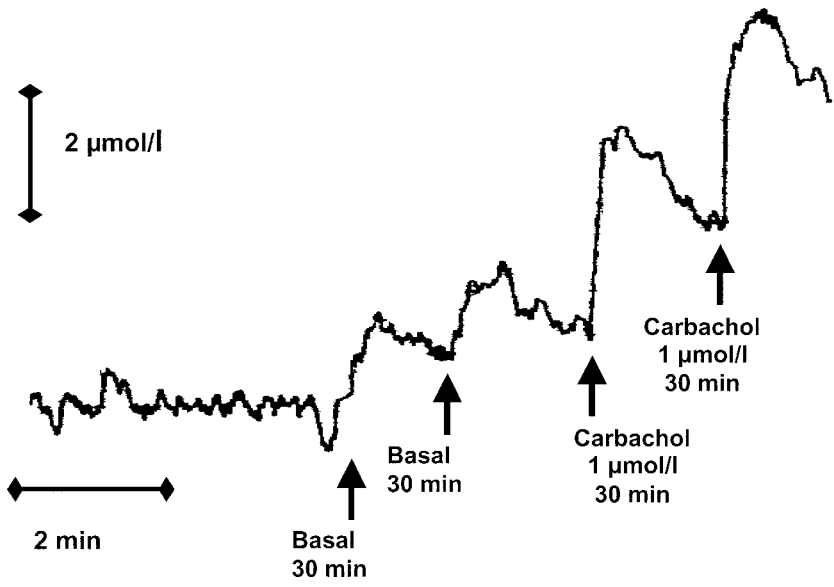

Fig. 3. This original recording shows the basal and carbachol induced nitrite/NO peaks elicited by 50 µL of the incubate solution in which the vessel pieces had been placed (30 min). Nitrate was converted to nitrite and the aliquot was added to 10 mL of the acidic iodide solution. After incubation with the agonist carbachol (1 µ*M*) under the same conditions, the nitrite/NO content was significantly increased.

1. Briefly, arteries were freshly prepared and opened longitudinally. They were fixed on a plastic rod (diameter 3 mm) with the endothelium outside and incubated for 30 min (longer time periods are also suitable) in 500 µL HEPES-buffered physiological solution at 25°C (without stirring; *see* **Note 5**). At this stage, it is possible to freeze the incubation probes for analysis at a later time (*see* **Note 6**).
2. Fifty microliters of a NADPH/FAD mixture [1.5:0.3 mg/mL] (*see* **Note 7**) were then added, followed 1 min later with 15 µL of nitrate reductase (10 U/mL) solution (final concentrations of 0.3 U/mL nitrate reductase) to convert nitrate to nitrite.
3. The resulting mixture was incubated at room temperature for a further 30 min.
4. Volumes of 50–200 µL of this solution were added to the acidic iodide calibration solution and the nitrite/NO concentration was estimated (*see* **Note 8**).

Using this method, it is possible to measure basal endothelial NO release over time (350 ± 17 pmol × 10 mg^{-1} × 30 min^{-1} [$n = 25$]) as well as agonist-induced NO releases. We used carbachol (1 µmol/L, 30 min) to induce an endothelial NO release and an example of our NO measurement is depicted in **Fig. 3**. Comparable amounts of NO/nitrite are formed in response to other agonists such as substance P (300 n*M*) or bradykinin (10 n*M*) (data not shown).

Finally, the amount of nitrite/NO formed in vessel pieces is dependent on size, specificacy on the size, and intactness of the endothelial area. Additionally, the amount of NO liberated by the endothelium is dependent on the presence of substrate of NO synthase, L-arginine. When L-arginine (1 m*M*) is added to the buffer, basal NO release increases by 30% (data not shown).

3.3. Measurement of NO From Endothelial Cell Cultures by Reconversion of Nitrite

The method is suitable for measuring basal NO release in endothelial cell cultures. We used porcine aortic endothelial cells (passage two) to perform our experiments, and it should be no problem to determine NO release in other endothelial cell lines that express a functional endothelial NO synthase (eNOS) or inducible NO synthase (iNOS) in a similar way (*see* **Note 5**). Cell culture techniques will not be described in this chapter.

1. Endothelial cell cultures were washed two times with the HEPES-buffered physiological solution and incubated for 120 min at 37°C.
2. Defined volumes (500 µL) of the supernatant (1.5 mL of HEPES buffer) of porcine aortic cell cultures (10-cm dishes) were treated with FAD/NADPH and nitrate reductase (*see* **Note 7**) in the same way as described in **Subheading 3.2.** Care should be taken that the amount of buffer is limited to achieve maximum nitrite/nitrate concentrations, although the cell monolayer must be completely covered.

4. Notes

1. The handling of the electrode as well as the interpretation of the results is not without difficulty because it is highly sensitive and will be disturbed easily. It is necessary to ground the experimentator and the recording devices thoroughly, otherwise small changes in electric currents will interfere with the recording and will produce slopes in the baseline or a very unstable and noisy baseline.
2. Temperature changes always affect the obtained signal; therefore, it is necessary that the calibration solution remain at a stable temperature and that the volumes added have the same temperature. Moreover, changes in pH and flow will also elicit a signal at the electrode. It is important that you do not place the tip of your pipet too close to the electrode and you do not use too much force to expel the volume out of the pipet because this may also cause a signal. Ideally, a fixed rack is recommended, in which you can place the pipet so that the point of injection is always the same. You should check the influence of the addition of your sample using either buffer without nitrite or the calibration solution.
3. Because of its high sensitivity, this method provides the possibility of measuring nitrite/NO in other biological samples, such as saline Langendorff heart perfusate ***(17)***.
4. When you use vessel segments from which NO is generated, it is always of advantage to use segments of the same vessel as controls for your experiments, because intraindividual experiments are more comparable and because there are

differences concerning the NO release and the function of different vessel preparations.

5. Because the endothelium releases NO when shear stress is applied (and thus increases nitrite/nitrate detected), you should be careful when adding your solutions or when you incubate your cells or vessel preparations. Even gentle shaking of the probes increases the nitrite values.
6. Because nitrate and nitrite are stable compounds, you do not need to worry about the short half-life of NO and it is possible to freeze biological samples at –80°C and measure them at a later date.
7. Aliquots of NADPH as well as FAD stock solutions may be stored frozen (–80°C). However, the reduction capacity must be controlled with nitrate reductase and a standard nitrate probe.
8. This assay is not affected by high concentrations of proteins such as bovine serum albumin (up to 1 mg/mL) or an SH-containing amino acid such as cysteine (up to 1 m*M*).

References

1 Ricciardolo, F. L. (2003) Multiple roles of nitric oxide in the airways. *Thorax* **58,** 175–182.
2 Anderson, T. J. (2003) Nitric oxide, atherosclerosis and the clinical relevance of endothelial dysfunction. *Heart Fail. Rev.* **8,** 71–86.
3 Shimokawa, H. (1999) Primary endothelial dysfunction: atherosclerosis. *J. Mol. Cell Cardiol.* **31,** 23–37.
4 Forstermann, U., Closs, E. I., Pollock, J. S., et al. (1994) Nitric oxide synthase isozymes. Characterization, purification, molecular cloning, and functions. *Hypertension* **23,** 1121–1131.
5 Moncada, S., Palmer, R. M., and Higgs, E. A. (1991) Nitric oxide: physiology, pathophysiology, and pharmacology. *Pharmacol. Rev.* **43,** 109–142.
6 Archer, S. (1993) Measurement of nitric oxide in biological models. *FASEB J.* **7,** 349–360.
7 Gryglewski, R. J., Moncada, S., and Palmer, R. M. (1986) Bioassay of prostacyclin and endothelium-derived relaxing factor (EDRF) from porcine aortic endothelial cells. *Br. J. Pharmacol.* **87,** 685–694.
8 Kelm, M., Feelisch, M., Spahr, R., et al. (1988) Quantitative and kinetic characterization of nitric oxide and EDRF released from cultured endothelial cells. *Biochem. Biophys. Res. Commun.* **154,** 236–244.
9 Henry, Y., Ducrocq, C., Drapier, J. C., et al. (1991) Nitric oxide, a biological effector. Electron paramagnetic resonance detection of nitrosyl–iron–protein complexes in whole cells. *Eur. Biophys. J.* **20,** 1–15.
10 Palmer, R. M., Ferrige, A. G., and Moncada, S. (1987) Nitric oxide release accounts for the biological activity of endothelium-derived relaxing factor. *Nature* **327,** 524–526.
11 Kelm, M., Preik-Steinhoff, H., Preik, M., et al. (1999) Serum nitrite sensitively reflects endothelial NO formation in human forearm vasculature: evidence for

biochemical assessment of the endothelial L-arginine–NO pathway [in process citation]. *Cardiovasc. Res.* **41,** 765–772.

12 Thomsen, L. L., Ching, L. M., and Baguley, B. C. (1990) Evidence for the production of nitric oxide by activated macrophages treated with the antitumor agents flavone-8-acetic acid and xanthenone-4-acetic acid. *Cancer Res.* **50,** 6966–6970.

13 Kikura-Hanajiri, R., Martin, R. S., and Lunte, S. M. (2002) Indirect measurement of nitric oxide production by monitoring nitrate and nitrite using microchip electrophoresis with electrochemical detection. *Anal. Chem.* **74,** 6370–6377.

14 Tsukahara, H., Gordienko, D. V., and Goligorsky, M. S. (1993) Continuous monitoring of nitric oxide release from human umbilical vein endothelial cells. *Biochem. Biophys. Res. Commun.* **193,** 722–729.

15. Berkels, R., Mueller, A., Roesen, R., et al. (1999) Nifedipine and Bay K 8644 induce an increase of $[Ca^{2+}]_i$ and NO in endothelial cells. *J. Cardiovasc. Pharmacol.* **4,** 175–181.

16 Malinski, T., Mesaros, S., Patton, S. R., et al. (1996) Direct measurement of nitric oxide in the cardiovascular system. *Physiol. Res.* **45,** 279–284.

17 Berkels, R., Purol-Schnabel, S., and Roesen, R. (2001) A new method to measure nitrate/nitrite with a NO-sensitive electrode. *J. Appl. Physiol.* **90,** 317–320.

18 Bannenberg, G., Xue, J., Engman, L., et al. (1995) Characterization of bronchodilator effects and fate of *S*-nitrosothiols in the isolated perfused and ventilated guinea pig lung. *J. Pharmacol. Exp. Ther.* **272,** 1238–1245.

19. Berkels, R., Bertsch, A., Breitenbach, T., et al. (1996) The calciumantagonist nifedipine stimulates endothelial NO release in therapeutical concentrations. *Pharm. Pharmacol. Lett.* **6,** 75–78.

2

High-Resolution Capillary Electrophoresis of Nitrite and Nitrate in Biological Samples

Dmitri Y. Boudko

Summary

Nitrite and nitrate are widely used reporters of endogenous nitric oxide (NO) and nitric oxide synthase (NOS) activity, which are crucial for a broad spectrum of physiological and pathophysiological pathways. Because of the great variety in spatial expression and activity of NOS in animal tissues, a high-resolution analysis of nitrite/nitrate concentrations in very small biological samples, such as individual cells or homogeneous cell clusters, is required. A high-performance capillary zone electrophoresis (CZE) system, which includes a PrinCE-476 computerized capillary electrophoresis and Crystal-1000 conductivity detector, was optimized to analyze nitrite/nitrate concentrations in submicroliter samples of mammalian neuronal tissues and large individual cells of invertebrates. Solid-phase microextraction (SPME) and Isotachophoretic stacking (ITS) were used. The method is highly reproducible and yield excellent limits of detection (LODs): 8.9 n*M* (0.41 ppb) and 3.54 n*M* (0.22 ppb) for nitrite and nitrate, respectively, relative to undiluted samples.

Key Words: Capillary zone electrophoresis (CZE); biological sample; single cell; solid-phase microextraction (SPME); chloride cleanup; Isotachophoretic stacking (ITS); nitric oxide (NO); nitric oxide synthase (NOS).

1. Introduction

Nitrite and nitrate are widely used reporters of endogenous nitric oxide (NO), a biogenic free-radical molecule crucial to a broad spectrum of physiological pathways and disorders, including neuronal functions, vasodilatation, inflammation, pain, and macrophage-mediated intervention of tumors and infections. Endogenous NO, a subproduct of two mono-oxygenations of L-arginine to L-citrulline, catalyzed by NO synthases, is rapidly oxidized [half-life in normoxic biological systems is <30 s ***(1)***], resulting in the formation of nitrites and nitrates ***(2–5)***. NO gas freely diffuse through cellular membranes, leading to an increase in the NO_2^-/NO_3^- levels in the vicinity of NO-producing cells;

From: *Methods in Molecular Biology, vol. 279: Nitric Oxide Protocols: Second Edition*
Edited by: A. Hassid © Humana Press Inc., Totowa, NJ

however, the largest portion of NO oxidation products are accumulated intracellularly in ionic form as a result of a deficiency in membrane mechanisms for its retrograde transport. Intracellular NO_2^-/NO_3^- mediates a variety of functions by themselves and also serves as a substrate in several nonenzymatic reactions that form a pool of secondary NO sources, buffering intracellular NO levels ***(6)***. Because of the great spatial variety in the expression and activity of NOSs in animal tissues, a high-resolution analytical evaluation of nitrite/nitrate concentrations in very small biological samples such as individual cells or homogeneous cell clusters is required. Here, we describe a high-performance capillary zone electrophoresis (CZE) technique that is optimized to analyze nitrite/nitrate concentrations in submicroliter samples of mammalian neuronal tissues and large individual neurons of invertebrates. High-throughput automatic measurements were made using a PrinCE-476 computerized capillary electrophoresis system with a Crystal-1000 conductivity detector. To improve nitrite detection, samples were precleaned from interfering high concentrations of chloride ions using solid-phase microextraction (SPME) techniques. Samples were diluted 1000- to 10,000-fold to obtain optimal isotachophoretic stacking conditions and to reach an adequate sample volume (>5 μL), which is necessary for reliable automatic injection. The method is highly reproducible, yields excellent limits of detection (LODs) of 8.9 n*M* (0.41 ppb) and 3.54 n*M* (0.22 ppb) for nitrite and nitrate, respectively, relative to undiluted samples ***(7)***, and is simple enough to be changed for different capillary electrophoresis (CE) configuration and biological samples.

1.1. Capillary Electrophoresis

Capillary electrophoresis is a high-resolution (10^5–10^6 theoretical plates), ultrasmall-volume sample (10–100 nL), and fast (0.2–10 min) separation technique that offers remarkable advantages for analytical evaluation of practically all types of metabolite in biological samples. Separation is carried out in a 20- to 75-mm-inner diameter (ID) polyimide-coated fused silica capillary. The capillary is loaded with alkaline buffer that induces formation of charge-coupled binary layers by facilitating dissociation of silanol on the inner surface of the capillary. Electrophoretic drag of mobile inner-layer elecro-osmotic flow (EOF) depends on electrolyte concentration and pH. EOF-modifying additives are used to adjust separation properties. The sample can be loaded by hydrostatic force or pressure, or injected electrophoretically. The CZE coupled to a conductivity detector (CD) is the technique of choice to detect ultraviolet (UV)-silent inorganic ions, providing approximately a 10-fold better LOD compared to UV-light-based detection ***(8,9)***. Several ionic assays for distincting samples using ion chromatography and CE with a CD have been described ***(7,10–19)***

and a commercial CD system suitable for CE integration has recently become available ***(9)***.

1.2. Sample SPME Chloride Cleanup

A typical problem in CE of nitrite/nitrate in biological samples is a high concentration of chloride ions, which interfere with the injection and detection of bromate, nitrite, and nitrate because these ions have similar electrophoretic properties and elution times. Chloride interference becomes more critical if electrophoretic injection and especially isotachophoretic stacking (ITP) preconcentration of the sample is used. To improve nitrite determinations, chloride ions can be removed by passing the sample through a silver-form sulfonated styrene-based resin. Because commercial solid-phase microextraction (SPME) cartridges are not available ***(20)***, we designed a microcartridge and procedure suitable for cleanup of 5- to 50-µL samples by the spin-enforced SPME technique ***(7)***.

2. Materials

2.1. Components (see *Note 1)*

1. PrinCE-C 465 (PrinCE Technologies, Netherlands), a computerized CE system with a robotic sample injector.
2. DAx 6 for Microsoft Windows NT/98 data acquisition and analysis software (Van Mierlo Software Consultancy, Netherlands). The software is used to control the CE unit and 22-bit acquisition board (SCPA L42M, SCPA, DE) and to perform data analysis. A data acquisition ratio of 10–20 data point per second is used).
3. Crystal-1000 conductivity detector (Thermo Bioanalysis, cat. no. 9435 250 02001).
4. ConCap™ I fused silica capillary assembly, 70 cm × 50 µm (Thermo Bioanalysis, cat. no. CD220307-A01 or 9435 250 02211).
5. ConTip™ I conductivity sensor assembly (Thermo Bioanalysis, cat. no. CD219812-A01).
6. Small laboratory centrifuge (>1000 rpm).
7. 2-mL vial, vial holder, and 13-mm vial cap for inlet buffer and standards (PrinCE Technology, cat. no. 8035.001, 2520.011, and 2520.810).
8. 250-µL Vial and vial holder for samples (PrinCE Technology, cat. nos. 8030.010 and 2520.014).
9. MilliCupTM-HV filter unit for filtering and degassing CE buffer (Milipore SJHV, cat. no. M4710).
10. Tru-Sweep™ sonicator bath for degassing CE and cleaning reusable analytical components (Crest Ultrasonics).
11. Polimer Luer-lock 10 and 30-cm^3 syringes (*see* **Note 2**).
12. OnGuard II A®, 2.5-cm^3 buffer preparation cartridges (Dionex, cat. no. 057092).
13. OnGuard II Ag®, 2.5-cm^3 (Dionex, cat. no. 057090) (*see* **Note 3**).
14. Polymer 1/8-in. female Luer-lock (Small Parts, cat. no. U-1005109).

Table 1
Stock Solutions

Anions	Formula	F.W.	m*M* (1000 ppm)	mg/250 mL (1000 ppm)
Chloride	NaCl	58.44	28.2	412
Nitrate	$NaNO_3$	84.99	16.1	342
Nitrite	$NaNO_2$	69.00	21.7	374
Sulfate	Na_2SO_4	142.04	10.4	370
Fluoride	NaF	41.99	52.6	553
Phosphate	Na_2PO_4	141.96	10.5	374

15. 0.1- to 10-μL Filter tips (USA Scientific, cat. no. 1121-3810).
16. 1- to 20-μL Tips (*see* **Note 4**).
17. Falcon BlueMax 15-mL graduated tubes (Fisher, cat. no. 14-959-49D).

*2.2. Reagents and Stock Solutions (***see** ***Note 5)***

1. 1*M* NaOH cleaning solution for SPME cartridge and capillary cleanup. Prepare 200 mL solution by dissolving 8 g of NaOH in 200 mL of distilled water (DW).
2. 25 m*M* EOF modifier solution (TTAB). Prepare 250-mL solution by dissolving 2.10 g TTAB in DW. Apply ultrasonic agitation (*see* **Note 6**).
3. 12 m*M* LiOH leading solution. Dissolve 0.05 g of lithium hydroxide monohydrate in 100 mL of DW. A fresh solution should be prepared weekly.
4. 1000 ppm terminating solution. Dissolve 0.12 g of sodium octanesulfonate (monohydrate) in 100 mL of DW. A fresh solution should be prepared weekly.
5. Stock standards. Dilute reagent in 250 mL of DW (*see* **Table 1**, column 5).
6. Mixed standards for calibration (1/10/100/1000 ppb). Prepare 10 mL of 10 ppm mixed standard by pipetting 100 μL of each standard solution into 15-mL graduated tubes and add DW to reach 10-mL volume. Add 900 μL of DW into four 2-mL sampling vials. Pipet 100 μL of 100 ppm mixed standard into the first vial and mix the solution by gentle pipetting it three times. Sequentially dilute mixed standard by transferring 100 μL of solution to each next vial after mixing it in previous vial. (Use fresh tips for each solution transfer.) Replace DW by 10 ppm terminating solution if one is used for sample preparation. The mixed standard can be stored for a month.

3. Methods

3.1. Preparation of 250 mL of CE Buffer

The CE buffer with the EOF-modifying solution of tetradecyltrimethylammonium hydroxide includes 25 m*M* arginine, 81.5 m*M* borate, and 0.5 m*M* TTAOH, pH 9.5, with 1 *M* NaOH. TTAB is converted to TTAOH by replacing bromide ions with hydroxyl ions using ion-exchange cartridge OnGuard II A.

1. Dissolve 1.09 g Arg and 1.25 g boric acid in 250-mL polypropylene flask filled with approx 100 mL DW.
2. Attach OnGuard II A cartridge to a 10-cm^3 syringe with plunger removed, backfill with approx 10 mL of DW, reinsert plunger, and pump all DW volume through the cartridge.
3. Detach cartridge, remove plunger, and repeat **step 2** except for backfilling syringe with 10 mL of 1*M* NaOH.
4. Repeat **step 2** with DW to wash residual NaOH.
5. Repeat **step 2** with 10 mL of 25 m*M* TTAB, first disposing 5 mL and collecting the next 5 mL into the polypropylene flask from **step 1**.
6. Add DW to reach 250-mL volume.
7. Degas and filter buffer solution by passing through a 22-μm membrane filter using a vacuum pump and appropriate filtering assembly. New buffer solution should be prepared daily.

3.2. Preparation of Chloride SPME Cartridges

1. Open OnGuard Ag cartridge using pliers and collect resin on a waxed balance paper and then in an Eppendorf tube. The resin from one OnGuard Ag cartridge is enough to prepare about 200 SPME cartridges (*see* **Fig. 1**). Backload approx 3.5 mg of the resin into 0.1- to 10-μL filter tips, which then will be used as SPME cartridges (*see* **Note 7**).
2. Attach the SPME cartridge to a plastic syringe using a 1/8-in. female Luer-lock and slowly (approx 10 s) pump about 0.1–0.2 mL of 1*M* NaOH.
3. Repeat **step 2**, pumping about 0.5 mL of DW.
4. Balance cartridges in centrifuge using 1- to 20-μL tips and 1.5-mL Eppendorf tubes as a cartage support (*see* **Fig. 2**).
5. Spin cartridges for 30 s to remove residual DW. Ready SPME cartridges can be stored and used during several days; however, the best results are obtained with a freshly prepared cartridge.

3.3. Sample Preparation

1. Acquire liquid or solid samples following an appropriate procedure ***(7,21–25)***.
2. Estimate volume of samples and resuspend samples in DW 1:1,000 to 1:100,000 final sample dilution and at least 10 μL volume (*see* **Note 8**).
3. Break down tissue by freezing and ultrasonic agitation (*see* **Note 9**).
4. Backload diluted samples into SPME cartridge–sample vial assembly, balance, and spin for approx 30 s (*see* **Fig. 1**, *positions 5* and *6*).
5. Deposit sample vial into a holder, seal holder with a cap, and place in a sampling carousel from PrinCE.

3.4. CE Running Protocol (see *Note 10*)

1. Deposit a set of analysis-ready samples, along with a set of four gradually diluted standards (*see* **step 5** of **Subheading 3.2.**) into a sampling carousel from PrinCE.

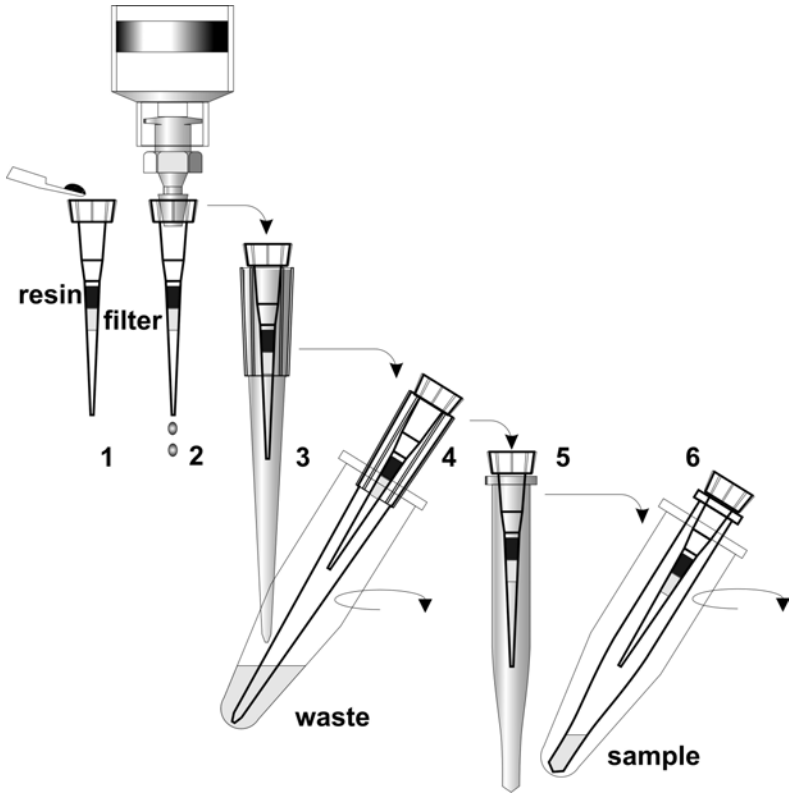

Fig. 1. Solid-phase microextraction-chloride cleanup cartridge preparation *(1–4)* and sample cleanup *(5, 6)* procedures. SPME cartridge is inserted into a 1- to 20-μL tip and sampling vial at 3 and 5, respectively, are shown.

2. Enter CE Global Configuration, and Crystal 1000 Configuration values according to manufacturer instructions.
3. Enter "Run Table" values (run number; separation method, sample/standard location).
4. Enter CE "Running Method" values (*see* **Table 2**).
5. Precondition CE capillary: Load capillary with 1*M* NaOH prior to run and flush it with DW after 5 min (*see* **Note 11**).
6. Postcondition CE capillary: After analysis, flush capillary sequentially for 2 min with CE buffer and then for 2 min with DW (*see* **Note 12**).
7. Refresh running buffer after each 10 separation cycles by switching to another running buffer vial.
8. Examples of electrophoretograms for different sample types are presented in **Fig. 2**.

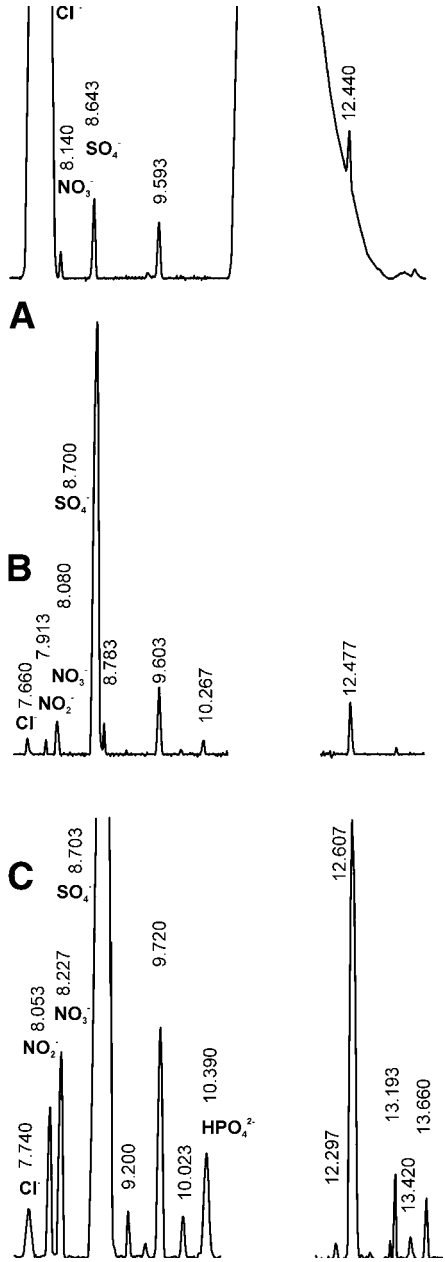

Fig. 2. Representative electropherograms of different tissue samples (modified from **ref. *7***). **A–C**: 10,000-fold diluted rat dorsal root ganglia before **(A)** and after **(B)** SPME chloride removal. Absolute retention times along with anion identities are shown. **B** and **C:** different ITP staking injection intervals, 3 and 12 s, respectively.

Table 2
Running Method (for 50-μm Bore, 500-mm-Length Capillary)

Procedure	Inlet vial	Pressure (mbar)	Voltage (kV)	Time (s)
1. Clean	1*M* NaOH	2000	0	100
2. Wash	18 *M*Ω DW	2000	0	100
3. Fill	Buffer load	2000	0	100
4. Stacking plug	12 m*M* LiOH	30	0	10
5.1 Sample injection[a]	Sample load	0	–5	5[b]
5.2 Sample injection[a]	Sample load	20	0	10[b]
6. Separation	Running buffer[c]	0	–20	900

[a]Value for electrophoretic and hydrodynamic injection 5.1 and 5.2, respectively, are shown.
[b]Average values of injection time for 1:1000 diluted samples are shown.
[c]This step is synchronized with data acquisition start.

3.5. Data Analysis

1. Here, we provide a brief summary of analysis procedure for DAx 6 software, which includes CE control and many special futures for automatic analysis of electrophoretograms (*see* **Note 13**).
2. Open electrophoretograms of four dilutions of mixed calibrations standard in a DAx "Graphic Window."
3. Construct and subtract baseline sequentially selecting individual electrophoretograms.
4. Select 10-ppb graph and annotate peaks and their concentrations. Anions in standards can be identified by relative-to-chloride retention times: chloride < nitrate < nitrite < sulfate < fluoride < phosphate < carbonate (carbonate from air).
5. Sequentially select 1, 100, and 1000 ppb and run "Detect Peak" analysis procedure.
6. Use the data tag peak menu to display "Peak List" for each of the measurements you want to include in the calibration.
7. Enter peak annotations if they are absent and correct concentration values in the "Peak List."
8. Save calibration procedures, which can be used with the same capillary length and CE protocols for an extended period of time.
9. Subtract baseline and run automatic analysis procedure for each sample.
10. Ion concentrations are determined from relative peak areas and calibration slopes using DAx 6 software. A four-point calibration database with linear or nonlinear point-to-point interpolation is used for quantitative analysis. Finally, electrophoretograms are exported into "Windows Metafile" vector format (*.wmf) and assembled into representative graphs (*see* **Fig. 2**).

4. Notes

1. Suppliers' URL: Dionex, www.dionex.com; PrinCE Technologies, www.princetechnologies.nl; Sigma-Aldrich, www.sigmaaldrich.com; SCPA, www.scpa.de; Van Mierlo Software Consultancy, www.dax.nl/mierlo/vmsc; Small Parts, www.smallparts.com.
2. Syringes are used to prepare buffer components and SPME cartridge cleanup.
3. OnGuard II Ag resin is used for preparing chloride SPME cartridges.
4. The 1- to 20-μL tips are used as a support and protect SPME cartridges.
5. Analytical-grade chemicals (99+%, A.C.S.) and water (>18 MΩ) must be used throughout.
6. The TTAB solution can be stored for 1 mo at room temperature. Do not refrigerate to avoid precipitation.
7. OnGuard-Ag resin can be stored in the dark.
8. In our experience, the terminating additive may improve separation if the sample dilution is < 1:1000; if dilution is > 1:1000, analytical-grade DW can be used. Diluted samples can be stored in Eppendorf tubes at –20°C for several days.
9. Most samples are broken down by hypo-osmotic shock, which provides sufficient conditions for equalizing of ionic concentrations. However, ultrasonic agitation and sample freezing can be beneficial in some instances.
10. Detailed PrinCE- and Cristal 1000-specific setup procedures can be found in the manufacturers' instructions.
11. Preconditioning is obligatory for new and previously dried CE capillaries.
12. Postconditioning increases the lifetime of CE capillaries. In the PrinCE interface, preconditioning and postconditioning of the separation capillary can be included as first and last lines in the "Run Table."
13. A detailed manual and demonstration of newer version of DAx CE is available at www.dax.nl/daxce. Alternatively, appropriate acquisition system and data analysis software can be used.

Acknowledgments

This work was supported by NIH grants RO1AI30464 (to William R. Harvey) and R01NS39103 and R01MH60261 (to Leonid L. Moroz). Dorsal root ganglia tissue samples were provided by Brian Y. Cooper (Department of Oral and Maxillofacial Surgery and Department of Neuroscience, University of Florida).

References

1. Lincoln, J., Hoyle, C. H. V., and Burnstock, G. (1997) *Nitric Oxide in Health and Disease*, Cambridge University Press, Cambridge.
2 Kharitonov, V. G., Sundquist, A. R., and Sharma, V. S. (1994) Kinetics of nitric oxide autoxidation in aqueous solution. *J. Biol. Chem.* **269(8),** 5881–5883.
3 Lewis, R. S. and Deen, W. M. (1994) Kinetics of the reaction of nitric oxide with oxygen in aqueous solutions. *Chem. Res. Toxicol.* **7(4),** 568–574.

4 Ignarro, L. J., et al. (1993) Oxidation of nitric oxide in aqueous solution to nitrite but not nitrate: comparison with enzymatically formed nitric oxide from L-arginine. *Proc. Natl. Acad. Sci. USA* **90(17),** 8103–8107.
5. Fukuto, J. M., Cho, J. Y., and Switzer, C. H. (2000) The chemical properties of nitric oxide and related nitrogen oxides., in *Nitric Oxide. Biology and Pathobiology* (Ignarro, L. J., ed.), Academic, San Diego, CA, pp. 23–40.
6. Moroz, L. L. (2001) Gaseous transmission across time and species. *Am. Zool.* **41,** 304–320.
7 Boudko, D. Y., et al. (2002) High-resolution microanalysis of nitrite and nitrate in neuronal tissues by capillary electrophoresis with conductivity detection. *J. Chromatogr B Analyt. Technol. Biomed. Life Sci.* **774(1),** 97–104.
8 Buchberger, W. W. (2000) Detection techniques in ion analysis: what are our choices? *J. Chromatogr. A* **884(1–2),** 3–22.
9 Haber, C., et al. (1996) Conductivity detection in capillary electrophoresis—a powerful tool in ion analysis. *J. Capillary Electrophor.* **3(1),** 1–11.
10 Stratford, M. R., et al. (1997) The role of nitric oxide in cancer. Improved methods for measurement of nitrite and nitrate by high-performance ion chromatography. *J. Chromatogr. A* **770(1–2),** 151–155.
11 Boudko, D. Y., Harvey, W. R., and Moroz, L. L. (2001) Single-cell NO^{2-}/NO^{3-} assay: concentrations, activities and transmembrane fluxes, in *Society for Neuroscience Abstracts*, Society for Neuroscience.
12. Boudko, D. Y., et al. (2001) Alkalinization by chloride/bicarbonate pathway in larval mosquito midgut. *Proc. Natl. Acad. Sci. USA* **98(26),** 15354–15359.
13 Valsecchi, S., Tartari, G., and Polesello, S. (1997) Determination of anions in rainwater by capillary electrophoresis with conductivity detection. *J. Chromatogr. A* **760(2),** 326–332.
14 Wiliams, R. C., et al. (1997) Analysis of acetate counter ion and inorganic impurities in pharmaceutical drug substances by capillary ion electrophoresis with conductivity detection. *J. Pharm. Biomed. Anal.* **16(3),** 469–479.
15 Monaghan, J. M., et al. (1997) Determination of nitrite and nitrate in human serum. *J. Chromatogr. A* **770(1–2),** 143–149.
16 Hilder, E. F., et al. (2001) Anion-exchange capillary electrochromatography with indirect UV and direct contactless conductivity detection. *Electrophoresis* **22(7),** 1273–1281.
17. Jackson, L. K., et al. (1998) Determination of trace level bromate in drinking water by direct injection ion chromatography. *J. Chromatogr. A* **829(1–2),** 187–192.
18 Kaniansky, D., Zelenska, V., and Baluchova, D. (1996) Capillary zone electrophoresis of inorganic anions with conductivity detection. *Electrophoresis* **17(12),** 1890–1897.
19 Helaleh, M. I. H. and Korenaga, T. (2000) Ion chromatographic method for simultaneous determination of nitrate and nitrite in human saliva. *J. Chromatogr. B* **744(2),** 433–437.
20 Saari-Nordhaus, R. and Anderson, J. M., Jr. (1995) Membrane-based solid-phase extraction as a sample clean-up technique for anion analysis by capillary electrophoresis. *J. Chromatogr. A* **706(1–2),** 563–569.

21 Bories, P. N., Scherman, E., and Dziedzic, L. (1999) Analysis of nitrite and nitrate in biological fluids by capillary electrophoresis. *Clin. Biochem.* **32(1),** 9–14.
22 Everett, S. A., et al. (1995) Nitric oxide in biological fluids: analysis of nitrite and nitrate by high-performance ion chromatography. *J. Chromatogr. A* **706(1–2),** 437–442.
23. El-Menyawi, I., et al. (1998) Measurement of serum nitrite/nitrate concentrations using high-performance liquid chromatography. **706(2),** 347–351.
24 Ferslew, K. E., Hagardorn, A. N., and Robert, T. A. (2001) Capillary ion electrophoresis of endogenous anions and anionic adulterants in human urine. *J. Forensic Sci.* **46(3),** 615–626.
25. Friedberg, M. A., Hinsdale, M. E., and Shihabi, Z. K. (1997) Analysis of nitrate in biological fluids by capillary electrophoresis. *J. Chromatogr. A* **781(1–2),** 491–496.

3

Nitrite and Nitrate Measurements in Human Urine by Capillary Electrophoresis

Edward Morcos and N. Peter Wiklund

Summary

Nitrite and nitrate represent relatively stable nitric oxide (NO) end products in several biological fluids. The amounts of nitrite and/or nitrate in urine have been shown to reflect local and/or systemic involvement of NO in pathological conditions, including urinary tract infections and cardiac and renal allograft rejection. Capillary electrophoresis (CE) has been used in analysis of several ions and micromolecules. Electrokinetic and hydrodynamic sample injections are the main methods of injecting samples onto capillary columns. The urine sample matrix may widely vary depending on urine concentration, urine pH, and ion intake. This chapter illustrates the measurement of nitrite and nitrate in urine by CE and the comparison between electrokinetic and hydrodynamic sample injections.

Key Words: Nitrite; nitrate; urine; capillary electrophoresis (CE); nitric oxide (NO).

1. Introduction

Nitrite and nitrate are commonly used as indicators of nitric oxide (NO) formation in many biological fluids, including urine ***(1–11)***. NO is involved in several physiologic functions, including neurotransmission and endothelium-dependent vasorelaxation ***(12)***. Furthermore, it is involved in host defense reactions, including inflammatory conditions and bacterial infections ***(13)***. NO is very short lived in biological fluids and its fate depends on different factors, including the presence of several agents such as oxyhemoproteins and reactive oxygen species (ROS) ***(14)***. Thus, the NO formed in blood is rapidly oxidized to nitrate, whereas NO formed locally in the urinary tract may be detected as nitrite because the lower urinary tract lacks NO-oxidizing mechanisms ***(15,16)***.

Capillary electrophoresis (CE) has several uses in the clinical laboratory because of its high efficiency of separation and short analysis time, compared

From: *Methods in Molecular Biology, vol. 279: Nitric Oxide Protocols: Second Edition*
Edited by: A. Hassid © Humana Press Inc., Totowa, NJ

to other techniques such as high-performance liquid chromatography (HPLC) ***(17)***. CE has also been used in nitrite and nitrate measurements in many biological fluids ***(8–11)***. Coelectro-osmotic capillary electrophoresis or capillary ion analysis (CIA) is widely used for measurement of small ions because rapid detection, high efficiency, and sharp separation is achieved ***(18)***. Application of either electrokinetic or hydrodynamic sample injection has been reported ***(18)***. While injecting samples onto capillary columns using electrokinetic sample injection, the amount of sample loaded depends on sample concentration, sample mobility, and variations in conductivity ***(19)***. These variables may be influenced by matrix effects such as the presence of larger quantities of ions other than those analyzed, including sodium and chloride ***(19)***. On the other hand, the volume of sample loaded onto the capillary column while using hydrodynamic sample injection is almost unaffected by the sample matrix, allowing high reproducibility of detection ***(19)*** (*see* **Note 1**).

Unlike other biological fluids, the urine matrix may vary widely among different individuals and even in the same individual. Such variation may include urinary pH, urine concentration, and contents of other ions mainly as sodium and chloride. Urinary pH may range as widely as from 4.5 to 8.0 ***(20)***, whereas urine concentration and its content of sodium and chloride is dependent on fluid and ion intake. This chapter illustrates a method for nitrite and nitrate measurement in human urine using CE. Also, effects of variations in urine matrix on nitrite and nitrate detection using either electrokinetic or hydrodynamic sample injection are shown.

2. Materials

1. Osmotic flow modifier (OFM) Anion-BT CIA-Pak™ (Waters-Millipore, Bedford, MA, USA).
2. Sodium sulfate (Merck, Darmstadt, Germany).
3. Sodium nitrite and sodium nitrate (Sigma, St. Louis, MO, USA).
4. Ultrapure water (Elgastat, Bucks, UK).
5. Ultrafree-MC filter devices with cutoff of 5 kDa molecular mass (Millipore, MA, USA).
6. HP 3D CE and Chem Station Data System (Hewlett Packard, Waldbrunn, Germany).
7. Extended-light-path fused-silica capillary column of 104-cm effective path length, 75-μm internal diameter, and 200-μm optical path length (Hewlett Packard, Waldbrunn, Germany).

3. Methods

1. Urine samples are collected as midstream urine from volunteers with no diet or fluid restrictions and stored at –80°C until analysis. The main purpose of collecting samples as midstream urine is to avoid contamination with nitrite and/or nitrate from external urethral meatus.

2. For analysis, samples are diluted 10X with freshly obtained deionized water, followed by centrifugation for 30 min at 5000*g*, using prewashed ultrafree-MC filter devices with a molecular mass cutoff of 5 kDa. At the end of centrifugation, filters are removed and the filtrates are kept on ice until immediate analysis.
3. The background electrolyte (BGE) consists of 25 m*M* sodium sulfate and 5% NICE-Pack OFM Anion-BT, dissolved in Milli-Q water, filtered with 0.2-μm filters and freshly prepared for daily analysis. The pH of the BGE is about 4.8.
4. Conditioning of capillary columns used for the first time is done by injecting sodium hydroxide (1*M* and 0.1*M*) and BGE for 5 min each, with the capillary column temperature set to 60°C.
5. The analysis is done at an applied voltage of –300V/cm in a column maintained at 40°C and ultraviolet (UV) detection at a 214-nm wavelength. The negatively charged electrode is set to the injection site, whereas the positively charged electrode is set behind the detector (*see* **Note 2**).
6. Data analysis is via an HP 3D CE Chem Station Data System having an initial peak width of 0.01, response time of 0.1 s, UV wavelength of 214 nm, and bandwidth of 2 nm.
7. Injection of samples onto the capillary column using electrokinetic sample injection is by an applied negative potential of –6 kV for 20 s (*see* **Note 3**). The detection of nitrite and nitrate is achieved in less than 5 min. Electeropherograms of urine samples loaded onto capillary columns by electrokinetic sample injection are illustrated in **Fig. 1A**, whereas **Fig. 1B** shows spiking of a volunteer sample with standard nitrite. **Figure 1C**,**D** shows spiking of a urine sample from a patient with urinary tract infection with nitrate.
8. Hydrodynamic sample injection is achieved by injecting samples at 30 mbar for 60 s. A negative pressure of 5 mbar is applied at the start of sample electrophoresis (*see* **Note 4**). Before each analysis, capillaries are washed with 1*M* NaOH and deionized water for 1 min each and BGE for 2 min. The electropherogram of urine loaded onto capillary by hydrodynamic sample injection is shown in **Fig. 2**.
9. Linear regression is used for analysis of standard nitrite and nitrate addition curves, as shown in **Fig. 3**. The Student's *t*-test for unpaired comparisons is used as indicated. Intra-assay coefficient of variations (CVs) is used for determining the intra-assay of variability in detection of nitrite and nitrate standards as measured by in-between peak areas of 10 urine samples in duplicates or as indicated.

3.1. Results

Intra-assay CVs for a nitrite concentration of 10 μ*M* was 0.95% for electrokinetic and 2.07% for hydrodynamic sample injection. For a nitrate concentration of 100 μ*M*, CVs was 1.05% for electrokinetic and 1.42% hydrodynamic sample injection. Using hydrodynamic sample injection, CVs for nitrite and nitrate over the range 0.1–1 μ*M* and 10–300 μ*M* are 4.3% and 2.1%, respectively (*see* **Fig. 3A**,**B).** Linear regressions for nitrite and nitrate over the range 0.1–1 μ*M* and 10–300 μ*M* gave 0.99 for both nitrite and nitrate (*see* **Fig. 3A**,**B**).

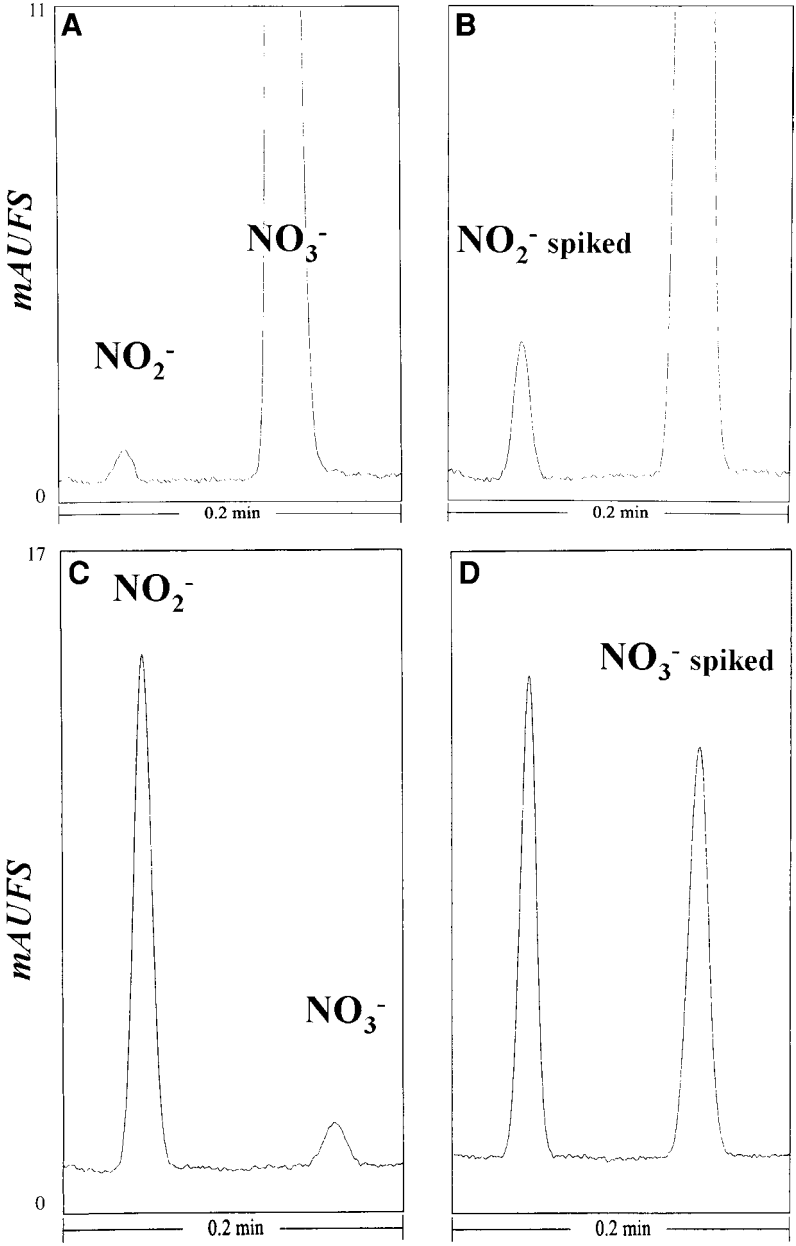

Fig. 1. Electropherograms of nitrite and nitrate peaks detected in a volunteer urine loaded by electrokinetic sample injection, as shown in **(A)**, whereas **(B)** shows spiking of this urine sample with 1 μ*M* nitrite. **(C)** Low nitrate concentration was seen in urine of a patient with urinary tract infection with nitrate reductase containing bacteria; **(D)** spiking sample shown in (C) with 100 μ*M* nitrate. (Reproduced from **ref.** ***21*** with permission.)

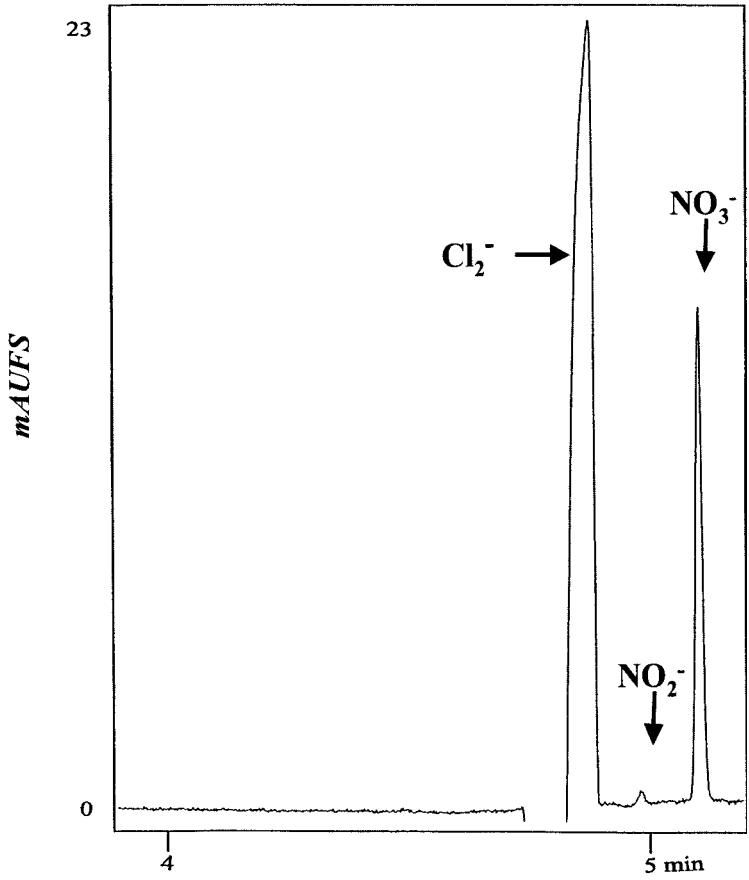

Fig. 2. Electropherogram of a volunteer urine sample loaded by hydrodynamic sample injection. Detection of chloride (Cl_2^-), nitrite (NO_2^-) and nitrate (NO_3^-) peaks was sharp and symmetric with complete resolution from each other. (Reproduced from **ref. *21*** with permission.)

Nitrite and nitrate concentrations in 20 urine samples from male volunteers were 0.366 ± 0.075 and 720 ± 103 μ*M*, respectively.

3.1.1. Urinary pH

The effect of urine pH on nitrite and nitrate detection was determined by adjusting the pH of urine samples to range from 4.5 to 8. The detection of nitrite and nitrate ranged widely when electrokinetic sample injection was applied, as shown in **Fig. 4A**,**C** (*see* **Note 3**). However, such a variance for urinary pH on nitrite and nitrate detection was not seen when hydrodynamic

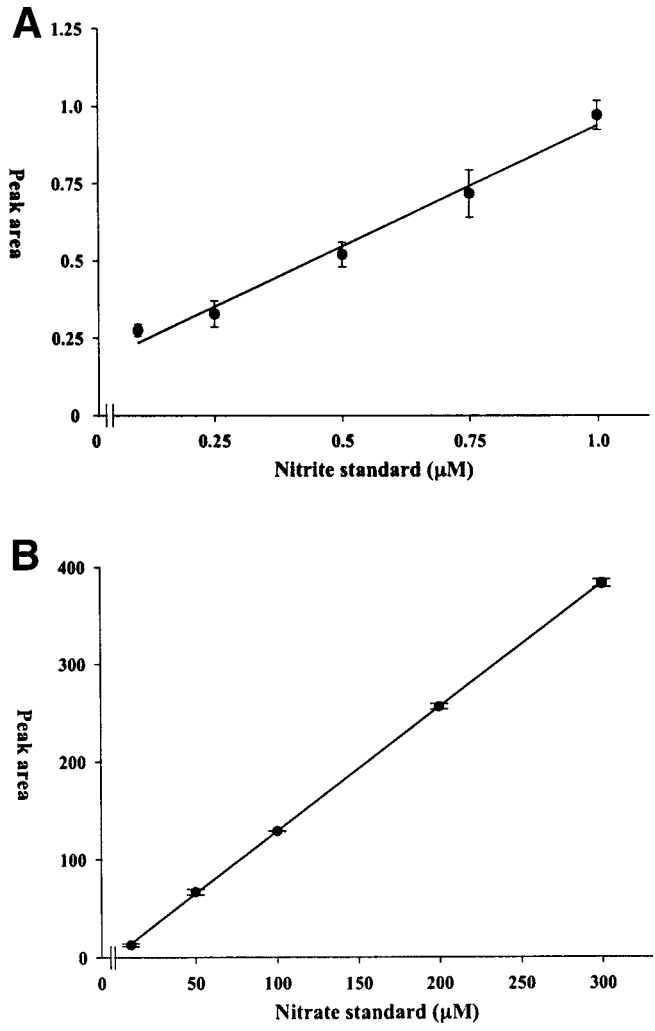

Fig. 3. Curves of standard addition of nitrite and nitrate to urine samples. Four urine samples were diluted in deionized water, spiked with standard nitrite and nitrate, and loaded by hydrodynamic injection (30 mbar for 60 s) onto the capillary. (Reproduced from **ref. *21*** with permission.)

sample injection was used (*see* **Fig. 4B,D)** (*see* **Note 4**). On the other hand, the sensitivity of detection was higher when using electrokinetic sample injection.

3.1.2. Urine Concentration

Either low or highly diluted (1 part to 10 or 1 part to 100) urine was loaded onto a capillary column using either electrokinetic or hydrodynamic sample

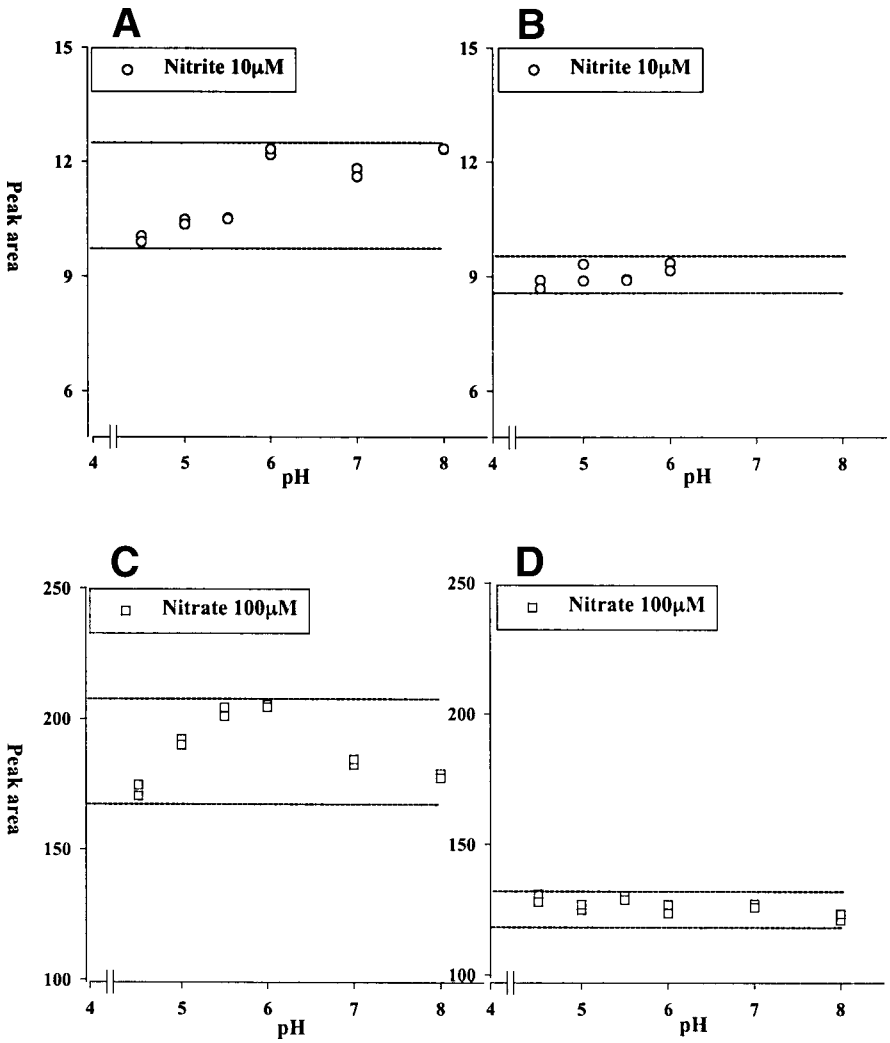

Fig. 4. Urine pH effect on detection of standard nitrite and nitrate. The pH of urine samples was adjusted to range from 4.5 to 8.0 in duplicates. Samples were loaded by electrokinetic sample injection **(A,C)** or hydrodynamic sample injection **(B,D)**. Detection of nitrite and nitrate shows high variability in different urine pH when electrokinetic sample injection was used **(A,C)**. However, such effect for urine pH was not seen when samples were injected hydrodynamically **(B,D)**. (Reproduced from **ref.** ***21*** with permission.)

injection. Significant increase of standard nitrite and nitrate detection was seen when highly diluted urine samples were loaded by electrokinetic sample injection (*see* **Fig. 5A)** (*see* **Note 3**). On the other hand, no difference in detection of

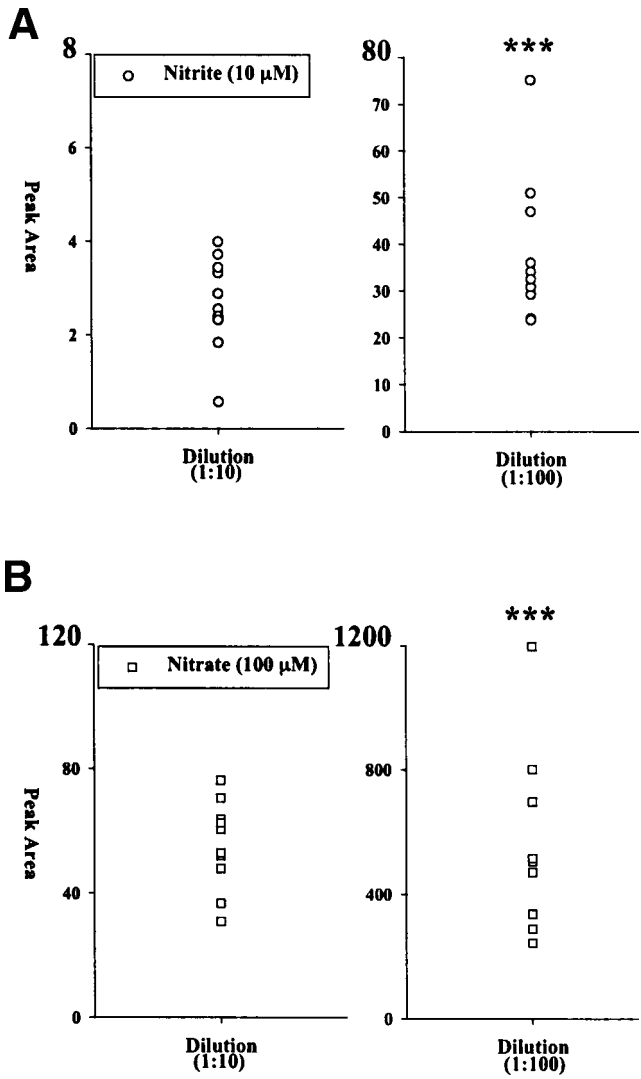

Fig. 5. Effect of sample dilution on standard nitrite and nitrate detection. Samples were loaded by electrokinetic sample injection **(A,B)** or hydrodynamic sample injection **(C,D)**. Significant increase in detection of standard nitrite and nitrate was seen with higher dilution of samples when electrokinetic sample injection was used **(A,B)**. ***$p < 0.001$ using Student's *t*-test for unpaired comparison. Such an increase in detection was not seen when samples were injected hydrodynamically **(C,D)**. (Reproduced from **ref. *21*** with permission.)

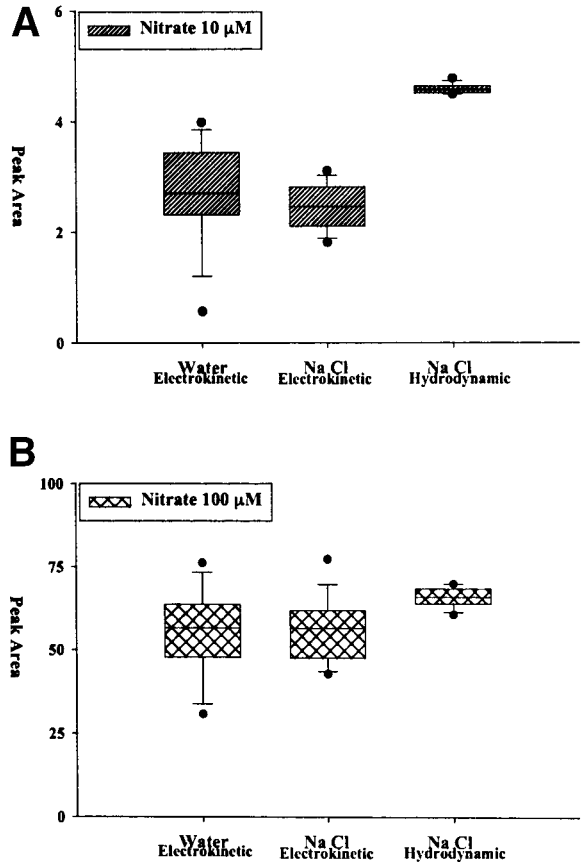

Fig. 6. Ionic sodium and chloride effect on detection of standard nitrite and nitrate. Urine samples were diluted 1 to 10 either in deionized water or freshly prepared physiologic saline solution (0.9% NaCl) in duplicates. Injection was done by –6 kV for 20 s for electrokinetic sample injection or 30 mbar for 30 s for hydrodynamic sample injection. Detection of standard nitrite and nitrate showed a high variability on different urine pH when samples were loaded by electrokinetic sample injection. Such effect was not seen with the hydrodynamic sample injection. (Reproduced from **ref. *21*** with permission.)

standard nitrite or nitrate was seen when hydrodynamic sample injection was applied (*see* **Fig. 5A**) (*see* **Note 4**).

3.1.3. Contents of Sodium and Chloride in Urine

Samples were diluted either in water or in physiologic saline (0.9% NaCl). Using electrokinetic sample injection, dilution of urine samples in physiologic saline led to a decrease in variability of detection compared to samples diluted in water (*see* **Fig. 6A**,**B** and **Note 3**). Dilution of urine samples either in water

or in physiologic saline gave the same results for the detection of nitrite and nitrate when hydrodynamic sample injection was used (*see* **Figs. 6A**,**B** and **Fig. 5C**,**D** and **Note 4**).

3.2. Discussion

3.2.1. Urinary Nitrite and Nitrate

Urinary nitrate reflects NO formed locally in organs or tissues located far from the urinary tract because gaseous NO is converted to nitrite and later to nitrate by local agents or other agents in systemic circulation, including oxyhemoglobins and ROS ***(14,16)***. Thus, increased urinary nitrate has been reported in atopic dermatitis and infective gastroenteritis ***(5,22,23)***. Furthermore, urinary nitrate has indicated increase of NO levels in systemic circulation, following cardiac and renal allograft rejections ***(7,24)***. On the other hand, nitrite detected in urine represents the main end products of NO formed locally in the urinary tract because there is a lack of converting mechanisms, including oxyhemoproteins in the urinary tract ***(15)***. Reports indicate increased NO formation in bladder inflammatory diseases, including interstitial inflammation, irradiation, and infectious as well as noninfectious cystitis ***(25,26)***. A simple dipstick test is routinely used as a marker of urinary tract infection where infecting bacterial agents contain nitrate reductase enzyme, which accounts for nitrate reduction into nitrite ***(27)***. Several methods, including Griess reaction, chemiluminescence, HPLC, and gas chromatography–mass spectrometry (GC-MS) have been mainly used for nitrite and nitrate measurements for research studies ***(28–32)***. However, indirect detection and a long analysis procedure is time-consuming and expensive.

3.2.2. CE in Nitrite and Nitrate Measurement

Capillary electrophoresis is an advanced technique for the analysis of biologically active molecules and ions ***(17,33)***. It is a powerful electromigration separation method for different ions and micromolecules. Capillary ion electrophoresis (CIE) has been shown to directly quantify nitrite and nitrate in biological fluids close to the millimolar range ***(34)***. Because of the low concentrations of nitrite in biological fluids, CIE has been used to indirectly determine nitrite and nitrate by their reduction into gaseous NO, which is detected subsequently by chemiluminescence ***(34)***. Moreover, CIE was also used for measurement of other NO metabolites such as nitrosylated glutathione ***(35)***. CIE allowed detection of nitrosylated glutathione with high separation from glutathione and glutathione disulfide, where extremely high current was applied and a low-pH buffer was used ***(35)***.

4. Notes

1. As previously established, detection of different ions using CE may be affected by quantity of sample loaded onto the capillary ***(19)***. It may also be affected by sample electrophoresis if the quantity of sample loaded is fixed ***(19)***. The urine matrix had an effect on nitrite and nitrate detection, which may be explained by differences in sample amount loaded onto the capillary depending on parameters such as urine pH, urine concentration, and contents of sodium and chloride. The most likely explanation is that these parameters may lead to currency drops and voltage differences while loading samples onto capillaries. On the other hand, the urine matrix had no effect on the detection of nitrite and nitrate while using hydrodynamic sample injection. It is also known that the sample quantity loaded onto the capillary is almost independent of the sample matrix when hydrodynamic sample injection is used ***(19)***. This suggests that the electrophoresis of urine loaded onto the capillary has not been affected by the urine sample matrix when hydrodynamic sample injection is used. Such effect of the urine matrix on sample electrophoresis cannot be totally excluded when electrokinetic sample injection was used. Thus, the effect of the sample matrix leading to wide range of detection of nitrite and nitrate using electrokinetic sample injection is mainly dependent on the sample volume loaded.
2. Coelectro-osmotic capillary electrophoresis is an approach used for optimizing CE separation for different ions of the same charge. When first introduced, it was called capillary ion analysis (CIA) ***(18)***. To analyze ions of negative charge, negative polarity is set to injection site, whereas the EOF direction is forward of the positively charged electrode settled behind the detector. Thus, either slow- or fast-migrating ions of the same charge are detected in the same analysis within a short run time. Thus, the major advantage of this technique is the detection of different ions of the same charge in a single electropherogram with shorter analysis times. Using the CIA technique, a method for nitrite and nitrate measurements in plasma has been developed, allowing detection of basal nitrite and nitrate in plasma using electrokinetic sample injection ***(36)***. Furthermore, a method for the measurement of nitrate in urine using electrokinetic sample injection has been described ***(37)***. However, no detection of urinary nitrite was achieved ***(37)***. Using hydrodynamic sample injection, a method for measurement of nitrite and nitrate in biological fluids was described ***(38)***. However, the low sensitivity of detection of nitrite in urine and long analysis times were reported ***(38)***.
3. As indicated in **Subheading 4.**, electrokinetic sample injection allowed higher sensitivity of detection (*see* **Fig. 4**). Urinary pH, urine concentration, and urine contents of sodium and chloride interfered with optimality and quantity of nitrite and nitrate detection. A wide range of detection of standard amounts of nitrite and nitrate has been seen, depending on urine matrix when electrokinetic sample injection was used (*see* **Figs. 4A**,**C**, **5A**,**B**, and **6A**,**B**). Thus, each urine sample has its own standards of detection when electrokinetic sample injection is used, depending on urine pH, concentration, and contents of sodium and chloride.

4. While using hydrodynamic sample injection, the detection of nitrite and nitrate was not dependent on urine sample matrices. Neither urine pH, urine concentration, nor urine contents of sodium and chloride had an effect on variability in detection of nitrite and nitrate (*see* **Figs. 4B**,**D**, **5C**,**D**, and **6A**,**B**). Thus, hydrodynamic sample injection presents the injection of choice while analyzing urine samples by CE because detection is not affected by urine matrix.

Acknowledgment

The work was supported by grants from the Swedish Medical Research Foundation (project 11199).

References

1. Kraftes-Jacobs, B., Brilli, R., Szabo, C., et al. (1997) Circulating methemoglobin and nitrite/nitrate concentrations as indicators of nitric oxide overproduction in critically ill children with septic shock. *Crit. Care Med.* **25,** 1588–1593.
2 Winlaw, D. S., Schyvens, C. G., Smythe, G. A., et al. (1994) Urinary nitrate excretion is a noninvasive indicator of acute cardiac allograft rejection and nitric oxide production in the rat. *Transplantation* **58,** 1031–1036.
3 Reimund, J. M., Duclos, B., Koehl, C., et al. (1999) Nitric oxide end products in patients hospitalized for diarrhoea. *Eur. J. Gastroenterol. Hepatol.* **11,** 1013–1018.
4 Kakoki, M., Matsumoto, A., Nagata, D., et al. (1999) Analysis of nitric oxide in the exhaled air of patients with chronic glomerulonephritis. *Clin. Nephrol.* **52,** 83–90.
5 Omata, N., Tsukahara, H., Ito, S., et al. (2001) Increased oxidative stress in childhood atopic dermatitis. *Life Sci.* **69,** 223–228.
6 Tsukahara, H., Hiraoka, M., Hori, C., et al. (1997) Urinary nitrite/nitrate excretion in infancy: comparison between term and preterm infants. *Early Hum. Dev.* **47,** 51–56.
7 Mugge, A., Kurucay, S., Boger, R. H., et al. (1996) Urinary nitrate excretion is increased in cardiac transplanted patients with acute graft rejection. *Clin. Transplant.* **10,** 298–305.
8. Morcos, E., Jansson, O. T., Adolfsson, J., et al. (2001) Bacillus–Calmette–Guerin induces long-term local formation of nitric oxide in the bladder via the induction of nitric oxide synthase activity in urothelial cells. *Urology* **165,** 678–682.
9 Lundberg, J. O., Herulf, M., Olesen, M., et al. (1997) Increased nitric oxide production in collagenous and lymphocytic colitis. *Eur. J. Clin. Invest.* **27,** 869–871.
10 Brundin, L., Morcos, E., Olsson, T., et al. (1999) Increased intrathecal nitric oxide formation in multiple sclerosis; cerebrospinal fluid nitrite as activity marker. *Eur. J. Neurol.* **6,** 585–590.
11 Brundin, L., Svenungsson, E., Morcos, E., et al. (1998) Central nervous system nitric oxide formation in cerebral systemic lupus erythematosus. *Ann. Neurol.* **44,** 704–706.
12 Moncada, S. and Higgs, E. A. (1995) Molecular mechanisms and therapeutic strategies related to nitric oxide. *FASEB J.* **9,** 1319–1330.

13. Maeda, H. and Akaike, T. (1998) Nitric oxide and oxygen radicals in infection, inflammation, and cancer. *Biochemistry (Mosc.)* **63,** 854–865.
14 Palmer, R. M., Rees, D. D., Ashton, D. S., et al. (1988) L-Arginine is the physiological precursor for the formation of nitric oxide in endothelium-dependent relaxation. *Biochem. Biophys. Res. Commun.* **153,** 1251–1256.
15. Kelm, M. and Yoshida, K. (1988) in *Methods in Nitric Oxide Research* (Feelisch, M. and Stamler, J. S., eds.), Wiley, London, pp. 47–58.
16 Ignarro, L. J., Fukuto, J. M., Griscavage, J. M., et al. (1993) Oxidation of nitric oxide in aqueous solution to nitrite but not nitrate: comparison with enzymatically formed nitric oxide from L-arginine. *Proc. Natl. Acad. Sci. USA* **90,** 8103–8107.
17 Landers, J. P. (1995) Clinical capillary electrophoresis. *Clin. Chem.* **41,** 495–509.
18. Jandik, P. and Bonn, G. (1993) In *Capillary Electrophoresis of Small Molecules and Ions* (Jandik, P. and Bonn, G., eds.), VCH, New York, pp. 5–78.
19. Heiger, N. D. (eds.) (1992) *High Performance Capillary Electrophoresis*, Hewlett-Packard, Germany, pp. 77–84.
20. Brendler, C. B. (1998) In *Campbell's Urology* (Walsh, P. C., Retik, A. B., Vaughan, E. D., et al., eds.), WB Saunders, Philadelphia, pp. 131–157.
21 Morcos, E. and Wiklund, N. P. (2001) Nitrite and nitrate measurement in human urine by capillary electrophoresis. *Electrophoresis* **22,** 2763–2768.
22 Dykhuizen, R. S., Copland, M., Smith, C. C., et al. (1995) Plasma nitrate concentration and urinary nitrate excretion in patients with gastroenteritis. *J. Infect.* **31,** 73–75.
23 Forte, P., Dykhuizen, R. S., Milne, E., et al. (1999) Nitric oxide synthesis in patients with infective gastroenteritis. *Gut* **45,** 355–361.
24 Smith, S. D., Wheeler, M. A., Zhang, R., et al. (1996) Nitric oxide synthase induction with renal transplant rejection or infection. *Kidney Int.* **50,** 2088–2093.
25 Ehren, I., Iversen, H., Jansson, O., et al. (1994) Localization of nitric oxide synthase activity in the human lower urinary tract and its correlation with neuroeffector responses. *Urology* **44,** 683–687.
26 Lundberg, J. O., Ehren, I., Jansson, O., et al. (1996) Elevated nitric oxide in the urinary bladder in infectious and noninfectious cystitis. *Urology* **48,** 700–702.
27. Schaeffer, J. A. (1998) In *Campbell's Urology* (Walsh, P. C., Retik, A. B., Vaughan, E. D., et al., eds.), WB Saunders, Philadelphia, pp. 533–614.
28. Griess, J. P. (1864) On a new series of bodies in which nitrogen is substituted for hydrogen. *Phil. Trans. R. Soc. (Lond.)* **154,** 667–731.
29. Griess, J. P. (1879) Bemerkungen zu der Abandlung der HH. Wesely und Benedikt "uber einige Azoverbindungen." *Ber. Deutsch. Chem. Ges*. **12,** 426–428.
30 Lee, K., Greger, J. L., Consaul, J. R., et al. (1986) Nitrate, nitrite balance, and de novo synthesis of nitrate in humans consuming cured meats. *Am. J. Clin. Nutr.* **44,** 188–194.
31 Tsikas, D., Fuchs, I., Gutzki, F. M., et al. (1998) Measurement of nitrite and nitrate in plasma, serum and urine of humans by high-performance liquid chromatography, the Griess assay, chemiluminescence and gas chromatography-mass spectrometry: interferences by biogenic amines and *N*(*G*)-nitro-L-arginine analogs. *J. Chromatogr. B. Biomed. Sci. Appl.* **715,** 441–445.

32 Kage, S., Kudo, K., and Ikeda, N. (2000) Determination of nitrate in blood by gas chromatography and gas chromatography-mass spectrometry. *J. Chromatogr. B. Biomed. Sci. Appl.* **742,** 363–368.
33 Shihabi, Z. K. and Friedberg, M. A. (1997) Analysis of small molecules for clinical diagnosis by capillary electrophoresis. *Electrophoresis* **18,** 1724–1732.
34 Trushina, E. V., Oda, R. P., Landers, J. P., et al. (1997) Determination of nitrite and nitrate reduction by capillary ion electrophoresis. *Electrophoresis* **18,** 1890–1898.
35 Trushina, E. V., Oda, R. P., McMurray, C. T., et al. (1999) Effective and reproducible capillary electrophoretic separation of thiols under conditions where exceptionally high current is generated. *Anal. Chem.* **71,** 5569–5573.
36 Leone, A. M., Francis, P. L., Rhodes, P., et al. (1994) rapid and simple method for the measurement of nitrite and nitrate in plasma by high performance capillary electrophoresis. *Biochem. Biophys. Res. Commun.* **200,** 951–957.
37 Meulemans, A. and Delsenne, F. (1994) Measurement of nitrite and nitrate levels in biological samples by capillary electrophoresis. *J. Chromatogr. B. Biomed. Sci. Appl.* **660,** 401–404.
38. Friedberg, M. A., Hinsdale, M. E., and Shihabi, Z. K. (1997) Analysis of nitrate in biological fluids by capillary electrophoresis. *J. Chromatogr. A* **781,** 491–496.

4

In Vivo Nitric Oxide Measurements Using a Microcoaxial Electrode

Yoshiichiro Kitamura, Hirosuke Kobayashi, Kazuo Tanishita, and Kotaro Oka

Summary

Nitric oxide (NO) is a vital molecule contributing to numerous physiological phenomena in various biological systems. To investigate the physiological role of NO, a range of NO-specific electrodes allowing direct and continuous NO measurement have been developed for in vitro and in vivo NO detection. A microcoaxial electrode has also been developed for the measurement of real-time NO levels. Because the working and reference electrodes in this device are situated close together, the microcoaxial electrode is considered to be ideal for the measurement of local NO concentrations with high spatial resolution. The microcoaxial electrode has been successfully applied to the real-time measurement of NO in endothelial cells, thereby demonstrating its effectiveness as an NO-specific electrode. In this chapter, we describe our experimental protocol for performing real-time NO measurements that was developed during physiological experiments using the microcoaxial electrode.

Key Words: Nitric oxide (NO); NO-specific electrode; electrochemistry; microcoaxial electrode; NO donor; *S*-nitroso-*N*-acetyl-DL-penicillamine (SNAP); endothelial cells; acetylcholine (ACh).

1. Introduction

Nitric oxide (NO) is usually produced on demand from constitutive NO synthase in various biological systems ***(1–5)***. Because small amounts of NO are released and quickly oxidized in tissues, NO exerts its effects only on a limited local area because of its short lifetime (less than 30 s) ***(6)***. Several methods have been developed to estimate NO concentrations in biological tissues. These methods include chemiluminescence measurement ***(7,8)***, electron paramagnetic resonance spectrometry ***(9)***, and the Griess method ***(10)***. However, these methods are discontinuous, indirect, or have other drawbacks (e.g., not local), meaning that it is therefore difficult to determine real-time local NO concentrations

From: *Methods in Molecular Biology, vol. 279: Nitric Oxide Protocols: Second Edition*
Edited by: A. Hassid © Humana Press Inc., Totowa, NJ

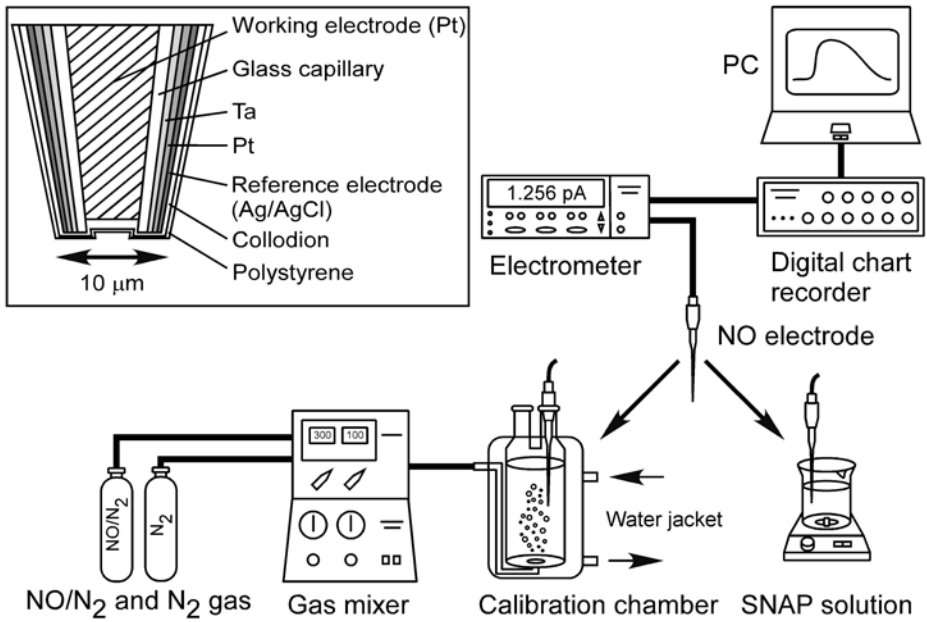

Fig. 1. Experimental setup for real-time NO measurements (see text). (Reprinted with permission from **ref. *25***.)

with high spatial and temporal resolutions. To overcome these disadvantages, a microelectrode technique for real-time NO measurement, based on electrochemical principles, has been developed ***(11)***. From this, various NO-specific electrodes have been described that enable the direct and continuous measurement of NO in vitro and in vivo ***(12–24)***. We also developed a microcoaxial electrode for selective NO measurement with high spatial and temporal resolutions within a confined area of tissue ***(25)***. Because the working and reference electrodes are oriented coaxially and close together, the microcoaxial electrode can be used to great effect for NO measurements in tissues or in isolated cells.

In this chapter, we describe in detail the procedure for making NO measurements with the microcoaxial electrode. We also present the results of real-time NO measurements made with the electrode for demonstration of its usefulness.

2. Materials

2.1. Calibration of Microcoaxial Electrode

1. Microcoaxial electrode for real-time NO measurement (*see* **Fig. 1**, *inset*) ***(25)*** (*see* **Note 1**). Preparation of the electrode has been described elsewhere in detail ***(25)*** (*see* **Note 2**).

2. Nitric oxide standard solution for calibration: Submicromolar NO solutions prepared from phosphate-buffered saline (PBS) or HEPES-buffered saline (HBS) (Dojindo, Kumamoto, Japan) bubbled with NO gas. The pH of these buffers must be kept at 7.4. Prepare fresh PBS or HBS for each experiment.
3. Experimental setup for electrochemical measurement (*see* **Fig. 1**). The electrode is connected to an electrometer (Model 6517; Keithley Instruments, Cleveland, OH), and the NO oxidation current is recorded by a digital chart recorder (PowerLab/8S, ADInstruments, Castle Hill, Australia) with the application program, Chart (4.1).

2.2. NO Measurement From NO Donor

S-nitroso-*N*-acetyl-DL-penicillamine (SNAP) solution: 100 μ*M* SNAP (Dojindo, Kumamoto, Japan) is dissolved in PBS (*see* **Note 3**). For examination of the selectivity of the electrode for NO, 10 μ*M* hemoglobin is used. Before each experiment, a 1 m*M* hemoglobin solution in PBS is prepared and diluted.

2.3. Measurement of NO in Endothelial Cells

1. Incubation buffer: Dulbecco's modified Eagle's medium (DMEM; Gibco, Grand Island, NE) supplemented with 10% heat-inactivated fetal bovine serum (JRH Biosciences, Lenexa, KS), 100 U/mL penicillin (Gibco), and 100 μg/mL streptomycin (Gibco).
2. External bathing medium used in experiments: HBS.
3. Acetylcholine (ACh) solution for stimulating cells: 1 μ*M* ACh (Sigma, St. Louis, MO) is dissolved in HBS. ACh solution (10 μ*M*) in HBS should be prepared and diluted before each experiment.
4. NO synthase (NOS) inhibitor solution: 1 m*M* N^G-nitro-L-arginine methyl ester (L-NAME; Dojindo) is dissolved in HBS.

3. Methods

3.1. Calibration

Calibration of the microcoaxial electrode is performed using submicromolar NO solutions. In our experiments, each solution was prepared by bubbling NO gas (Takachiho Chemical Industry, Tokyo, Japan) into deoxygenated PBS or HBS. Each NO gas was prepared using a gas mixer (GB-2C; KOFLOC, Tokyo, Japan) that combined 738 ppm NO gas and 100% N_2 gas in appropriate ratios. A fume hood should be used in the procedure to calibrate the electrode using NO gas.

1. Immerse the electrode tip in 200 mL of calibration buffer (e.g., PBS or HBS) in a calibration chamber maintained at 37°C (*see* **Fig. 1**).
2. Connect the electrode to the electrometer and apply voltage for NO oxidation between the working and reference electrodes (+0.6 V) (*see* **Notes 4** and **5**).
3. To deoxygenate the buffer, bubble it with N_2 for at least 30 min (*see* **Note 6**). Then, bubble with each concentration of NO and, finally, bubble with N_2 again (*see* **Fig. 2A**).

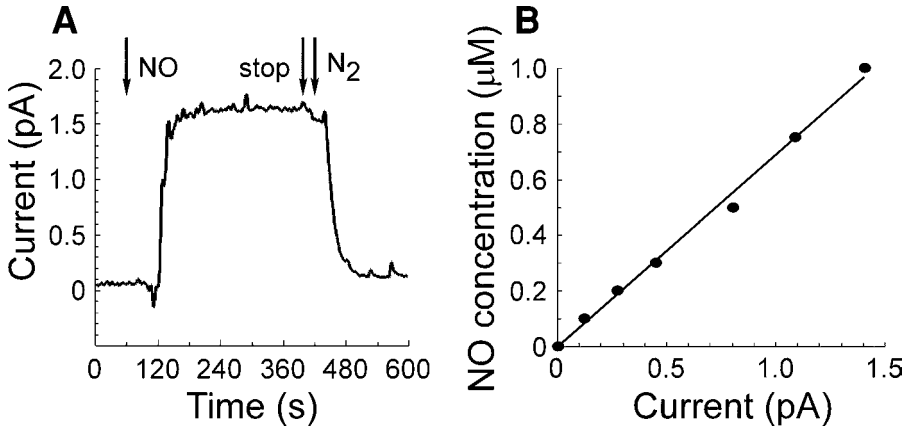

Fig. 2. Response of the electrode to NO. **(A)** N_2 was bubbled into the PBS while a stable current was being established. When this was followed by NO bubbling into the PBS (indicated by NO), the oxidation current started to increase and then stabilized. Even after the cessation of NO bubbling (labeled stop), the current stabilized at a slightly lower (approx 10%) level. When N_2 was rebubbled (labeled N_2) into the solution, the current returned to the baseline level seen before NO bubbling. **(B)** Calibration curve for submicromolar NO solutions (0, 0.1, 0.2, 0.3, 0.5, 0.75, and 1.0 μ*M*, $r = 0.99$). The response to 1 μ*M* NO solution is usually 1–5 pA. (Reprinted with permission from **ref. *25***.)

4. Molarity of NO (C_{NO} [*M*]) in PBS is given by the partial pressure of a gas (*p*NO [mm Hg]) and the solubility of NO (α [cm^3]) according to equation

$$C_{NO} = (pNO)\ (\alpha) \quad (1)$$

   (*see* **Note 7**). The concentration of NO is approx 1 μ*M* at 37°C when 738 ppm NO gas is bubbled ***(25)***.
5. Record oxidation current at a sampling rate of 10 Hz.
6. The current for each concentration of NO is calculated from an averaged NO oxidation current at the time at which the bubbling of NO gas was stopped. This value is then used for constructing a calibration curve (*see* **Fig. 2B**).
7. Keep the electrode tip in distilled water when it is not in use and avoid allowing the double membrane to dry out.

3.2. Measurement of NO Generated by SNAP

1. Immerse the electrode tip in PBS stirred with a magnetic bat (*see* **Fig. 1**).
2. Add appropriate amount of SNAP powder (final concentration: 100 μ*M*) into PBS (100 mL).
3. To examine the selectivity of the electrode for NO, add 1 m*M* hemoglobin (Hb) (1 mL; final concentration: 10 μ*M*) to PBS (99 mL) after the electrode response reaches a peak (*see* **Notes 8** and **9**).

3.3. Real-Time Measurement of Acetylcholine-Induced NO Production From Endothelial Cells

1. Incubate endothelial cells to confluence on glass cover slips in plastic culture dishes filled with DMEM (3 mL) at 37°C.
2. Replace DMEM with HBS (2.7 mL). The temperature of the HBS is maintained at 37°C using a warming plate (DC-MP 100 DM; Kitazato Supply, Shizuoka, Japan).
3. Place the electrode tip near the cell layer (less than 10 μm away) using a hydraulic micromanipulator (Model MO-103; Narishige Scientific Instrument Lab., Tokyo, Japan) under microscopic observation.
4. Stimulate the cells with ACh (1 μ*M* final concentration). For this, the ACh (10 μ*M*; 0.3 mL) solution in a glass capillary tube connected to a plastic syringe (1 mL) is injected into the bathing medium.
5. For inhibition of NO synthesis, incubate cells in HBS containing the NOS inhibitor. L-NAME (1 m*M*), for 10 min before ACh addition. Cells are then stimulated with ACh in the presence of L-NAME.
6. For examination of reproducibility of NO synthesis, remove L-NAME and stimulate cells again with ACh (*see* **Note 10**).

4. Notes

1. The microcoaxial electrode was originally developed as an amperometric oxygen (O_2) electrode ***(26)***. The design is basically the same for the NO electrode, with the exception of the thickness of the double membrane of collodion and polystyrene at the electrode tip (O_2: 5% w/v each; NO: 3% w/v each) because of the short lifetime of NO in vivo.
2. In brief, an electrically etched platinum wire (Tanaka Kikinzoku, Tokyo, Japan) serving as the working electrode is inserted into a lead-free glass capillary tube (Schott Glaswerke, Mainz, Germany). A layer of silver is then sputtered onto the glass capillary surface. This acts as the reference electrode. The Ag layer is easily chlorinated by constant electrolysis at –0.7 V. The electrode should not respond to 10 μ*M* NO_2^- after placement of the double membrane on the tip.
3. *S*-Nitroso-*N*-acetyl-DL-penicillamine is usually dissolved in dimethyl sulfoxide (DMSO) or ethanol in a relatively high concentration as stock solution, and this stock solution is added to the PBS. However, the microcoaxial electrode is slightly responsive to DMSO as well as to ethanol even after placing the double membrane on the tip of the electrode. Therefore, the SNAP solution should be prepared by adding SNAP powder directly to the PBS, which is stirred constantly with a magnetic bat.
4. From the relationship between the voltage of the working electrode and the oxidation current in 100 μ*M* NO solution prepared from 73,800 ppm NO gas, the voltage for NO oxidation is around +0.6 V ***(25)***.
5. Because the AgCl layer of the reference electrode is ideally decreased during NO oxidation as described by Eqs. (2) and (3), it is better to chlorinate the reference electrode at –0.7 V in the calibration buffer before calibration.

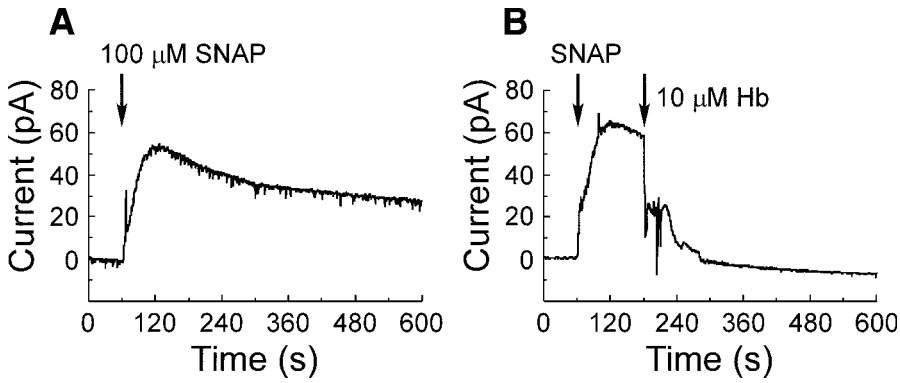

Fig. 3. Continuous NO measurement in the presence of an NO donor. **(A)** Addition of 100 μ*M* SNAP increased the current, and this increase continued for at least 30 min (data not shown). **(B)** After the current had reached a peak value, it rapidly decreased to the baseline level when a putative NO scavenger, hemoglobin (Hb, 10 μ*M*), was added to the SNAP-containing PBS. (Reprinted with permission from **ref. *25***.)

$$NO + 4OH^- \rightarrow NO_3^- + 3e^- \quad (2)$$

$$AgCl + e^- \rightarrow Ag^+ + Cl^- \quad (3)$$

6. Dark current gradually decreases after application of the NO oxidation voltage. If the dark current is relatively large, the electrode response to NO is difficult to detect. Therefore, an appropriate period for decreasing the dark current is required before calibration.
7. The molarity of NO is calculated using Eq. (1). Here, the α for NO solubility in water at 37°C was used for PBS and HBS.
8. It took about 60 s for the peak response to SNAP to be observed (*see* **Fig. 3A**,**B**). Because SNAP powder was added to the buffer in these experiments, time was taken for SNAP to gradually dissolve and release NO. Indeed, the electrode response decreased more rapidly after the addition of the NO scavenger Hb into the SNAP solution (*see* **Fig. 3B**). Therefore, the relatively slow response to SNAP did not always indicate that the response time of the electrode was slow.
9. When the electrode is immersed in a protein-rich solution or biological tissue, the tip must be washed carefully with distilled water. Also, buildup at the tip may be removed during the process of calibration after measurement. After each experiment, the tip should be kept in distilled water to prevent drying.
10. When real-time NO measurements in biological systems are performed, the reliability of the measurement must be examined directly by applying the NOS inhibitors and/or the NO scavengers to these systems. In our NO measurement on ACh-stimulated endothelial cells, the electrode response was significantly suppressed by treating the cells with the NOS inhibitor L-NAME (*see* **Fig. 4A**), following which, the response recovered after removal of the L-NAME (*see* **Fig. 4B**).

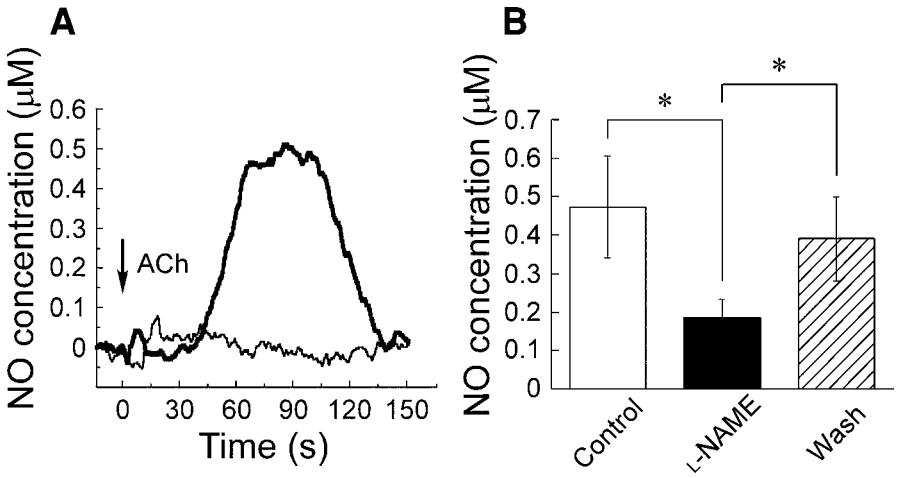

Fig. 4. Direct, continuous measurement of NO released from endothelial cells. **(A)** Transient NO release was detected (0.50 μ*M* peak) after acetylcholine (ACh, 1 μ*M*) administration (thick line). This release was suppressed (peak decreased to 0.13 μ*M*) in the presence of the putative NOS inhibitor L-NAME (1 m*M*, thin line). **(B)** Statistics of peak ACh-stimulated NO release in the presence and absence of L-NAME. Values are means ± SD (error bars). Compared to control (white bar, 0.47 ± 0.13 μ*M*), NO release was significantly inhibited by L-NAME (black bar, 0.18 ± 0.04 μ*M*, $p < 0.01$). After removal of L-NAME (shaded bar), NO release (0.39 ± 0.10 μ*M*) partially recovered. (Reprinted with permission from **ref. *25***.)

From these experiments, we can confidently state that the electrode response reflects NO production.

Acknowledgments

We thank Dr. D. W. Lübbers and Dr. H. Baumgältl at the Max-Planck-Institute für Molekulare Physiologie for teaching us the technique of fabricating the microcoaxial electrode. We also thank Dr. H. Sano, Institute of Biomedical Engineering, Faculty of Science and Technology, Keio University, and Dr. T. Aomatsu, Department of Aerospace Engineering, Graduate School of Engineering, Nagoya University, Chikusa, for advice on proper use of the electrode.

References

1 Collier, J. and Vallance, P. (1989) Second messenger role for NO widens to nervous and immune systems. *Trends Pharmacol. Sci.* **10,** 427–431.

2 Moncada, S., Palmer, R. M., and Higgs, E. A. (1991) Nitric oxide: physiology, pathophysiology, and pharmacology. *Pharmacol. Rev.* **43,** 109–142.

3 Bredt, D. S. and Snyder, S. H. (1992) Nitric oxide, a novel neuronal messenger. *Neuron* **8,** 3–11.

4 Garthwaite, J. and Boulton, C. L. (1995) Nitric oxide signaling in the central nervous system. *Annu. Rev. Physiol.* **57,** 683–706.
5 MacMicking, J., Xie, Q. W., and Nathan, C. (1997) Nitric oxide and macrophage function. *Annu. Rev. Immunol.* **15,** 323–350.
6 Palmer, R. M., Ferrige, A. G., and Moncada, S. (1987) Nitric oxide release accounts for the biological activity of endothelium-derived relaxing factor. *Nature* **327,** 524–526.
7 Braman, R. S. and Hendrix, S. A. (1989) Nanogram nitrite and nitrate determination in environmental and biological materials by vanadium (III) reduction with chemiluminescence detection. *Anal. Chem.* **61,** 2715–2718.
8 Beckman, J. S. and Conger, K. A. (1995) Direct measurement of dilute nitric oxide in solution with an ozone chemiluminescent detector. *Methods* **7,** 35–39.
9 Wennmalm, A., Lanne, B., and Petersson, A. S. (1990) Detection of endothelial-derived relaxing factor in human plasma in the basal state and following ischemia using electron paramagnetic resonance spectrometry. *Anal. Biochem.* **187,** 359–363.
10 Green, L. C., Wagner, D. A., Glogowski, J., et al. (1982) Analysis of nitrate, nitrite, and [^{15}N]nitrate in biological fluids. *Anal. Biochem.* **126,** 131–138.
11 Shibuki, K. (1990) An electrochemical microprobe for detecting nitric oxide release in brain tissue. *Neurosci. Res.* **9,** 69–76.
12 Malinski, T. and Taha, Z. (1992) Nitric oxide release from a single cell measured *in situ* by a porphyrinic-based microsensor. *Nature* **358,** 676–678.
13 Ichimori, K., Ishida, H., Fukahori, M., et al. (1994) Practical nitric oxide measurement employing a nitric oxide-selective electrode. *Rev. Sci. Instrum.* **65,** 2714–2718.
14. Broderick, M. P. and Taha, Z. (1995) Nitric oxide detection using a popular electro-chemical sensor—recent applications and the development of a new generation of highly sensitive and selective NO-microsensors, 4th IBRO World Congress of Neuroscience, Kyoto, Japan.
15 Xu, W., Yao, S. J., and Wolfson, S. K., Jr. (1995) A nitric oxide sensor using reduction current. *ASAIO J.* **41,** M413–M418.
16 Friedemann, M. N., Robinson, S. W., and Gerhardt, G. A. (1996) *o*-Phenylenediamine-modified carbon fiber electrodes for the detection of nitric oxide. *Anal. Chem.* **68,** 2621–2628.
17 Maskus, M., Pariente, F., Wu, Q., et al. (1996) Electrocatalytic reduction of nitric oxide at electrodes modified with electropolymerized films of $[Cr(v\text{-}tpy)_2]^{3+}$ and their application to cellular NO determinations. *Anal. Chem.* **68,** 3128–3134.
18 Bedioui, F., Trevin, S., Devynck, J., et al. (1997) Elaboration and use of nickel planar macrocyclic complex-based sensors for the direct electrochemical measurement of nitric oxide in biological media. *Biosens. Bioelectr.* **12,** 205–212.
19 Park, J. K., Tran, P. H., Chao, J. K., et al. (1998) *In vivo* nitric oxide sensor using nonconducting polymer-modified carbon fiber. *Biosens. Bioelectron.* **13,** 1187–1195.
20 Barker, S. L. and Kopelman, R. (1998) Development and cellular applications of fiber optic nitric oxide sensors based on a gold-adsorbed fluorophore. *Anal. Chem.* **70,** 4902–4906.

21 Barker, S. L., Kopelman, R., Meyer, T. E., et al. (1998) Fiber-optic nitric oxide-selective biosensors and nanosensors. *Anal. Chem.* **70,** 971–976.
22 Barker, S. L., Clark, H. A., Swallen, S. F., et al. (1999) Ratiometric and fluorescence-lifetime-based biosensors incorporating cytochrome c' and the detection of extra- and intracellular macrophage nitric oxide. *Anal. Chem.* **71,** 1767–1772.
23 Barker, S. L., Zhao, Y., Marletta, M. A., et al. (1999) Cellular applications of a sensitive and selective fiber-optic nitric oxide biosensor based on a dye-labeled heme domain of soluble guanylate cyclase. *Anal. Chem.* **71,** 2071–2075.
24 Mochizuki, S., Himi, N., Miyasaka, T., et al. (2002) Evaluation of basic performance and applicability of a newly developed in vivo nitric oxide sensor. *Physiol. Meas.* **23,** 261–268.
25 Kitamura, Y., Uzawa, T., Oka, K., et al. (2000) Microcoaxial electrode for *in vivo* nitric oxide measurement. *Anal. Chem.* **72,** 2957–2962.
26. Baumgältl, H. and Lübbers, D. W. (1983) Microcoaxial needle sensor for polarographic measurement of local O_2 pressure in the cellular range of living tissue. Its construction and properties, in *Polarographic Oxygen Sensors* (Gnaiger, E. and Forstner, H., eds.), Springer-Verlag, Berlin, pp. 37–65.

5

Measurement of Exhaled Nitric Oxide

Peter A. Steerenberg and Jan G. C. van Amsterdam

Summary

Assessment of the value of exhaled NO (eNO) is an attractive tool for studying pulmonary disease, considering its wide advantages (i.e., fast analysis, noninvasive sampling, ability to measure large numbers of subjects [including children], and inexpensive in use). Increased concentrations of eNO have been observed in asthmatic patients' airway infections, allergic rhinitis, and bronchiectasis. During inflammation, specific and nonspecific stimuli elicit expression and *de novo* synthesis of inducible nitric oxide (iNOS). Once generated in the bronchiolar cells, NO is released from the tissue and diffuses to the lumen of the bronchiolis. Of the two sampling ways (on-line and off-line), the off-line method is suitable for monitoring environmental health effects of air pollution and for obtaining an impression of the prevalence of atopy in epidemiological surveys. For this off-line measurement, a balloon method is developed (sampling exhaled air at location) that includes a sample device assuring inflation of balloons at a controlled flow rate and back-pressure. Cigaret smoking and alcohol consumption significantly reduces NO levels in exhaled air because of downregulation of iNOS. Although eNO can be reliably measured and analyzed, the prospective value to detect asthma or allergy is rather low (low sensitivity and low specificity), which makes the diagnostic value of eNO for predicting either allergy or asthma doubtful. Promising results have, however, been observed in corticoid-sparing therapies under guidance of eNO. In addition, measurement of eNO helps to understand the mechanisms of pulmonary disease and may be useful in detecting adverse effects of air pollution.

Key Words: Exhaled nitric oxide (eNO); off-line; asthma; atopy; nitric oxide synthase (NOS); inducible NOS (iNOS).

1. Introduction

Sampling of exhaled air is a noninvasive procedure that can be easily performed in adults, children, and patients with respiratory disease. Several studies have demonstrated increased levels of nitric oxide (NO) in exhaled air of patients with pulmonary disease, including asthma. In addition, exhaled NO (eNO) may be an elegant tool for monitoring environmental health effects of

From: *Methods in Molecular Biology, vol. 279: Nitric Oxide Protocols: Second Edition*
Edited by: A. Hassid © Humana Press Inc., Totowa, NJ

air pollution and for obtaining an impression of the prevalence of atopy in epidemiological surveys. However, considering its low sensitivity, the level of eNO is no reliable diagnostic measure of an atopic status. eNO can be measured in exhaled air sampled either on-line (direct exhalation into the NO analyzer) or off-line after remote collection of exhaled air into balloons. In this chapter, attention will be mainly focused on the balloon procedure to measure eNO.

2. Basic Aspects of eNO

2.1. Generation and Functions of Nitric Oxide

The enzyme nitric oxide synthase (NOS) catalyzes the conversion of L-arginine to L-citrulline + NO. Although citrulline exerts no biological activity, NO serves many functions throughout the body, including the pulmonary compartment. Constitutive NOS (cNOS) generates relatively low amounts of NO in a large variety of cells, like platelets, renal mesangial cells, osteoblasts, osteoclasts, epithelium, and endothelium. NO is also involved in neurotransmission and the regulation of vascular and bronchiolar tone. Neuronal NOS (nNOS) is predominantly located in discrete sites of the brain and modulates neuronal development, synaptic plasticity, memory, and vision ***(1)***.

The third type of NOS, inducible NOS (iNOS), is the cytokine-inducible form of NOS and is implicated in a variety of diseases, including allergic asthma. Following its induction, iNOS produces relatively high amounts of NO (i.e., 100- to 1000-fold more NO than cNOS does). The presence of iNOS has been established in epithelial cells, macrophages, endothelial cells, Kupffer cells, neutrophils, fibroblasts, astrocytes, and vascular smooth-muscle cells ***(1–3)***. iNOS is induced by interferon-γ, tumor necrosis factor-α (TNF-α) ***(4)***, and interleukin-1β (IL-1β) ***(5)***. Other cytokines, like transforming growth factor-β (TGF-β) ***(6)***, IL-4 ***(7)***, and IL-10 inhibit iNOS induction and certain L-arginine analogs may be used to inhibit NO production ***(8)***. Of special interest is the inhibition of iNOS by corticosteroids that are commonly used in the treatment of asthma.

During inflammation specific and nonspecific stimuli elicit expression and *de novo* synthesis of iNOS ***(9)***. Being a cytotoxic compound, NO is directly involved in the nonspecific host defense against pathogens and may react with proteins causing tissue injury. NO may also serve an immunomodulatory role, as it may shift the Th_1/Th_2 balance in favor of Th_2, thus promoting IgE-mediated allergy. IL-10 produced by Th_2 cells further downregulates Th_1 cells and may also directly inhibit the induction of iNOS ***(2,10,11)*** (*see* **Fig. 1**).

2.2. Sources of eNO

Nitric oxide may be derived from cNOS expressed in healthy lung epithelium, whereas under inflammatory conditions, induction of iNOS will lead to

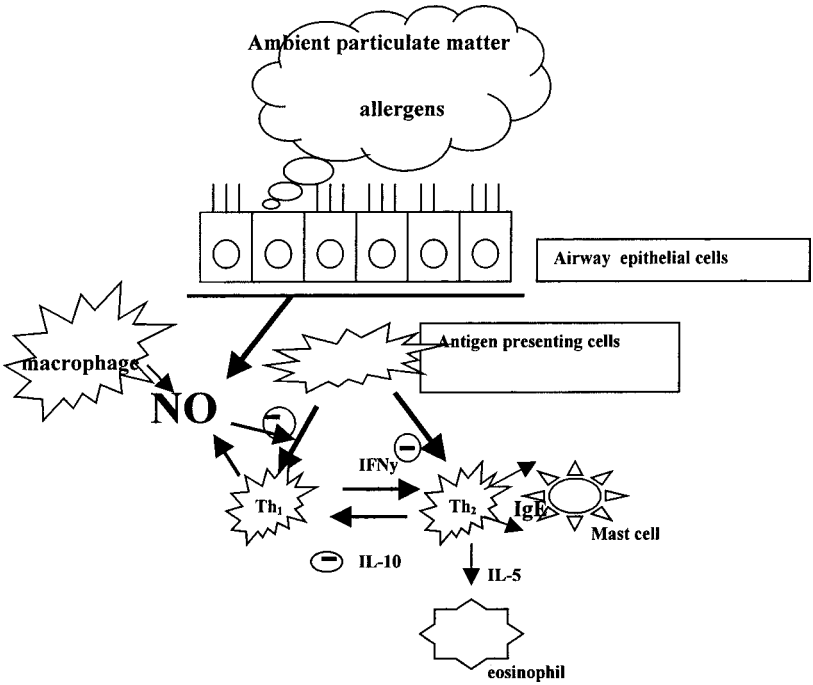

Fig. 1. The functions of nitric oxide in the lung. (Modified from **ref. *2***.)

increased levels of eNO ***(12)***. Alveolar air contains very low amounts of NO because it diffuses through the alveolar membrane, where it is rapidly bound by hemoglobin. To demonstrate the strong diffusion of NO, eNO was measured in four regular smokers after inhaling cigaret smoke containing 6000–25,000 μg/m^3 NO (*see* **Fig. 2**). Only 2% of inhaled NO was recovered in the exhaled air following inhalation ***(13)***.

Once generated in the bronchiolar cells, NO is released from the tissue and diffuses to the lumen of the bronchiolis. The concentration of eNO in exhaled air decreases when sampling progressively down the respiratory tract at the nose, mouth, and below the focal chords ***(14)***. From a comparative study between CO_2 and NO, it was concluded that the bulk of NO is produced proximal to the alveolar membrane ***(15)***.

High levels of NO are detected in the nose of healthy subjects, constitutively produced by steroid-resistant NOS ***(16,17)***. Gerlach and colleagues ***(18)*** suggested that eNO represents autoinhalation of NO produced in the nose. Exhaled air should therefore be sampled either by using a nose clip or via exhalation against a low resistance to ensure closure of the nasopharynx with the soft palate ***(19)***.

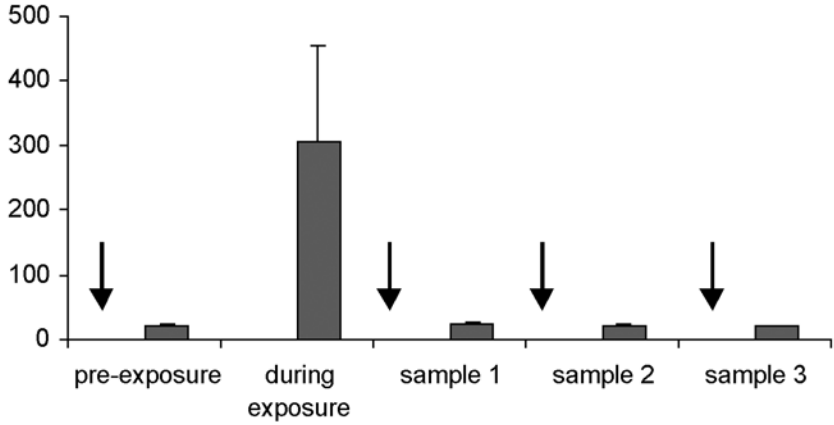

Fig. 2. Levels of eNO (expressed as means ± SEM) have been measured before, during, and after cigaret smoking in four regular smokers. Cigaret smoke contained 6000–25,000 μg/m^3 NO. Arrows indicate 1-min breathing and final inhalation of clean air prior to sampling exhaled air. The two final samples were obtained following 2-min breathing and final inhalation of clean air. The entire postexposure sampling procedure took 6.5 min.

2.3. NO in Respiratory Disease

Nitric oxide produced in the (upper) airways is partly exhaled and the presence of nitric oxide in exhaled air of animals and healthy human subjects was first reported by Gustafsson and colleagues in 1991 ***(20)*** and later confirmed by many others. In clinical pulmonology, the observed increase in eNO in patients with respiratory diseases like allergic asthma (*see* **Table 1**) led to its application as biomarker for therapeutic interventions in pulmonary disease. Increased concentrations of eNO are observed in asthmatic patients ***(21–27)***, airway infections ***(28,29)***, allergic rhinitis ***(30,31)***, and bronchiectasis ***(32)***.

Treatment with anti-inflammatory corticosteroids that inhibit iNOS ***(33,34)*** reduces eNO in subjects with allergic asthma but not in normal subjects ***(35–37)***. This suggests that eNO in healthy subjects is derived from cNOS, whereas in asthmatics, the additional amounts of eNO are generated by iNOS ***(12)***. Indeed, biopsies from asthmatic patients but not healthy subjects express iNOS in airway epithelial cells. Pro-inflammatory cytokines, known to be increased in the airways of asthmatics, have been shown to induce iNOS expression in human epithelial cells in vitro ***(38)***. However, in one study, no significant difference in nasal NO level was observed between asthmatics and nonasthmatics ***(39)***, but this may be the result of the presence of chronic obstructive pulmonary disease (COPD) in the subjects. In contrast to patients with asthma, eNO is decreased in patients with chronic obstructive pulmonary disease

Table 1
eNO in Pulmonary Disease

	eNO	Ref.
Allergic asthma	Increased	***22,24–26,29,47–49***
Steroid treatment of asthma	Decrease	***35–37,50,51***
COPD	Decreased	***40,41***
	Increase	***44,45***
Bronchiectasis	Increased	***32***
Airway infection	Increased	***28,29***
Cystic fibrosis	No change	***24,42***
Allergic rhinitis	Increased	***30,31,52***
	No change	***53***
Atopy	Increased	***54–56***
	No change	***57***

(40,41), whereas the level of NO is unchanged in cystic fibrosis patients ***(24,42)***. The variable results observed in COPD patients ***(43–45)*** may be the result of the high number of smokers included in the COPD studies, as cigaret smoking is known to profoundly decrease exhaled ***(46)*** but not nasal NO ***(39)***.

Of particular interest for epidemiological studies is the observation that atopy is positively associated with an increased level of eNO. Following inhaled allergen challenge, asthmatics show a progressive elevation of eNO during the late response but not during the early bronchoconstrictive response ***(33,58)***. Interestingly, at 4 h following allergen challenge, a sixfold increase in the expression of iNOS mRNA was observed in rodents ***(59)***.

Atopic probable asthmatic children had significantly higher geometric mean eNO (13 ppb) than did nonatopic probable asthmatic children (3 ppb). A similar difference was observed between atopic (8 ppb) and nonatopic children (3 ppb) ***(55)***. Studying a rather small group of 13 children, Lanz et al. ***(57)*** observed no difference in eNO between atopic and nonatopic children. A study on subjects allergic to laboratory animals showed that eNO was three times higher in symptomatic atopic persons than in asymptomatic atopic persons (18 vs 6 ppb) ***(54)***. Recently, Franklin et al. ***(56)*** showed increased eNO in children with a positive skin-prick test relative to nonatopic children. This is in line with our observation that nonsymptomatic atopic subjects exhale higher levels of NO relative to nonatopic subjects (*see* **Fig. 3**) ***(56,60)***.

Subjects with allergic rhinitis show compared with controls increased exhaled ***(61)*** and nasal NO ***(61–63)***. This was recently confirmed by Henriksen et al. ***(30)***, who showed elevated eNO in allergic rhinitis patients in the nonpollen season, as compared with controls, which was further increased in the pol-

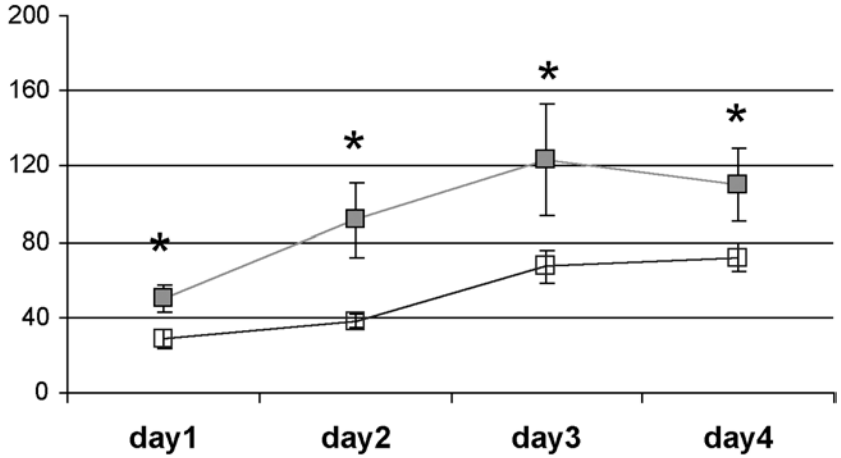

Fig. 3. Levels of eNO in atopics and nonatopics on 4 d with a different level of air pollution. Open bars: nonatopic subjects; hatched bars: atopic subjects. *$p < 0.05$, compared to nonatopics.

len season. Kharitonov et al. reported that during the pollen season, nasal NO, but not eNO, was significantly increased in subjects with seasonal allergic rhinitis compared with control subjects ***(53)***. The latter study further showed the remarkable observation that 1 h after nasal challenge with allergens, nasal NO had decreased again, which significantly correlated with increased rhinitis symptoms ***(53)***.

Application of eNO as a biomarker of effect of air pollution is presently under investigation. In healthy subjects, it was demonstrated ***(13,64,65)*** that the level of endogenous NO in exhaled air is increased on days with high levels of outdoor air pollution (up to 20% increase), indicating that eNO may serve as a biomarker of exposure to air pollution. Piacentini et al. ***(66)*** observed no effect of ambient NO on eNO. Which specific air pollutant is responsible for this increase in eNO remains to be determined.

3. Factors Affecting eNO Value

3.1. Lifestyle Factors

Cigaret smoking significantly reduces NO levels in exhaled air but not nasal NO ***(39)*** and the reduction in eNO appears to be related to the number of cigarets smoked ***(46)***. Cigarets generate very high levels of NO that induce a fall in eNO because of downregulation of iNOS ***(33)***. Alcohol consumption also inhibits iNOS and reduces eNO ***(67)***. Administration of L-arginine dose-dependently increases both exhaled and nasal NO, but it is unlikely that consumption of daily food, which does not contain substantial amounts of

L-arginine, affects the level of eNO. Attention should, however, be paid to belching. Eating lettuce known to contain large amounts of nitrate after a period of fasting causes a fourfold increase in belching air ***(68)***. No consistent evidence for differences in exhaled air levels based on gender, age and body size has been established. In women, low NO concentrations were observed just before and during the menses and a midcycle increase in eNO has been reported ***(69)***.

3.2. Breathholding and Exercise

Breathholding increases NO levels because of an accumulation of NO in the upper or lower respiratory tracts ***(21,70)***. The effect of exercise is complex, with a progressive fall in eNO with increasing exercise, but correction for increased ventilation shows an increased production of NO ***(71,72)***. Hyperventilation at rest shows also an increment in NO production, albeit to a lesser extent than exercise ***(72)***. To eliminate the effect of recent exercise on measured levels of NO, it is recommended ***(71)*** that the subject should be seated at least 5 min before actual sampling and remain seated throughout the procedure.

3.3. Contamination of Air Sample by Nasal NO

High concentrations of NO have been detected in nasal air of normal subjects ***(14,21,47,73,74)***. The nasal cavity and the paranasal sinuses, in particular, excrete high concentrations relative to the lower respiratory tract. Normal oral exhalations, when the vellum is open, allow contamination of the eNO level by nasal NO ***(19,73)***. Wearing a nose clip partly prevents such contamination.

Contamination by nasal NO can also be opposed by breathing against low resistance that causes vellum closure ***(19)***. Using this approach, the same values were found as those measured directly from the lower airways via a bronchoscope ***(73)***. The low resistance pressure should not be higher than 20 cm water, because eNO increases at higher end-respiratory pressure ***(75)***. Measurement of a single breath in subjects wearing a nose clip shows an initial NO peak followed by a NO plateau. The peak indicates that even in subjects wearing a nose clip, a substantial part of eNO is derived from upper airways, including the nasal cavity ***(27)***. The plateau is independent of the inhalation route, via the nose or mouth ***(76)***. Slow exhalation from vital capacity to residual volume through a mouthpiece, which creates resistance, appears to be the best manoeuvre to obtain the most reproducible NO samples, free of nasal contamination ***(53)***.

3.4. Contamination of Air Sample by Ambient NO

Despite the rapid absorption of inhaled ambient NO by the alveoli, residual NO and environmental NO in the dead volume may contaminate the sample of exhaled air ***(42,63,64,77–79)***.

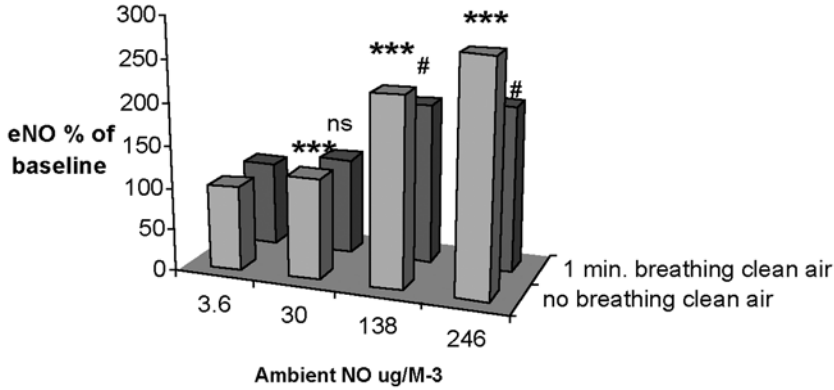

Fig. 4. Levels of eNO (means ± SEM) on 4 d with different levels of outdoor air 1-min breathing and final inhalation of clean air (solid bars). Outdoor air pollution was read as ambient NO level, which amounted 4, 30, 138, and 246 μg/m^3. Individual eNO values were expressed as percentage of their baseline value and the averaged value of the group on separate days was calculated (*see* **ref. *13***). ***$p < 0.001$, compared to respective eNO level on the day with negligible outdoor air pollution (3.6 μg/m^3 ambient NO); $^{\#}p < 0.001$, compared to first sample; ns: no significant difference compared to the first sample.

To exclude contamination of exhaled air by ambient NO, breathing clean air for 1 min and subsequent inhalation of clean air appears to be sufficient to completely remove residual exogenous NO from the respiratory tract ***(13)***. Alternatively, one may discard the dead volume (containing ambient NO) in a preballoon ***(80)*** or via an outlet connected to a three-way valve ***(81)***.

Figure 4 shows not only the contamination of the sample by ambient NO but also the increase of endogenous NO resulting from activation of lung by ambient pollution.

4. Measurement of eNO and Sampling Procedures

4.1. Equipment to Sample and Measure eNO

Levels of NO in exhaled air can be determined by direct exhalation into a NO analyzer detecting NO via chemiluminescence (*see* **Fig. 5**). In nonambulant patients or in epidemiological field studies dealing with large numbers of subjects at different locations, this technique is not practicable. Collection of exhaled air in NO-impermeable Mylar sampling balloons offers an elegant alternative (*see* **Fig. 6**). To circumvent the effect of water vapor ***(82)***, the analyzer is equipped with a Naflon drier and a particle filter. Materials used in NO measurement should be inert. Sulfhydryl groups in rubber may react with NO and should not be used.

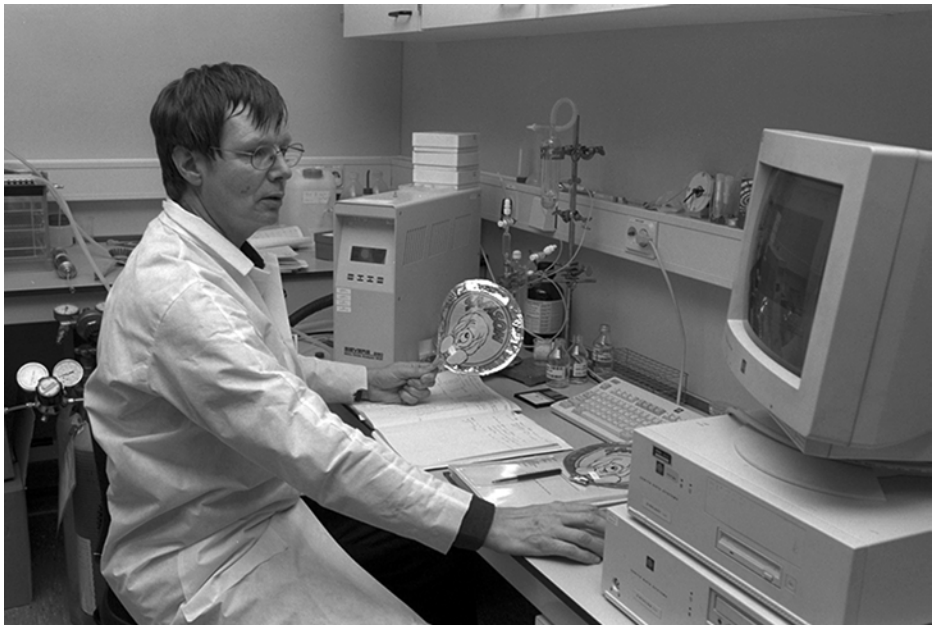

Fig. 5. The concentration of eNO in a Mylar foil balloon measured by a rapid-response chemiluminescence analyzer. (Courtesy of Sievers, Boulder, CO, USA.)

Levels of eNO are routinely analyzed by chemiluminescence (Sievers 280B; Sievers, Boulder, CO) using a response time < 200 ms. The analyzer sample flow rate is kept constant at 200 mL/min. **Figure 5** reflects the measurement of NO in balloons using the chemiluminescence analyzer of a Sievers 280B, but other brands are available and may be purchased in combination with certain software to enable biofeedback (e.g., Eco Physics, Dürnten, Switzerland and Aerocrine, Danderyd, Sweden).

4.2. On-Line Sampling and Measurement

The European Respiratory Society (ERS) Task Force "Measuring of nitric oxide in exhaled air" ***(71)*** recommends on-line measurement of eNO. Using this procedure, subjects exhale directly into the tubing of the NO analyzer during their visit to the laboratory and the NO level is analyzed continuously during exhalation. This results in a NO profile versus time or exhaled volume, together with other exhalation variables (e.g., airway flow and/or pressure) and displayed in real time ***(83)***. In short, the patient should be seated comfortably, with a mouthpiece at a proper height and position. The patient inserts the mouthpiece and inhales NO-free air (containing < 5 ppb) through the mouth to total lung capacity (TLC) over 2–3 s and then exhales immediately. A flow rate

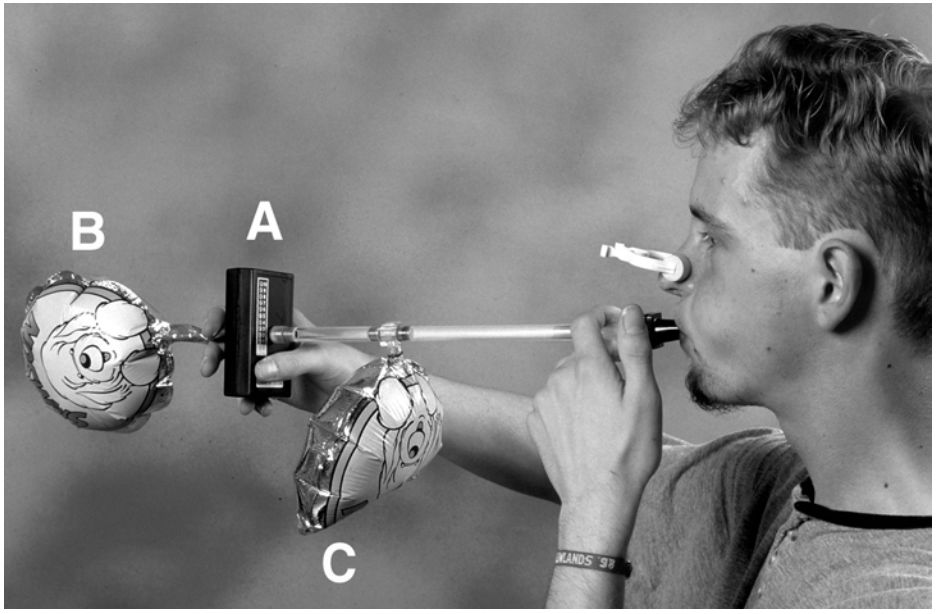

Fig. 6. Sampling of exhaled air was carried out with a sampling device equipped with a 18-G needle as flow restriction and a manometer. Ten indicator lamps on the metallic strip are connected to the manometer and each lamp reflects a certain pressure. Guided by the indicator lamps **(A)** subjects exhaled at the desired flow rate of 500 mL/min at 20 cm water pressure. A preballoon of 500 mL **(B)** without a restriction is attached to the blowpipe just before restriction and sampling balloon **(C)**.

of 0.05 L/s (limits: 0.045–0.055 L/s) is desired. However, eNO measurement can be performed at higher or lower flow rates if this is desirable in certain situations. A constant expiration flow is normally achieved by displaying the pressure or flow to the subject. In this way (visual biofeedback), a constant pressure or flow is attained by to the subject, who maintains these parameters within specified limits. In all cases, however, the expiration flow should be clearly recorded and reported in any publication.

4.3. Off-Line Sampling

For field studies in epidemiology (sampling exhaled air at location), we have developed a balloon technique that includes a sample device assuring inflation of balloons at controlled flow rate and back-pressure *(13)*. **Figure 6** depicts such a sampling device and **Fig. 7** gives further technical details. The balloon procedure offers a sound and convenient alternative for the on-line procedure to measure eNO in large populations as required in epidemiological studies

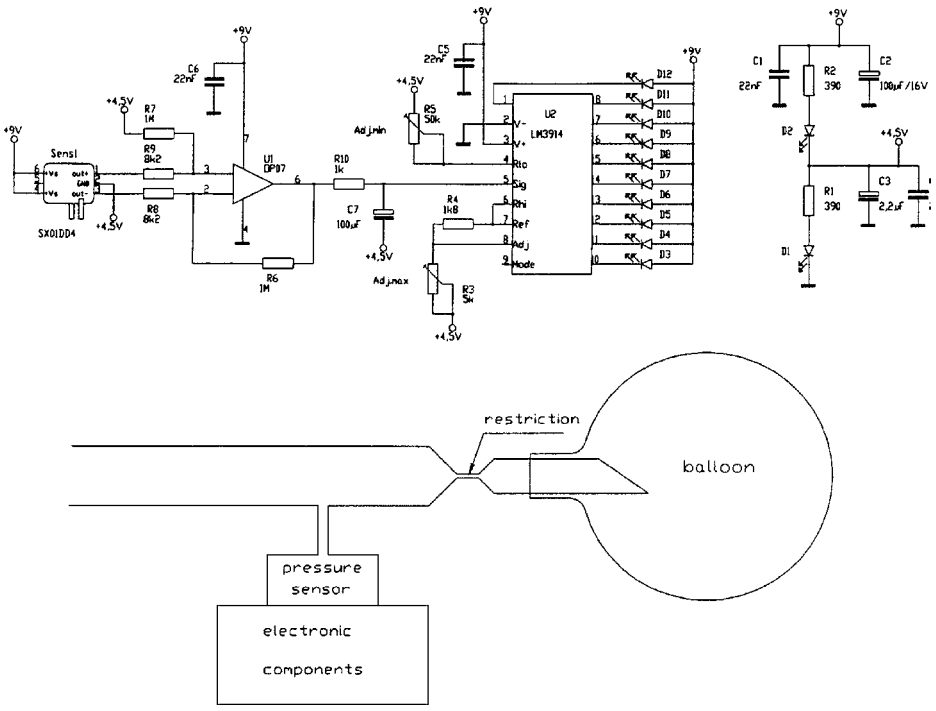

Fig. 7. Technical scheme of the sample device.

(84). Other groups have described similar off-line sampling equipments ***(77,80,81,83)***.

Routinely, exhaled air of the children is sampled in balloons (Mylar balloon, ABC ballonnen; Zeist, The Netherlands) using the sampling device, equipped with a preballoon of 750 mL to prevent contamination of the sample with ambient NO ***(80)***. The flow rate is 550 mL/min at 20 cm water backpressure (*see* **Figs. 6** and **8**).

The content of NO remains stable in the Mylar balloons for at least 48 h and is measured by chemiluminescence (*see* **Fig. 5**) after transportation of the balloons to the laboratory. Outdoor air, to monitor ambient NO as measure of outdoor air pollution, can be similarly sampled in foil air balloons by a permissible air sampling pump (Model P-200; Dupont de Nemours & Company Inc., Wilmington, DE, USA).

The balloon procedure offers a valid alternative for on-line measurements, as comparable levels were obtained by both techniques (balloon vs on-line) in a sample of healthy subjects ***(84–87)***. **Figure 9** show the results of this comparison.

Fig. 8. Sampling eNO of a young volunteer in an epidemiological study at an elementary school.

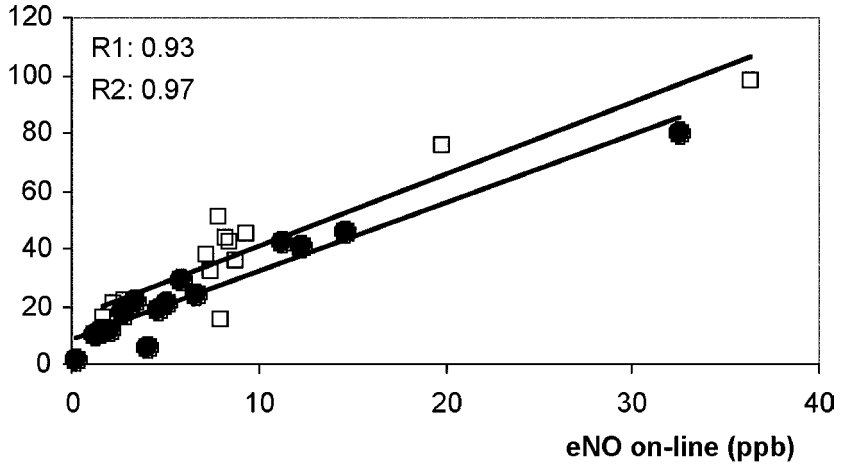

Fig. 9. Regression analysis of NO values measured on-line versus off-line (balloon method) on 2 d with a different level of air pollution. ●: d 1 with a low level of air pollution, $r = 0.97$, $p < 0.001$; □: d 2 with a high level of air pollution, $r = 0.93$, $p < 0.001$. Each point represents one subject.

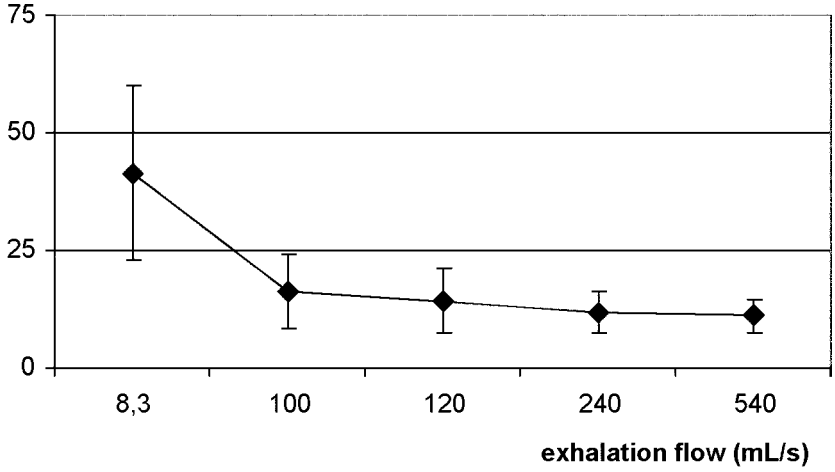

Fig. 10. Flow dependency of eNO in healthy subjects.

5. Flow Dependency of eNO

The level of eNO depends on the exhalation rate below 200–250 mL/s ***(19,76,77)***.

In the higher range of exhalation flow rates (i.e., above a cutoff value of 250 mL/s, eNO is virtually flow independent) (*see* **Fig. 10**). Therefore, exhaled air should be sampled at a given and constant exhalation flow to respectively allow comparison of the data and to obtain reproducible values.

Guidelines to measure eNO have been formulated by the ERS ***(88,89)*** and ATS ***(83)***. The ERS recommends using a flow rate of 150–250 mL/s, but gives no further specifications for off-line sampling. In contrast, the ATS ***(83)*** recommends an exhalation flow of 350 mL/s for off-line measurements in adults and children.

5.1. Selection of the Exhalation Rate in Air Sampling

Silkoff et al. ***(19,85)*** studied the flow dependency of eNO in detail and advocated measuring eNO at flow rates of 10–40 mL/s, which results in higher eNO values than would be obtained after sampling at high flow. In addition, asthma may be considered a disease of the conducting airways because in asthmatic patients, steroids decrease bronchiolar but not alveolar NO output ***(90)***. This pleads to sample exhaled air at a low flow rate, reflecting bronchial NO flux, rather than to sample air at a high flow rate (reflecting alveolar NO flux).

Using different approaches (i.e., the comparison of eNO and carbon dioxide ***[91]*** and intrabronchiolar air sampling with a catheter ***[92]***), it has been demonstrated that eNO originates primarily from the conducting and not the alveolar airways. In addition, in single-flow maneuvers, the NO level rapidly reaches

plateau values ***(19)***, whereas gases released in the alveolar space, such as carbon dioxide, typically show a sloping curve and never reach a constant level. At very high expiratory flows, the diffusion from the bronchiolar tissue to exhaled air is negligible ***(93)***, and eNO is virtually of alveolar origin only. In contrast, eNO obtained at 350 mL/s represents NO originating mainly from the alveolar space, which is of less interest because asthma is regarded as a disease of the conducting (broncheolar) airways. However, using high exhalation flows, several groups reported a significant difference between eNO of healthy and asthmatic subjects ***(24,94,95)***. This indicates that even at high flow rates, a minor amount of NO is still released from the conducting airways, which is large enough to differentiate between healthy and asthmatic subjects.

5.2. Discriminating Power of eNO at Different Flow Rates

It appears that the power of eNO to discriminate between atopic and nonatopic children does not depend on the exhalation flow. This was in a study with atopic ($N = 21$, mean age 9.9 yr) and nonatopic children ($N = 25$, mean age 9.9 yr) who were sampled at low (8.3 mL/s) and high (> 350 mL/s) exhalation flow rates. Both at low and high exhalation flow rates, children with skin-prick positivity to house dust mites have statistically significant ($p < 0.001$) twofold higher eNO values as compared to children lacking such a sensitivity (low flow: 50.0 ± 8.3 ppb vs 26.9 ± 1.3 ppb; high flow: 13.2 ± 1.7 vs 7.8 ± 0.2 ppb). The differences in eNO because of the difference in flow rate were highly significant ($p < 0.001$) and the same is the case for the allergy status ($p < 0.001$). The differences at low flow rate between allergic and nonallergic subjects did not differ from those at high flow rates (p-value of the "flow × allergy" interaction = 0.389). The receiver operating characteristics (ROC) area under the curve (AUC) for low and high flow rate were 0.766 and 0.754 ($p = 0.002$ and $p = 0.004$), respectively, but the difference in AUC did not differ from zero (95% confidence interval –0.11 to 0.12; $p = 0.892$). Therefore, atopic (i.e., skin-prick positive) subjects can be well distinguished from control subjects using eNO values measured in air samples obtained at either a low or high flow rate, and this implies that measurement of eNO is suitable to detect allergy at young age.

6. Diagnostic Value of eNO

Hypersensitivity for specific allergens is routinely diagnosed using clinical anamnesis in combination with skin-prick tests or the radioallergosorbent (RAST) assay. In addition to allergic asthma, the exposure to perennial and seasonal allergens may lead to increased eNO levels in sensitized subjects ***(53,60,96–102)***. Second, an increase in eNO has been shown to accompany eosinophilic inflammation (i.e., the eosinophilic count in sputum is significantly and positively associated with eNO) ***(103–105)***.

The diagnostic value of eNO to predict either allergy or asthma is still doubtful. The studies that evaluated the predictability of eNO have been mainly performed in asthmatic and allergic patients and showed a close association between eNO and the disease. Such studies, however, suffer from selection bias, as the subjects are recruited from populations who visit the clinic because they seem to have some pulmonary complaint. Obviously, nonsymptomatic asthmatics and allergic subjects without asthmatic symptoms do not visit the clinic and are not included in such studies. We therefore assessed the diagnostic value of eNO to predict allergy in a nonselected sample of 506 school children (6–12 yr of age) without applying specific inclusion or exclusion criteria. The atopic profile was assessed by skin-prick tests (to common aeroallergens).

The mean value ± SD of eNO in nonatopic (N = 371) and atopic children (N = 135) was 33.1 ± 15.3 and 57.2 ± 49.5 ppb, respectively (ranges: 4.0–100.3 ppb and 15.4–355 ppb, respectively). This difference in eNO indicates that an atopy-related inflammation in the lower airways elicits an increase in the release of eNO. Indeed, it has been suggested that mild airway inflammation is present in atopic, nonasthmatic subjects regarding signs of mild eosinophilia in biopsies ***(106)*** previously observed in subjects without bronchial hyperreactivity (BHR) that eNO was higher in atopic than in nonatopic subjects. Further, this is in agreement with the observation that eNO levels in allergic asthmatics were significantly higher than in nonatopic asthmatic subjects ***(99,107)***. Further research is required to understand why eight nonatopic subjects exhaled such high levels of NO. Does it have a genetic basis or does the high value represent an early risk factor for the subsequent development of allergy/asthma?

To assess the predictability of eNO with respect to the presence of an atopic constitution in the children, we defined "a high eNO value" as follows: A child has a high eNO if its eNO exceeds a cutoff value of 63.7 ppb (mean value of nonatopic subjects + 2 × standard deviation). Using this cutoff value and the skin-prick test results, the children were categorized in four groups (*see* **Table 2**).

Based on the number of subjects in each of the four groups (*see* **Table 2**), the diagnostic value of a high eNO to predict the presence of atopy was assessed. Diagnostic value can be well described by calculating the following predictive values: positive (PV+) and negative (PV–) predictive value, selectivity (Se), and specificity (Sp).

As depicted in **Table 3**, the positive predictive value of eNO for atopy (PV+; reflects how many of the subjects with a high eNO value are atopic) is considerable and shows that high levels of eNO are associated with the presence of atopy. The level of eNO, however, cannot serve as a reliable diagnostic measure of an atopic status. It is concluded that eNO is of inferior value to diagnose allergy as compared to the routinely used tests like skin-prick test and RAST, as it lacks sensitivity for allergy.

Table 2
Number of Subjects Categorized According to Level of eNO, and Atopic Constitution as Assessed by the Skin-Prick Test in 506 Children

	Atopy +	Atopy –	Total
High eNO	40	18	58
Low eNO	94	354	448
Total	134	372	506

Note: High eNO value is defined as an eNO value > 63.7 ppb (which is the mean value of nonatopic subjects + 2× standard deviation).

Table 3
Descriptive Parameters of Diagnostic Value of High eNO (> 63.7 ppb) With Respect to Atopic Constitution as Assessed by the Skin-Prick Test in 506 Children Based on the Data in Table 2

	Positive predictive value	Negative predictive value	Sensitivity	Specificity	False positive	False negative
eNO vs atopy	69%	79%	30%	95%	5%	70%

7. Conclusions

The measurement of eNO is an attractive tool for studying pulmonary disease considering its wide advantages (i.e., fast analysis, noninvasive sampling, ability to assess large numbers of subjects [including children], and inexpensive in use). The main disadvantage is, however, its low sensitivity as a biomarker to detect respiratory illness. It is now well recognized that inducible eNO is implicated in a variety of diseases, including asthma. In the lung, eNO is generated by epithelial cells and macrophages. NO is accounted for in many functions throughout the body. During respiratory problems, it regulates the vascular and bronchiolar tone, and during inflammation, it is directly involved in the nonspecific host defense against pathogens. NO may also serve an immunomodulatory role, as it shift the Th_1/Th_2 balance in favor of Th_2, thus promoting IgE-mediated responses. In most respiratory diseases, such as allergic asthma, allergic rhinitis, bronchiectasis, cystic fibrosis, airway infections, and irritation induced by air pollution, eNO is increased. In contrast, COPD, smoking cigarets, and steroid treatment of asthma decrease the level of eNO.

Although eNO is simple to sample and to analyze, confounding factors, like lifestyle (smoking), gender, and ambient NO, can easily diminish the reliabil-

ity of the test. Confounding by ambient NO can be avoided by discarding the first 750 mL of exhaled air from the dead space, although one should be aware that exposure to high levels of air pollution (ambient NO levels > 100 ppb) may increase endogenous eNO.

Reproducibility of the eNO sampling can be frustrated by technical inaccuracy. Contamination of eNO by nasal NO can be opposed by the use of a nose clip or breathing against low resistance that causes vellum closure. Most important is the flow dependency of eNO (*see* **Fig. 10**), which compels one to standardize flow at exhalation flows below 250 mL/s; this is not required for higher flows.

Many studies have shown that eNO values measured on-line correlate well with those measured off-line, so that both approaches give comparable results. Generally, eNO of ambulant patients is routinely measured in the clinic on-line, whereas in epidemiological studies with high numbers of children, the off-line approach is preferable.

Although eNO can be reliably measured and analyzed, the prospective value to detect asthma or allergy is rather low (low sensitivity and low specificity), which makes the diagnostic value of eNO to predict either allergy or asthma doubtful. Promising results have, however, been observed in corticoid-sparing therapies under guidance of eNO. In addition, measurement of eNO helps to understand the mechanisms of pulmonary disease and may be useful for detecting the adverse effects of air pollution.

References

1 Moncada, S., Palmer, R. M., and Higgs, E. A. (1991) Nitric oxide: physiology, pathophysiology, and pharmacology. *Pharmacol. Rev.* **43,** 109–142.

2 Barnes, P. J. and Liew, F. Y. (1995) Nitric oxide and asthmatic inflammation. *Immunol. Today* **16,** 128–130.

3 Barnes, P. J. (1996) NO or no NO in asthma? *Thorax* **51,** 218–220.

4 Ding, A. H., Nathan, C. F., and Stuehr, D. J. (1988) Release of reactive nitrogen intermediates and reactive oxygen intermediates from mouse peritoneal macrophages. Comparison of activating cytokines and evidence for independent production. *J. Immunol.* **141,** 2407–2412.

5 Suschek, C., Fehsel, K., Kroncke, K. D., et al. (1994) Primary cultures of rat islet capillary endothelial cells. Constitutive and cytokine-inducible macrophage like nitric oxide synthases are expressed and activities regulated by glucose concentration. *Am. J. Pathol.* **145,** 685–695.

6 Ding, A., Nathan, C. F., Graycar, J., et al. (1990) Macrophage deactivating factor and transforming growth factors-beta 1, -beta 2, and -beta 3 inhibit induction of macrophage nitrogen oxide synthesis by IFN-gamma. *J. Immunol.* **145,** 940–944.

7 Bogdan, C., Vodovotz, Y., Paik, J., et al. (1994) Mechanism of suppression of nitric oxide synthase expression by interleukin-4 in primary mouse macrophages. *J. Leukocyte Biol.* **55,** 227–233.

8 Yates, D. H., Kharitonov, S. A., Thomas, P. S., et al. (1996) Endogenous nitric oxide is decreased in asthmatic patients by an inhibitor of inducible nitric oxide synthase. *Am. J. Respir. Crit. Care Med.* **154,** 247–250.
9. Gustafsson, L. E. (1998) Exhaled nitric oxide as a marker in asthma. *Eur. Respir. J.* **26(Suppl.),** 49S–52S.
10 Curran, A. D. (1996) The role of nitric oxide in the development of asthma. *Int. Arch. Allergy Immunol.* **111,** 1–4.
11 Steerenberg, P. A., van Amsterdam, J. G., Vandebriel, R. J., et al. (1999) Environmental and lifestyle factors may act in concert to increase the prevalence of respiratory allergy including asthma. *Clin. Exp. Allergy* **29,** 1303–1308.
12. Kharitonov, S. A. and Barnes, P. J. (1996) Nitric oxide in exhaled air is a new marker of airway inflammation. *Monaldi Arch. Chest Dis* **51,** 533–537.
13 Steerenberg, P. A., Snelder, J. B., Fischer, P. H., et al. (1999) Increased exhaled nitric oxide on days with high outdoor air pollution is of endogenous origin. *Eur. Respir. J.* **13,** 334–337.
14 Lundberg, J. O., Weitzberg, E., Nordvall, S. L., et al. (1994) Primarily nasal origin of exhaled nitric oxide and absence in Kartagener's syndrome. *Eur. Respir. J.* **7,** 1501–1504.
15 Byrnes, C. A., Dinarevic, S., Shinebourne, E. A., et al. (1997) Exhaled nitric oxide measurements in normal and asthmatic children. *Pediatr. Pulmonol.* **24,** 312–318.
16 Lundberg, J. O., Lundberg, J. M., Alving, K., et al. (1997) Nitric oxide and inflammation: the answer is blowing in the wind. *Nature Med.* **3,** 30–31.
17 Tracey, W. R., Xue, C., Klinghofer, V., et al. (1994) Immunochemical detection of inducible NO synthase in human lung. *Am. J. Physiol.* **266,** L722–L727.
18 Gerlach, H., Rossaint, R., Pappert, D., et al. (1994) Autoinhalation of nitric oxide after endogenous synthesis in nasopharynx. *Lancet* **343,** 518–519.
19 Silkoff, P. E., McClean, P. A., Slutsky, A. S., et al. (1997) Marked flow-dependence of exhaled nitric oxide using a new technique to exclude nasal nitric oxide. *Am. J. Respir. Crit. Care Med.* **155,** 260–267.
20 Gustafsson, L. E., Leone, A. M., Persson, M. G., et al. (1991) Endogenous nitric oxide is present in the exhaled air of rabbits, guinea pigs and humans. *Biochem. Biophys. Res. Commun.* **181,** 852–857.
21 Dillon, W. C., Hampl, V., Shultz, P. J., et al. (1996) Origins of breath nitric oxide in humans. *Chest* **110,** 930–938.
22 Hamid, Q., Springall, D. R., Riveros-Moreno, V., et al. (1993) Induction of nitric oxide synthase in asthma. *Lancet* **342,** 1510–1513.
23 Kharitonov, S. A., Yates, D., Springall, D. R., et al. (1995) Exhaled nitric oxide is increased in asthma. *Chest* **107,** 156S–157S.
24 Lundberg, J. O., Nordvall, S. L., Weitzberg, E., et al. (1996) Exhaled nitric oxide in paediatric asthma and cystic fibrosis. *Arch. Dis. Child* **75,** 323–326.
25 Massaro, A. F., Gaston, B., Kita, D., et al. (1995) Expired nitric oxide levels during treatment of acute asthma. *Am. J. Respir. Crit. Care Med.* **152,** 800–803.

26 Persson, M. G., Zetterstrom, O., Agrenius, V., et al. (1994) Single-breath nitric oxide measurements in asthmatic patients and smokers. *Lancet* **343,** 146–147.
27 Tsujino, I., Miyamoto, K., Nishimura, M., et al. (1996) Production of nitric oxide (NO) in intrathoracic airways of normal humans. *Am. J. Respir. Crit. Care Med.* **154,** 1370–1374.
28 de Gouw, H. W., Grunberg, K., Schot, R., et al. (1998) Relationship between exhaled nitric oxide and airway hyperresponsiveness following experimental rhinovirus infection in asthmatic subjects. *Eur. Respir. J.* **11,** 126–132.
29 Kharitonov, S. A., Yates, D., and Barnes, P. J. (1995) Increased nitric oxide in exhaled air of normal human subjects with upper respiratory tract infections. *Eur. Respir. J.* **8,** 295–297.
30 Henriksen, A. H., Sue-Chu, M., Lingaas-Holmen, T., et al. (1999) Exhaled and nasal NO levels in allergic rhinitis: relation to sensitization, pollen season and bronchial hyperresponsiveness. *Eur. Respir. J.* **13,** 301–306.
31 Martin, U., Bryden, K., Devoy, M., et al. (1996) Increased levels of exhaled nitric oxide during nasal and oral breathing in subjects with seasonal rhinitis. *J. Allergy Clin. Immunol.* **97,** 768–772.
32 Kharitonov, S. A., Wells, A. U., O'Connor, B. J., et al. (1995) Elevated levels of exhaled nitric oxide in bronchiectasis. *Am. J. Respir. Crit. Care Med.* **151,** 1889–1893.
33 Barnes, P. J. and Kharitonov, S. A. (1996) Exhaled nitric oxide: a new lung function test. *Thorax* **51,** 233–237.
34 Di Rosa, M., Radomski, M., Carnuccio, R., et al. (1990) Glucocorticoids inhibit the induction of nitric oxide synthase in macrophages. *Biochem. Biophys. Res. Commun.* **172,** 1246–1252.
35 Kharitonov, S. A., Yates, D. H., and Barnes, P. J. (1996) Inhaled glucocorticoids decrease nitric oxide in exhaled air of asthmatic patients. *Am. J. Respir. Crit. Care Med.* **153,** 454–457.
36 Kharitonov, S. A., Yates, D. H., Chung, K. F., et al. (1996) Changes in the dose of inhaled steroid affect exhaled nitric oxide levels in asthmatic patients. *Eur. Respir. J.* **9,** 196–201.
37 Yates, D. H., Kharitonov, S. A., Robbins, R. A., et al. (1995) Effect of a nitric oxide synthase inhibitor and a glucocorticosteroid on exhaled nitric oxide. *Am. J. Respir. Crit. Care Med.* **152,** 892–896.
38 Robbins, R. A., Springall, D. R., Warren, J. B., et al. (1994) Inducible nitric oxide synthase is increased in murine lung epithelial cells by cytokine stimulation. *Biochem. Biophys. Res. Commun.* **198,** 835–843.
39 Robbins, R. A., Floreani, A. A., Von Essen, S. G., et al. (1996) Measurement of exhaled nitric oxide by three different techniques. *Am. J. Respir. Crit. Care Med.* **153,** 1631–1635.
40 Clini, E., Bianchi, L., Pagani, M., et al. (1998) Endogenous nitric oxide in patients with stable COPD: correlates with severity of disease. *Thorax* **53,** 881–883.
41 Rutgers, S. R., Meijer, R. J., Kerstjens, H. A., et al. (1998) Nitric oxide measured with single-breath and tidal-breathing methods in asthma and COPD. *Eur. Respir. J.* **12,** 816–819.

42 Dotsch, J., Demirakca, S., Terbrack, H. G., et al. (1996) Airway nitric oxide in asthmatic children and patients with cystic fibrosis. *Eur. Respir. J.* **9,** 2537–2540.
43 Maziak, W., Loukides, S., Culpitt, S., et al. (1998) Exhaled nitric oxide in chronic obstructive pulmonary disease. *Am. J. Respir. Crit. Care Med.* **157,** 998–1002.
44 Hogman, M., Holmkvist, T., Wegener, T., et al. (2002) Extended NO analysis applied to patients with COPD, allergic asthma and allergic rhinitis. *Respir. Med.* **96,** 24–30.
45 Silkoff, P. E., Martin, D., Pak, J., et al. (2001) Exhaled nitric oxide correlated with induced sputum findings in COPD. *Chest* **119,** 1049–1055.
46 Kharitonov, S. A., Robbins, R. A., Yates, D., et al. (1995) Acute and chronic effects of cigarette smoking on exhaled nitric oxide. *Am. J. Respir. Crit. Care Med.* **152,** 609–612.
47 Alving, K., Weitzberg, E., and Lundberg, J. M. (1993) Increased amount of nitric oxide in exhaled air of asthmatics. *Eur. Respir. J.* **6,** 1368–1370.
48 Hadjikoumi, I., Hassan, A., and Milner, A. D. (2002) Exhaled nitric oxide measurements in childhood asthma: comparison of two sampling techniques. *Pediatr. Res.* **52,** 745–749.
49 Silvestri, M., Sabatini, F., Spallarossa, D., et al. (2001) Exhaled nitric oxide levels in non-allergic and allergic mono- or polysensitised children with asthma. *Thorax* **56,** 857–862.
50 Jones, S. L., Herbison, P., Cowan, J. O., et al. (2002) Exhaled NO and assessment of anti-inflammatory effects of inhaled steroid: dose-response relationship. *Eur. Respir. J.* **20,** 601–608.
51 Warke, T. J., Fitch, P. S., Brown, V., et al. (2002) Exhaled nitric oxide correlates with airway eosinophils in childhood asthma. *Thorax* **57,** 383–387.
52 Gratziou, C., Lignos, M., Dassiou, M., et al. (1999) Influence of atopy on exhaled nitric oxide in patients with stable asthma and rhinitis. *Eur. Respir. J.* **14,** 897–901.
53 Kharitonov, S. A., Rajakulasingam, K., O'Connor, B., et al. (1997) Nasal nitric oxide is increased in patients with asthma and allergic rhinitis and may be modulated by nasal glucocorticoids. *J. Allergy Clin. Immunol.* **99,** 58–64.
54 Adisesh, L. A., Kharitonov, S. A., Yates, D. H., et al. (1998) Exhaled and nasal nitric oxide is increased in laboratory animal allergy. *Clin. Exp. Allergy* **28,** 876–880.
55 Frank, T. L., Adisesh, A., Pickering, A. C., et al. (1998) Relationship between exhaled nitric oxide and childhood asthma. *Am. J. Respir. Crit. Care Med.* **158,** 1032–1036.
56 Franklin, P. J., Taplin, R., and Stick, S. M. (1999) A community study of exhaled nitric oxide in healthy children. *Am. J. Respir. Crit. Care Med.* **159,** 69–73.
57 Lanz, M. J., Leung, D. Y., McCormick, D. R., et al. (1997) Comparison of exhaled nitric oxide, serum eosinophilic cationic protein, and soluble interleukin-2 receptor in exacerbations of pediatric asthma. *Pediatr. Pulmonol.* **24,** 305–311.
58 Kharitonov, S. A., O'Connor, B. J., Evans, D. J., et al. (1995) Allergen-induced late asthmatic reactions are associated with elevation of exhaled nitric oxide. *Am. J. Respir. Crit. Care Med.* **151,** 1894–1899.

59 Liu, S. F., Haddad, E. B., Adcock, I., et al. (1997) Inducible nitric oxide synthase after sensitization and allergen challenge of Brown Norway rat lung. *Br. J. Pharmacol.* **121,** 1241–1246.
60 van Amsterdam, J. G., Hollander, A., Snelder, J. D., et al. (1999) The effect of air pollution on exhaled nitric oxide of atopic and nonatopic subjects. *Nitric Oxide* **3,** 492–495.
61 Martin, U., Bryden, K., Devoy, M., et al. (1996) Increased levels of exhaled nitric oxide during nasal and oral breathing in subjects with seasonal rhinitis. *J. Allergy Clin. Immunol.* **97,** 768–772.
62 Arnal, J. F., Didier, A., Rami, J., et al. (1997) Nasal nitric oxide is increased in allergic rhinitis. *Clin. Exp. Allergy* **27,** 358–362.
63 Baraldi, E., Azzolin, N. M., Carra, S., et al. (1998) Effect of topical steroids on nasal nitric oxide production in children with perennial allergic rhinitis: a pilot study. *Respir. Med.* **92,** 558–561.
64 Corradi, M., Pelizzoni, A., Majori, M., et al. (1998) Influence of atmospheric nitric oxide concentration on the measurement of nitric oxide in exhaled air. *Thorax* **53,** 673–676.
65 van Amsterdam, J. G., Verlaan, B. P., van Loveren, H., et al. (1999) Air pollution is associated with increased level of exhaled nitric oxide in nonsmoking healthy subjects. *Arch. Environ. Health* **54,** 331–335.
66 Piacentini, G. L., Bodini, A., Vino, L., et al. (1998) Influence of environmental concentrations of NO on the exhaled NO test. *Am. J. Respir. Crit. Care Med.* **158,** 1299–1301.
67 Yates, D. H., Kharitonov, S. A., Robbins, R. A., et al. (1996) The effect of alcohol ingestion on exhaled nitric oxide. *Eur. Respir. J.* **9,** 1130–1133.
68 Lundberg, J. O., Weitzberg, E., Lundberg, J. M., et al. (1994) Intragastric nitric oxide production in humans: measurements in expelled air. *Gut* **35,** 1543–1546.
69 Kharitonov, S. A., Logan-Sinclair, R. B., Busset, C. M., et al. (1994) Peak expiratory nitric oxide differences in men and women: relation to the menstrual cycle. *Br. Heart J.* **72,** 243–245.
70 Kharitonov, S. A. and Barnes, P. J. (1997) Nasal contribution to exhaled nitric oxide during exhalation against resistance or during breath holding. *Thorax* **52,** 540–544.
71 Kharitonov, S., Alving, K., and Barnes, P. J. (1997) Exhaled and nasal nitric oxide measurements: recommendations. The European Respiratory Society Task Force. *Eur. Respir. J.* **10,** 1683–1693.
72 Persson, M. G., Wiklund, N. P., and Gustafsson, L. E. (1993) Endogenous nitric oxide in single exhalations and the change during exercise. *Am. Rev. Respir. Dis* **148,** 1210–1214.
73 Kharitonov, S. A., Chung, K. F., Evans, D., et al. (1996) Increased exhaled nitric oxide in asthma is mainly derived from the lower respiratory tract. *Am. J. Respir. Crit. Care Med.* **153,** 1773–1780.
74 Lundberg, J. O., Weitzberg, E., Lundberg, J. M., et al. (1996) Nitric oxide in exhaled air. *Eur. Respir. J.* **9,** 2671–2680.

75 Persson, M. G., Lonnqvist, P. A., and Gustafsson, L. E. (1995) Positive end-expiratory pressure ventilation elicits increases in endogenously formed nitric oxide as detected in air exhaled by rabbits. *Anesthesiology* **82,** 969–974.
76 Hogman, M., Stromberg, S., Schedin, U., et al. (1997) Nitric oxide from the human respiratory tract efficiently quantified by standardized single breath measurements. *Acta Physiol. Scand.* **159,** 345–346.
77 Byrnes, C. A., Dinarevic, S., Busst, C. A., et al. (1997) Effect of measurement conditions on measured levels of peak exhaled nitric oxide. *Thorax* **52,** 697–701.
78. Gomez, F. P., Martinez-Palli, G., Barbera, J. A., et al. (1998) Medicion del oxido nitrico exhalado en sujetos sanos. *Med. Clin. (Barc.)* **111,** 1–5.
79 Therminarias, A., Flore, P., Favre-Juvin, A., et al. (1998) Air contamination with nitric oxide: effect on exhaled nitric oxide response. *Am. J. Respir. Crit. Care Med.* **157,** 791–795.
80 Steerenberg, P. A., Nierkens, S., van Loveren, H., et al. (2000) A simple method to sample exhaled NO not contaminated by ambient NO from children and adults in epidemiological studies. *Nitric Oxide* **4,** 168–174.
81 Paredi, P., Loukides, S., Ward, S., et al. (1998) Exhalation flow and pressure-controlled reservoir collection of exhaled nitric oxide for remote and delayed analysis. *Thorax* **53,** 775–779.
82 van der Mark, T. W., Kort, E., Meijer, R. J., et al. (1997) Water vapour and carbon dioxide decrease nitric oxide readings. *Eur. Respir. J.* **10,** 2120–2123.
83. Anonymous (1999) Recommendations for standardized procedures for the on-line and off-line measurement of exhaled lower respiratory nitric oxide and nasal nitric oxide in adults and children. *Am. J. Respir. Crit. Care Med.* **160,** 2104–2117.
84 van Amsterdam, J. G., Verlaan, A. P., van Loveren, H., et al. (1999) The balloon technique: a convenient method to measure exhaled NO in epidemiological studies. *Int. Arch. Occup. Environ. Health* **72,** 404–407.
85 Kissoon, N., Duckworth, L. J., Blake, K. V., et al. (2000) FE(NO): relationship to exhalation rates and online versus bag collection in healthy adolescents. *Am. J. Respir. Crit. Care Med.* **162,** 539–545.
86 Kissoon, N., Duckworth, L. J., Blake, K. V., et al. (2002) Exhaled nitric oxide concentrations: online versus offline values in healthy children. *Pediatr. Pulmonol.* **33,** 283–292.
87 Pijnenburg, M.-W. H., Lissenberg, E. T., Hofhuis, W., et al. (2002) Exhaled nitric oxide measurements with dynamic flow restriction in children aged 4–8 yrs. *Eur. Respir. J.* **20,** 919–924.
88 Baraldi, E. and de Jongste, J. C. (2002) Measurement of exhaled nitric oxide in children, 2001. *Eur. Respir. J.* **20,** 223–237.
89 Kharitonov, S., Alving, K., and Barnes, P. J. (1997) Exhaled and nasal nitric oxide measurements: recommendations. The European Respiratory Society Task Force. *Eur. Respir. J.* **10,** 1683–1693.

90 Lehtimaki, L., Kankaanranta, H., Saarelainen, S., et al. (2001) Inhaled fluticasone decreases bronchial but not alveolar nitric oxide output in asthma. *Eur. Respir. J.* **18,** 635–639.
91 Byrnes, C. A., Dinarevic, S., Busst, C., et al. (1997) Is nitric oxide in exhaled air produced at airway or alveolar level? *Eur. Respir. J.* **10,** 1021–1025.
92 Silkoff, P. E., McClean, P. A., Caramori, M., et al. (1998) A significant proportion of exhaled nitric oxide arises in large airways in normal subjects. *Respir. Physiol.* **113,** 33–38.
93 Silkoff, P. E., Sylvester, J. T., Zamel, N., et al. (2000) Airway nitric oxide diffusion in asthma: role in pulmonary function and bronchial responsiveness. *Am. J. Respir. Crit. Care Med.* **161,** 1218–1228.
94 Baraldi, E., Azzolin, N. M., Zanconato, S., et al. (1997) Corticosteroids decrease exhaled nitric oxide in children with acute asthma. *J. Pediatr.* **131,** 381–385.
95 Nelson, B. V., Sears, S., Woods, J., et al. (1997) Expired nitric oxide as a marker for childhood asthma. *J. Pediatr.* **130,** 423–427.
96 Adisesh, L. A., Kharitonov, S. A., Yates, D. H., et al. (1998) Exhaled and nasal nitric oxide is increased in laboratory animal allergy. *Clin. Exp. Allergy* **28,** 876–880.
97 Arnal, J. F., Didier, A., Rami, J., et al. (1997) Nasal nitric oxide is increased in allergic rhinitis. *Clin. Exp. Allergy* **27,** 358–362.
98 Baraldi, E., Carra, S., Dario, C., et al. (1999) Effect of natural grass pollen exposure on exhaled nitric oxide in asthmatic children. *Am. J. Respir. Crit. Care Med.* **159,** 262–266.
99 Gratziou, C., Lignos, M., Dassiou, M., et al. (1999) Influence of atopy on exhaled nitric oxide in patients with stable asthma and rhinitis. *Eur. Respir. J.* **14,** 897–901.
100 Henriksen, A. H., Sue-Chu, M., Lingaas-Holmen, T., et al. (1999) Exhaled and nasal NO levels in allergic rhinitis: relation to sensitization, pollen season and bronchial hyperresponsiveness. *Eur. Respir. J.* **13,** 301–306.
101 Martin, U., Bryden, K., Devoy, M., et al. (1996) Increased levels of exhaled nitric oxide during nasal and oral breathing in subjects with seasonal rhinitis. *J. Allergy Clin. Immunol.* **97,** 768–772.
102 Moody, A., Fergusson, W., Wells, A., et al. (2000) Increased nitric oxide production in the respiratory tract in asymptomatic pacific islanders: an association with skin prick reactivity to house dust mite. *J. Allergy Clin. Immunol.* **105,** 895–899.
103 Horvath, I., Donnelly, L. E., Kiss, A., et al. (1998) Raised levels of exhaled carbon monoxide are associated with an increased expression of heme oxygenase-1 in airway macrophages in asthma: a new marker of oxidative stress. *Thorax* **53,** 668–672.
104 Jatakanon, A., Lim, S., Kharitonov, S. A., et al. (1998) Correlation between exhaled nitric oxide, sputum eosinophils, and methacholine responsiveness in patients with mild asthma. *Thorax* **53,** 91–95.
105 Silvestri, M., Spallarossa, D., Frangova-Yourukova, V., et al. (1999) Orally exhaled nitric oxide levels are related to the degree of blood eosinophilia in atopic children with mild-intermittent asthma. *Eur. Respir. J.* **13,** 321–326.

106. Howarth, P. H., Wilson, J., Djukanovic, R., et al. (1991) Airway inflammation and atopic asthma: a comparative bronchoscopic investigation. *Int. Arch. Allergy Appl. Immunol.* **94,** 266–269.
107. Ludviksdottir, D., Janson, C., Hogman, M., et al. (1999) Exhaled nitric oxide and its relationship to airway responsiveness and atopy in asthma. BHR Study Group. *Respir. Med.* **93,** 552–556.

6

Nitric Oxide Imaging in Neurons Using Confocal Microscopy

Xiaoxiang Zheng, Gangmin Ning, Dihui Hong, and Mu Zhang

Summary

The instability and low concentration of nitric oxide (NO) in specimens make it difficult to be detected directly. In this chapter, a method for imaging nitric oxide using laser scanning confocal microscopy (LSCM) is presented. A cultured hippocampal neuron is dyed with DAF-2 and observed under a Zeiss LSM 510 laser scanning confocal microscope. A 488-nm laser power is applied as excitation and the emission light from the labeled nitric oxide in the neuron is detected. In this way, nitric oxide is imaged and its intracellular kinetic change is monitored. Furthermore, image processing and visualization techniques are employed to help analyze the image data.

Key Words: Nitric oxide imaging; confocal microscopy.

1. Introduction

Nitric oxide (NO) is a type of short-lived, endogenously produced gas. It was first described in the 1980s as an endothelium-derived relaxant of vascular smooth muscle. However, in the past decade, it has been shown to be involved in many physiological processes, such as vascular homeostasis, neurotransmission, and inflammation. In the central nervous system (CNS), NO has been shown to be a physiological neurotransmitter or neuromodulator ***(1–9)***. Because NO is labile, existing in vivo for about 6–10 s before conversion into nitrates and nitrites and its concentration is in the nanomolar range, it has been difficult to perform direct NO detection with satisfactory sensitivity. Several methods have been used to measure nitric oxide, including a NO-selective electrode, fluorescence probes, Griess reagents, and so forth ***(10–15)***. DAF-2 was developed recently as a NO-sensitive fluorescent dye and widely used in biological studies ***(16,17)***. Laser scanning confocal microscopy (LSCM) is a valuable tool for obtaining high-resolution images and stacking two-dimensional (2-D) optical sections of a variety of biological specimens. Confocal micro-

From: *Methods in Molecular Biology, vol. 279: Nitric Oxide Protocols: Second Edition*
Edited by: A. Hassid © Humana Press Inc., Totowa, NJ

scopy combined with fluorescent probe provides a practical approach to recording intracellular nitric oxide dynamics ***(18–23)***.

2. Materials

2.1. Specimen

Cultured neurons from Sprague–Dawley rat pups (postnatal d 3–5).

2.2. Specific Equipment

1. Humidified CO_2 incubator.
2. Laminar-flow hood.
3. Centrifuge.
4. Laser scanning confocal microscope.

2.3. Chemicals, Reagents, and Solutions

1. Dulbecco's modified Eagle's medium (DMEM).
2. Phosphate-buffered saline (PBS): 8.0 g/L NaCl, 0.2 g/L KCl, 1.15 g/L Na_2HPO_4, 0.2 g/L K_2HPO_4, pH 7.4.
3. 75% Ethanol.
4. Fetal calf serum (FCS).
5. Trypsin.
6. Poly-D-lysine.
7. 5-Fluoro-2'-deoxyuridine.
8. DMEM solution: Dissolve 10 g in 1 L water; add 3.7 g of $NaHCO_3$, add 10% FCS, 100 U/mL penicillin, and 100 U/mL streptomycin.
9. Artificial cerebrospinal fluid (ACSF): 125 m*M* NaCl, 2.5 m*M* KCl, 26 m*M* $NaHCO_3$, 1.25 m*M* NaH_2PO_4, 2 m*M* $CaCl_2$, 1 m*M* $MgCl_2$, and 10 m*M* glucose, pH 7.4.
10. 4,5-Diaminofluorescein diacetate (DAF-2 DA).
11. *S*-Nitroso-*N*-acetyl-DL-penicillamine (SNAP).

3. Methods

Laser scanning confocal microscopy is a well-established technique in biology and medicine, which provides three-dimensional (3-D) images by means of microscopic tomography. The principle of confocal detection is as follows: An aperture (pinhole) is placed in front of the light detector, at a position such that the light from out-of-focus planes is blocked and only the light coming from the focal plane of the sample is collected. Microscopic tomography is made by moving the focal plane in the *z* direction. Stacks of optical sections obtained from successive focal planes can be reconstructed, to produce a 3-D view of the specimen. Advantages of this system include the following:

1. Higher resolution than conventional fluorescence microscopy ***(24)***.
2. Ability to optically section the whole specimen of cells and small organisms that have been tagged with fluorescent probes.
3. No bleaching outside the focal plane and less phototoxicity.

3.1. Neuronal Culture

1. Cover slips are washed with 75% ethanol and flame-sterilized before placement into dishes. Each cover slip is coated with 10 μg/mL poly-D-lysine.
2. The head of a rat is quickly rinsed with 75% ethanol and decapitated using sterile scissors.
3. Small scissors are used to peel away the scalp and then the skull. The entire brain is removed using a spatula and transferred to a sterile dish containing PBS at 4°C.
4. The hippocampus is separated from the cortex and sliced into small pieces.
5. The minced tissue is transferred to a conical tube, and once the tissue has settled, the supernatant solution is removed.
6. Five milliliters of 0.25% trypsin is added and the mixture is incubated at 37°C for 15 min.
7. Trypsin-containing solution is removed and the same volume of warmed DMEM solution is added.
8. Cells are dissociated by trituration with a fire-polished Pasteur pipet.
9. Cells are centrifuged at 1000 rpm for 10 min and then resuspend in DMEM solution.
10. Cells are plated at a density of about 1×10^5 cells/mL in a total of 2 mL of medium per 35-mm dish.
11. Cultures are maintained in an incubator at 37°C in a humidified atmosphere of 5% CO_2/95% air.
12. After 24 h, the plating medium is replaced with fresh culture medium. On the third day of culture, the media are supplemented with 5-fluoro-2'-deoxyuridine to block the proliferation of non-neuronal cells.
13. Half the volume of cultured media is replaced twice a week.

3.2. Nitric Oxide Dyeing

1. Cover slip with attached cells is removed from the culture medium and washed three times with fresh ACSF.
2. Cells are incubated with 10 μ*M* DAF-2 DA in incubator for 30 min.
3. Cover slip is washed three times with fresh ACSF.

3.3. Detecting Fluorescence by LSCM

3.3.1. Observation in the Eyepieces

1. Cultured neurons are transferred to a culture dish (*see* **Note 1**).
2. The culture dish is mounted on the microscope stage and the specimen is brought into focus. We routinely use a ×20 objective. A higher-resolution image can be obtained by using an immersion objective at a numerical aperture greater than 1.0.
3. Using stage movement controls, appropriate neurons are placed in the field of view.

3.3.2. Fixing Parameters of LSCM for Image Acquisition

We collect images using the Zeiss LSM 510 laser scanning microscope equipped with a 15-mW argon laser that provides 488-nm illumination. DAF-2 DA has excitation peak with maximum at 495 nm and emits green light with a

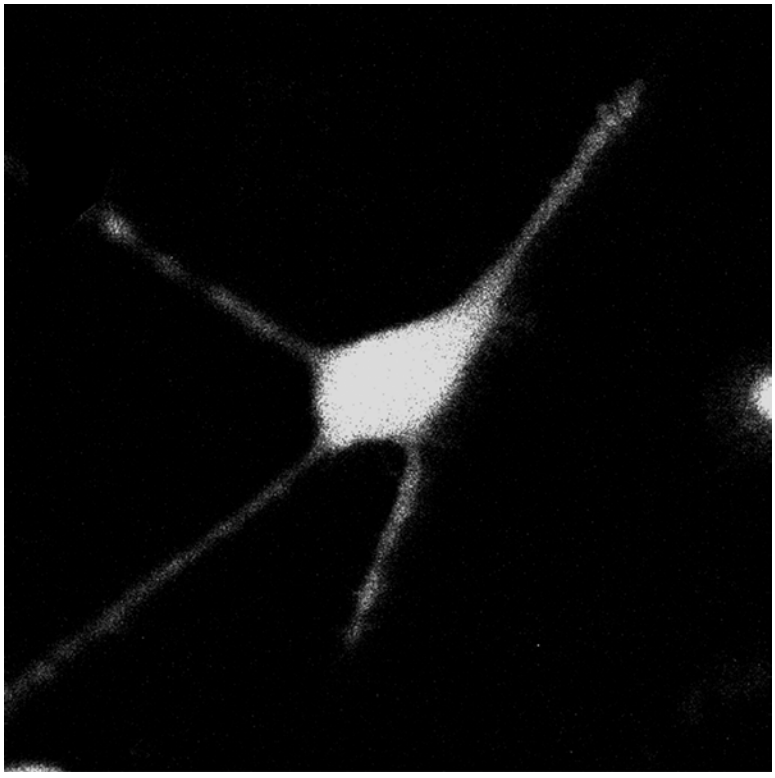

Fig. 1. Confocal imaging of neuronal nitric oxide. This image was collected using an LSM510 with a ×20 (NA = 0.75) objective, zoom = 4.2, laser output = 25%, laser intensity = 10%, pinhole size = 4.4 Airy units and then saved at a resolution of 512 × 512 with 256 gray scales.

peak wavelength of 515 nm. An argon laser (488 nm) is used as excitation source in our experiments.

1. Setting scanning configuration: The main dichroic (HFT 488) prevents the laser from reaching the detectors. The fluorescence between 500 and 550 nm is detected using an additional cutoff filter (BP 500-550) in front of the detector.
2. Choose scanning parameters, including image size, scan speed, averaging, and zooming. Fluorescence images are usually scanned and stored at a resolution of 512 × 512 with 256 gray scales (*see* **Fig. 1**).

3.3.3. Optimizing the Image

Optimizing the image requires a balance between high image quality and avoiding bleaching the sample.

1. Pinhole diameter: The pinhole diameter determines the thickness of the optical section. Contrast and resolution are improved as the pinhole diameter decreases; however, the amount of light getting to the detector is also attenuated. We do not recommend the use a pinhole less than 1 Airy unit, because it will lead to noisy images resulting from the inefficiency of photons.
2. Laser intensity: Even though high laser intensity may make the image appear more distinct, it may also increase the rate of photobleaching and make the data less biologically reliable.
3. Adjustment of the photomultiplier tube (PMT) effect (detector gain, amplifier gain, and amplifier offset): These parameters determine the range of light intensity that will be detected by the PMT. These parameters should be adjusted for high contrast without saturation or loss of detail ***(25)*** (*see* **Note 2**).

3.4. Time-Series Analysis of Intracellular Nitric Oxide Dynamics

Laser scanning confocal microscopy allows precise temporal analysis of intracellular nitric oxide levels. Using a scan-time-series menu, some definite cells can be repeatedly scanned to monitor the dynamic changes in fluorescent intensity of intracellular nitric oxide levels over time. For example, 10 μmol SNAP was added to the medium in the experiment and intracellular nitric oxide dynamics was recorded as shown in **Fig. 2A**.

3.4.1. Adding Reagent

Add reagent to the medium using a microliter pipet. This operation should be done carefully to avoid washing off neurons or hitting the dish. A large volume of added reagent may cause the object to move out of the focus plane. In this case, the focal plane should be reestablished.

3.4.2. Time Series of Images Acquisition

Time-lapse intracellular nitric oxide imaging acquisition starts 30 s after the addition of reagent. Successful imaging of live cells requires extreme care to maintain a steady environment during the whole process. Photodamage from the illuminating laser beam can be cumulative over multiple scans; thus, the exposure to the beam should be kept to the minimum necessary to acquire the image. In most cases, the physiological process of nitric oxide generation in the neuron takes place relatively slowly and can be effectively captured by LSCM. An acquisition rate at 1 frame (512 × 512)/min can provide both satisfactory temporal and spatial resolution for most physiological studies (*see* **Notes 3** and **4**).

3.4.3. Dynamic Intensity Measurement

1. Select the area to be measured: Drag mouse to outline an ROI to be measured. In LSM 510, once an ROI is selected, the information about it (intensity histogram, size in pixels, and mean intensity) will be displayed (*see* **Fig. 2B**).

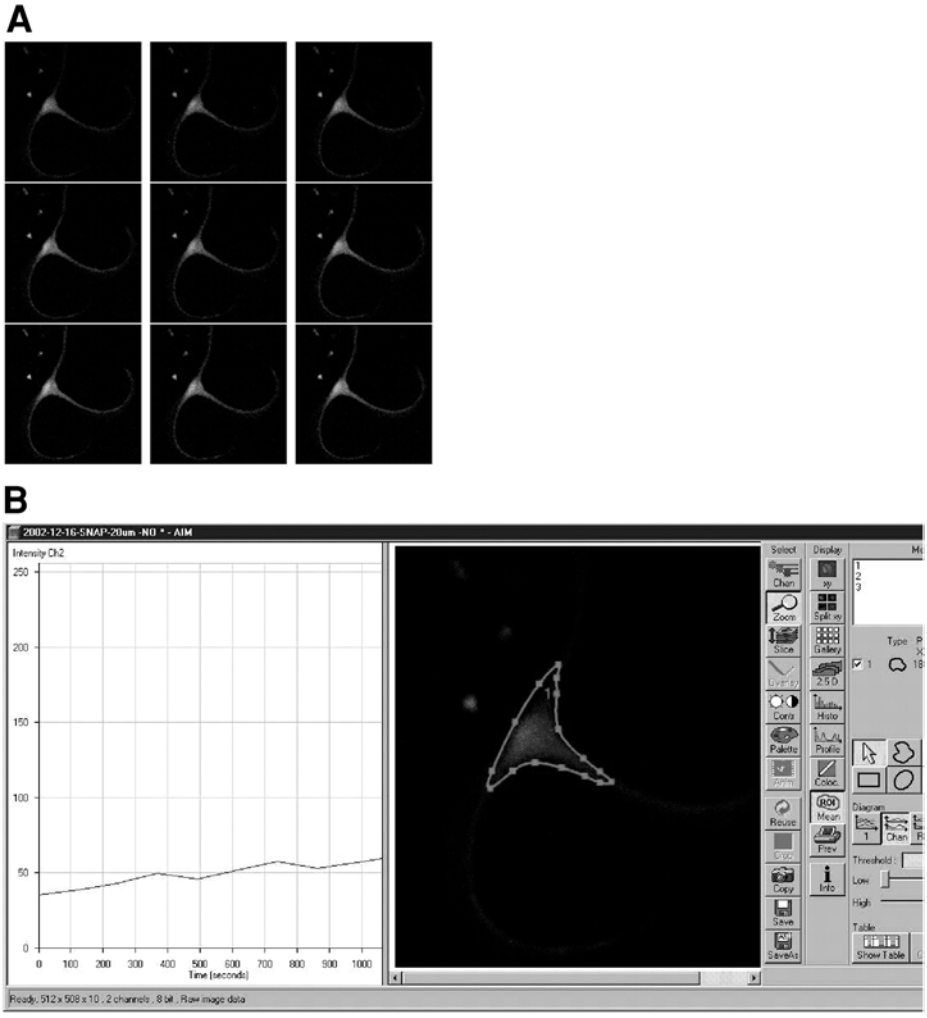

Fig. 2. Time series of intracellular nitric oxide dynamics and measurement. **(A)** A series of images shows intracellular nitric oxide dynamics after applying 10 μmol SNAP. The images were recorded every 2 min and for 18 min immediately after SNAP was applied. **(B)** When a region of interest (ROI) is selected (*right middle*), mean ROI function in LSM 510 software is activated to calculate and plot the mean fluorescent intensity in the ROI during the time-course (*left*).

2. Increases in intracellular nitric oxide are expressed as the ratio of fluorescence intensity of DAF-2 over baseline (F/F_0). The self-ratio method (F/F_0) is used because it is independent of factors such as dye concentration, excitation intensity, and detector efficiency ***(26,27)***.

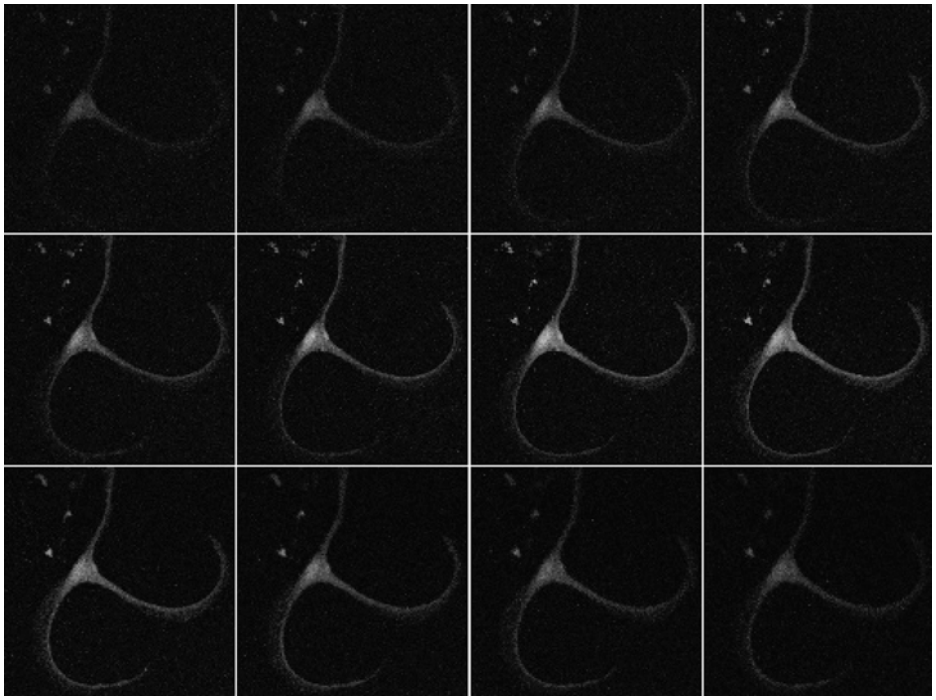

Fig. 3. Confocal optical sections of fluorescence-labeled intracellular nitric oxide. This specimen is scanned with a distance of 1.3 μm between the optical sections. The parameters of LSM510 for these volume data were ×20 (NA = 0.75) objective, zoom = 2.2, pinhole size = 2.6 Airy units, saved at a resolution of 512 × 512 with 256 gray scales.

3.5. Intracellular Nitric Oxide Distribution Evaluation

By changing the focal plane, a sequence of 2-D images is obtained to form 3-D volume data. The volume data can be reconstructed into 3-D images, then rotated or tilted to view the intracellular fluorescence-labeled nitric oxide distribution.

3.6. Image Stacks Acquisition

1. Use the focus knob to set the top and bottom of the scan section.
2. Decide the size of the image and the desired *Z*-step distance between the successive optical sections (*see* **Note 5**).
3. Start to collect the *Z*-stack (*see* **Fig. 3**).

3.6.1. Reconstruction and Visualization

It is conceptually difficult to understand intracellular fluorescence distribution from a series of optical sections taken by LSCM. Once collected, optical

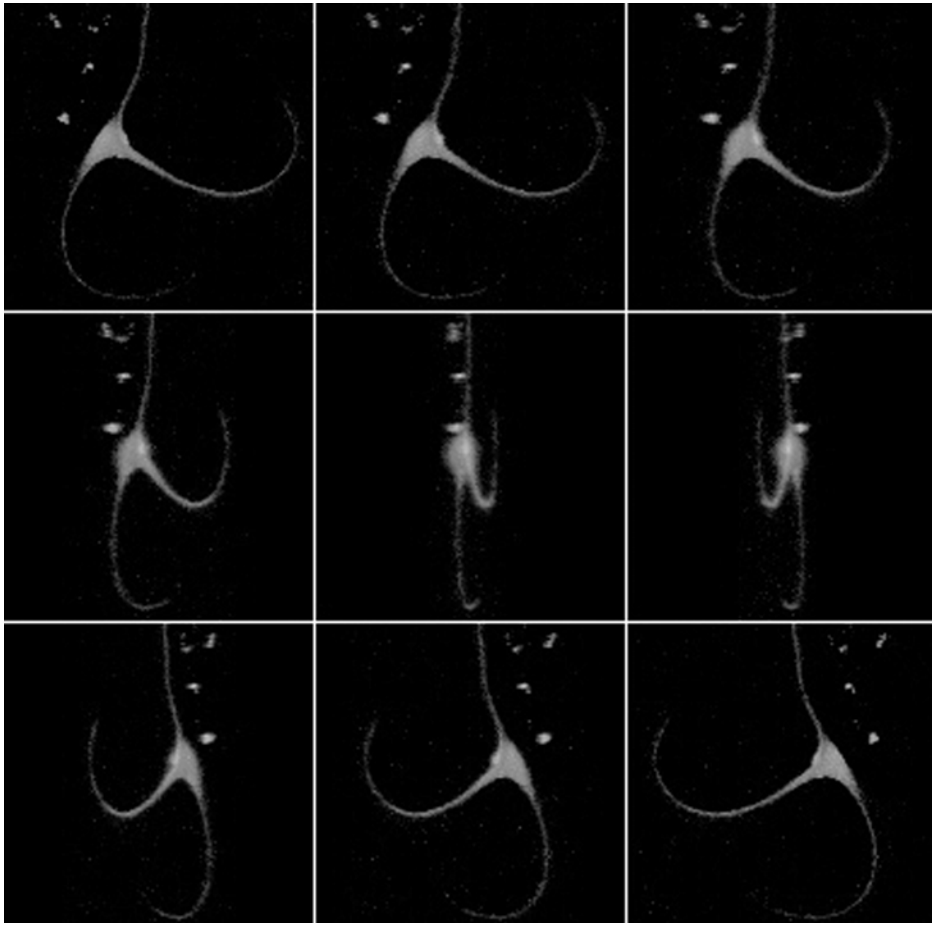

Fig. 4. Three-dimensional projection of fluorescence-labeled nitric oxide in the neuron. The volume data in **Fig. 3** were projected on a 2-D screen by LSM510 software. The projection was rotated along the *y*-axis with a step of 20°, which allowed viewing the object from different angles.

sections are ideal for further processing into a 3-D representation of the specimen, using visualization techniques. The intracellular distribution of fluorescence-labeled nitric oxide can be viewed by the *projection* functions in LSM510 as shown in **Fig. 4** (*see* **Note 6**).

1. Choose the turning axis, the *x*-, *y*-, or *z*-axis and specify the difference angle numerically.
2. Use a transparency to compensate for bright exterior to allow the inner structures to be seen in the projection.

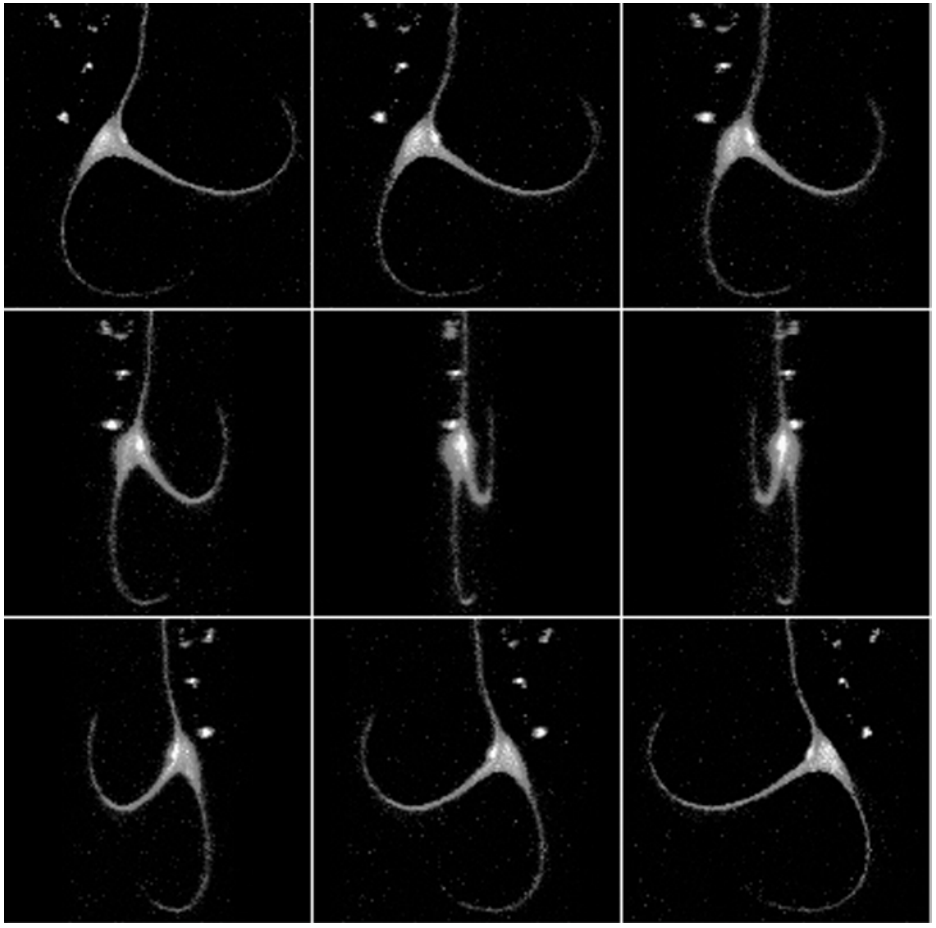

Fig. 5. Pseudocolor map of intracellular fluorescence-labeled nitric oxide. According to the pseudocolor lookup table, a different color was assigned to **Fig. 4** to map the different fluorescence-labeled nitric oxide concentration in the neuron.

3. Pseudocolor can be used to map the different fluorescence-labeled nitric oxide levels in the neuron (*see* **Fig. 5**).

4. Notes

1. Use thin glass-bottomed culture dishes to ensure that the use of a short working distance objective is feasible; thus, high magnification and a thin optical section can be achieved.
2. The black level of the PMT amplifier must be set so the full range of signal can be detected. While the photonic signal is linearly amplified, the electronic noise is exponentially increased; this should be used only in the case when the other

settings have been exploited. When the PMT is properly adjusted, the pixels in the brightest areas of the image should be bright white in order to utilize the full gray-scale range of the data. In LSM510 software, option RANGE INDICATOR can be used to indicate if a proper matching is achieved, whereas the blue color indicates below detector threshold and red indicates the PMT is saturated. Usually, first set the background to be just black using the offset control; then, set the detector gain to just produce red pixels on the bright part of the image.

3. Some physiological processes will induce cellular edema during the time-course, which leads the neuron of interest to move out of focus. Cellular edema also obstructs the light path, making the slice more opaque and thereby producing a blurred image. To counteract this, we use a large pinhole, enlarging the optical section, thus keeping the neuron in focus throughout the entire experiment. However, this approach also reduces the "confocal degree" to some extent.
4. If the stimulus increases the intracellular nitric oxide concentration during the time-course, one must be careful that the PMT not be saturated.
5. The optical section thickness refers to the thickness of the section of the sample imaged by the microscope and it is largely governed by the numerical aperture of the objective and the diameter of confocal pinhole. The step size should not be larger than the optical section thickness. In LSM510, clicking on option OPTIMAL INTERVAL and optimal interval set is suggested. It is about half the optical slice thickness. Using immersion objectives with a relatively high numerical aperture will generate thin sections and improve the resolution.
6. Usually, the resolution on the *z*-axis is lower than that on *x*- or *y*-axis. An important consideration when using other software to perform 3-D reconstructions from optical sections is to make sure that the sampling in the *z* direction matches that on the *x*-*y* plane. This can be done through the interpolation on the *z* plane after the images have been captured.

Acknowledgments

This work was supported by the National Natural Science Foundation of China (grant 30170275), The Key Laboratory on Biomedical Engineering of the Ministry of Education, China, and The Key Laboratory on Screening and Evaluating Chinese Cardio- and Cerebral-vascular Medicine, Zhejiang Province, China.

References

1 Palmer, R. M., Ferrige, A. G., and Moncada, S. (1987) Nitric oxide release accounts for the biological activity of endothelium-derived relaxing factor. *Nature* **327,** 524–526.
2 Prast, H. and Philippu, A. (2001) Nitric oxide as modulator of neuronal function. *Prog. Neurobiol.* **64,** 51–68.
3 Stuart-Smith, K. (2002) Demystified. Nitric oxide. *Mol. Pathol.* **55,** 360–366.
4 Esplugues, J. V. (2002) NO as a signaling molecule in the nervous system. *Br. J. Pharmacol.* **135,** 1079–1095.

5. Muller, F. and Koch, K. W. (1998) Calcium-binding proteins and nitric oxide in retinal function and disease. *Acta Anat. (Basel).* **162,** 142–150.
6 Burney, S., Tamir, S., Gal, A., et al. (1997) A mechanistic analysis of nitric oxide-induced cellular toxicity. *Nitric Oxide* **1,** 130–144.
7 Lala, P. K. and Chakraborty, C. (2001) Role of nitric oxide in carcinogenesis and tumour progression. *Lancet Oncol.* **2,** 149–156.
8 Murohara, T. and Asahara, T. (2002) Nitric oxide and angiogenesis in cardiovascular disease. *Antioxid Redox Signal* **4,** 825–831.
9 Lipton, P. (1999) Ischemic cell death in brain neurons. *Physiol. Rev.* **79,** 1431–1586.
10 Mordvintcev, P., Mulsch, A., Busse, R., et al. (1991) On-line detection of nitric oxide formation in liquid aqueous phase by electron paramagnetic resonance spectroscopy. *Anal Biochem.* **199,** 142–146.
11 Kikuchi, K., Nagano, T., Hayakawa, H., et al. (1993) Detection of nitric oxide production from a perfused organ by a luminol–H_2O_2 system. *Anal Chem.* **65,** 1794–1799.
12 Malinski, T. and Taha, Z. (1992) Nitric oxide release from a single cell measured in situ by a porphyrinic-based microsensor. *Nature* **358,** 676–678.
13 Malinski, T., Taha, Z., and Grunfeld, S. (1993) Diffusion of NO in the aorta wall monitored in-situ by porphyrinic microsensor. *Biochem. Biophys. Res. Commun.* **193,** 1076–1082.
14 Shibuki, K., (1990) An electrochemical microprobe for detecting nitric oxide release in brain tissue. *Neurosci. Res.* **9,** 69–76.
15. Zhang, X. and Broderick, M. Amperometric detection of nitric oxide. *Mod. Aspects Immunobiol.* **1,** 160–165.
16 Kojima, H., Nakatsubo, N., Kikuchi, K., et al. (1998) Detection and imaging of nitric oxide with novel fluorescent indicators: diaminofluoresceins. *Anal. Chem.* **70,** 2446–2453.
17 Al-Mehdi, A. B., Song, C., Tozawa, K., et al. (2000) Ca2+- and phosphatidylinositol 3-kinase-dependent nitric oxide generation in lung endothelial cells in situ with ischemia. *J. Biol. Chem.* **275,** 39,807–39,810.
18 Zanella, B., Calonghi, N., Pagnotta, E., et al. (2002) Mitochondrial nitric oxide localization in H9c2 cells revealed by confocal microscopy. *Biochem. Biophys. Res. Commun.* **290,** 1010–1014.
19 Lopez-Figueroa, M. O., Caamano, C., Morano, M. I., et al. (2000) Direct evidence of nitric oxide presence within mitochondria. *Biochem. Biophys. Res. Commun.* **272,** 129–133.
20 Chen, X., Sheng, C., and Zheng, X. (2001) Direct nitric oxide imaging in cultured hippocampal neurons with diaminoanthraquinone and confocal microscopy. *Cell Biol. Int.* **25,** 593–598.
21 Chen, X., Sheng, C., and Zheng, X. (2001) Inhibitive Effect of *N*-nitro-L-arginine on hippocampal neurons excitation. *Acta Biochimica et Biophysica Sinica* **33,** 437–442.
22. Chen, X., Sheng, C., and Zheng, X. (2000) Jujuboside A inhibited penicillin G stimulated releasing of glutamate and a later increase of nitric oxide in hippocam-

pal cells, Proceedings of IEEE–EMBS 2000' Asia–Pacific Conference on Biomedical Engineering, pp. 785–786.
23. Sheng, C., Chen, X., and Zheng, X. (2000) A novel method of direct detection of nitric oxide, Proceedings of IEEE–EMBS 2000' Asia–Pacific Conference on Biomedical Engineering, pp. 530–531.
24. Sheppard, C. J. R. and Gu, M. (1992) The significance of 3-D transfer functions in confocal scanning microscopy. *J. Microsc.* **165,** 377–390.
25. Sheppard, J. R., Gu, M., and Roy, M. (1992) Signal to noise ratio in confocal microscopy systems. *J. Microsc.* **168,** 209–218.
26 Koizumi, S., Bootman, M. D., Bobanovic, L. K., et al. (1999) Characterization of elementary Ca^{2+} release signals in NGF-differentiated PC12 cells and hippocampal neurons. *Neuron* **22,** 125–137.
27. Maravall, M., Mainer, Z. F., Sabatini, B. L., et al. (2000) Estimating intracellular calcium concentration and buffering without wavelength ratioing. *Biophys. J.* **78,** 2655–2667.

7

Measurement of Nitric Oxide Synthase Activity In Vivo and In Vitro by Gas Chromatography–Mass Spectrometry

Dimitrios Tsikas

Summary

Measurement of the nitric oxide (NO) metabolites nitrite and nitrate in biological matrices is a reliable method to assess NO synthase (NOS) activity. Unlike the "L-citrulline assay," the "nitrite/nitrate assay" is generally applicable and permits acquisition of maximum information about what NOS did actually produce. From the various analytical approaches and methods available so far for the quantitation of nitrite and nitrate, mass-spectrometry-based methods, notably gas chromatography–mass spectrometry (GC-MS), offer the highest reliability in terms of accuracy, precision, specificity, minimum of interferences, sensitivity, and no limitation regarding biological matrix. Among the GC-MS methods, that one utilizing the derivatization reagent pentafluorobenzyl bromide is the single assay permitting measurement of nitrite and nitrate. This method possesses the unique opportunity to measure simultaneously stable-isotope-labeled nitrite and nitrate (i.e. [^{15}N]nitrite and [^{15}N]nitrate), which are exclusively produced by NOS-catalyzed oxidation of L-[*guanidino*-$^{15}N_2$]-arginine, the stable-isotope-labeled L-arginine analog. ˙NOS may concomitantly produce ˙NO and $O_2^{\cdot -}$, thus forming peroxynitrite ($ONOO^-$), which also degrades to nitrite and nitrate. Thus, the GC-MS nitrite/nitrate assay provides information about biologically relevant NOS activity. This chapter describes GC-MS protocols for the measurement of NOS activity in vitro (e.g., of isolated NOS preparations and in cells) and in vivo (in animals and humans).

Key Words: Nitric oxide (˙NO); ˙NO synthase (NOS); NOS activity; nitrite; nitrate; stable isotopes; L-[*guanidino*-$^{15}N_2$]-arginine; [^{15}N]nitrite; [^{15}N]nitrate; peroxynitrite; pentafluorobenzyl bromide; gas chromatography–mass spectrometry (GC-MS); negative-ion chemical ionization; selected-ion monitoring.

1. Introduction

1.1. Assessment of NOS Activity

Measurement of nitric oxide synthase (NOS) activity in vitro and in vivo is the most frequently used tool in the field of nitric oxide (˙NO) research.

From: *Methods in Molecular Biology, vol. 279: Nitric Oxide Protocols: Second Edition*
Edited by: A. Hassid © Humana Press Inc., Totowa, NJ

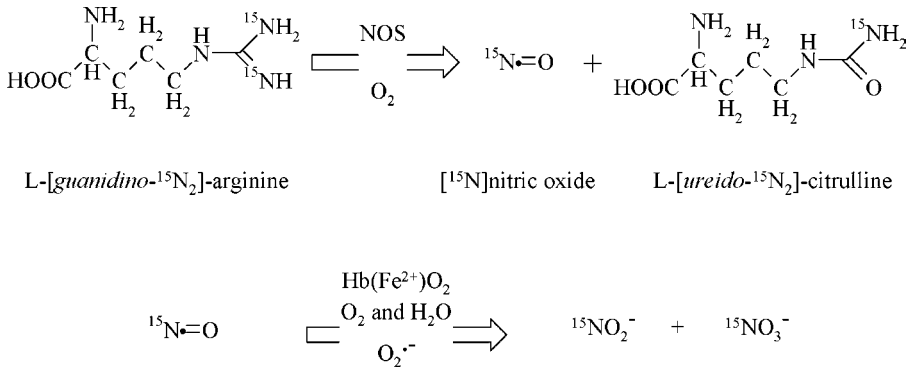

Fig. 1. Utilizing molecular oxygen (O_2) as the cosubstrate, NOS oxidizes L-[*guanidino*-$^{15}N_2$]-arginine to [^{15}N]nitric oxide (^{15}•NO) and L-[*ureido*-^{15}N]-citrulline. Upon release, ^{15}•NO undergoes several reactions. Auto-oxidation in aqueous solution yields [^{15}N]nitrite. In erythrocytes, ^{15}•NO as well as [^{15}N]nitrite are oxidized to [^{15}N]nitrate by oxyhemoglobin. ^{15}•NO may also react with superoxide ($O_2^{\bullet -}$), either coproduced by nitric oxide synthase (NOS) or from other sources, to form peroxynitrite ($O^{15}NOO^-$) that degrades to [^{15}N]nitrite and [^{15}N]nitrate. Thus, [^{15}N]nitrite and [^{15}N]nitrate reflect NOS-catalyzed conversion of L-[*guanidino*-$^{15}N_2$]-arginine to ^{15}•NO.

In principle, activity of nitric oxide synthase (NOS) can be assessed by measuring L-arginine-derived •NO and/or L-citrulline (*see* **Fig. 1**). However, in vivo •NO is not accessible to quantitative analysis because of its very short half-life of less than 0.1 s ***(1)***. Furthermore, the L-arginine/•NO pathway negligibly contributes to whole-body L-citrulline production (i.e., by much less than 1%) ***(2)***. The so-called L-citrulline assay, which uses radiolabeled L-arginine as substrate ***(3)***, is the most frequently used NOS assay in vitro, because of its ease and simple laboratory performance. However, the L-citrulline assay is limited to situations that exclude contribution to L-citrulline by other pathways, notably the urea cycle; that is, this assay is limited to investigations in vitro. Both in vitro and in vivo, •NO and other •NO-derived species, particularly peroxynitrite ($ONOO^-$), the reaction product of the combination of •NO and superoxide, $O_2^{\bullet -}$, which may be produced concomitantly by NOS ***(4)***, are also converted to nitrite and nitrate (e.g., from degradation or oxidation in erythrocytes) (*see* **Fig. 1**).

A detailed picture of what NOS did produce and how much •NO has been actually produced is provided by measuring nitrite and nitrate (i.e., by the nitrite/nitrate assay). Nitrite and nitrate can be measured by a variety of analytical methods from which, however, only very few allow their accurate quantitation in vitro and in vivo in urine and plasma or serum ***(5)***. Among them, mass-spectrometry-based methods, notably gas chromatography–mass spectrometry (GC-MS), offer versatile facilities and the highest analytical

reliability. GC-MS methods possess the unique opportunity of measuring L-[*guanidino*-$^{15}N_2$]-arginine-derived [^{15}N]nitrite and [^{15}N]nitrate that avoids uncertainties arising from L-arginine-unrelated, ubiquitous nitrite and nitrate (*see* **Note 1**).

1.2. Measurement of Nitrite and Nitrate by GC-MS

1.2.1. Derivatization Procedures

Chemical conversion of nitrite and nitrate into thermally stable, volatile derivatives accessible to GC analysis is an absolute requirement for the analysis of these anions by GC-MS techniques. From the numerous derivatization reactions available, only one permits simultaneous derivatization and quantitation of nitrite and nitrate, thus overcoming severe methodological problems arising from the need of separate analysis resulting from oxidation of nitrite to nitrate or reduction of nitrate to nitrite before derivatization. Simultaneous derivatization and quantitation of nitrite and nitrate is possible by using the versatile derivatization reagent pentafluorobenzyl bromide (PFB-Br; 2,3,4,5,6–pentafluorobenzyl bromide or α-bromo-pentafluorotoluene) (*see* **Fig. 2**). PFB-Br undergoes substitution reactions with a variety of nucleophiles, including organic and inorganic anions ***(6)***. In these reactions, the leaving group Br of PFB-Br is substituted (most likely through a S_N2 mechanism) by the nucleophiles to produce *N*-, *O*-, and *S*-PFB derivatives (*see* **Fig. 2**). Nitrite reacts with PFB-Br to form almost exclusively the nitro PFB derivative (i.e., PFB-NO_2), whereas the reaction of nitrate produces the PFB nitric acid derivative (i.e., PFB-ONO_2) (*see* **Fig. 2**) ***(7)***. PFB-NO_2 and PFB-ONO_2 are freely soluble in and quickly extractable with water-nonmiscible organic solvents such as toluene.

1.2.2. Gas Chromatography–Mass Spectrometry

PFB–NO_2, PFB–$^{15}NO_2$, PFB–ONO_2, and PFB–$O^{15}NO_2$ are volatile, thermally stable compounds. Using chemically bonded fused silica capillary columns of middle polarity (*see* **Note 2**), such as Optima 17, PFB-ONO_2 elutes in front of PFB–NO_2. PFB–$O^{15}NO_2$ and PFB–$^{15}NO_2$ have almost identical retention times with their unlabeled analogs. The electrically uncharged gaseous molecules are released directly into the ion source of the GC-MS instrument, where they ionize in a manner depending on the ionization mode and the GC-MS instrument (*see* **Figs. 3** and **4**). PFB derivatives are strongly electron-capturing substances. Under negative-ion chemical ionization (NICI) conditions (e.g., using methane as the reagent gas), PFB–NO_2, PFB–$^{15}NO_2$, PFB–ONO_2, and PFB–$O^{15}NO_2$ readily ionize to yield various anions (*see* **Figs. 3** and **4**), the most characteristic and important being NO_2^-, $^{15}NO_2^-$, ONO_2^-, and $O^{15}NO_2^-$, respectively, which differ in their mass-to-charge ratios (*m*/*z*), and can, therefore, be discriminated mass spectrometrically.

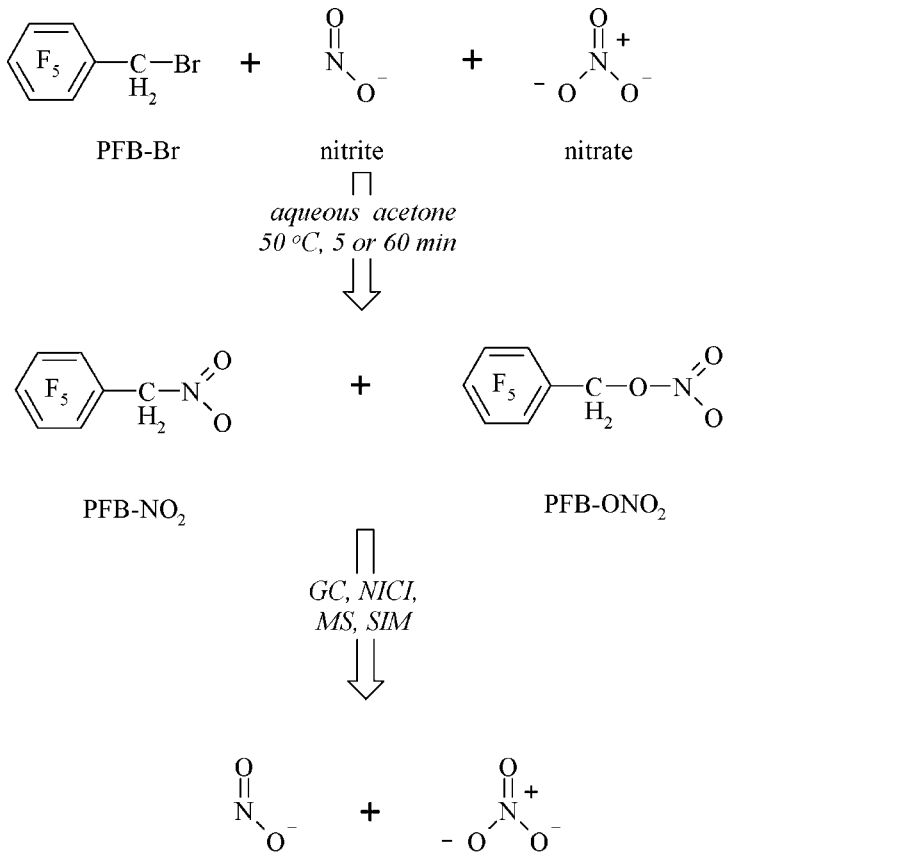

m/z	46	62	for unlabelled anions
m/z	47	63	for ^{15}N-labelled anions

Fig. 2. In aqueous acetonic solutions (i.e., buffered solutions), NOS incubates, cell culture supernatants, tissue homogenates, whole blood, plasma, serum, saliva, seminal fluid, exhaled breath condensate, and lavage, unlabeled and stable-isotope-labeled nitrite and nitrate react with pentafluorobenzyl bromide (PFB-Br) to form the corresponding PFB derivatives (i.e., $PFBNO_2$ and $PFBONO_2$). These compounds are separated gas chromatographically and ionized to nitrite and nitrate, respectively, in the negative-ion chemical ionization (NICI) mode. Subsequently, nitrite and nitrate are separated mass spectrometrically and finally monitored in the selected-ion monitoring (SIM) mode.

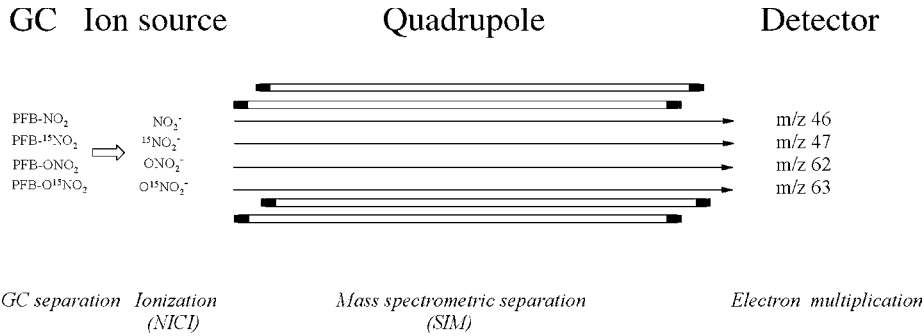

Fig. 3. Simplified schematic of the simultaneous quantitative analysis of nitrite, nitrate, and their ^{15}N-labeled analogs as their PFB derivatives using GC, single-stage quadrupole MS. NICI, negative-ion chemical ionization; SIM, selected-ion monitoring; *m/z*, mass-to-charge ratio.

Quantitative determination of nitrite and nitrate as their PFB derivatives with GC-MS instruments (e.g., with single-stage quadrupole instruments) is performed in the selected-ion monitoring (SIM) mode, because this scanning technique provides the most sensitive detection (*see* **Fig. 3**). The mass spectrometer is set to pass alternately four specific and intense ions with *m/z* corresponding to the same ions of the analytes and the internal standards, respectively (*see* **Fig. 3**) (i.e., *m/z* 46 and *m/z* 47 for NO_2^- and $^{15}NO_2^-$, respectively, and *m/z* 62 and *m/z* 63 for ONO_2^- and $O^{15}NO_2^-$, respectively.

Calculation of concentrations of nitrite and nitrate ($[NO_x^-]$; $x = 2$ for nitrite and $x = 3$ for nitrate) present in a certain matrix can be simply performed by using the known concentrations of the internal standards ($[^{15}NO_x^-]$) added to the sample (*see* **Note 3**) and the following equation:

$$[NO_x^-] = (R - R_0)\,[^{15}NO_x^-] \quad (1)$$

where R is the peak area ratio of *m/z* 46 to *m/z* 47 for nitrite or of *m/z* 62 to *m/z* 63 for nitrate measured in the sample and R_0 is the peak area ratio of *m/z* 46 to *m/z* 47 for [^{15}N]nitrite or *m/z* 62 to *m/z* 63 for [^{15}N]nitrate measured in their stock solutions. Typical R_0 values are of the order of 0.015 for both anions.

The concentrations of [^{15}N]nitrite and [^{15}N]nitrate formed in vitro or in vivo (e.g., from L-[*guanidino*-$^{15}N_2$]-arginine) can be calculated by using Eq. (2), which is a transformation of Eq. (1):

$$[^{15}NO_x^-] = (R' - R'_0)\,[NO_x^-] \quad (2)$$

In this equation, R' is the peak area ratio of *m/z* 47 to *m/z* 46 for [^{15}N]nitrite or of *m/z* 63 to *m/z* 62 for [^{15}N]nitrate measured in the sample and R'_0 is the corresponding peak area ratio measured in the sample without addition or formation

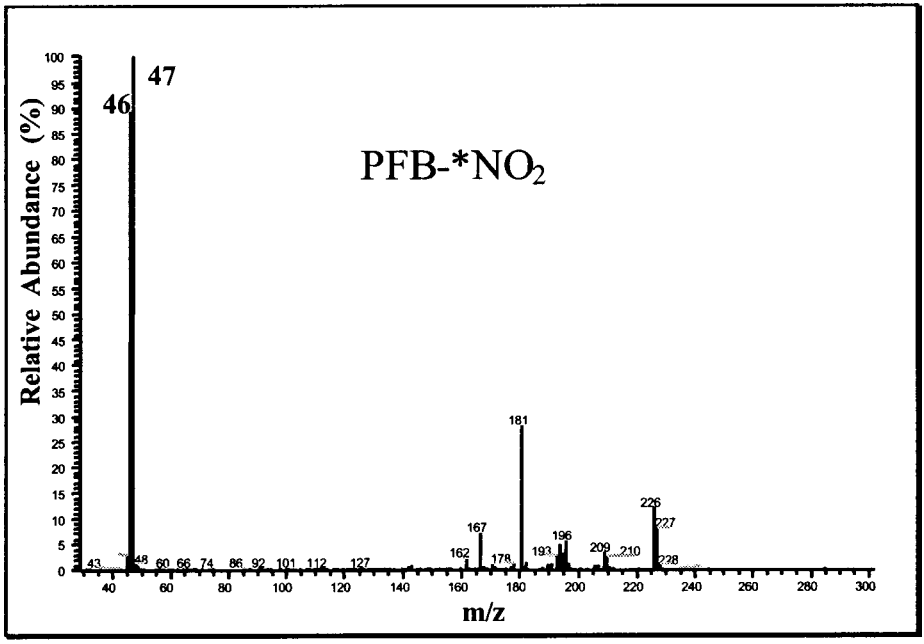
PFB-*NO2
Relative Abundance (%)
m/z
46
47
181
167
196
226
227
162
178
193
209
210
228

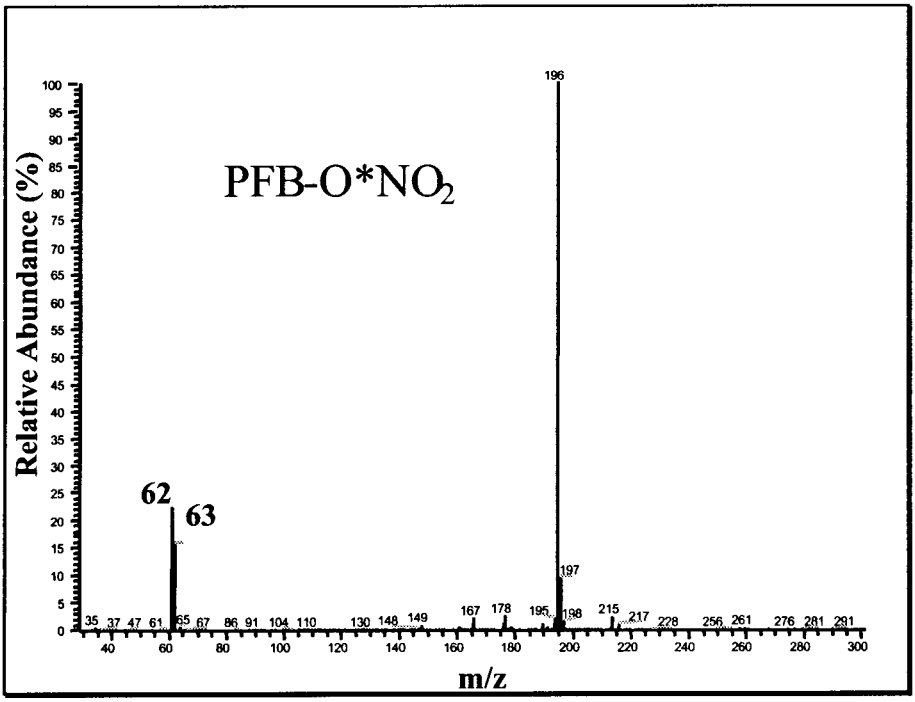
PFB-O*NO2
Relative Abundance (%)
m/z
62
63
196
197
167
178
195
198
215
217
228
256
261
276
281
291

Fig. 4.

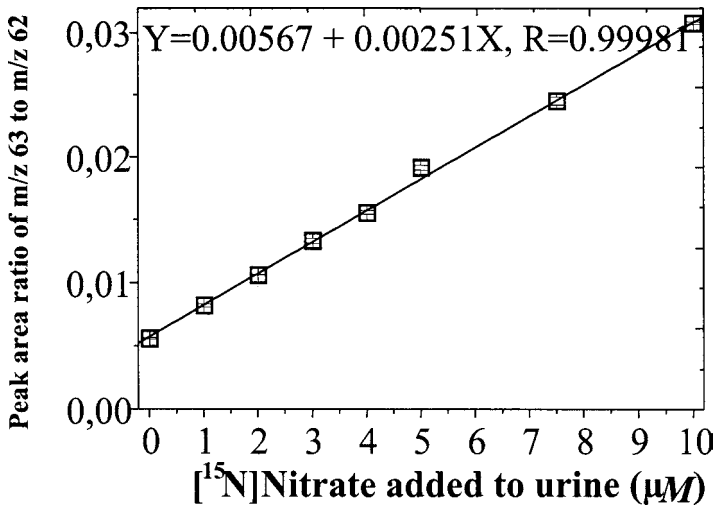

Fig. 5. A GC-MS standard curve for [^{15}N]nitrate added to human urine. [^{15}N]Nitrate was added to urine samples at the indicated final concentrations. Samples were derivatized with PFB-Br and SIM of *m/z* 63 and *m/z* 62 was performed. The peak area ratio is plotted versus the [^{15}N]nitrate concentration added. Linear regression analysis between the peak area ratio measured (*Y*) and the [^{15}N]nitrate concentration added (*X*) revealed a straight line with the regression equation $Y = 0.00567 + 0.00251X$ (regression coefficient, $R = 0.99981$).

of [^{15}N]nitrite or [^{15}N]nitrate or in their stock solutions. Typically, R_0 amounts to approx 0.005 for unlabeled nitrite (*m/z* 47 to 46) and 0.006 (*m/z* 63 to 62) for unlabeled nitrate. Usually, enrichment values ($^{15}NO_x$), expressed as atom percent ^{15}N, rather than concentrations of [^{15}N]nitrite or [^{15}N]nitrate in a certain matrix are reported ***(8)***. For this purpose, Eq. (3) can be used:

$$^{15}NO_x = \frac{100 \cdot R'}{1 + R'} \tag{3}$$

Figure 5 shows a standard curve for [^{15}N]nitrate that was externally added to a human urine sample. The peak area ratio of *m/z* 63 to *m/z* 62 increases linearly with increasing added [^{15}N]nitrate concentration. The *y*-axis intercept (i.e., 0.00567) and the reciprocal value of the slope (i.e., 1/0.00251) of the

Fig. 4. *(previous page)* Negative-ion chemical ionization (NICI) mass spectra of the PFB derivatives of unlabeled and ^{15}N-labeled nitrite (upper panel) and nitrate (lower panel). The ^{15}N-label is indicated by asterisks. The relevant mass fragments (i.e., *m/z*) are emphasized by bold numbers (i.e., *m/z* 46 and *m/z* 47 for NO_2^- and $^{15}NO_2^-$, respectively, and *m/z* 62 and *m/z* 63 for NO_3^- and $^{15}NO_3^-$, respectively.

regression equation yield R'_0 and $[NO_3^-]$ (i.e., the endogenous urinary mean concentration of nitrate), respectively, which amounts to 398 μ*M* in this urine sample. The concentration of endogenous [^{15}N]nitrate in the urine sample is calculated to be approx 1.4 μ*M*. [^{15}N]Nitrate externally added at 1 μ*M* can be discriminated from endogenous [^{15}N]nitrate (*see* **Fig. 5**). Similar results are also obtained for [^{15}N]nitrite. The limit of quantitation (LOQ) of the method for [^{15}N]nitrate and [^{15}N]nitrite present in addition to the naturally occurring ^{15}N-labeled anions is mainly determined by the concentration of endogenous nitrate and nitrite. Addition of 10 μ*M* of [^{15}N]nitrate to the urine sample yields an approximate enrichment value of 2.9% [^{15}N]nitrate.

2. Materials

1. Sodium [^{15}N]nitrate (98 atom% at ^{15}N; Sigma, Munich, Germany) (*see* **Note 3**).
2. Sodium [^{15}N]nitrite (98 atom% at ^{15}N) and L-[*guanidino*-$^{15}N_2$]-arginine HCl (98% at both ^{15}N atoms) (Cambridge Isotope Laboratories, Andover; MA, USA) (*see* **Note 3**).
3. 2,3,4,5,6–Pentafluorobenzyl bromide (PFB-Br) (Aldrich, Steinheim, Germany) (*see* **Note 4**).
4. Purified recombinant bovine endothelial NOS (eNOS) (Cayman Chemical, Ann Arbor, MI; isolated from a Baculovirus overexpression system in Sf9 cells) supplied in 50 m*M* HEPES, pH 7.4, with 10% glycerol, 5 m*M* CHAPS, and 100 μ*M* dithiothreitol (DTT). The specific activity of eNOS was declared by the supplier as 1.3 nmol ˙NO/min × mg as measured spectrophotometrically using the oxyhemoglobin assay (1 m*M* $CaCl_2$, 1.2 μ*M* calmodulin, 0.1 mM NADPH, 50 μ*M* L-arginine, 12 μ*M* H_4B, 170 μ*M* DTT). The original eNOS preparation (1.07 mL, 6.18 mg eNOS) is thawed, aliquoted to 10-μL portions and frozen (–80°C) immediately. eNOS stock solutions are used once without re-refrigerating.
5. eNOS cofactors: NADPH, H_4B (tetrahydrobiopterin), FAD (flavin adenine dinucleotide), and FMN (flavin adenine mononucleotide) (Sigma, Munich, Germany); calmodulin (CaM; Biomol, Hamburg, Germany); $CaCl_2$ (Merck, Darmstadt, Germany).
6. NOS inhibitors: N^G,N^G-dimethylarginine (asymmetric dimethylarginine, ADMA), N^G-nitro-L-arginine (L-NNA), N^G-methyl-L-arginine (L-NMA) (Sigma, Munich, Germany).
7. GC-MS instruments. Single-stage quadrupole MS engine 5890A connected to a gas chromatograph 5890 series II equipped with an autosampler model 7673 (Hewlett Packard, Waldbronn, Germany); triple-stage quadrupole (TSQ 7000) connected to a gas chromatograph Trace 2000 equipped with an autosampler model AS 2000 (Finnigan MAT, San Jose, CA, USA). The GC–tandem MS instrument is operating in the single-stage quadrupole mode.
8. GC high-resolution capillary columns. Optima 17 (length, 15 m; inner diameter, 0.25 mm; film thickness, 0.25 μm (Macherey-Nagel, Düren, Germany). Optima 17 is a fused silica capillary column with immobilized phenylmethylpolysiloxane

(50% phenyl) groups and has middle polarity. Similar chemically bonded GC phases are OV-17, DB-17, HP-50+, HP-17, SPB-50, SP-2250, Rtx-50, CP-SIL 24 CB, and ZB-50 (*see* **Note 2**).
9. Thermostat (Bioblock Scientifics); sample tray capacity for 60 samples; Thermolyne Corp., Iowa, USA).
10. Nitrogen evaporator (TurboVap LV evaporator; sample tray capacity for 50 vials; Zymark, Idstein/Taunus, Germany).
11. Apact dual-channel aggregometer (LAbor, Hamburg, Germany).
12. Glassware (Macherey-Nagel, Düren, Germany). Snap ring vials N11-1 (32.5 × 11.5 mm); snap ring caps N11; microinserts for snap ring vials (30 × 5 mm).
13. Autosampler/injector syringe (5-µL SGE syringe, SK-5F-HP-0.63; SGE International Pty. Ltd, Australia).
14. Vortex mixer (Model Reax 2000; Heidolph, Germany).

3. Methods

3.1. Derivatization and Extraction Procedures (see Note 4)

1. Introduce a 100-µL aliquot of the sample into a glass snap ring vial.
2. Add a 400-µL aliquot of acetone.
3. Add a 10-µL aliquot of PFB-Br.
4. Close the vial with a snap ring cap.
5. Put the vial onto a thermostat at 50°C.
6. Incubate for 5 or 60 min.
7. Evaporate acetone with a nitrogen stream.
8. Extract by vortexing for 60 s with a 300- to 1000-µL aliquot of toluene.
9. Let phases separate or separate phases by short centrifugation.
10. Decant a 200- to 800-µL aliquot of the toluene phase into a snap ring vial and close the vial with a snap ring cap; for small volumes, introduce sample into microinserts.

PFB-Br (*see* **Note 4**) is a liquid insoluble in water, but soluble in most organic solvents, including those being water miscible such as acetone, acetonitrile, and ethanol. PFB-Br is also soluble in other organic solvents that are not miscible with water (e.g., toluene).

Because derivatization of nitrite and nitrate with PFB-Br must take place in aqueous phase, a water-miscible organic solvent has to be used. The most suitable organic solvent is acetone, because it can be quickly removed after derivatization. In order to obtain a homogenous liquid phase, acetone has to be used in the fourfold volume of the aqueous phase (e.g., buffer, plasma), regularly 400 µL of acetone per 100 µL of the aqueous phase and for up to 10 µL of PFB-Br. In protein-rich matrices such as plasma, proteins precipitate on the addition of acetone as well as during derivatization. However, this does not affect derivatization. Preceding precipitation or removal of proteins is not necessary.

The yield of the reaction products depends on various experimental conditions, including temperature, time, and amount of PFB-Br. When using acetone as the organic solvent, a reaction temperature of 50°C is recommended. Derivatization should be performed in autosampler airtight glass vials in a well-ventilated fume hood (*see* **Note 4**). Maximum yield of PFB-NO_2 and PFB-ONO_2 requires use of PFB-Br at high excess (10 µL equivalent to 17.3 mg or 48 µmol) over nitrite and nitrate—in particular, in biological samples such as plasma and urine rich in other anions, notably chloride, which readily react with PFB-Br. For maximum sensitivity of nitrite analysis, the reaction time should be limited to 5 min *(7)*. For simultaneous analysis of nitrite and nitrate, a reaction time of 60 min is required *(7)*.

Upon derivatization, the samples are put into a nitrogen evaporator and acetone is evaporated by means of a gentle nitrogen stream. This process lasts a few minutes, the sample becomes cool, and excess PFB-Br remains as a small drop on the aqueous phase. PFB–NO_2, PFB–ONO_2, other PFB derivatives, and the remaining PFB-Br are subsequently extracted with an organic solvent, preferably with toluene. Use of this solvent has weighty advantages over use of other solvents such as ethyl acetate. PFB–NO_2 and PFB–ONO_2 are readily soluble in toluene, and their extraction by this solvent is quantitative and fast; it takes no more than 60 s when vortexed. As a rule, phase separation occurs spontaneously and quickly (*see* **Note 4**). If necessary, samples may be centrifuged (e.g., for 1 min at 800*g*); drying of the toluene phase over anhydrous sodium sulfate is not necessary. The volume of toluene to be used for extraction is directed toward the concentration of nitrite and nitrate in the matrix to be analyzed. Thus, in NOS incubates, use of 100–300 µL of toluene is recommended, whereas in plasma and urine, a toluene volume of 1 mL suffices. If necessary, the toluene extract should further be diluted with toluene.

3.2. Gas Chromatography–Mass Spectrometry

1. Inject a 0.5-µL aliquot of the toluene phase (*see* **Note 5**).
2. Use an oven temperature program, starting at 70°C.
3. Perform selected-ion monitoring (SIM) of *m/z* 46, 47, 62, and 63 with a dwell time of 50 ms for each ion in the negative-ion chemical ionization (NICI) mode (*see* **Note 6**).
4. Separate chromatograms of the single ions and integrate peaks.
5. Calculate peak area ratios of *m/z* 46 to 47 and of *m/z* 62 to 63.
6. Calculate concentrations by using Eq. (1) or (2).

Aliquots (0.5 µL) are injected in the splitless mode and analyzed using an oven temperature program (e.g., the column is held at 70°C for 1 min and then increased to 280°C at a rate of 30°C/min). Helium (50 kPa) and methane (200 Pa) are used as the carrier and the reagent gases, respectively, for NICI. Electron

energy and electron current are set to 230 eV and 300 mA, respectively, for NICI. Constant temperatures of 180°C, 280°C, and 200°C are kept at the ion source, interface, and injector of the instrument, respectively. SIM of *m/z* 46 ($[NO_2]^-$) for nitrite, 47 ($[^{15}NO_2]^-$) for [^{15}N]nitrite, 62 ($[NO_3]^-$) for nitrate, and 63 ($[^{15}NO_3]^-$) for [^{15}N]nitrate is performed with a dwell time of 50 ms for each ion. The electron multiplier voltage is set to 1200 V for urine samples, 1600 V for plasma samples, and 2600 V or higher when measuring L-[*guanidino*-$^{15}N_2$]-arginine-derived [^{15}N]nitrite and [^{15}N]nitrate. These conditions are valid for the Hewlett-Packard GC-MS single-stage quadrupole instrument MS Engine. If using other GC-MS instruments, such as the triple-stage quadrupole instrument TSQ 7000, adapt GC-MS conditions, if necessary.

3.3. Measurement of NOS Activity In Vitro

*3.3.1. Enzyme Assay Using Isolated NOS Preparations (*see ***Note 7****)*

1. Prepare a stock solution of NOS cofactors in potassium phosphate buffer (e.g., 50 m*M*, pH 7.0, 5 mL) with the following final concentrations: 10 μ*M* H_4B, 5 μ*M* FAD, 5 μ*M* FMN, 500 μ*M* $CaCl_2$, 0.8 m*M* NADPH, 500 n*M* CaM. If necessary, adapt cofactor concentrations. Make 400-μL aliquots and store at –20°C (*see* **Note 8**).
2. Take a 400-μL aliquot of the cofactor solution, spike with L-[*guanidino*-$^{15}N_2$]arginine (concentration range: 0–40 μ*M*), and preincubate for 10 min at 37°C.
3. Start the reaction by adding NOS (final protein concentration ranging between 5 and 90 μg/mL, or appropriately).
4. Stop the reaction after an appropriate time of incubation (range: 0–30 min) by transferring aliquots (100 μL) of NOS incubates into 1.5-mL glass snap ring vials that contain an ice-cold aqueous acetone solution (400 μL) of [^{14}N]nitrite and [^{14}N]nitrate for use as internal standards, resulting in an appropriate final concentration (e.g., 1.0 μ*M* each with respect to 100-μL aliquots of the incubation mixture). Mix the samples immediately by vortexing and put on ice until derivatization.
5. Derivatize by using the derivatization procedure.

Typical results from such experiments are shown in **Fig. 6**. Using a commercially available purified eNOS preparation, formation of [^{15}N]nitrate and [^{15}N]nitrite was found to depend linearly on incubation time for at least 10 min (*see* **Fig. 6A**) and on eNOS concentrations up to 45 μg/mL (data not shown). From these experiments, mean specific eNOS activity is calculated as 0.41 nmol [^{15}N]nitrate/min × mg eNOS and 0.48 nmol [^{15}N]nitrite/min × mg eNOS. Thus, the total mean specific eNOS activity amounts to 0.89 nmol ^{15}·NO/min × mg eNOS. This value is comparable with that declared by the supplier (i.e., 1.3 nmol ·NO/min × mg eNOS, as obtained by means of the oxyhemoglobin assay. By using the same GC-MS nitrite/nitrate assay, we have measured a specific

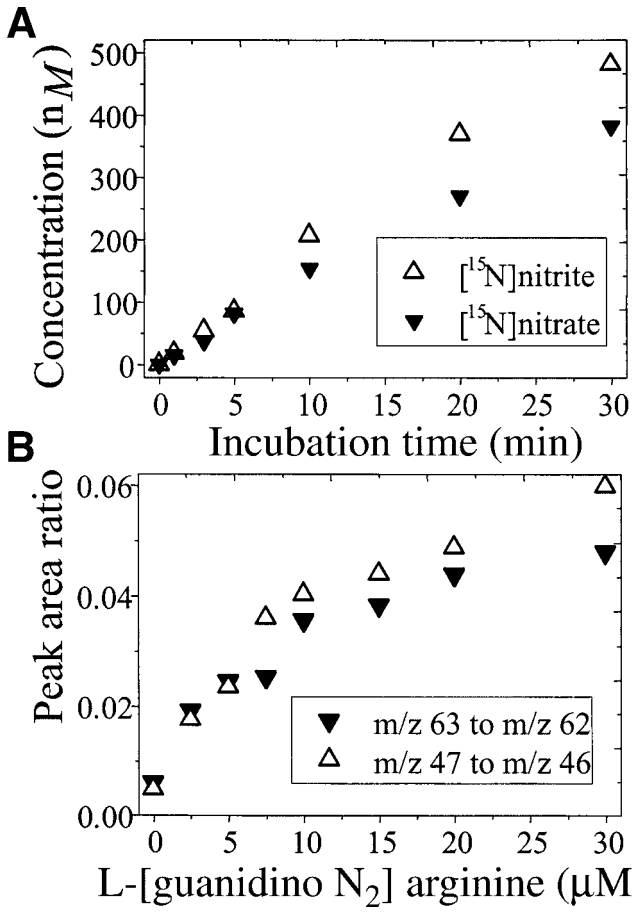

Fig. 6. **(A)** Dependence of eNOS-catalyzed (45 μg/mL) formation of [^{15}N]nitrite and [^{15}N]nitrate from L-[*guanidino*-$^{15}N_2$]arginine (20 μ*M*) on the incubation time. **(B)** Dependence of [^{15}N]nitrite and [^{15}N]nitrate formation (expressed as peak area ratio of *m/z* 47 to *m/z* 46 and of *m/z* 63 to *m/z* 62, respectively) on L-[*guanidino*-$^{15}N_2$]arginine concentration (range: 0–30 μ*M*) after an incubation time of 10 min with eNOS (45 μg/mL).

activity for an isolated recombinant rat neuronal NOS (nNOS) of about 280 nmol ^{15}NO/min × mg nNOS ***(9)***, which is approx 300 times higher than that of the recombinant bovine eNOS.

To investigate the effect of NOS inhibitors (*see* **Note 9**) on NOS-dependent formation of [^{15}N]nitrite and [^{15}N]nitrate, proceed as follows. Find optimal conditions for incubation time and NOS concentration (*see* above). Use L-[*guanidino*-$^{15}N_2$]arginine at fixed concentrations of 0, 2.5, 5, 7.5, 10, 12.5,

15, 20, 30, and 40 μ*M*. Measure NOS activity in the absence and in the presence of an NOS inhibitor at varying appropriate concentrations (e.g., 1, 2, 5, 10, and 30 μ*M* [e.g., in quadruplicate]). Determine [^{15}N]nitrite and [^{15}N]nitrate concentrations, calculate initial NOS velocities, and determine inhibitory mechanism and constants (e.g., by primary and secondary Lineweaver–Burk or Hanes plots using mean specific NOS activities) ***(9)***.

3.3.2. Enzyme Assay of Cellular NOS

3.3.2.1. Enzyme Assay of Endothelial NOS

The above-described assay for purified, isolated NOS preparations is adaptable to measure NOS activity in whole cells ***(10)***. Required modifications include concentration of L-[*guanidino*-$^{15}N_2$]arginine and NOS inhibitors, incubation time, and other experimental conditions such as preincubation, stimulation, and need of cofactors. Usually, assessment of NOS activity in whole cells requires considerably higher concentrations of L-[*guanidino*-$^{15}N_2$]arginine (e.g., 1 m*M*) and of NOS inhibitors (e.g., > 5 μ*M*) and considerably longer incubation times (e.g., 3–24 h) ***(10)***.

3.3.2.2. Enzyme Assay of Platelet NOS

1. Prepare platelet-rich plasma (PRP) by centrifugation of citrated blood (200*g*, 15 min) and platelet poor plasma (PPP) by centrifugation (400*g*, 15 min) of the remaining blood.
2. Pipet 250-μL aliquots of PRP in aggregometer cuvets and put them in the instrument thermostated at 37°C. Add a small aliquot (e.g., 10 μL) of an aqueous solution of L-[*guanidino*-$^{15}N_2$]arginine to achieve a final concentration of 1 m*M* and incubate for 2 min.
3. Induce platelet aggregation by adding a small aliquot of an aqueous solution of collagen to achieve relevant concentrations (e.g., 0–25 μg/mL) and monitor light transmission toward PPP (e.g., for 3–5 min).
4. Take 100-μL aliquots from the cuvets and pipet them into 400-μL aliquots of ice-cold acetone. Store the samples at –20°C.
5. Derivatize by adding 10-μL aliquots of PFB-Br and incubating appropriately.
6. Extract reaction products with small volumes of toluene (e.g., 100–300 μL).

Maximum platelet aggregation is induced by 1 μg/mL of collagen (*see* **Fig. 7A**). **Figure 7B** shows that platelets exhibit NOS activity, with maximum [^{15}N]nitrite formation occurring at 0.5 μg/mL of collagen.

3.4. Measurement of NOS Activity In Vivo

In principle, the above-described protocol for the measurement of NOS activity in vitro can be applied to assess NOS activity in vivo, in animals and in humans, preferably by using L-[*guanidino*-$^{15}N_2$]arginine ***(9,11)***. Because only

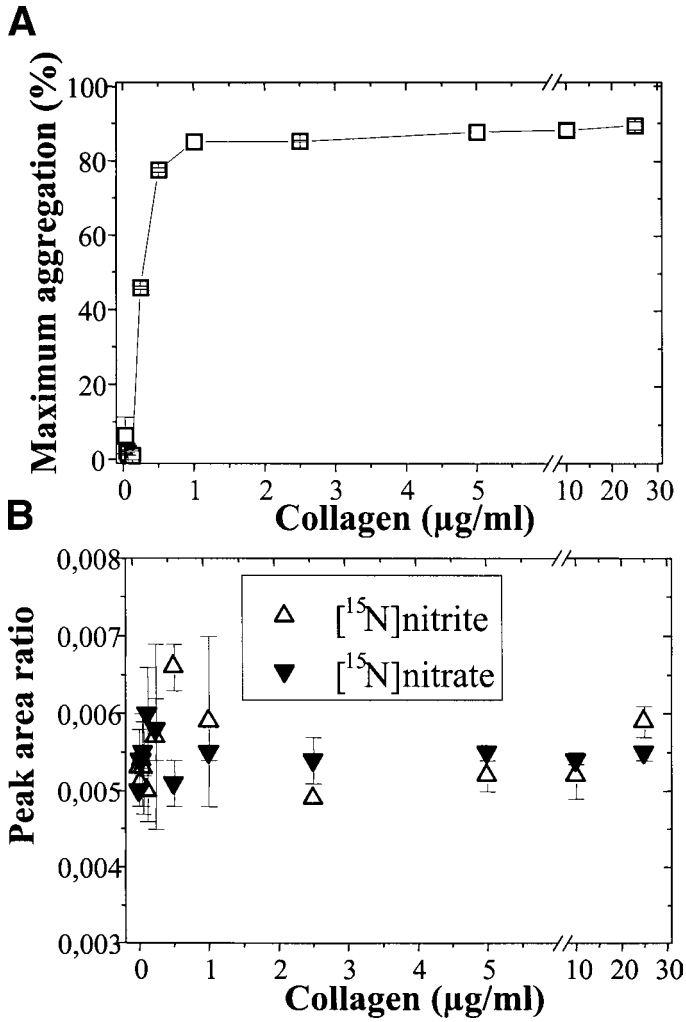

Fig. 7. **(A)** Maximum aggregation and **(B)** [^{15}N]nitrite and [^{15}N]nitrate formation in platelet-rich plasma preincubated for 2 min with L-[*guanidino*-$^{15}N_2$]arginine (1 m*M*). Aggregation was induced by collagen at the indicated concentrations and monitored for 3–5 min. Data are shown as mean ± SEM from duplicate incubations.

a small portion of L-arginine is metabolized via the ·NO pathway, large amounts of L-[*guanidino*-$^{15}N_2$]arginine may be required and relatively low enrichment of [^{15}N]nitrite and [^{15}N]nitrate may be expected. In addition, intake of foods rich in nitrite and nitrate should be avoided. Whole-body NOS activity is best assessed by measuring nitrate and nitrite in 24-h collected urine. If this is not possible, shorter collection intervals can be chosen. Nitrate and nitrite excre-

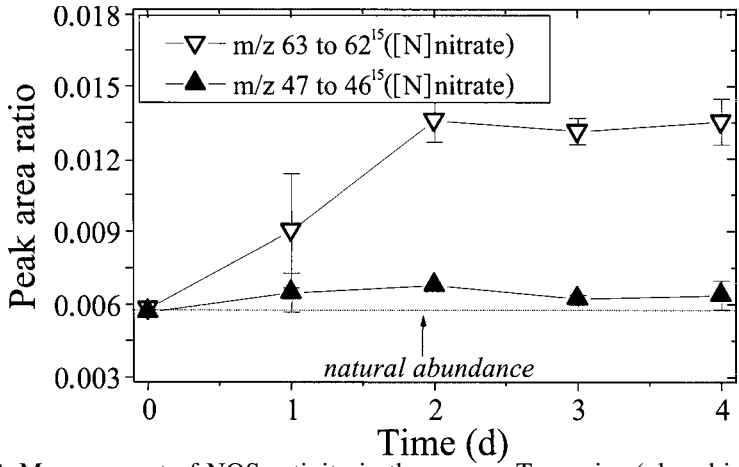

Fig. 8. Measurement of NOS activity in the mouse. Two mice (placed in a metabolic cage) received L-[*guanidino*-$^{15}N_2$]arginine in drinking water (10 mg/100 mL) for 4 d. Twenty-four-hour urine was collected and the peak area ratios of *m/z* 63 to *m/z* 62 ([^{15}N]nitrate to [^{14}N]nitrate) and of *m/z* 47 to *m/z* 46 ([^{15}N]nitrite to [^{14}N]nitrite) was determined by GC-MS in 100-µL urine aliquots. Data are shown as mean ± SEM. The horizontal dotted line shows the values of the peak area ratios for the natural abundances of [^{15}N]nitrite and [^{15}N]nitrate as measured by GC-MS (approx 0.0056 each).

tion should be corrected for creatinine excretion. Age dependence (*see* **Note 10**) and circadian rhythmicity of NOS activity must be considered ***(12)*** (*see* **Subheading 3.4.1.**). Use of circulating nitrite and nitrate to measure whole-body NOS activity is a less reliable method and may overlook important findings ***(13)***. On the other hand, however, short-lasting changes in NOS activity are best assessed by measuring circulating nitrite ***(14,15)***.

3.4.1. Measurement of NOS Activity in Animals

1. Adapt the animals of appropriate age (*see* **Note 10**); for example, for mice, for at least 2 d in metabolic cages in the housing facilities of the laboratory.
2. During this time, the animals are receiving normal chow and plain tap water ad libitum.
3. One day before starting of the experiment, collect urine for 24 h.
4. Change the drinking water to L-[*guanidino*-$^{15}N_2$]arginine-containing drinking water (e.g., 10 mg/100 mL).
5. Collect 24-h urine for several days.
6. Derivatize 100-µL aliquots of urine and analyze by GC-MS.
7. Continue urine collection until a constant peak area ratio of *m/z* 63 to 62 is achieved.

Figure 8 shows the profiles of the peak area ratios of *m/z* 63 to *m/z* 62, and of *m/z* 47 to *m/z* 46 in urine of mice that received L-[*guanidino*-$^{15}N_2$]arginine in

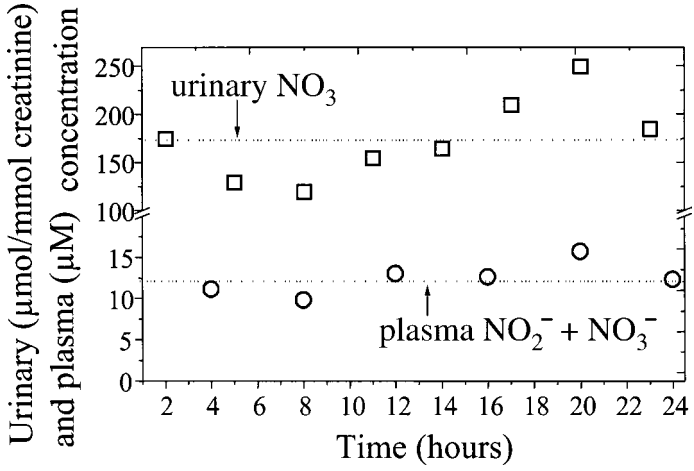

Fig. 9. Diurnal variation for urinary nitrate measured by GC-MS (open squares, $n = 8$ ***[12]***) and plasma nitrite+nitrate measured by the Griess assay (open circles; $n = 9$ ***[13]***) in healthy humans. Data are presented as mean values taken from Bode-Böger et al. ***(12)*** and Elherik et al. ***(13)***. The horizontal lines indicate the zero point of the corresponding wave functions.

drinking water. Both peak area ratios increased clearly above the respective values for the natural abundances of [^{15}N]nitrite and [^{15}N]nitrate after L-[*guanidino*-$^{15}N_2$]arginine administration. The peak area ratio of *m/z* 63 to *m/z* 62 reached and kept a constant value at d 2, 3, and 4. This animal model can be used to measure NOS activity in different conditions.

3.4.2. Measurement of NOS Activity in Humans

3.4.2.1. Use of L-[*Guanidino*-$^{15}N_2$]Arginine

By using this GC-MS methodology and by infusing L-[*guanidino*-$^{15}N_2$]arginine into fasted human volunteers (given as a priming dose of 10 μmol/kg and then at a constant dose of 10 μmol/kg/h), Rhodes et al. ***(8)*** have shown that the L-arginine/˙NO pathway is the major source of plasma nitrite. Over the 5-h infusion period, enrichment of [^{15}N]nitrite in plasma increased to 6.7% at 1 h, to 8.1% at 3 h, and to 8.3% at 5 h; similar enrichment values were also observed for plasma L-[*guanidino*-$^{15}N_2$]arginine ***(8)***.

3.4.2.2. Circadian Rhythmicity of NOS Activity

Systemic ˙NO production rates can be assessed noninvasively by determining urinary concentrations of nitrate ***(16)***. Circadian rhythmicity of NOS activity in humans can be successfully investigated by measuring nitrate concentrations in consecutively collected urine fractions for 24 h (*see* **Fig. 9**). Urine samples are aliquoted (e.g., 100 or 1000 μL), the internal standards are added (e.g., 10-μL

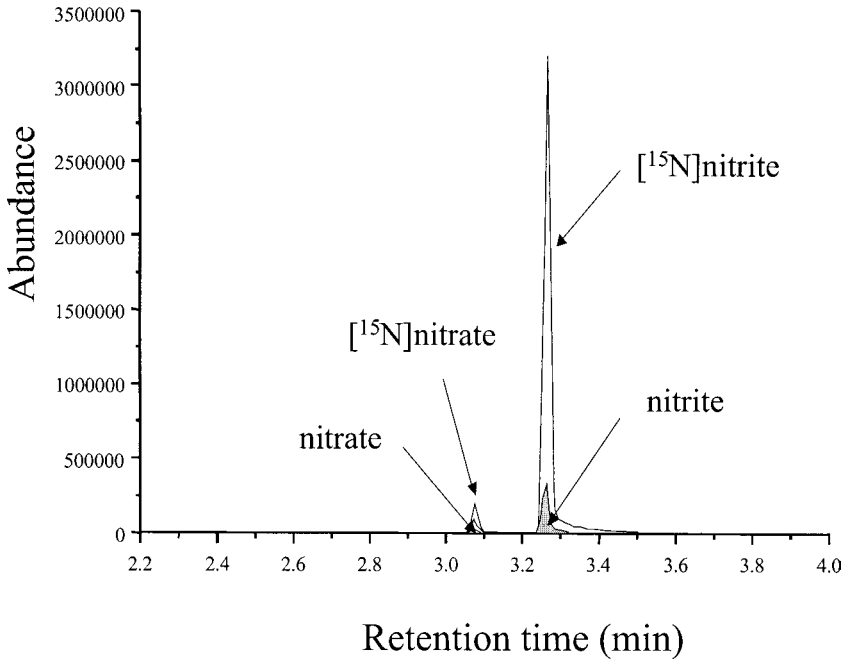

Fig. 10. A typical partial chromatogram from the simultaneous GC-MS analysis in human plasma of nitrate (SIM of *m/z* 62 and *m/z* 63; retention time, 3.08 min) and of nitrite (SIM of *m/z* 46 and *m/z* 47; retention time, 3.27 min) in the NICI mode. In this sample, the concentrations of the internal standards (open peaks) were 80 μ*M* each. Endogenous nitrite and nitrate (solid peaks) concentrations were 8.2 and 32.1 μ*M*, respectively. GC-MS instrument: Hewlett-Packard MS Engine.

aliquots of a stock solution containing 4000 μ*M* of [^{15}N]nitrate and 40 μ*M* of [^{15}N]nitrite) and stored at –20°C until further analysis.

3.4.2.3. Long-Term Measurement of NOS Activity

A similar protocol can be used to investigate systemic ·NO production rates by measuring nitrite and nitrate in 24-h collected urine samples for long period of time (i.e., for several days or weeks). In this case, urine should be collected in polypropylene bottles containing EDTA and 4-hydroxy-tempo (each at an approximate concentration of 1 m*M*). During urine collection, polypropylene bottles should be stored in a refrigerator at or below 4°C. Urine samples are aliquoted (e.g., 100 μL), the internal standards are added (e.g., 10-μL aliquots of a stock solution containing 4000 μ*M* [^{15}N]nitrate and 40 μ*M* [^{15}N]nitrite and stored at –20°C until GC-MS analysis (*see* **Fig. 10**).

Healthy humans with an uncontrolled nitrate diet excrete into the urine approx 100 μmol nitrate/mmol creatinine or 1200 μmol nitrate/24 h, and 0.5 μmol

nitrite/mmol creatinine or 5 μmol nitrite/24 h ***(16)***. The plasma concentrations amount to approx 68 μ*M* for nitrate and 4 μ*M* for nitrite. A standardized low-nitrate diet may considerably reduce urinary and plasma values both of nitrate and nitrite ***(16)***.

3.4.2.4. Short-Term Measurement of NOS Activity

The most sensitive and reliable method of measuring short-lasting changes of NOS activity is measuring of circulating nitrite ***(14,15)***. This protocol permits investigations of effects of growth hormone on ·NO release by infusing L-arginine ***(14)***.

1. After an overnight fast, the subjects rest in the supine position for at least 30 min before the start of L-arginine intravenous infusion.
2. Infuse an L-arginine solution in physiological saline (e.g., Fresenius, Bad Homburg, Germany; 30 g in 150 mL, pH 6.5; *see* **Note 11**) into an antecubital vein via an indwelling needle during 30 min.
3. Collect blood samples before (e.g., 30, 15, and 1 min) and after the start (e.g., 10, 20, 30, 40, 60, 90, and 120 min) of the L-arginine infusion.
4. Generate plasma or serum by immediate centrifugation (800*g*, 10 min, 2°C).
5. Add to 1-mL plasma or serum aliquots the internal standard [^{15}N]nitrite (e.g., 10 μL of a 400-μ*M* solution of sodium [^{15}N]nitrite in distilled water).
6. Generate ultrafiltrate by centrifugation (e.g., 1200*g*, 15 min, 2°C; Centrisart I cartridges, pore size 4 μm, cutoff 20 kDa; Sartorius, Göttingen, Germany).
7. Derivatize 100-μL aliquots and extract with 300-μL aliquots of toluene.

Using this protocol, typically plasma nitrite levels increase immediately upon infusion start, with concentration-time profiles depending on the experimental conditions ***(14)***.

3.4.3. Quality Control for Urinary and Circulating Nitrate and Nitrite

Analyze study urine (plasma/serum) samples alongside each three quality control (QC1, QC2, QC3) urine (plasma/serum) samples. For this purpose, choose a pooled urine collected for 24 h or pooled plasma or serum of medium nitrate concentrations (e.g., 400 μ*M* for urine and 40 μ*M* for plasma or serum) ***(7,17,18)***. The concentration of the internal standard [^{15}N]nitrate to be added to all study and QC urine (plasma/serum) samples should be 400 (40) μ*M*. This permits accurate quantitation of nitrate in a wide concentration range (i.e., between 50 [15] μ*M* and 2000 or even 4000 [120] μ*M*).

1. Analyze QC1 sample without external addition of nitrate.
2. Spike QC2 with 200 (20) μ*M* of nitrate.
3. Spike QC3 sample with 400 (40) μ*M* of nitrate.
4. Analyze QC samples in duplicate, study samples simply.
5. Determine recovery (in %) and imprecision (relative standard deviation [RSD] in %) from the QC samples (*see* **Note 12**); frequently, instead of recovery and imprecision, the terms accuracy and precision, respectively, are used.

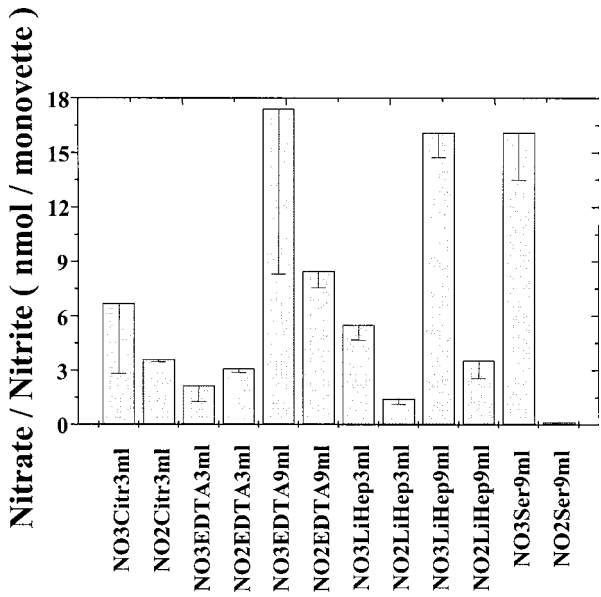

Fig. 11. Nitrite (NO2) and nitrate (NO3) content of various commercially available monovettes (Sarstedt, Germany) as measured by GC-MS. Each of the five monovettes of the volumes indicated (i.e., 3 mL and 9 mL) were filled with distilled water, shaken, and allowed to stay at room temperature for 10 min. Aliquots (100 µL) of the solutions and of distilled water were spiked with a mixture of [^{15}N]nitrite and [^{15}N]nitrate (10 µ*M* each), derivatized and analyzed by GC-MS. The nitrite and nitrate content of the monovettes was calculated by subtracting the nitrite and nitrate content of the distilled water used. Values are presented as mean ± SEM. Abbreviation of the monovettes: Citr, citrate; LiHep, lithium heparin; Ser, serum.

6. Recovery and imprecision values should be close to 100% and below 10%, respectively ***(17)***.
7. Define own values for recovery and imprecision for the QC samples (e.g., recovery ≥ 95 ± 5 %; RSD ≤ 10%).
8. Consider only those data from study samples, the corresponding QC samples of which fulfill these criteria; otherwise, repeat analysis of study and QC samples.

Establish QC systems for nitrite in urine, plasma or serum and in other biological fluids, considering the respective expected concentrations of nitrite.

3.4.4. Contribution of Monovettes to Endogenous Nitrite and Nitrate

Commercially available monovets containing EDTA or citrate but not lithium heparin as anticoagulating agents may contain considerable amounts of nitrite and nitrate, which may significantly contribute to endogenous levels (*see* **Fig. 11**) ***(19)***. Because the contribution of nitrite present in monovettes will depend on

the blood volume taken, this contribution may vary greatly and lead to erroneous plasma nitrite levels. It is, therefore, recommended to draw the same volume of blood. It can be calculated that when 3-mL EDTA and 3-mL citrate monovettes are used, their nitrite content would contribute by about 1 μ*M* to endogenous plasma nitrite, which is of the same order of magnitude. By contrast, monovette-derived nitrate will not considerably contribute to endogenous nitrate because of its relatively high endogenous level. The monovettes should be tested prior to use. With respect to circulating nitrite, use of serum monovettes is recommended. Nevertheless, serum should be generated under conditions not permitting significant oxidation of nitrite to nitrate. Thus, venous blood is collected into serum monovettes and centrifuged at 2°C ***(20)***.

4. Notes

1. The element nitrogen (N) consists of two stable, naturally occurring isotopes (i.e., ^{14}N and ^{15}N), with a natural abundance of 99.635% and 0.365%, respectively. The element oxygen (O) consists of three stable, naturally occurring isotopes (i.e., ^{16}O, ^{17}O, and ^{18}O), with a natural abundance of 99.759%, 0.037%, and 0.204%, respectively. Thus, naturally occurring nitrite and nitrate contain these isotopes. When monitoring the ions *m/z* 46, 47, 62, and 63, the ^{18}O isotope does not contribute to them. Theoretically, the ratios of the abundances of [^{15}N]nitrite to [^{14}N]nitrite and of [^{15}N]nitrate to [^{14}N]nitrate can be calculated ***(21)*** and amount to 0.00442 and 0.00479, respectively. These ratios are constant; that is, they do not depend on the concentration of nitrite and nitrate in a certain matrix. However, for maximum sensitivity, chemicals, solutions, and materials of low nitrate and nitrite should be used.
2. PFB–NO_2 and PFB–ONO_2 coelute on the DB-5 MS capillary colum (DB-5 MS, 30 m × 0.25 mm inner diameter, 0.25 μm film thickness, from J & W Scientific, Rancho Cordova, CA, USA).
3. Use commercially available salts of [^{15}N]nitrate, [^{15}N]nitrite, and L-[*guanidino*-$^{15}N_2$]arginine of the highest isotopic purity available. For quantitative measurements, prepare stock solutions (each 8 m*M*) of unlabeled nitrate and nitrite as well as of [^{15}N]nitrate and [^{15}N]nitrite in distilled water and dilute with distilled water appropriately when needed. For simultaneous quantitation of nitrite and nitrate, prepare a stock solution containing both anions at appropriate concentrations.
4. PFB-Br is corrosive and an eye irritant. Inhalation and contact with skin and eyes should be avoided. All work should be performed in a well-ventilated fume hood. After GC-MS analysis of the samples, remove and combine toluene phases in an appropriate container. Leave all glassware open in a fume hood until no liquid is visible. Do not dispose of the remaining PFB-Br into wash basin.
5. Use toluene to clean glass syringes. The injector temperature should not exceed 200°C because PFB–NO_2 degrades with increasing injector temperature, leading to loss of sensitivity.

6. PFB–ONO_2 and PFB–NO_2 are completely separated on capillary columns such as Optima 17 and differentially ionize in the ion source of GC-MS instruments under NICI conditions. Detection of nitrate and nitrite is superior over detection of other ions formed by NICI of PFB–NO_2 and PFB–ONO_2 that contain carbon atoms. The number and the natural abundance of ^{15}N atoms (0.366%) and ^{17}O atoms (0.037%) is considerably lower than that of ^{13}C (1.107%) in the molecules of PFB–NO_2 and PFB–ONO_2. The contribution of *m/z* 47 and 63 originating from the ^{15}N isotope of nitrite and nitrate to *m/z* 47 and 63 of the internal standards [^{15}N]nitrite and [^{15}N]nitrate, respectively, is negligible. The consequences of this are linear calibrations over a much larger concentration range and simple calculation of nitrite and nitrate concentrations.
7. Take special precautions to avoid contamination of samples, solutions, materials, and instruments by [^{15}N]nitrite and [^{15}N]nitrate from other sources. A special workplace is recommended.
8. Prepare fresh solutions of NADPH, H_4B, FAD, FMN, L-[*guanidino*-$^{15}N_2$]arginine, and all NOS inhibitors in distilled water. Dilute calmodulin (1 mg) in distilled water (1 mL), aliquot, and store frozen.
9. L-Arginine analogs containing nitro groups, such as L-NNA, and other nitro groups containing compounds, such as 3-nitrotyrosine ***(19)***, do not interfere with the measurement of nitrite and nitrate when analyzed as their PFB derivatives ***(7)***.
10. The endogenous ˙NO production rate is greatly decreasing in the first months of human life ***(22)***, and this may also be expected for animals.
11. Check the pH value of the L-arginine solution prior to infusion.
12. By definition, recovery [100·mean concentration measured in QC2 or QC3) minus (mean concentration measured in QC1)/added concentration QC2 or QC3] applies to QC2 and QC3. Imprecision [100·(standard deviation divided by the corresponding mean concentration of QC1 or QC2 or QC3)] applies to all QC samples. For details regarding method validation and quality control, *see* the literature in **refs. *23*** and ***24***.

Acknowledgments

The expert laboratory assistance of I. Fuchs, M. T. Suchy, and A. Mitschke is gratefully acknowledged. The excellent technical assistance of F.-M. Gutzki in GC-MS is also gratefully acknowledged. This work was supported in part by the Deutsche Forschungsgemeinschaft (TS 60/2-1).

References

1 Kelm, M. and Schrader, J. (1990) Control of coronary vascular tone by nitric oxide. *Circ. Res.* **66,** 1561–1570.
2 Hibbs, J. B., Jr., Westenfelder, C., Taintor, R., et al. (1992) Evidence for cytokine-inducible nitric oxide synthesis from L-arginine in patients receiving interleukin-2 therapy. *J. Clin. Invest.* **89,** 867–877.
3. Marletta, M. A. (1993) Nitric oxide synthase structure and mechanism. *J. Biol. Chem.* **268,** 12,231–12,234.

4. Pou, S., Pou, W. S., Bredt, D. S., et al. (1992) Generation of superoxide by purified brain nitric oxide synthase. *J. Biol. Chem.* **267,** 24,173–24,1176.
5 Ellis, G., Adatia, I., Yazdanpanah, M., et al. (1998) Nitrite and nitrate analyses: a clinical biochemistry perspective. *Clin. Biochem.* **31,** 195–220.
6 Wu, H.-L., Chen, S.-H., Lin, S.-J., et al. (1983) Gas chromatographic determination of inorganic anions as pentafluorobenzyl derivatives. *J. Chromatogr.* **269,** 183–190.
7 Tsikas, D. (2000) Simultaneous derivatization and quantification of the nitric oxide metabolites nitrite and nitrate in biological fluids by gas chromatography/mass spectrometry. *Anal. Chem.* **72,** 4064–4072.
8 Rhodes, P., Leone, A. M., Francis, P. L., et al. (1995) The L-arginine:nitric oxide pathway is the major source of plasma nitrite in fasted humans. *Biochem. Biophys. Res. Commun.* **209,** 590–596.
9 Tsikas, D., Sandmann, J., Savva, A., et al. (2000) Assessment of nitric oxide synthase activity in vitro and in vivo by gas chromatography–mass spectrometry. *J. Chromatogr. B* **742,** 143–153.
10. Böger, R. H., Sydow, K., Borlak, J., et al. (2000) LDL cholesterol upregulates synthesis of asymmetrical dimethylarginine in human endothelial cells. Involvement of *S*-adenosylmethionine-dependent methyltransferases. *Circ. Res.* **87,** 99–105.
11 Tsikas, D., Sandmann, J., Lueßen, P., et al. (2001) *S*-Transnitrosylation of albumin in human plasma and blood in vitro and in vivo in the rat. *Biochem. Biophys. Acta* **1546,** 422–434.
12. Bode-Böger, S. M., Böger, R. H., Kielstein, J. T., et al. (2000) Role of endogenous nitric oxide in circadian blood pressure regulation in healthy humans and in patients with hypertension or atherosclerosis. *J. Invest. Med.* **48,** 125–132.
13 Elherik, K., Khan, F., McLaren, M., et al. (2002) Circadian variation in vascular tone and endothelial cell function in normal males. *Clin. Sci.* **102,** 547–552.
14. Bode-Böger, S. M., Böger, R. H., Löffler, M., et al. (1999) L-Arginine stimulates NO-dependent vasodilation in healthy humans—effect of somatostatin pretreatment. *J. Invest. Med.* **47,** 43–50.
15 Kelm, M., Preik-Steinhoff, H., Preik, M., et al. (1999) Serum nitrite sensitively reflects endothelial NO formation in human forearm vasculature: evidence for biochemical assessment of the endothelial L-arginine–NO pathway. *Cardiovasc. Res.* **41,** 765–772.
16 Tsikas, D., Böger, R. H., Bode-Böger, S. M., et al. (1994) Quantification of nitrite and nitrate in human urine and plasma as pentafluorobenzyl derivatives by gas chromatography–mass spectrometry using their ^{15}N-labelled analogs. *J. Chromatogr. B* **661,** 185–191.
17. Tsikas, D., Gutzki, F.-M., and Frölich, J. C. (2002) Quantitation of members of the L-arginine/nitric oxide (NO) pathway by gas chromatography–mass spectrometry. *Recent Res. Devel. Anal. Biochem.* **2,** 1–27.
18 Becker, A. J., Ückert, S., Tsikas, D., et al. (2000) Determination of nitric oxide metabolites by means of the Griess assay and gas chromatography-mass spectrometry in the cavernous and systemic blood of healthy males and patients with

erectile dysfunction during different functional conditions of the penis. *Urol. Res.* **28,** 364–369.

19 Tsikas, D., Gutzki, F. M., Rossa, S., et al. (1997) Measurement of nitrite and nitrate in biological fluids by gas chromatography–mass spectrometry and by the Griess assay: problems with the Griess assay—solutions by gas chromatography–mass spectrometry. *Anal. Biochem.* **244,** 208–220.

20 Keimer, R., Stutzer, F. K., Tsikas, D., et al. (2003) Lack of oxidative stress during sustained therapy with isosorbid dinitrate and pentaerythrityl tetranitrate in healthy humans: a randomized, double-blind crossover study. *J. Cardiovasc. Pharmacol.* **41,** 284–292.

21. Beynon, J. H. (1960) *Mass Spectrometry and Its Application to Organic Chemistry*, Elsevier, Amsterdam.

22 Tsukahara, H., Hiraoka, M., Hori, C., et al. (1997) Age-related changes of urinary nitrite/nitrate excretion in normal children. *Nephron* **76,** 307–309.

23. Lawson, A. M., Gaskell, S. J., and Hjelm, M. (1985) Methodological aspects on quantitative mass spectrometry used for accuracy control in clinical chemistry. *J. Clin. Chem. Clin. Biochem.* **23,** 433–441.

24. Shah, V. P., Midha, K. K., Dighe, S., et al. (1992) Analytical methods validation: bioavailability, bioequivalence, and pharmacokinetic studies. *J. Pharm. Sci.* **81,** 309–312.

8

A Nonradioactive Assay for Nitric Oxide Synthase Activity in Tissue Extracts

Hazel Sutherland, Olga Zolle, Roba Khundkar, Alec W. M. Simpson, Jonathan C. Jarvis, and Stanley Salmons

Summary

We describe a fluorescence assay for nitric oxide synthase activity based on a new indicator, 4,5-diaminofluorescein (DAF-2). The method offers the advantage of being safer and more convenient than the citrulline radioassay in common use. The rapid and irreversible binding of DAF-2 to oxidized nitric oxide (NO) enables NO production to be measured in real time. The protocol is applied to the measurement of nitric oxide synthase in crude extracts of skeletal muscle.

Key Words: DAF-2; skeletal muscle; nitric oxide (NO); nitric oxide synthase (NOS); NO donor; NOS inhibitor.

1. Introduction

The activity of nitric oxide synthase (NOS), the enzyme that synthesizes nitric oxide (NO), is conventionally measured in tissue by the citrulline assay ***(1)***. However, this assay involves the use of radioactive material and does not allow the production of NO to be followed in real time. We describe a method based on the citrulline assay as described by Reiser ***(2)***, in which the radioactive component is replaced by a fluorescent indicator that can measure directly the amount of NO produced in the tissue. We have used the procedure to measure NOS activity in crude extracts derived from skeletal muscle and this is the context in which the methods will be described ***(3)***. The recently developed fluorescent indicator 4,5-diaminofluorescein (DAF-2) and the membrane-permeable DAF-2 diacetate (DAF-2 DA) bind rapidly and irreversibly to oxidized NO under neutral conditions to form a green-fluorescing triazole compound, DAF-2T (*see* **Fig. 1**). This can be measured spectrofluorometrically ***(4,5)*** with high sensitivity, the detection limit being 5 n*M*.

From: *Methods in Molecular Biology, vol. 279: Nitric Oxide Protocols: Second Edition*
Edited by: A. Hassid © Humana Press Inc., Totowa, NJ

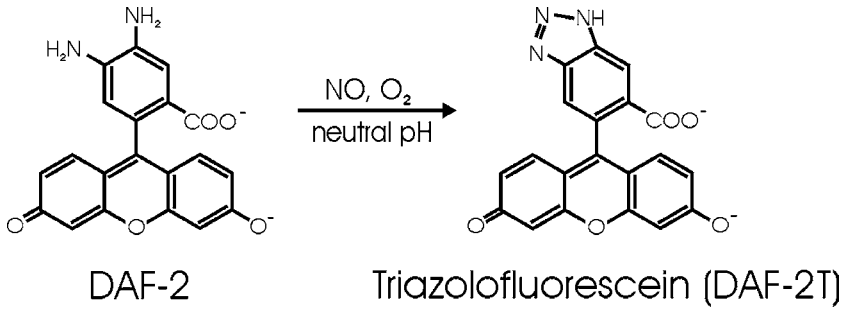

Fig. 1. 4,5-Diaminofluorescein (DAF-2) binds to NO in the presence of oxygen to produce a fluorescent product, triazolofluorescein (DAF-2T).

Both DAF-2 DA and DAF-2 have been receiving increasingly widespread use in the measurement of NOS activity via real-time production of NO (for references, *see* **ref. *6***). To date, this technique has been applied only to isolated cells. The present assay employs DAF-2 to measure real-time NO production in whole-muscle extracts, and this was achieved in spite of the presence of fluorescent substrates and cofactors that are necessary to maintain the NOS activity in the muscle.

Much remains to be learned about the functional significance of NO within muscle. This assay can be used in conjunction with specific NOS blockers to elucidate the roles of the three NOS isoforms that are expressed in skeletal muscle ***(9)***.

2. Materials (*see* Note 1)

2.1. Isolation Buffer

The isolation buffer consists of 50 m*M* Tris-HCl, pH 7.4, 1 m*M* EDTA, 0.5 m*M* PMSF, 1 m*M* iodoacetamide, 1 μ*M* leupeptin, 1 μ*M* pepstatin A. For 1 mL of isolation buffer, add 100 μL of each of the above stock solutions to 400 μL distilled water and store on ice until used (*see* **Note 2**). The buffer is prepared from the following stock solutions.

1. 500 m*M* Tris-HCl: Dissolve in distilled water and adjust pH to 7.4. Store at 4°C.
2. 10 m*M* Ethylene diaminetetraacetic acid (EDTA): Dissolve in distilled water. For EDTA to dissolve, the pH of the solution needs to be adjusted to between 7 and 8 with NaOH. Store at 4°C.
3. 5 m*M* Phenylmethyl sulfonylfluoride (PMSF): Dissolve in absolute ethanol and store frozen at –20°C; very unstable in water (50% hydrolyzed after 100 min at 25°C).
4. 10 m*M* Iodoacetamide: Dissolve in distilled water and store in a dark bottle at –20°C (photolabile).

5. 10 m*M* leupeptin: Dissolve in distilled water and store at 4°C for up to 1 wk or frozen at –20°C for up to 1 mo.
6. 10 μ*M* Pepstatin A: Dissolve in dimethyl sulfoxide (DMSO) or methanol and store at 4°C for up to 1 wk or frozen at –20°C for up to several months.

2.2. Assay Buffer

The assay buffer consists of 55 m*M* HEPES, 20 m*M* Tris-HCl, 2 m*M* L-arginine (*see* **Note 4**), 0.8 m*M* DTT, 0.4 m*M* EDTA, 0.8 μ*M* NADPH, 1 m*M* $MgCl_2$ ***(1)***; 1 m*M* $CaCl_2$, 10 μg/mL calmodulin ***(7)***, 0.8 μ*M* FMN, 6 μ*M* BH_4, 0.8 μ*M* FAD; 0.2 m*M* PMSF, 0.4 m*M* iodoacetamide, 0.4 μ*M* leupeptin, 0.4 μ*M* pepstatin A, 10 mg/mL muscle extract, 12 μ*M* DAF-2. Volumes added to make 1 mL are as follows: 50 μL HEPES; 40 μL Tris-buffer; 10 μL L-arginine; 50 μL DTT; 40 μL EDTA; 50 μL NADPH; 50 μL $MgCl_2$; 100 μL $CaCl_2$; 10 μL calmodulin; 40 μL FMN; 40 μL BH_4; 40 μL FAD; 40 μL PMSF; 40 μL iodoacetamide; 40 μL leupeptin; 40 μL pepstatin A; 100 μL muscle extract; 8 μL DAF-2. Adjust volume to 1 mL with distilled water. Store on ice until use (*see* **Note 2**). The buffer is made from the following stock solutions.

1. 1.1 *M N*-2-Hydroxyethylpiperazine-*N*'-2-ethane-sulfonic acid (HEPES): Dissolve in distilled water and store at room temperature.
2. 500 m*M* Tris-HCl, pH 7.4: Solution prepared and stored as in **step 1** of **Subheading 2.1.**
3. 200 m*M* L-Arginine: Dissolve in distilled water and store frozen at –20°C.
4. 16 m*M* Dithiothreitol (DTT): Dissolve in distilled water and store in the short term at 4°C or in the longer term (more than 3 mo) at –20°C.
5. 10 m*M* EDTA. Solution prepared and stored as in **step 2** of **Subheading 2.1.**
6. 16 μ*M* NADPH: Dissolve in distilled water and store frozen at –20°C for over 2 mo.
7. 10 m*M* $MgCl_2$: Dissolve in distilled water and store at 4°C.
8. 10 m*M* $CaCl_2$: Dissolve in distilled water and store at 4°C.
9. 1 mg/mL Calmodulin: Dissolve in distilled water and store frozen at –20°C for up to 2 mo or at –70°C for up to 4 mo.
10. 20 μ*M* Riboflavin monophosphate (FMN): Dissolve in distilled water and adjust pH to 6. Store in a dark bottle (photolabile) at –20°C.
11. 150 μ*M* (6*R*)-5,6,7,8-Tetrahydrobiopterin (BH_4): Dissolve in distilled water, after which it can be stored at –70°C for several months. It is completely destroyed within 90 min at room temperature.
12. 20 μ*M* Flavin–adenine dinucleotide (FAD): Dissolve in distilled water and adjust pH to 7.0. Store as for FMN, in a dark bottle at –20°C.
13. 5 m*M* PMSF; 10 m*M* iodoacetamide; 10 μ*M* leupeptin; 10 μ*M* pepstatin A . Stock solutions as for the isolation buffer (**steps 3–6** of **Subheading 2.1.**).
14. 1.5 m*M* DAF-2: Dilute in dimethyl sulfoxide (DMSO). Store at 4°C, in a dark bottle in the presence of nitrogen (*see* **Note 3**).
15. NO donor: (±)-*S*-nitroso-*N*-acetylpenicillamine (SNAP).

3. Method

1. To prepare the crude muscle extracts, frozen muscle samples, stored previously at –70°C are first ground to a powder under liquid nitrogen in a precooled pestle and mortar. Place the muscle powder (approx 100 mg) in a precooled 1.5-mL Eppendorf vial and weigh. Add nine times this weight in volume of ice-cold isolation buffer to give a concentration of 100 mg/mL. Mix each sample thoroughly with a benchtop vortex mixer. Store samples on ice for immediate use or freeze them rapidly in liquid nitrogen for storage at –70°C.
2. In a dark room, add all of the components of the assay buffer (omitting only the muscle extract and DAF-2) to an Eppendorf vial and mix. Alternatively thaw a frozen aliquot of the assay buffer (*see* **Note 2**). Add to a quartz cuvet and record the fluorescence at 37°C with an excitation wavelength of 510 nm and an emission wavelength of 530 nm (bandwidth: 5 nm) (refer to **Note 5** for information on choice of wavelengths). Set the rate of the fluorescence count to two per second for 25 min. Stir the mixture throughout the procedure. When the baseline has stabilized (approx 3 min), add the muscle extract and the DAF-2. Record the fluorescence for the remainder of the 25 min.
3. In the presence of active NOS, the production of NO, and hence the level of fluorescence, will increase with time as it binds to DAF-2. The gradient of this increase is a measure of the NOS activity. This can be calculated by transferring the data from each assay to a spreadsheet application such as Microsoft Excel™.
4. To confirm that the rise in fluorescence is associated with the production of NO, add a NOS inhibitor, such as N^G-monomethyl-L-arginine monoacetate (L-NMMA) or N^G-allyl-L-arginine. This should produce a significant decrease in activity. Ensure that the concentration of the inhibitor is sufficiently high to block all three NOS isoforms. As an additional check, removal of the substrate, arginine, from the assay should likewise result in a significant drop in the production of NO.
5. To express the fluorescence counts in terms of NO production, the method must be calibrated with an NO donor, such as SNAP. Add the known concentrations of SNAP to the full assay buffer containing DAF-2 and measure the peak fluorescence. Subtract the value of fluorescence originating from the assay buffer alone from the mean data. This can be obtained at the start of each assay, before any muscle extract or DAF-2 is added. Under the conditions of this assay, the fluorescent counts corresponding to molarities of SNAP from 0.05 to 0.5 m*M* are found to fit a Boltzmann sigmoidal curve with the origin at zero. The equation for the best-fit sigmoidal curve can then be rearranged to convert readings of fluorescence from each of the assays into moles of SNAP or NO.
6. The NOS activity or rate of NO production is normally expressed as pmol NO/min/mg muscle. For each assay, divide the NO value by the time in minutes over which it was produced and then by the weight in milligrams of muscle added to each assay.

4. Notes

1. Many of the stock solutions used are extremely sensitive to light and heat. For this reason, we prepared aliquots, which could then be stored in the dark at a suitably low temperature.
2. To reduce pipetting errors, make up larger volumes of both the isolation buffer and the assay buffer (minus muscle and DAF-2), freeze in aliquots, and store in the dark in a freezer at –70°C. When the aliquots have been removed from the freezer, they should be stored in the dark on ice for as little time as possible. This also applies to the muscle samples, the DAF-2, and the SNAP solutions.
3. DAF-2 is supplied by Calbiochem in DMSO at a concentration of 5 m*M*. It is hydrolyzed in water, which results in an increase in the basal fluorescence from 4000 to more than 20,000 in a matter of days. It is readily oxidized and is photolabile and thermolabile. Either use DAF-2 neat (2.4 μL in 1 mL gives a concentration of 12 μ*M*) or dilute an aliquot with DMSO (100 μL of 5 m*M* in 234.56 μL DMSO gives a 1.5-μ*M* solution, of which 8 μL added to the assay produces a concentration of 12 μ*M*). We prefer to work with the 1.5-μ*M* solution because the larger volume can be pipetted more accurately. To eliminate oxidation, displace the air in the top of the bottle with nitrogen. Store at 4°C in a dark bottle.
4. L-Arginine is added to the assay at a concentration of 2 m*M*. This is greater than that used in previous NO assays [Hevel and Marletta ***(1)*** quoted values of 200 μ*M* to 1 m*M* in other studies.] Additional arginine does not produce an increase in fluorescence, suggesting that the reaction is not substrate limited under the conditions of this assay.
5. We used a Photon Technology International (PTI) Deltascan dual-excitation photometer. With the emission wavelength set at 530 nm (bandwidth: 5 nm), we performed an excitation scan of the isolation and assay buffer. The isolation buffer showed only a basal level of fluorescence, whereas the assay buffer showed high levels of fluorescence (*see* **Fig. 2**). Therefore, we performed an excitation scan of the assay buffer, adding each of the components in turn.

   NADPH and BH_4 fluoresced at 370 nm, FAD and FMN fluoresced at 370 and 450 nm, and, in addition, FMN fluoresced to a small extent at 280 nm. When DAF-2 and the NO donor SNAP were added to the assay buffer, a new fluorescent peak was observed at 510 nm, distinct from those emanating from the components of the buffer itself (*see* **Fig. 2**). We therefore chose 510 nm as the excitation wavelength for this procedure. The manufacturer's specifications for DAF-2 are that the maximum excitation is at 495 nm and maximum emission is 515 nm. However, because the components of the buffer fluoresced up to 500 nm, we were obliged to use an emission wavelength of 530 nm, which is longer than the manufacturer's stated optimum.
6. DMSO has a low surface tension, so use a Hamilton syringe rather than a Gilson pipet to draw up both the DAF-2 and SNAP solutions.
7. Three isoforms of NOS are expressed in muscle tissue. The neuronal isoform (nNOS) has been demonstrated in both the cytoplasm and the sarcolemma of muscle fibers. The endothelial isoform (eNOS) has been found to be closely

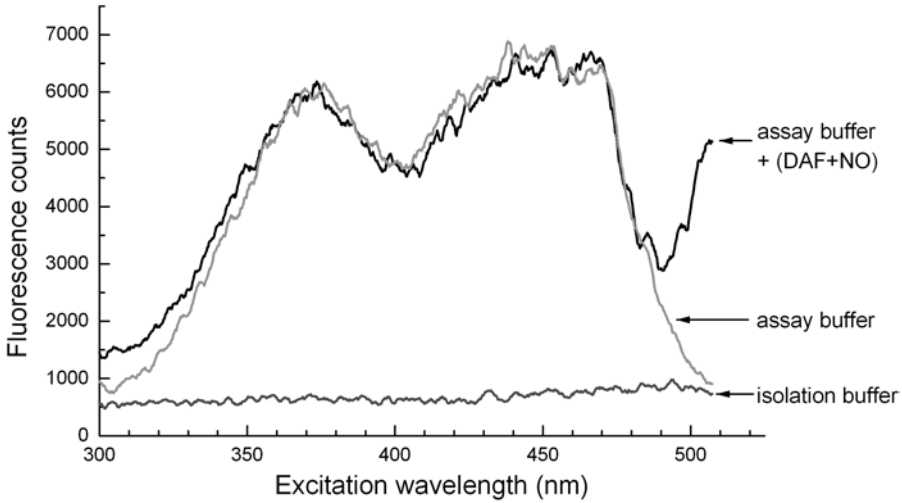

Fig. 2. Excitation wavelength scan (from 300 to 510 nm) for the isolation buffer and the assay buffer in the absence and presence of DAF-2 and the NO donor SNAP. Fluorescence was detected at 530 nm with a Photon Technology International (PTI) Deltascan Photometer at 37°C. Bandwidths were set at 5 nm. Fluorescence was recorded for scan steps of 1 nm and the data were smoothed with PTI software. (Reproduced from **ref. *3*** with permission.)

associated with vascular endothelium and muscle mitochondria ***(7,8)***. Under conditions of stress, skeletal muscle expresses the inducible isoform of NOS (iNOS) within capillaries, macrophages, and myocytes ***(9)***. The contribution of each isoform to overall NOS activity can be isolated by using a commercially available NOS blocker to inhibit the specific isoform. In this case, adjust the volume of water to allow for the addition of the blocker to the assay, maintaining the total assay volume at 1 mL.

8. 4,5-Diaminofluorescein, (DAF-2), N^G-monomethyl-L-arginine monoacetate (L-NMMA), N^G-allyl-L-arginine, and (–$^+$)-S-nitroso-*N*-acetylpenicillamine (SNAP) were purchased from Calbiochem-Novabiochem (UK) Ltd. (Beeston, UK). All other reagents were purchased from Sigma–Aldrich Company Ltd. (Dorset, UK).

5. Comment

Studies of NOS activity tend to focus on differences between tissues, the response to changing experimental conditions, and the contribution of the different isoforms. For these purposes it is the relative, rather than the absolute, levels of NOS activity that are of interest, and the fluorescent assay described here would appear to offer a satisfactory alternative to the existing radioactive assay. We feel less confident about the conversion of fluorescent counts to

absolute values of NO for several reasons. First, the standard curve obtained with SNAP is highly nonlinear. Second, we have assumed that under the nonequilibrium conditions of assaying the standards, SNAP dissociates fully on a mole-to-mole basis ***(10)***. Third, assay of standards takes place in aqueous solution and should be corrected for the efficiency with which NO binds to DAF-2 in the presence of biologic material ***(5)***. That efficiency is said to be 9.6% in the presence of biologic material but the concentration-dependence of this figure does not appear to have been determined. We look forward to seeing improved techniques for calibrating the fluorescence, definitive comparison of the fluorescence-based with the radioactivity-based assay, and further refinement of the fluorescent assay itself.

Acknowledgments

H.S. was supported by the British Heart Foundation (RG/97001). O.Z. was a Wellcome Prize Fellow (044516/Z/98). R.K. was supported by a Physiological Society Vacation Studentship.

References

1 Hevel, J. M. and Marletta, M. A. (1994) Nitric-oxide synthase assays. *Methods Enzymol.* **233,** 250–258.
2 Reiser, P. J., Kline, W. O., and Vaghy, P. L. (1997) Induction of neuronal type nitric oxide synthase in skeletal muscle by chronic electrical stimulation in vivo. *J. Appl. Physiol.* **82,** 1250–1255.
3 Sutherland, H., Khundkar, R., Zolle, O., et al. (2001) A fluorescence-based method for measuring nitric oxide in extracts of skeletal muscle. *Nitric Oxide* **5,** 475–481.
4 Kojima, H., Nakatsubo, N., Kikuchi, K., et al. (1998) Detection and imaging of nitric oxide with novel fluorescent indicators: diaminofluoresceins. *Anal. Chem.* **70,** 2446–2453.
5 Nakatsubo, N., Kojima, H., Kikuchi, K., et al. (1998) Direct evidence of nitric oxide production from bovine aortic endothelial cells using new fluorescence indicators: diaminofluoresceins. *FEBS Lett.* **427,** 263–266.
6 Nagano, T. and Yoshimura, T. (2002) Bioimaging of nitric oxide. *Chem. Rev.* **102,** 1235–1270.
7 Kobzik, L., Stringer, B., Balligand, J.-L., et al. (1995) Endothelial type nitric oxide synthase in skeletal muscle fibers: mitochondrial relationships. *Biochem. Biophys. Res. Commun.* **211,** 375–381.
8 Frandsen, U., Lopez-Figueroa, M., and Hellsten, Y. (1996) Localization of nitric oxide synthase in human skeletal muscle. *Biochem. Biophys. Res. Commun.* **227,** 88–93.
9 Thompson, M., Becker, L., Bryant, D., et al. (1996) Expression of the inducible nitric oxide synthase gene in diaphragm and skeletal muscle. *J. Appl. Physiol.* **81,** 2415–2420.
10. Southam, E. and Garthwaite, J. (1991) Comparative effects of some nitric oxide donors on cyclic GMP levels in rat cerebellar slices. *Neurosci. Lett.* **130,** 107–111.

9

Measurement of Nitric Oxide-Related Enzymes in the Brain by *In Situ* Hybridization

Olivier Braissant

Summary

Functional genomic increasingly requires the cell-specific localization of gene expression. The histological analysis of mRNA expression is performed by *in situ* hybridization (ISH), whereas proteins are detected by immunohistochemistry. ISH allows the rapid detection of any transcript with the same protocol provided that its cDNA is known. This is an advantage compared to immunohistochemistry, which necessitates the raise of specific antibodies and the test of different procedures depending on the antigens to detect. However, ISH is subject to multiple technical difficulties. We have developed a nonradioactive ISH protocol allowing the simultaneous coupling of immunohistochemistry to follow gene expression at the protein level on the same section as the mRNA detection. This chapter describes the neuronal nitric oxide synthase (nNOS), argininosuccinate synthetase (AS), and argininosuccinate lyase (AL) mRNA expression in the rat brain to illustrate the methods allowing the nonradioactive localization of transcripts by ISH, coupled to immunohistochemistry to identify the specific cell types of central nervous system (CNS) on the same section.

Key Words: *In situ* hybridization; brain; nitric oxide synthase (NOS); argininosuccinate synthetase (AS); argininosuccinate lyase (AL); tissue sections; nonradioactive; immunohistochemistry; gene expression; riboprobe; digoxigenin.

1. Introduction

The cell-specific localization of gene expression is increasingly used and most often a prerequisite to understand the role of complex multigenic pathways. *In situ* hybridization (ISH) for analyzing gene expression at the mRNA level allows the rapid detection of any transcript with the same protocol, provided that its cDNA is known. This is an advantage compared to immunohistochemistry, which necessitates the raise of specific antibodies and the test of different procedures (e.g., type of fixation), depending on the antigens to detect. However, ISH and the work with RNA on tissue section or whole organisms is subject to multiple technical difficulties ***(1–5)***.

From: *Methods in Molecular Biology, vol. 279: Nitric Oxide Protocols: Second Edition*
Edited by: A. Hassid © Humana Press Inc., Totowa, NJ

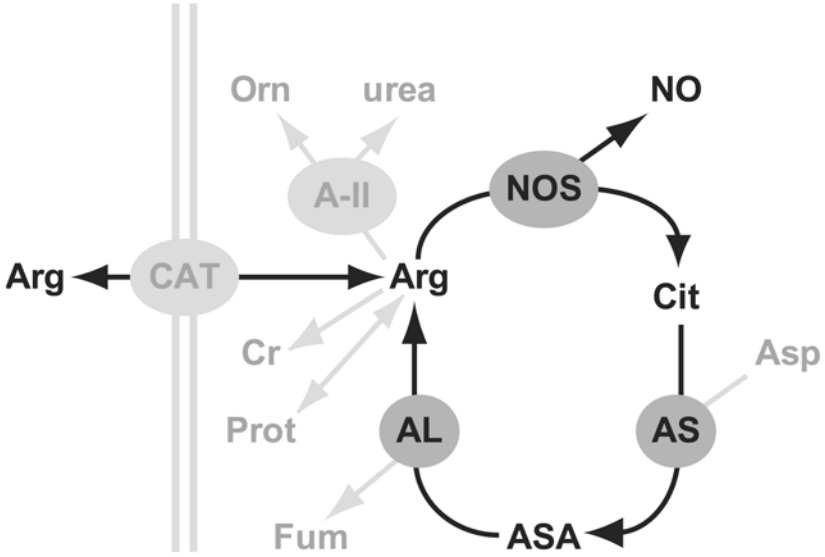

Fig. 1. The citrulline–NO cycle in the CNS. A-II: arginase II, AL: argininosuccinate lyase, Arg: arginine, AS: argininosuccinate synthetase, ASA: argininosuccinic acid, Asp: aspartate, CAT: cationic amino acid transporter, Cit: citrulline, Cr: creatine, Fum: fumarate, NO: nitric oxide, NOS: nitric oxide synthase, Orn: ornithine, Prot: proteins. The enzymes analyzed in this chapter (NOS, AS, and AL) are depicted in black.

We have developed a nonradioactive ISH protocol sensitive enough to detect mRNA levels as low as 20 transcripts per cell ***(5)***, which allows the simultaneous coupling to immunohistochemistry to follow gene expression at the protein level or cellular typing with specific protein markers on the same tissue section as the mRNA detection ***(6)***.

Nitric oxide (NO), an important cell–cell signaling molecule in the central nervous system (CNS) ***(7)***, is synthesized from a unique precursor, L-arginine (Arg), through nitric oxide synthase (NOS) activity ***(8)***. The NO production capacity is dependent on the intracellular concentration of Arg, which, in the brain, is supplied by protein breakdown or extracted from the blood through cationic amino acid transporters. Arginine can be recycled from the citrulline produced in the NOS reaction, through argininosuccinate synthetase (AS) and argininosuccinate lyase (AL) activities, and metabolized by arginase (*see* **Fig. 1**). Neuronal NOS (nNOS), AS, and AL have been shown to be differentially expressed by specific brain cells ***(9,10)***. The analysis of nNOS, AS, and AL mRNA expression in the rat brain will be used to illustrate the methods allowing the nonradioactive localization of transcripts by ISH, coupled to immuno-

histochemistry against MAP2, GFAP, and MBP to identify neurons, astrocytes, and oligodendrocytes, respectively.

2. Materials

1. nNOS, AS, and AL cDNAs; pGEM-3Zf(+) vector (Promega; Madison, WI).
2. Plasmid DNA amplification equipment (including *Escherichia coli* strain DH5α).
3. Restriction enzymes; T7/SP6 RNA polymerases; RQI-DNase; RNasin (Promega).
4. ATP; GTP; CTP; UTP; digoxigenin-11-UTP (DIG-UTP) (Roche, Basel, Switzerland).
5. Agarose gel electrophoresis and DNA gel extraction equipment.
6. Dithiothreitol (DTT).
7. NH_4–acetate.
8. Tris-ethylene diamine tetraacetic acid (EDTA) (TE) 10 m*M*/1 m*M*, pH 8.0.
9. Spectrophotometer for optical density measure of riboprobe concentration.
10. Nylon membrane (Qiabrane; Qiagen, Basel, Switzerland).
11. Isopentane (2-methylbutane); liquid nitrogen.
12. Cryostat; tissue-freezing medium (Jung, Nussloch, Germany).
13. Phosphate-buffered saline (PBS); diethylpyrocarbonate (DEPC).
14. Containers/baskets for histological sections; Superfrost$^+$ slides (Menzel Gläser, Germany).
15. Oven (for hybridization, 58°C) and water baths (37°C, 65°C, 80°C, and 95°C).
16. Incubation boxes.
17. Parafilm (American National Can, Greenwich, CT).
18. Paraformaldehyde (PFA).
19. Formamide.
20. Salmon sperm DNA.
21. 20X Sodium citrate buffer (SSC): 3*M* NaCl, 0.3*M* Na–citrate.
22. Buffer 1 (100 m*M* Tris-HCl, 150 m*M* NaCl, pH 7.5); blocking reagent (Roche, cat. no. 1 096 176).
23. Buffer 2: 100 m*M* Tris-HCl, 100 m*M* NaCl, 50 m*M* $MgCl_2$, pH 9.5.
24. Anti-DIG antibody alkaline phosphatase coupled (Roche); NBT/BCIP.
25. Glycerol.
26. EtOH.
27. Xylene.
28. Eukitt resin (O. Kindler GmbH & Co., Freiburg, Germany).
29. Bovine serum albumin (BSA).
30. Permeabilization buffer: 0.1% Na–citrate, 0.1% Triton X-100.
31. Anti-MAP2, anti-GFAP, and anti-MBP monoclonal antibodies (Chemicon International, Temecula, CA).
32. Anti-mouse IgG biotinylated secondary antibody (Zymed, San Francisco, CA).
33. Streptavidin-coupled peroxidase; H_2O_2; aminoethylcarbazole (AEC) (Zymed).

3. Methods

The methods described outline (1) the riboprobe synthesis, (2) the preparation of tissue and cryosections, (3) the detection of mRNA by nonradioactive ISH, and (4) the colabeling of *in situ* hybridized sections by immunohistochemistry.

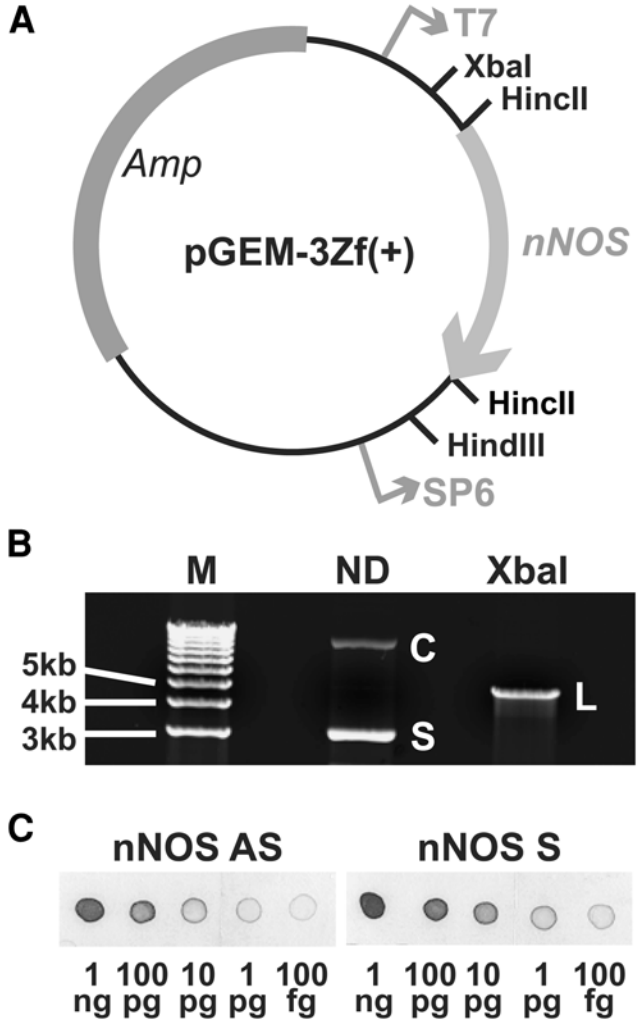

Fig. 2. Synthesis of nNOS ISH antisense and sense riboprobes. **(A)** Schematic drawing of pGEM-3Zf(+) plasmid adapted from Promega (Madison, WI). nNOS cDNA (1850 bp) is cloned into the *Hinc*II site. Linearization with *Xba*I and transcription with SP6 RNA polymerase will yield an nNOS antisense probe. Linearization with *Hin*dIII and transcription with T7 RNA polymerase will yield an nNOS sense probe. **(B)** Linearization of pGEM-3Zf(+)–nNOS with *Xba*I. The linearized plasmid *(L)* is gel purified before transcription. *C*: circular plasmid; kb: kilobase; *M*: DNA size marker; *ND*: nondigested; *S*: supercoiled plasmid. **(C)** Control of DIG incorporation by dot spotting of decreasing (1 ng to 100 fg) amount of antisense (AS) and sense (S) nNOS riboprobes.

3.1. Riboprobe Synthesis

Specific cDNA fragments for rat nNOS (1850 bp), AS (450 bp), and AL (470 bp) were obtained by reverse transcription coupled to polymerase chain reaction (PCR) ***(10)*** and cloned in the vector pGEM-3Zf(+) (*see* **Note 1**) into the *Hin*cII site (*see* **Fig. 2A**). The resulting plasmids are linearized with *Xba*I to yield antisense probes (i.e., test probes, complementary to mRNA), and with *Hin*dIII to yield sense probes (i.e., control probes, which should not hybridize). The linearized plasmids are agarose gel purified (*see* **Fig. 2B**) and used as templates for digoxigenin-labeled riboprobe synthesis (*see* **Note 2**). For a typical preparation of linearized cDNA template, 10 µg of plasmid containing the specific cDNA insert are restriction enzyme digested (*see* **Note 3**).

The transcription mixture (50 µL) includes 1 µg of linearized template cDNA, ATP, GTP, and CTP at 1 m*M* each, 0.7 m*M* UTP, 0.3 m*M* DIG-UTP, 10 m*M* DTT, RNasin (1 unit/µL of transcription mix), and SP6 or T7 RNA polymerase (1 unit/µL of transcription mix). Transcription is performed for at least 2 h at 37°C. The template cDNAs are then digested by RQI-DNase (2 µL at 1 unit/µL, 30 min at 37°C), and all reactions are stopped by adjusting the reaction volume to 100 µL with TE 10 m*M*/1 m*M*; pH 8.0. The riboprobes are then purified through two precipitation steps by the addition of 100 µL NH_4–acetate (4*M*) and 500 µL EtOH (100%), and centrifuged for 30 min at 4°C in a microfuge. The pellet is resuspended in 200 µL DEPC-treated water. The DIG incorporation into the probes is controlled by dot spotting of successive 1:10 dilutions of riboprobes on a Nylon membrane, from 1 ng to 100 fg (*see* **Fig. 2C**). DIG is visualized with an anti-DIG antibody coupled to alkaline phosphatase as described in **Subheading 3.3.2.** The concentration of the synthesized riboprobe is measured by spectrophotometry at 260 nm and 280 nm. Twenty to forty micrograms (100–200 ng/µL in 200 µL final resuspension) of synthesized riboprobe are obtained routinely from 1 µg of cDNA template.

3.2. Preparation of Tissue and Cryosections

3.2.1. Tissue Preparation

Adult rats (300 g) are deeply anesthetized (10 mg/rat Ketalar; Parke Davis, USA) and sacrificed by decapitation. Their brain is extracted within 2 min, rinsed in ice-cold DEPC-treated PBS (*see* **Note 4**), immediately embedded in tissue-freezing medium, and frozen in a bath of isopentane (2-methylbutane) cooled in liquid nitrogen. Brains are kept at –80°C until used for cryosections.

3.2.2. Cryosections

Cryosections (10–20 µm thick) are prepared on a cryostat (–20°C to –25°C) and mounted on positively charged superfrost$^+$ slides that are maintained at

room temperature (RT), let to dry for 30 s at room temperature (RT), and postfixed for 10 min in 4% PFA–PBS at RT (*see* **Note 5**). Cryosections are then washed at RT two times for 15 min in PBS containing 0.1% fresh DEPC and finally equilibrated 15 min in DEPC-treated 5X SSC (0.75*M* NaCl, 0.075*M* Na–citrate) (*see* **Note 6**). At this stage, sections are ready for prehybridization and hybridization with riboprobes (*see* **Note 7**).

3.3. In Situ *Hybridization*

3.3.1. Prehybridization and Hybridization

Prehybridization and hybridization of sections are performed horizontally in a box saturated with a solution of 5X SSC and 50% formamide, to avoid evaporation. Sections are prehybridized for 2 h at 58°C in the hybridization mix (50% formamide, 5X SSC, 40 μg/mL salmon sperm DNA; 500 μL on each section) (*see* **Note 8**). Riboprobes are denatured 5 min at 80°C and added to the hybridization mix (400 ng/mL). The hybridization is carried out at 58°C overnight (O/N) (15 h; abundant transcripts) or 40 h (rare transcripts) (*see* **Note 9**) with 200 μL of hybridization mix on each section, covered by a parafilm rectangle.

3.3.2. Removal of Excess Probe and Staining of Sections

After incubation, the sections are washed under agitation for 30 min in 2X SSC (RT), 1 h in 2X SSC (65°C), and 1 h in 0.1X SSC (65°C). Sections are equilibrated 5 min in buffer 1 (100 m*M* Tris-HCl and 150 m*M* NaCl, pH 7.5) and then incubated for 2 h at RT with alkaline phosphatase-coupled anti-digoxigenin antibody diluted 1:5000 in buffer 1 containing 0.5% blocking reagent. Excess antibody is removed by 2X 15-min wash in buffer 1, and the sections are equilibrated 5 min in buffer 2 (100 m*M* Tris-HCl, 100 m*M* NaCl, 50 m*M* $MgCl_2$, pH 9.5). Color development is performed at RT (30 min to 3 d, depending on the amount of transcripts to be detected) in buffer 2 containing NBT (450 μg/mL) and BCIP (175 μg/mL) (*see* **Note 10**). Staining is stopped by a 10 min wash in TE 10/1 m*M*, pH 8.0, and nonspecific staining is removed 1 h in 95% EtOH with gentle agitation. Sections are rehydrated 15 min in deionized water to remove the precipitated Tris-HCl and dehydrated through successive baths of EtOH (70%, 95%, and 100%) and xylene (2X 15 min each) (*see* **Note 11**). ISH-only slides are mounted in Eukitt resin. **Figure 3** shows the expression of nNOS, AS, and AL mRNAs in the telencephalic cortex of an adult rat. nNOS (**Fig. 3A**) and AS (**Fig. 3B**) mRNAs are found in isolated neurons, with nNOS mRNA being particularly abundant and also localized in neuronal processes (*see* **Note 12**). AL (**Fig. 3C**) presents a more diffuse signal and is expressed both by neurons and astrocytes of the cortex ***(10)***. Hybridization with the respective control sense probes (**Fig. 3D–F**) does not yield any signal.

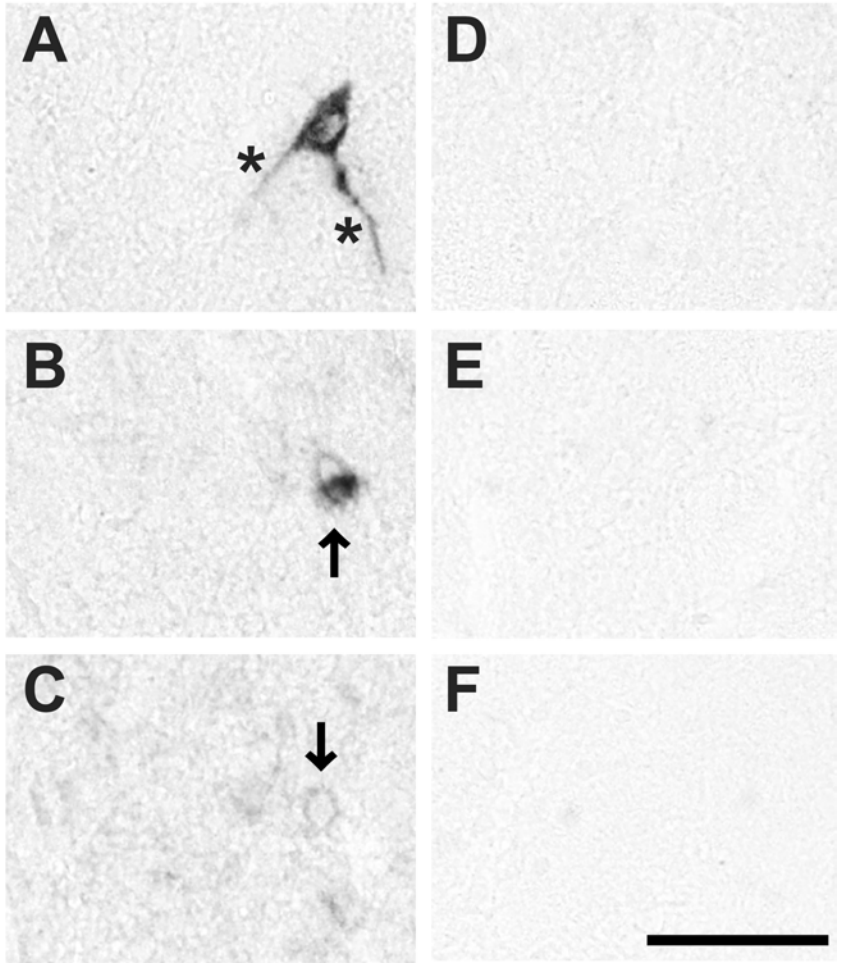

Fig. 3. Expression of nNOS, AS, and AL mRNAs in the rat cortex. **(A, D)** nNOS; **(B, E)** AS; **(C, F)** AL. **(A–C)** Antisense riboprobes; **(D–F)** sense riboprobes. nNOS mRNA is abundantly expressed in scattered neurons of the cortex and can even be localized to neuronal processes (asterisk in **A**). AS mRNA is also localized in scattered neurons of cortex (arrow in **B**), but is not found in processes. AL mRNA is much less abundant and presents a more diffuse signal throughout cortex, with a higher concentration in the perinuclear zone of neurons (arrow in **C**). Hybridization with control sense probes does not yield any signal. Scale bar: 50 μm.

3.4. ISH Colabeling by Immunohistochemistry

Antisense ISH stained sections can be further processed for immunohistochemistry, in order to follow the expression of the same gene at the protein

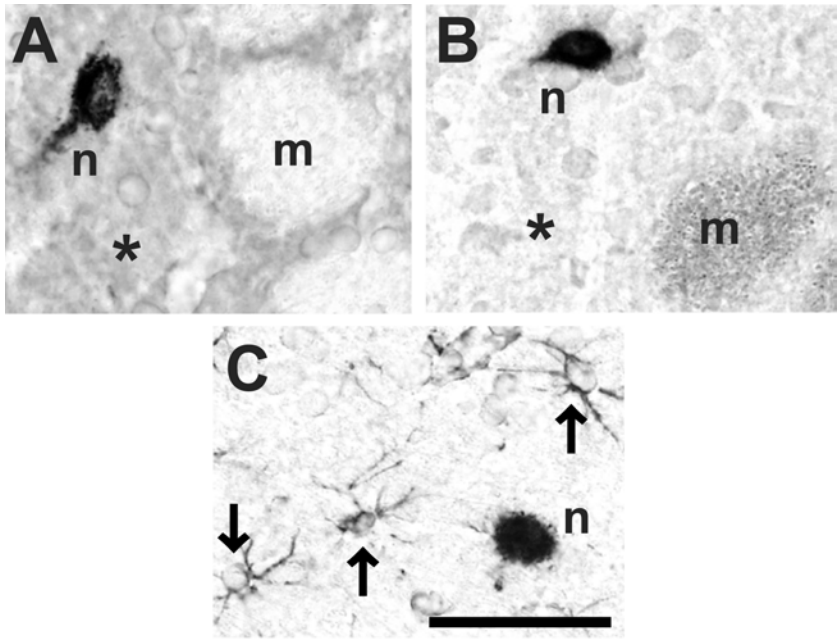

Fig. 4. nNOS expression by ISH, coupled to CNS cell typing by immunohistochemistry. **(A)** Neurons (cell bodies and dendites) identified with anti-MAP2 antibody. **(B)** Oligodendrocytes and myelin sheath identified with anti-MBP antibody. **(C)** Astrocytes identified with anti-GFAP antibody (*arrows*). Micrographs illustrate the very high expression of nNOS by scattered neurons (*n*) of the striatum. Bundles of myelinated axons (*m*, **panels A** and **B**) are negative with anti-MAP2, but stained with anti-MBP antibodies. Neuronal cell bodies and dendrites (asterisk, **panels A** and **B**) are stained with anti-MAP2, but negative with anti-MBP antibodies. Scale bar: 50 μm.

level, or for identifying the specific cell types expressing the mRNA. In this study, neurons, astrocytes, and oligodendrocytes are identified using monoclonal antibodies directed against microtubule-associated protein 2 (MAP2), glial fibrillary acidic protein (GFAP), and myelin basic protein (MBP), respectively.

3.4.1. Rehydration, Fixation, and Permeabilization of ISH Stained Sections

The ISH stained sections are first rehydrated at RT through successive bathes of EtOH (100%, 95%, 70%), H_2O, and PBS. After rehydration, the sections are fixed 1 h in 4% PFA–PBS (RT) and washed 3X 5 min in PBS. Cell membranes are permeabilized for 5 min in 0.1% sodium citrate and 0.1% Triton X-100, and sections are washed 3X 3 min in PBS.

3.4.2. Immunohistochemistry

Sections are processed for immunohistochemistry using the Histostain-Plus kit (Zymed Laboratories). Sections are blocked 10 min in 1% BSA in PBS. The monoclonal primary antibodies are diluted 1:100 in the same blocking solution and applied for 1 h at RT on the sections. After washing away the primary antibodies, sections are incubated with an anti-mouse IgG biotinylated secondary antibody followed by a streptavidin–peroxidase conjugate. Peroxidase staining is performed using AEC and H_2O_2 (*see* **Note 13**). The staining is stopped in H_2O. The double-stained sections (blue signal for ISH by NBT/BCIP and alkaline phosphatase; red signal for immunohistochemistry by AEC and peroxidase) are mounted in glycerol (*see* **Note 14**). The cover slip is sealed with Eukitt resin. **Figure 4** illustrates the expression of nNOS mRNA in the caudate putamen of the adult rat, where nNOS is expressed by scattered neurons ***(10)***. After ISH, the same sections were colabeled by immunohistochemistry against MAP2, GFAP, and MBP to reveal neurons (cell bodies and dendrites), astrocytes, and oligodendrocytes respectively, showing the absence of nNOS mRNA from GFAP-positive cells (astrocytes) and MBP-positive axon bundles (myelinated axons) of caudate putamen (*see* **Note 15**).

4. Notes

1. Any classical cloning plasmid vector can be used (e.g., equipped with ampicilline resistance and a multiple cloning site flanked by either SP6, T3, or T7 RNA promoters).
2. Different kinds of probe can be used for the detection of mRNA in ISH experiments. However, in vitro-transcribed riboprobes are the best choice on tissue sections, as they are single stranded, may span hundreds of nucleotides (we typically use probes ranging from 100 to 2000 nt), and consequently include numerous labeled nucleotides. Thus, specific test antisense riboprobes are obtained, with a high sensitivity of detection allowing the localization of as low as 20 mRNA molecules per cell ***(5)***. Moreover, to ascertain the specificity of hybridization, in vitro transcription allows the synthesis of adequate control sense probes, which have the same length, G+C content, and thus similar properties of hybridization as the antisense probes. As shown here with nNOS, probes as long as 2000 nt penetrate well into the cryosections and do not need to be hydrolyzed in smaller pieces, thus avoiding potential background troubles.
3. It is important to purify the linearized plasmids through agarose gel electrophoresis followed by extraction from the gel of the band of adequate size, as the restriction enzyme digestion is never complete. This pitfall results in the presence of very low levels (i.e., not detectable on agarose gel) of circular or supercoiled plasmids, which yield too long riboprobes after in vitro transcription, and this with a totally nonspecific plasmid sequence. This can lead to hybridization and background troubles (*see* **Fig. 2B**).

4. Depending on the tissue to analyze, one might prefer perfusing the rat transcardially with DEPC-treated PBS, to remove blood and decrease RNase activity.
5. 4% PFA–PBS has been shown to be one of the best fixatives to preserve tissue quality, to keep RNA within cells and to allow a sensitive detection of mRNA ***(11–13)***. To maximize the sensitivity of mRNA detection, we generally omit fixation of the tissue after dissection, freeze, and store it immediately at –80°C until used for ISH. However, this is only possible for tissues having an homogeneous texture (e.g., brain). For tissues with heterogeneous textures (e.g., embryos), immediate fixation after dissection can be necessary, sometimes for a long time (e.g., overnight), to allow for a good quality of cryosections. In this instance, fixed samples have to be cryoprotected by a 6-h incubation in 12% sucrose–PBS (4°C) followed by 18% sucrose–PBS (4°C overnight) before freezing.

   Other tissues are extremely difficult to cut by cryosectioning (e.g., adipose tissue) and need to be embedded in paraffin. After dissection, these are fixed in 4% PFA–PBS, dehydrated through successive baths of EtOH (70%, 95%, and 100%) and xylene (2X 30 min each), and embedded in three successive baths of paraffin (58°C). After paraffin solidification at RT, the tissue is kept at 4°C until used. Paraffin sections (8–12 μm thick) are prepared and mounted on slides, air-dried overnight, and stored at 4°C in a dry atmosphere until used for ISH. Sections are rehydrated through successive baths of xylene, EtOH (100%, 95%, 70%), DEPC-treated water, and DEPC-treated PBS.

   After cryosection of fixed tissues or rehydration of paraffin-embedded sections, ISH is performed from the postfixation point on (*see* **Subheading 3.2.2.**). However, probes penetrate less easily between the covalently linked structures of tissues that have been fixed after dissection for a long time; thus, the sensitivity of detection will be decreased considerably, and hybridization and staining times will have to be lengthened to reach the same level of signal as with unfixed tissues. In this case, a mild digestion of the sections with proteinase K and/or permeabilization with Triton X-100 before the prehybridization step might help and allow a better penetration of the probes and increase the sensitivity of detection. This, however, should not be done on cryosections of unfixed tissues, where digestion reduces tissue preservation and signal intensity considerably ***(5)***.
6. Before and during hybridization, all solutions (H2O, PBS, SSC) must be DEPC treated and autoclaved to work in the best RNase-free conditions. To inhibit endogenous RNase activities in the tissue, we have shown that adding 0.1% fresh DEPC in the 2X 15-min washes in PBS following postfixation of sections was more efficient and easier to handle than the acetylation process used in most of classical ISH protocols ***(3,5)***. The histological baskets and containers used to handle slides must also be RNase-free (wash in detergent, rinse in bidistilled water, and final wash in EtOH).
7. Fixation inactivates RNases and, therefore, sections of tissues fixed for a long time may be stored at –20°C (cryosections) or 4°C (paraffin embedded sections) until used for ISH. In contrast, for cryosections of unfixed tissues, the ISH protocol must follow the cutting immediately, in order to keep rare transcripts intact

and to further maximize the sensitivity of their detection. This procedure is convenient for a single person to process up to 200 ISH slides per week.

8. Many variations in hybridization solutions are proposed in ISH protocols, all aiming at achieving the right stringency to favor specific signals, while avoiding unspecific signals. We aimed at simplifying the hybridization solution and found that a 5X SSC solution with 50% formamide used at 58°C for hybridization confers the desired stringency for RNA–RNA hybrids of 100–2000 nt of length ***(5,10)***. The probe concentration was tested from 100 ng/mL to 2 μg/mL, and the best specific versus unspecific signal ratio was obtained with riboprobes at 400 ng/mL. The use of blockers was also simplified, and a 100X excess (40 μg/mL for 400 ng/mL of probe) of salmon sperm DNA was found to be satisfactory. Specific hybridization resists to the final 1 h stringent wash in 0.1X SSC at 65°C.
9. Abundant transcripts (> 1000 mRNA molecules/cell) allow a short hybridization time (overnight). In contrast, we have observed that the detection of rare transcripts (approx 20 mRNA molecules/cell) requires a much longer hybridization time (40 h) to maximize and ensure the encounter of riboprobes with their target mRNAs ***(5)***.
10. Under our hybridization conditions (58°C, 50% formamide), endogenous alkaline phosphatase activity is inactivated. Therefore, alkaline phosphatase inhibitors such as levamizole in the staining solution are not necessary.
11. In the protocol presented here, dehydration and rehydration after ISH of sections processed for immunohistochemistry against MAP2, GFAP, and MBP gave better results.

    However, this step depends on the antigen epitope to be detected, which may require the sections to stay in acquous buffer to remain detectable by immunohistochemistry. Moreover, some antigens might not survive to the ISH procedures (58°C, 40 h, 50% formamide, followed by washes at 65°C) or might be altered by the 4% PFA postfixation step (*see* **Subheading 3.4.1.**).
12. In most cases, mRNAs analyzed by ISH will be localized or concentrated in the perinuclear region of cells. However, as shown here with nNOS, some transcripts appear to be transported along cell processes, which might allow translation into proteins near their functional site.
13. Depending on the tissue observed, endogenous peroxidase should be inactivated before immunohistochemistry, using H_2O_2.
14. Very low levels of mRNAs might be difficult to observe after immunohistochemistry. In those cases, the cell identification for mRNA expression is realized on adjacent sections labeled by immunohistochemistry.
15. In the case of colocalization of mRNAs and proteins in the same cell and depending on their abundance, the resulting signal of colabeling will appear purple (same subcellular localization) or will stain different part of the same cell with blue for mRNAs and red for proteins ***(6)***.

Acknowledgments

I thank Dr. Masataka Mori, Dr. Tomomi Gotoh, and Dr. Masaki Takiguchi for the kind gift of rat AS, AL, and nNOS cDNAs. I also thank Marc Loup for

excellent technical assistance, and Professor Claude Bachmann for a critical reading of this manuscript. This work was funded in part by the Swiss National Science Foundation (grant no. 3100-063892).

References

1 Dagerlind, A., Friberg, K., Bean, A. J., et al. (1992) Sensitive mRNA detection using unfixed tissue: combined radioactive and non-radioactive in situ hybridization histochemistry. *Histochemistry* **98,** 39–49.

2 Schaeren-Wiemers, N. and Gerfin-Moser, A. (1993) A single protocol to detect transcripts of various types and expression levels in neural tissue and cultured cells: in situ hybridization using digoxigenin-labelled cRNA probes. *Histochemistry* **100,** 431–440.

3 Hayashi, S., Gillam, I. C., Delaney, A. D., et al. (1978) Acetylation of chromosome squashes of *Drosophila melanogaster* decreases the background in autoradiographs from hybridization with ^{125}I-labeled RNA. *J. Histochem. Cytochem.* **26,** 677–679.

4 Komminoth, P., Merk, F. B., Leav, I., et al. (1992) Comparison of ^{35}S- and digoxigenin-labeled RNA and oligonucleotide probes for in situ hybridization. Expression of mRNA of the seminal vesicle secretion protein II and androgen receptor genes in the rat prostate. *Histochemistry* **98,** 217–228.

5 Braissant, O. and Wahli, W. (1998) A simplified in situ hybridization protocol using non-radioactively labelled probes to detect abundant and rare mRNAs on tissue sections. *Biochemica* **1,** 10–16.

6. Braissant, O., Henry, H., Loup, M., et al. (2001) Endogenous synthesis and transport of creatine in the rat brain: an in situ hybridization study. *Mol. Brain Res*. **86,** 193–201.

7 Garthwaite, J. and Boulton, C. L. (1995) Nitric oxide signaling in the central nervous system. *Annu. Rev. Physiol*. **57,** 683–706.

8 Palmer, R. M., Ashton, D. S., and Moncada, S. (1988) Vascular endothelial cells synthesize nitric oxide from L-arginine. *Nature* **333,** 664–666.

9 Iwase, K., Iyama, K., Akagi, K., et al. (1998) Precise distribution of neuronal nitric oxide synthase mRNA in the rat brain revealed by non-radioisotopic in situ hybridization. *Mol. Brain Res*. **53,** 1–12.

10 Braissant, O., Gotoh, T., Loup, M., et al. (1999) L-Arginine uptake, the citrulline–NO cycle and arginase II in the rat brain: an in situ hybridization study. *Mol. Brain Res*. **70,** 231–241.

11 Angerer, L. M. and Angerer, R. C. (1981) Detection of poly A$^+$ RNA in sea urchin eggs and embryos by quantitative in situ hybridization. *Nucleic Acids Res*. **9,** 2819–2840.

12 Singer, R. H. and Ward, D. C. (1982) Actin gene expression visualized in chicken muscle tissue culture by using in situ hybridization with a biotinated nucleotide analog. *Proc. Natl. Acad. Sci. USA* **79,** 7331–7335.

13. Lawrence, J. B. and Singer, R. H. (1985) Quantitative analysis of in situ hybridization methods for the detection of actin gene expression. *Nucleic Acids Res*. **13,** 1777–1799.

10

Real-Time Polymerase Chain Reaction to Quantify mRNA for Endothelial Nitric Oxide Synthase

Yi Chu and Frank M. Faraci

Summary

The endothelial isoform of nitric oxide synthase (eNOS) plays a major role in vascular biology and emerging evidence suggests it may serve diverse biological functions in nonvascular cells. To be able to study the eNOS at the molecular level, including regulation of mRNA levels, we developed real-time reverse transcription-polymerase chain reaction methodology for sensitive and precise quantification of mRNA levels. In addition to providing quantification of mRNA levels, the method should be attractive because of its high sensitivity and the fact that blood vessels from small species such as genetically altered mice can be studied. Here, we demonstrate that the method can measure mRNA levels in cerebral and coronary arteries from mice, in addition to larger blood vessels.

Key Words: Nitric oxide; nitric oxide synthase; endothelium; vascular biology; cerebral artery.

1. Introduction

Endothelium is known to exert a major influence on vascular structure and tone. For example, endothelium affects basal vascular tone and mediates vasorelaxation in response to increased blood flow (shear stress) and a variety of receptor-mediated agonists. Endothelium-dependent relaxation is mediated by a family of endothelium-derived relaxing factors (EDRFs), including nitric oxide (NO), endothelium-derived hyperpolarizing factors, and prostacyclin. Although there are differences between species, between different vascular beds, and along the vascular tree, NO produced by the endothelial isoform of NO synthase (eNOS) is the predominant EDRF. For example, in human cerebral and coronary blood vessels (both large arteries and resistance vessels), NO mediates the majority of the response to endothelium-dependent stimuli

From: *Methods in Molecular Biology, vol. 279: Nitric Oxide Protocols: Second Edition*
Edited by: A. Hassid © Humana Press Inc., Totowa, NJ

(1–3). Similar findings have been obtained in mice *(4,5)*. Thus, eNOS plays a major role in vascular biology. In addition, expression of eNOS in nonendothelial cells may serve other diverse biological functions, including control of mitochondrial biogenesis, as revealed recently *(6)*.

To better define mechanisms of eNOS-mediated signaling in health and disease, it is important to be able to study the eNOS enzyme at the molecular level, including regulation of mRNA levels. The development of real-time reverse transcription-polymerase chain reaction (RT-PCR) methodology allows more sensitive and precise quantification of mRNA levels than traditional Northern blotting, RNase protection, or end-point RT-PCR assays (for a review, *see* **ref. *7***). The purpose of this chapter is to describe in detail the real-time RT-PCR methodology that we developed that allows reliable quantification of eNOS mRNA *(8)*.

2. Materials

2.1. Reagents

1. RNase-free deionized water.
2. RNA extraction buffer: for example, TriReagent (Molecular Research Center) or TRIzol reagent (Invitrogen).
3. Chloroform.
4. Glycogen.
5. Ethanol and isopropanol.
6. Random deoxynucleotide hexamer.
7. Deoxynucleotide triphosphates (dNTPs).
8. Moloney murine leukemia virus reverse transcriptase (Invitrogen).
9. Reverse-transcription buffer: containing 50 m*M* Tris-HCl, pH 8.3, 75 m*M* KCl, 3 m*M* $MgCl_2$, and 10 m*M* dithiothreitol (DTT) (provided when purchasing Reagent 8).
10. The sense primer (1419–1437 *[9]*; spanning exons 10 and 11 corresponding to the human eNOS genomic sequence *[10]*), 5'-CCTTCCGCTACCAGCCAGA-3', and the antisense primer (1523–1500, spanning exons 11 and 12), 5'-CAGAGATCTTCA CTGCATTGGCTA-3'.
11. TA cloning plasmid vector: for example, pCR3.1 (Invitrogen).
12. T4 DNA ligase, RNase, and restriction enzymes.
13. Quick Spin Sephadex G-50 column (Roche).
14. Dual-labeled TaqMan probe (1467–1497, within exon 11), 5'-6-carboxy fluorescein-CAGGCATCACCAGGAAGAAGACCTTTAAGGA-6-carboxy tetramethylrhodamine-3'.
15. A kit including the primers and probe for TaqMan real-time RT-PCR for 18S rRNA, TaqMan ribosomal control reagents, cat. no. 4308329, purchased from Applied Biosystems Inc. (ABI).
16. TaqMan 2X PCR master mix (ABI) (Concentrations at 1X: 5.5 m*M* $MgCl_2$, 200 μ*M* dATP/dCTP/dGTP, 400 μ*M* dUTP, 0.01 U/μL AmpErase, and 0.025 U/μL

AmpliTaq Gold DNA polymerase, provided in the mix with inclusion of primers at 200 n*M* and probe at 100 n*M*).

2.2. Equipment

1. Real-time PCR machinecycler: for example, ABI Prism Sequence Detection System 7000.
2. Primer/probe design software: for example, Primer Express (ABI).
3. PCR cycler: for example, ABI GeneAmp System 2400.
4. Microcentrifuge: for example, Eppendorf 5415C.
5. Water baths.
6. Electrophoresis apparatus.
7. Ultraviolet spectrophotometer: for example, Beckmen DU640B.

3. Methods

3.1. RNA Preparation

1. For studies in C57BL/6 mice, the thoracic aorta and carotid artery are harvested with careful removal of fat surrounding the adventitia and blood inside the lumen.
2. The vessels are minced with a razor blade (*see* **Note 1**) and immediately added to a 1.5-mL tube (RNase-free) containing 1.0 mL of TriReagent.
3. After vigorous shaking and incubation (15 min to several hours), 300 μL of chloroform is added to the tube and it is vigorously shaken and incubated for 15 min.
4. The tube is then centrifuged at 15,000*g* for 15 min at 4°C, and the aqueous supernatant is collected into a fresh 1.5-mL tube, taking care not to touch pipet tips to the interface or the organic phase. Twenty micrograms of glycogen is added to coprecipitate RNA, followed by the addition of 800 μL of isopropanol.
5. After mixing, the tube containing RNA is stored in a –80°C freezer for future use. RNA precipitate is obtained after centrifugation at 15,000*g* at 4°C for 20 min and subsequently rinsed in 70% ethanol.
6. After centrifugation for 10 min, the precipitate is resuspended in 10 μL of RNase-free water. One microliter of RNA is added to 69 μL of water for measurement of RNA concentration using a Beckmen Beckman DU640B spectrophotometer (*see* **Note 2**). The remaining 9 μL of RNA is immediately placed in a –80°C freezer for storage. The yield of total RNA from thoracic aorta and carotid artery of a mouse is approx 1.4 μg and 0.7 μg, respectively ***(8)***.
7. Cerebral and coronary arteries, after careful isolation, are directly added into a 1.5-mL tube containing TriReagent, and processed as described in **steps 3–6** above. Arteries are pooled from two to three mice to increase RNA yield. The yield of total RNA from cerebral and coronary arteries per mouse is approx 0.32 μg and 0.25 μg, respectively ***(8)***.

3.2. Reverse-Transcription Reaction

1. Four hundred nanograms of RNA (occasionally 350 or 300 ng, when the RNA yield is low) is used for RT in a final volume of 20 μL.

2. The reaction mixture consists of 3.125 μ*M* random hexamer, 0.5 m*M* deoxynucleotide triphosphates, 50 m*M* Tris-HCl, pH 8.3, 75 m*M* KCl, 3 m*M* $MgCl_2$, 10 m*M* DTT, and 10 units/μL Moloney murine leukemia virus reverse transcriptase (Invitrogen) (*see* **Note 3**).
3. The reaction is incubated at 37°C for 90 min and subsequently stored at –20°C until use.

3.3. Design and Preparation of Primers and Probe

1. Primers and probe for mouse eNOS were designed to satisfy the following conditions. First, both 5' and 3' primers, in addition to being specific for eNOS, overlap two neighboring exons so that they only hybridize with cDNA but not the genomic sequence of eNOS. This approach ensures that only mRNA, after RT, is measured in the sample.
2. Second, primers, probe, and the length of the PCR product satisfy the requirements as specified in the Primer Express software (ABI).
3. Third, primers and probe, with minor modifications, may be adapted to be used for quantification of eNOS mRNA in other species (*see* **Note 4**). The primers and the dual-labeled probe for mouse eNOS, designed based on the above criteria, and the commercial set for 18S rRNA as a control for RNA input and RT efficiency, are described in **Subheading 2.1.**

3.4. Preparation of DNA Standards

1. The products of conventional PCR for mouse eNOS (105 bp) and 18S rRNA (187 bp), amplified from cDNA derived from mouse aorta with the use of the primers designed for the real-time PCR, are cloned into pCR3.1 vector (Invitrogen), using standard cloning procedures that are also detailed in the manufacturer's product sheet.
2. A clone each of pCR3.1/eNOS and pCR3.1/18S, after confirmation of correct sequences by DNA sequencing, is propagated.
3. Plasmid DNA is purified by extensive digestion and removal of RNA by RNase and extractions with phenol and chloroform, followed by passing through a Quick Spin Sephadex G-50 column (Roche).
4. The plasmid DNA is then linearized by digestion with *Bam*HI and *Xho*I, respectively, both being single cutters in pCR3.1 and neither site existing in the PCR segment.
5. The linearized plasmid DNA is purified and then quantified using a Beckman DU640B spectrophotometer. Concentration in molecules of single-stranded DNA (ssDNA) per microliter was obtained using the formula: Concentration of plasmid DNA (mg/mL) × 6.022×10^{23} × 2/(no. of basepairs of plasmid DNA × 650), 650 being the average molecular weight of 1 bp. The standards used in real-time PCR increase in 10-fold intervals from 20 to 2×10^7 molecules (ssDNA) for mouse eNOS and from 300 to 3×10^8 molecules (ssDNA) for 18S rRNA. The range of standards is determined with pilot experiments and covers the range of eNOS or 18S copies in samples to be quantified.

3.5. Real-Time PCR

Real-time PCR is performed following the recommendations by ABI.

1. Briefly, 1.1 μL of DNA standard or RT product (22 ng equivalent of total RNA) is added (using a P2 pipetman and aerosol-free tips; *see* **Note 5**) to an aliquot of 26.4 μL of the stock buffer, making the mixed solution to a final concentration of 1X TaqMan mixture (described in **Subheading 2.1.**) using TaqMan 2X PCR Master Mix.
2. From the 27.5-μL mixture, 25.0 μL (20 ng total RNA in 1X TaqMan mix) is transferred to a 96-well plate. PCR is performed at 50°C for 2 min, at 95°C for 10 min, and then run for 40 cycles at 95°C for 15 s, and at 60°C for 1 min on the ABI Prism 7700 or 7000 Detection System. C_T, which is the threshold cycle number at which the initial amplification becomes detectable by fluorescence (defined as $\Delta R_n = 0.1$ in our experiments), is determined.
3. A standard curve is established in C_T vs copy number of ssDNA (equivalent to cDNA after RT), and the copy number of cDNA is determined for each RT sample as an approximation of mRNA copies. All analyses are standard procedures of the 7700 or 7000 detection system. For 18S rRNA PCR, 2 pg equivalent of total RNA after RT (1 μL of 1:10,000 diluted RT product) was used because of the great abundance of 18S RNA. Quantification of eNOS mRNA is expressed as both copy numbers per nanogram of total RNA and the ratio of eNOS and 18S rRNA.

3.6. An Example of Application

We have published results using this methodology to measure eNOS mRNA levels in several blood vessels from mice *(8)*. As an additional example, we recently compared eNOS mRNA levels in cerebral blood vessels from age-matched (approx 20 wk) male spontaneously hypertensive rats (SHR) and normotensive control Wistar–Kyoto rats (WKY) using the primers and probe specific for rat eNOS *(8)* (*see* **Fig. 1**). These data demonstrate that there is no significant difference in eNOS mRNA levels in cerebral arteries between 5-mo-old SHR and WKY rats. In addition, the data demonstrate that the levels of 18S rRNA are consistent between SHR and WKY rats and thus can be used to normalize RNA input and RT efficiency.

Although the levels of eNOS mRNA and 18S rRNA are expressed in absolute values (because of the use of the standards), we must bear in mind that the values are only an approximation and, certainly, an underestimation of the true values, because RT efficiency is always <100% (this efficiency ranges from 24 to 60%, according to the manufacturer of MMLV–reverse transcriptase). Thus, the power of the methodology lies in the ability to obtain accurate approximations of eNOS mRNA levels in small samples and accurate comparison between samples.

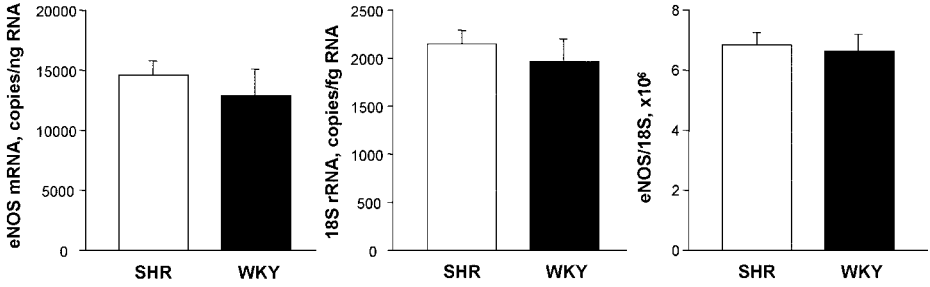

Fig. 1. Levels of eNOS mRNA (*left*) and 18S rRNA (*middle*), and the ratio of eNOS to 18S (*right*) in cerebral arteries from 20-wk-old male SHR (n = 7, unpooled) and WKY (n = 8, unpooled) rats, determined by real-time RT-PCR methodology described in this chapter. Values are means ± SE. Neither eNOS nor 18S was detectable in RT samples with omission of reverse transcriptase.

4. Notes

1. We have found that the use of a razor blade to mince blood vessels on a plastic weighing boat for harvest of RNA, in comparison to the conventional use of a tissue homogenizer, has distinctive advantages. These advantages include (1) disposability, which ensures no contamination between tissue samples, and (2) rapidity of the procedure, which is beneficial in minimizing post-tissue-harvest RNA degradation.
2. It is best to perform RNA quantification (by $OD_{260\ nm}$) and RT reaction of all samples at one time to minimize procedural variation.
3. The use of random deoxynucleotide hexamers as primers, instead of oligo-dT or gene-specific primer, appears to produce higher yield of cDNA, and, more importantly, the resultant cDNA can be used for subsequent PCR for unlimited genes, including 18S rRNA, which would otherwise be undetectable. There are many products of reverse transcriptase to choose and we have used the classic MMLV–reverse transcriptase (Invitrogen), which produces consistent and reliable results. The RT reaction condition provided in the protocol is good for starting RNA that ranges from 100 ng to 4 μg.
4. The design of primers/probe is critically important for a real-time RT-PCR protocol. Every effort should be made to design cDNA-specific primers and/or probe so that no positive PCR can proceed with genomic DNA as the template. Although genomic DNA can theoretically be completely eliminated by an added step of DNase digestion of RNA samples prior to RT, the digestion may not be complete and, more importantly, the yield of RNA from small samples such as mouse vessels would suffer should the step of DNase digestion be added.
5. Extreme care must be taken in pipetting samples to ensure accuracy of volume and no contamination between samples. This step, next to contamination between samples during handling, may constitute a major source of inaccuracy in final

results. We recommend use of a P2 pipettor if a volume <2 μL is to be transferred. We also recommend that aerosol-free tips (certified DNase/RNase/pyrogen-free) and a dedicated area be used throughout the preparation for a real-time PCR run.

5. Concluding Remarks

We have developed the methods needed to use real time RT-PCR to quantify eNOS mRNA levels in blood vessels from mice and rats. Genetically altered mice are increasingly being used for studies of vascular biology. In addition to providing more precise quantification of mRNA levels, the method should be attractive because of its high sensitivity and the fact that blood vessels from mice are relatively small—limiting the amount of mRNA that can be extracted. We have demonstrated that the method can be used to measure mRNA levels in cerebral and coronary arteries from mice in addition to the largest blood vessel, the aorta ***(8)***. Recently, other laboratories have also begun to use real time RT-PCR to quantify eNOS mRNA levels in mice ***(11)*** and in other species (human, rat, pig) ***(12–15)***.

Acknowledgment

This work was supported by National Institutes of Health grants HL-38901, HL-62984, and NS-24621.

References

1 Egashira, K., Katsuda, Y., Mohri, M., et al. (1996) Role of endothelium-derived nitric oxide in coronary vasodilatation induced by pacing tachycardia in humans. *Circ. Res*. **79,** 331–335.

2 Kuga, T., Mohri, M., Egashira, K., et al. (1997) Bradykinin-induced vasodilation of human coronary arteries in vivo: role of nitric oxide and angiotensin-converting enzyme. *J. Am. Coll. Cardiol*. **30,** 108–112.

3 Elhusseiny, A. and Hamel, E. (2000) Muscarinic—but not nicotinic—acetylcholine receptors mediate a nitric oxide-dependent dilation in brain cortical arterioles: a possible role for the M5 receptor subtype. *J. Cerebr. Blood Flow Metabol*. **20,** 298–305.

4 Sobey, C. G. and Faraci, F. M. (1997) Effects of a novel inhibitor of guanylyl cyclase on dilator responses of mouse cerebral arterioles. *Stroke* **28,** 837–843.

5 Lamping, K. G., Nuno, D. W., Chappell, D. A., et al. (1999) Agonist-specific impairment of coronary vascular function in genetically-altered, hyperlipidemic mice. *Am. J. Physiol*. **276,** R1023–R1029.

6 Nisoli, E., Clementi, E., Paolucci, C., et al. (2003) Mitochondrial biogenesis in mammals: the role of endogenous nitric oxide. *Science* **299,** 896–899.

7 Giulietti, A., Overbergh, L., Valckx, D., et al. (2001) An overview of real-time quantitative PCR: applications to quantify cytokine gene expression. *Methods* **25,** 386–401.

8 Chu, Y., Heistad, D. D., Knudtson, K. L., et al. (2002) Quantification of mRNA for endothelial NO synthase in mouse blood vessels by real-time polymerase chain reaction. *Arteriosclerosis Thromb. Vasc. Biol*. **22,** 611–616.
9 Gnanapandithen, K., Chen, Z., Kau, C. L., et al. (1996) Cloning and characterization of murine endothelial constitutive nitric oxide synthase. *Biochim. Biophys. Acta* **1308,** 103–106.
10. Marsden, P. A., Heng, H. H. Q., Scherer, S. W., et al. (1993) Structure and chromosomal localization of the human constitutive endothelial nitric oxide synthase gene. *J. Biol. Chem.* **268,** 17,478–17,488.
11 Wang, Y. X., Martin-McNulty, B., Huw, L. Y., et al. (2002) Anti-atherosclerotic effect of simvastatin depends on the presence of apolipoprotein E. *Atherosclerosis* **162,** 23–31.
12 Gan, L. M., Selin-Sjogren, L., Doroudi, R., et al. (2000) Temporal regulation of endothelial ET-1 and eNOS expression in intact human conduit vessels exposed to different intraluminal pressure levels at physiological shear stress. *Cardiovasc. Res.* **48,** 168–177.
13. Reber, K. M., Su, B. Y., Clark, K. R., et al. (2002) Developmental expression of eNOS in postnatal swine mesenteric artery. *Am. J. Physiol*. **283,** G1328–G1335.
14 Hattori, Y., Nakanishi, N., Akimoto, K., et al. (2003) HMG-CoA reductase inhibitor increases GTP cyclohydrolase I mRNA and tetrahydrobiopterin in vascular endothelial cells. *Arteriosclerosis Thromb. Vasc. Biol*. **23,** 176–182.
15. Sasaki, Y., Noguchi, T., Yamamoto, E., et al. (2002) Effects of Ginkgo biloba extract (EGb 761) on cerebral thrombosis and blood pressure in stroke-prone spontaneously hypertensive rats. *Clin. Exp. Pharmacol. Physiol*. **29,** 963–967.

11

Dioxygen-Dependent Metabolism of Nitric Oxide

Paul R. Gardner, Anne M. Gardner, and Craig K. Hallstrom

Summary

Nitric oxide (NO) serves critical signaling, energetic, and toxic functions throughout the biosphere. NO steady-state levels and functions are controlled in part by NO metabolism or degradation. Dioxygen-dependent NO dioxygenases (EC 1.14.12.17) and dioxygen-independent NO reductases (EC 1.7.99.7) are being identified as major routes for NO metabolism in various life forms. Here we describe the use of the Clark-type NO electrode, mechanistic inhibitors, and nitrate/nitrite assays to measure, characterize, and identify major NO metabolic pathways and enzymes in bacteria, fungi, plants, mammalian cells, and organelles. The methods may prove to be particularly useful for mechanistic investigations and the development of inhibitors, inducers, and other novel NO-modulating therapeutics.

Key Words: Nitric oxide dioxygenase; flavohemoglobin; nitric oxide reductase; nitric oxide electrode; nitrate; cyanide; carbon monoxide.

1. Introduction

Nitric oxide (NO)-metabolizing NO dioxygenases (NODs) (EC 1.14.12.17) and NO reductases (NORs) (EC 1.7.99.7) are found in diverse organisms. In microbes, NO stress induces NODs and NORs, which prevent NO toxicity and regulate NO signaling pathways ***(1)***. NODs utilize dioxygen and NAD(P)H to convert NO to nitrate [Eq. (1)], whereas NORs are O_2-independent metalloenzymes that reduce NO to N_2O (Eq. 2) and are best known for their roles in energy-yielding denitrification pathways in microbes ***(2,3)***:

$$2NO + 2O_2 + NAD(P)H \rightarrow 2\ NO_3^- + NAD(P)^+ + H^+ \quad (1)$$

$$2NO + NAD(P)H + H^+ \rightarrow N_2O + NAD(P)^+ + H_2O \quad (2)$$

Microbial (flavo)hemoglobins ***(4–12)*** and mammalian myoglobins and hemoglobins ***(13–15)*** catalyze NO dioxygenation and are proposed to fulfill biological functions in NO metabolism. There is also emerging evidence for

From: *Methods in Molecular Biology, vol. 279: Nitric Oxide Protocols: Second Edition*
Edited by: A. Hassid © Humana Press Inc., Totowa, NJ

other NOD types in bacteria and mammals ***(11,16)***. Three types of microbial NOR have been demonstrated ***(2,3,17)***. In addition, *Escherichia coli* nitrite reductase is reported to bear low NOR activity ***(18)***, and the mammalian mitochondrial cytochrome-*c* oxidase shows limited NOR activity ***(19,20)***.

A variety of dioxygen-dependent reactions may also constitute pathways for NO metabolism in various tissues, cells, and organelles and, moreover, these reactions may serve important (patho)physiological roles. For example, 15-lipoxygenase, prostaglandin H synthase, peroxidases, and mitochondrial cytochrome-*c* oxidase oxidize NO to nitrite ***(19,21–26)***. Oxidations of NO by 12/15-lipoxygenase, prostaglandin H synthase, and peroxidase all require the cosubstrate H_2O_2 and are thus necessarily dioxygen dependent. In addition to the formation of nitrite, peroxidases catalyze nitrogen dioxide formation and the nitration of protein tyrosines, suggesting limited benefits to cells for this NO metabolic pathway ***(24)***. Nonenzymic reactions of NO with superoxide radical ($O_2^{\cdot -}$) and O_2 also form potential sinks for NO removal and for the formation of nitrite and nitrate within cells and tissues. However, the intermediates and products of these reactions are highly reactive and clearly toxic ***(27,28)***. NO-scavenging NODs and NORs and $O_2^{\cdot -}$-scavenging superoxide dismutases (SODs) limit the flux of NO metabolized via the diffusion-limited bimolecular reaction of NO and $O_2^{\cdot -}$ ***(4,29,30)*** as well as the slower termolecular reaction of NO with O_2.

Here, we describe applications of the Clark-type NO electrode to the measurement of NO metabolism by various cells, tissues, cell extracts, and purified components thereof. We focus on methods for measuring and characterizing dioxygen-dependent pathways. It is hoped that the methods described will facilitate (1) the elaboration of NO-metabolizing enzymes in various tissues and in diverse organisms and (2) the development and application of novel therapeutics to regulate NO levels, including antibiotics, antineoplastic agents, and blood pressure modulators.

1.1. Clark-Type NO Electrode Measurements

Measurements of NO in solution are based on the amperometric method for measuring O_2 invented by Leland Clark at Cincinnati Children's Hospital Medical Center in 1954. The major differences from the original design for O_2 measurements is the voltage applied to the NO-specific electrode and the magnitude of the current detectable as a result of NO oxidation rather than O_2 reduction. Electrodes employ a gas-permeable membrane that limits reactions with redox-active molecules in the assay medium. The size and area of the platinum electrode determines rates of NO oxidation, and the tip area is thus minimized to limit NO decomposition by the electrode. Principles for the

application of the NO electrode and improvements to its sensitivity have been previously discussed ***(31,32)***.

1.2. NO Metabolism by Tissues, Cells, Organelles, Extracts, and Isolated Enzymes

In addition to knowledge of NO synthesis, a full understanding of NO physiology requires knowledge of rates of NO metabolism by various tissues, cells, and specific organelles, as well as a detailed mechanistic knowledge of the reaction components and their contributions to overall NO metabolism. Although it is now well understood that various bacteria and fungi express efficient and inducible NO-metabolizing enzymes such as the NODs and NORs that modulate NO toxicity and signaling functions ***(1)***, significantly less is known about NO metabolism in complex multicellular organisms such as mammals. The half-life for NO in cardiac tissue has been estimated to be a mere 100 ms ***(33)***. It is clear that various mammalian tissues, cells, mitochondria and microsomes, and extracts exhibit distinct capacities for NO metabolism ***(16,20,29,34–39)***. Indeed, some mammalian cells consume NO at rates approaching those for O_2 respiration ***(29)***. It has been generally assumed that hemoglobin and myoglobin form major pathways for NO metabolism. Indeed, the abundant myoglobin and hemoglobin have been shown to function as NODs in myocytes and erythrocytes similar to the ancestral flavohemoglobins in microbes ***(4,13–15,40)***. The reaction of NO with $O_2^{\cdot -}$ is also a significant route for NO decomposition during the respiratory burst of neutrophils and other immune cells accompanying inflammation ***(41)***. On the other hand, there is growing evidence for specific NO-metabolizing enzymes in nonerythrocytic mammalian cells and tissues similar to those described for bacteria and fungi. Peroxidases, 12/15-lipoxygenase, prostaglandin H synthase, and cytochrome-*c* oxidase have been proposed to serve this function in mammalian cells ***(19–25,42)***. These enzymes metabolize NO to nitrite in vitro; yet, their relative contributions to overall NO metabolism in various cells and tissues under (patho)physiological conditions remain to be established. Knowledge of the kinetics of specific NO metabolic enzymes and, in particular, turnover numbers for particular pathway components provides valuable criteria for evaluating the physiological functions of various NO metabolic enzymes. Indeed, Lancaster and co-workers have argued the essential function for nonerythrocyte NO metabolism based on NO production rates, diffusion rates, and reaction rates within erythrocytes and hepatocytes ***(37)***.

1.3. NO, O_2, and NAD(P)H Dependence of NO Metabolism

Measurements of NO and O_2 dependencies and stoichiometries and other substrate requirements for NO metabolism within cells, isolated organelles, or

with purified enzymes provide information on the identity and function of a NO metabolic pathway. In *E. coli*, dioxygen-dependent NO metabolism occurs with apparent $K_M(O_2)$ and K_M(NO) values of 60 μ*M* and 400 n*M*, respectively ***(6)***. Anaerobic NO metabolism via NOR (NorVW) occurs with a similar apparent K_M(NO) of 400 n*M* ***(3,43)***. The isolated NOD (flavohemoglobin) and NorVW show similar NO saturation values and capacity for protection of NO-sensitive targets and cell growth. The dioxygen-dependent NO metabolic activity that we have previously characterized within an assortment of mammalian cell types is saturable by O_2 and NO and shows remarkably similar apparent K_M(NO) and $K_M(O_2)$ values of 200 n*M* and 17 μ*M*, respectively, to those measured for microbial NODs ***(5,6,29,44)***. It is noteworthy that Thomas et al. ***(37)*** did not observe saturation of hepatocyte NO consumption by NO, whereas Griffiths and Garthwaite ***(38)*** reported a saturability of the brain tissue NO consumption activity [K_M(NO) = 120 n*M*] roughly similar to that we reported for cultured cells ***(29)***.

1.4. Products of O_2-Dependent NO Metabolism

Nitrate and nitrite are terminal products of O_2-dependent NO metabolism, whereas N_2O is the product of anaerobic NO-metabolizing enzymes. Measurement of these relatively stable products can provide important information about the pathways utilized for NO metabolism within complex biological systems. Moreover, the distribution of products within cells can provide insights into the localization and identity of the major NO-metabolizing enzymes and pathways. For example, O_2-dependent metabolism of NO by cultured human CaCo-2 cells produced near-stoichiometric nitrate. Nitrate was contained within the cell membrane, thus demonstrating an intracellular NO dioxygenation ***(29)***. Nitrate is also produced via a dioxygen-dependent mechanism within brain tissue ***(39)*** and lung tissue ***(45,46)***. The finding of stoichiometric nitrate formation diminishes the likelihood of significant roles for peroxidases, cytochrome-*c* oxidase, 15-lipoxygenase, prostaglandin H synthase, $O_2^{\cdot -}$, or O_2 reactions in NO metabolism because these reactions produce nitrite. On the other hand, a finding of significant nitrite formation by a NO metabolic pathway under study would indicate significant involvement of a nitrite-generating reaction or enzyme, as reported for cytochrome-*c* oxidase in mitochondria rich cells ***(25)***.

1.5. Inhibitors of NO Metabolism and NODs

Measurements of the sensitivity of NO metabolism to inhibitors also provide information on the identity and mechanism of various proposed NO metabolic pathways. Dioxygen-dependent mammalian cell NO metabolism shows sensitivity to heme poisons, including cyanide, CO, NO, and phenylhydrazine, sug-

gesting a role for a heme-dependent NOD similar to the microbial NOD (flavohemoglobin) ***(5,16,29,44,47)***. NO and CO are competitive with respect to O_2 (K_i values ≤ 3 μ*M*) for the flavohemoglobin NODs ***(5,6)*** and for the mammalian NOD ***(29)***. Further, inhibition of the NO consumption activity in cultured mammalian cells, but not brain tissue ***(39)***, by the flavoenzyme inhibitor diphenyleneiodonium suggests a role for a flavin-dependent NO dioxygenase within some cells ***(29)***, but not others. Inhibitors that target metabolic pathways have also been used to test the roles of enzymes in NO metabolism. For example, the role of mitochondrial respiratory complexes such as cytochrome-*c* oxidase in cellular NO metabolism can be tested by applying upstream inhibitors of electron transport ***(29)***. In addition, extracellular superoxide dismutase, catalase or $O_2^{\cdot -}/H_2O_2$ generators can be used to evaluate relative roles for $O_2^{\cdot -}$- or H_2O_2-dependent pathways and enzymes in dioxygen-dependent NO metabolism. Interestingly, no significant contribution of extracellular or intracellular $O_2^{\cdot -}$ or H_2O_2 to NO metabolism was measured for cultured human epithelial-like A549 lung cells, nor did elevated $O_2^{\cdot -}$ or H_2O_2 stimulate cellular NO metabolism ***(29)***.

2. Materials

2.1. Clark-Type NO Electrode Apparatus

1. A 2-mm ISO-NOP electrode and ISO-NO Mark II meter was obtained from World Precision Instruments (Sarasota, FL).
2. A thermostatted water-jacketed, electrode-ported, glass-stoppered, 2-mL-capacity glass cell chamber originally designed for an 8-mm O_2 electrode was obtained from the Gilson, Inc. (Middleton, WI) (*see* **Fig. 1**) The 2-mm NO electrode was fitted to the O_2 electrode port by setting the NO electrode into a custom-cut plastic sleeve with epoxy resin. For this purpose, a 10-mL plastic disposable pipet was cut to length with a file and was modified with a groove to fit a rubber O-ring for a leakproof seal to the glass-walled port (*see* **Note 1**).
3. A circulating, temperature-controlled water bath is connected with Tygon® tubing to the NO electrode cell outer chamber.
4. A microcontrolled magnetic stirrer (Corning) is used for stirring a 2-mm × 8-mm micro stir bar in the NO electrode chamber cell.
5. A Kipp and Zonen BD111 chart recorder is used to record the NO signal. The recorder is generally set for a 80% full-scale response to 2 μ*M* NO at 1 V and a chart speed of 30 mm/min. A lower voltage is used for greater sensitivity. Devices and programs for computer data collection are available, but the chart system for data analysis suffices.
6. Hamilton syringes are used to deliver NO and other reagents through the narrow delivery port of the glass-stoppered cell. It is important that the saturated NO solution, cells, extracts, and substrates be delivered through the port of the glass stopper with minimal disturbance of the electrode cell and with rapid and homogenous mixing.

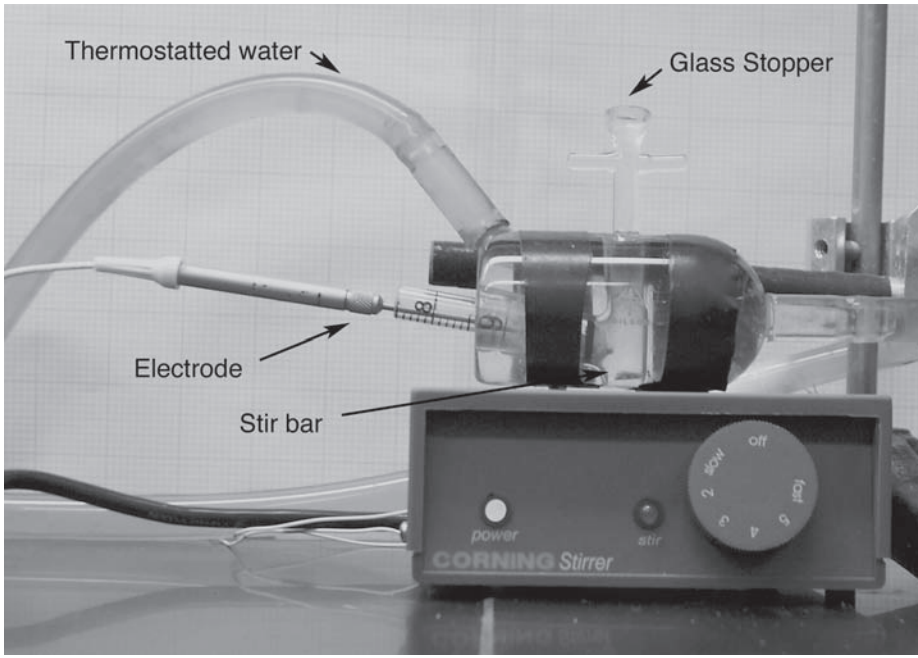

Fig. 1. Nitric oxide electrode chamber and cell. A 2-mm ISO-NOP NO electrode is custom fitted to a thermostatted, glass-stoppered, 2-mL cell (Gilson, Inc.) equipped with a stir bar and seated on a micromagnetic stirrer (Corning).

7. Rubber-septum-sealed glass tubes containing 3-mm × 10-mm micro stir bars and 1 mL pure water are used to prepare NO stock solutions. Glass tubes are custom sized from rubber-septum-sealed 10-mm × 100-mm (7-mL) Vacutainer® tubes (Becton-Dickinson) by cutting with a file to 45 mm and fire polishing the cut end. The rubber septum is reinserted in the tube for a gas-tight seal (*see* **Note 2**).
8. Thick-walled and limited gas (O_2, NO, CO)-permeability Tygon® R-3603 tubing (4.8 mm inner diameter [ID] × 14.3 mm outer diameter [OD]) is used to deliver gases to the septum-sealed glass tubes. Tube ends are connected to syringe needles using cut 1-mL Tuberculin syringe ends (Becton-Dickson) that fit tightly within the 4.8-mm-ID tubing. Syringe needles are used to deliver gases to rubber-septum-sealed tubes.
9. A 99.999% N_2 gas tank (Praxair, Bethlehem, PA) and regulator is used for purging O_2 from solutions. A calibrated flow meter can be used for controlling gas flow rates, but it is not essential (*see* **Note 3**).
10. A 98.5% NO gas lecture bottle (Aldrich, cat. no. 29,556-6) equipped with a regulator and backflow protection valve is used to prepare saturated (2 m*M*) NO stock solutions. Saturated NO stock solution is prepared by placing 1 mL of pure water in a 10-mm × 45-mm glass tube with a 3-mm × 10-mm micro stir bar that is

sealed with a rubber septum (*see* **Section 2.1.**, **item 7**). The water is purged by stirring for 5 min under 99.999% N_2 delivered at a rate of approx 30 mL/min to remove O_2. Then, 98.5% NO is bubbled at a rate of approx 5 mL/min for 7 min. NO gas is first passed through a rubber-septum-sealed 7-mL Vacutainer® tube containing 1*M* NaOH before being delivered in series via thick-walled Tygon R-3603 tubing to the stirring 1 mL water in the septum-sealed tube. Bubbling through NaOH is employed to remove higher oxides of nitrogen. All tubing connections are made with syringe needles. The system is vented at the terminus to a 125-mL Erlenmeyer flask containing 100 mL of 0.16*M* $KMnO_4$ and 2.5% H_2SO_4 to decompose exiting NO. Several NO stocks are prepared and are stored at 4°C. Each 1-mL tube provides up to 50, 2-μL aliquots for NO consumption assays before a significant decrease in NO is observed. Used NO stock solution can be tested by comparing the response with that for a fresh NO stock.

11. A squirting water bottle is used to rinse the electrode and chamber between assays (*see* **Note 4**).
12. An aspirator is used to carefully wash and evacuate the NO electrode cell.

2.2. NO Metabolism by Tissues, Cells, Organelles, Extracts, and Isolated Enzymes

1. Bovine erythrocyte copper- and zinc-containing superoxide dismutase (SOD) (5000 U/mg from Roche Diagnostics, Inc., cat. no. 0837113) is prepared by dissolving 100 mg in 1 mL of water. SOD is frozen on dry ice, stored at –80°C, and thawed in a 37°C water bath for repeated use.
2. A McIlwain tissue slicer (Brinkman Inst. Co., Westbury, NY, USA) is used to prepare 1-mm tissue slices.
3. A PowerGen 700 homogenizer (Fisher Scientific, Pittsburgh, PA) is used to homogenize tissues.
4. A Kontes glass–Teflon tissue homogenizer is used to prepare organelles.
5. A Virsonic 475 sonicator equipped with a microtip (Virtis Corp., Gardiner, NY) is used to prepare cell-free extracts.
6. Y-PER®-S yeast protein extraction reagent (Pierce Chemical Co., Rockford, IL, cat. no. 78999) is used to facilitate the lysis of yeasts by sonication.
7. NADH and NADPH (Roche Diagnostics, Inc., Indianapolis, IN) are prepared fresh as 10-m*M* stocks in water.
8. FAD (Sigma, F-6625) is prepared as a 1-m*M* stock in water and stored frozen at –20°C.
9. For bacterial NO consumption assays, a buffer containing minimal salts medium (60 m*M* K_2HPO_4, 33 m*M* KH_2PO_4, 7.6 m*M* $(NH_4)_2SO_4$, and 1.7 m*M* sodium citrate), 10 m*M* glucose, and 200 μg/mL chloramphenicol saturated with 200 μ*M* O_2 is prepared fresh at 37°C (*see* **Note 5**).
10. For fungal, mammalian cell, and tissue NO consumption assays, a buffer containing Dulbecco's phosphate-buffered saline (8.1 m*M* Na_2HPO_4, 1.1 m*M* KH_2PO_4, 138 m*M* NaCl, 2.7 m*M* KCl, 0.9 m*M* $CaCl_2$ and 0.5 m*M* $MgCl_2$), 5 m*M* glucose, 100 μg/mL cycloheximide, and saturated with 200 μ*M* O_2 at 37°C is used (*see* **Note 5**).

11. For microsome NO consumption assays, a buffer containing 100 m*M* sodium HEPES, pH 7.8, 0.25*M* sucrose, 1 m*M* EDTA, 1 m*M* EGTA, and saturated with 200 μ*M* O_2 at 37°C is used.
12. For extracts and purified NODs (flavohemoglobins), a buffer containing 100 m*M* sodium phosphate, pH 7.0, 0.3 m*M* EDTA, and saturated with 200 μ*M* O_2 at 37°C is used. NAD(P)H (100 μ*M*), FAD (1 μ*M*), and SOD (0.5 mg/mL) are added as required by the specific assay.
13. For mitochondria, measurements are made in a 100-m*M* HEPES, pH 7.8, buffer containing 0.25*M* sucrose with succinate, malate, and other oxidizable substrates as required for respiration and activity.
14. Cultured mammalian cells, bacteria, fungi, or other cells and tissues grown, prepared, or procured by standard methods.

2.3. NO, O_2, and NAD(P)H Dependence of NO Metabolism

1. A 99.99% O_2 tank (Bethlehem, PA) and regulator is used to prepare a saturated 1.14 m*M* O_2 solution (at 20°C) in buffer or media essentially as described for the NO stock (*see* **Subheading 2.1.**, **item 10**) except that NaOH scrubbing and N_2 purging are not required.
2. A 99.999% N_2 tank (Praxair, Bethlehem, PA) and regulator is used to purge solutions free of O_2.
3. *Aspergillus niger* glucose oxidase (4000 U/mL) (Sigma, G-9010) and bovine liver catalase (1.3×10^6 U/mL) (Roche Diagnostics, Inc., Indianapolis, IN) are used to catalytically remove O_2 from buffers and media in the NO electrode cell chamber.
4. NADH and NADPH (10 m*M*) (Roche Diagnostics, Inc., Indianapolis, IN) are prepared fresh in water and are used at 100 μ*M* for the assay of NO metabolic activities of cell extracts, microsomes, and purified components.
5. A Clark-type O_2 electrode (Yellow Springs Inst. Co., Yellow Springs, OH) fitted in a thermostatted 2-mL cell chamber is used for measurements of O_2 concentration.

2.4. Products of O_2-Dependent NO Metabolism

1. A Virsonic 475 sonicator (The Virtis Co., Gardiner, NY) equipped with a microtip is used to disrupt cells and organelles.
2. Griess reagents are used for determining nitrite and nitrate. Griess reagents are prepared and used essentially as previously described ***(48,49)***.
3. Nitrate reductase (10 U/mg) from *A. niger* (Roche Diagnostics, Inc.) is used for nitrate measurements.
4. An ultraviolet (UV)–visible Beckman DU-640 spectrophotometer is used for nitrite/nitrate assays and NAD(P)H measurements.

2.5. Inhibitors of NO Metabolism and NODs

1. A 99.5% CO tank (Praxair, Bethlehem, PA) and regulator is used to produce a saturated 1-m*M* CO stock in water in a rubber-septum-sealed tube essentially as described for the NO stock (*see* **Subheading 2.1.**, **item 10**) except that NaOH scrubbing and N_2 purging are not required.

2. Sodium cyanide (Sigma, S-3296) is prepared as a 250-m*M* stock in water and is stored frozen at –20°C. The solution is stable for months.
3. Diphenyleneiodonium chloride (Sigma, D-2926) is prepared as a 50-m*M* solution in dimethyl sulfoxide (DMSO) and is stored frozen at –20°C.
4. Rotenone (Sigma, cat. no. R8875), Antimycin A (Sigma, cat. no. A-8674), myxothiazole (Fluka, cat. no. 70183) are prepared in ethanol as 0.5–4 m*M* solutions and stored at –20°C.

3. Methods

3.1. Clark-Type NO Electrode Measurements

Saturated NO (2 μL) is removed from the 2-m*M* NO stock solution by piercing the rubber septum with a 10-μL Hamilton syringe. NO is quickly injected into the glass-stoppered 2-mL electrode cell chamber and the NO electrode current response is recorded on the chart paper. Cells, microsomes, extracts, or purified proteins are added when the signal reaches its apex (*see* **Fig. 2**). Rates of NO decomposition are calculated for specific NO concentrations, and background rates of NO decomposition under control conditions are subtracted from the test rates at a given NO concentration (*see* **Note 7**). Rates are calculated from the tangents of the curves (*see* **Fig. 2** and **Note 6**). Typically, measurements are made for 1 μ*M* NO, which is equal to the rate at the half-maximal response of the NO electrode to 2 μ*M* NO.

3.2. NO Metabolism by Tissues, Cells, Organelles, Extracts, and Isolated Enzymes

1. Nitric oxide consumption activity is measured for cells that have been first quantitated. Mammalian cells are counted with a hemacytometer. For bacteria and fungi, growth is measured by turbidity at 550 nm and by plating and counting.
2. Cells are washed with appropriate assay medium and kept on ice. Bacteria are generally resuspended at 10^6 cells/μL. Mammalian cells and yeasts are resuspended at 2×10^6 cells per 30 μL. Then, 2–60 μL of cells are delivered to the 2-mL assay medium containing an initial 2 μ*M* NO. Rates of NO metabolism are generally determined at 1 μ*M* NO. Cells are varied in concentration in the assay to obtain measurable rates of NO decomposition (*see* **Note 8**). The medium used for bacteria is the minimal salts medium containing glucose and chloramphenicol as described in **Subheading 2.2.** The medium used for fungi, yeasts, and mammalian cells is a Dulbecco's phosphate-buffered medium containing glucose and cycloheximide as described in **Subheading 2.2.** Chloramphenicol or cycloheximide is added to block nascent protein synthesis and the induction of NO metabolizing activity during the assay. Rates of cellular NO consumption are calculated and reported as nanomoles of NO per minute per 10^7 cells. Alternatively, for mammalian cells having large variations in size, values for nanomoles of NO per minute per wet weight can be determined for whole-cell activity comparisons.

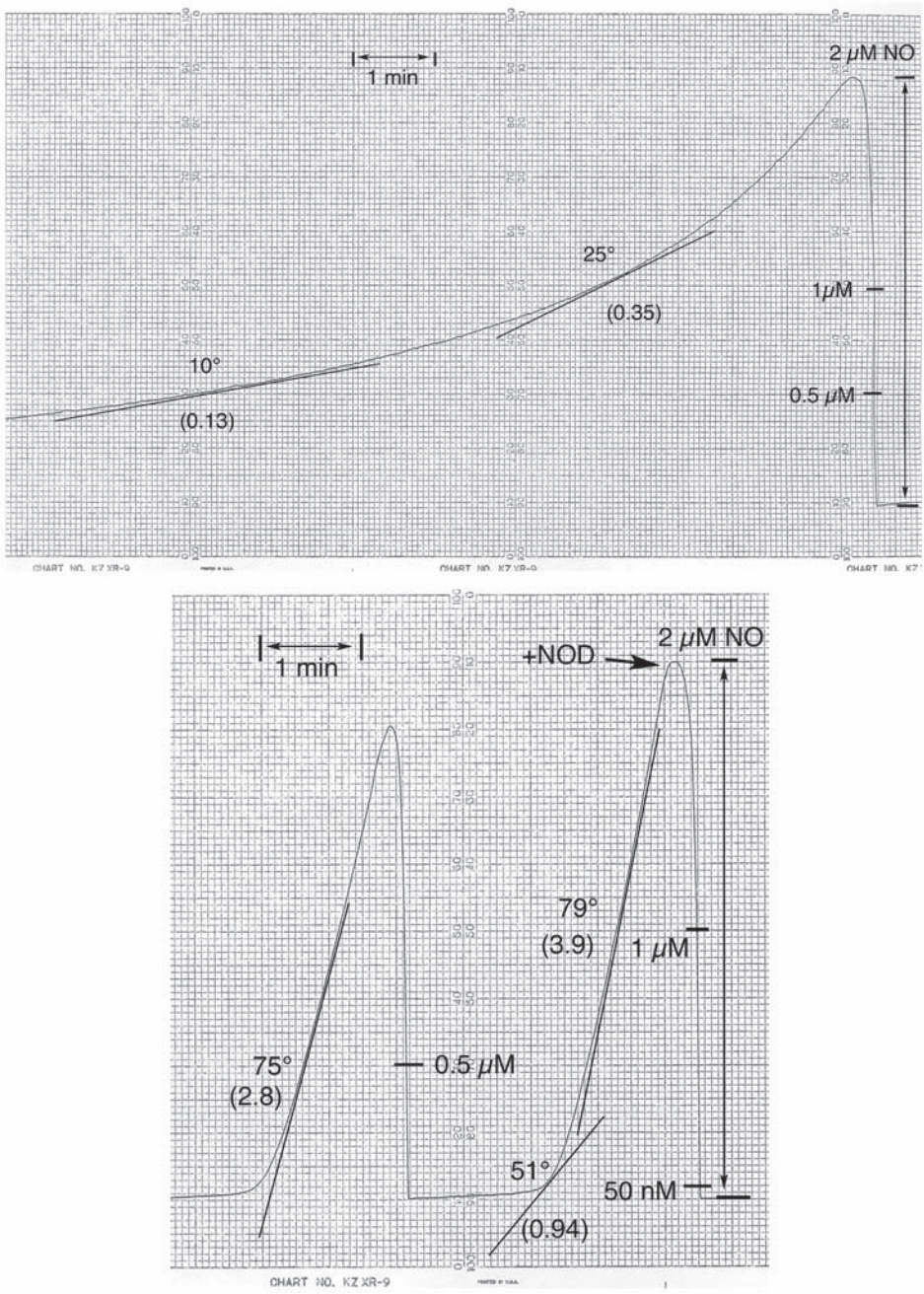

Fig. 2. Nitric oxide consumption rate measurements. Chart recording of NO decomposition in aerated buffer containing NADH, FAD, initial 2 μ*M* NO, and no catalyst (*top*) or *E. coli* NOD (flavohemogobin) is added at the apex of the NO response

3. Sliced tissues are prepared for NO consumption assay by first cutting tissues to approx 0.5 cm × 0.5 cm × 1 cm with a scalpel and then slicing with a McIlwain tissue slicer set for 1-mm slices. Slices are rinsed and kept in assay medium on ice in Petri dishes prior to assaying. Tissue slices (10–30 mg total wet weight) are placed in the 2-mL chamber prior to closing the cell with the glass stopper. Repetitive additions of 2 μ*M* NO are made to determine the catalytic rate of NO metabolism by the tissue because hemoglobin from contaminating erythrocytes rapidly and stoichiometrically consumes NO during the initial NO addition. Tissue slices are collected and saved following the assay to determine wet weight. Briefly, the assay volume containing tissue is removed to a preweighed 1.5-mL conical Eppendorf tube and centrifuged at 20,000*g* for 30 s. The supernatant is then aspirated and the tissue and tube weighed to determine the net tissue wet weight.
4. Nitric oxide consumption activities of microsomes and mitochondria are measured on isolated organelles. To prepare mitochondria and microsomes, frozen cell pellets containing 10^8–10^9 cells are thawed in a room-temperature water bath and immediately placed on ice. Cells are pooled and resuspended in sucrose buffer (0.25*M* sucrose, 100 m*M* sodium HEPES, pH 7.8, containing the protease inhibitors leupeptin [2 μg/mL] [Sigma, L-9783], pepstatin A [2 μg/mL] [Sigma, P-4265], phenylmethane sulfonylfluoride [1 m*M*] [Sigma, P-7626], EDTA [1 m*M*], and EGTA [1 m*M*] at a 3:1 volume ratio. Cells are homogenized with a Teflon–glass tissue homogenizer (Kontes Glass Company, Vineland, NJ) using seven passes at approx 500 rpm. The homogenate is then centrifuged at 1000*g* for 5 min at 4°C to remove cell membranes, intact cells, and nuclei. The supernatant is centrifuged at 10,000*g* for 10 min at 4°C to pellet mitochondria. The pellet is saved for measurements of the NO metabolic activity of mitochondria. Alternatively, mitochondria are isolated using a micro differential centrifugation method employing $<10^8$ cells ***(50)***. The supernatant is then centrifuged at 20,000*g* for 120 min at 4°C to pellet the lower-density microsome fraction. The microsome pellet is washed by overlaying with 2 mL of ice-chilled sucrose buffer containing 1 m*M* EDTA and 1 m*M* EGTA and centrifuging at 10,000*g* for 2 min. The wash is removed and the resulting microsomal pellet is suspended at a minimal 1:1 ratio of sucrose buffer containing 1 m*M* EDTA and 1 m*M* EGTA. Microsomes are frozen rapidly on dry ice and stored at –70°C. Microsomal protein is determined using the Peterson's modified Lowry method ***(51)*** with bovine serum albumin as the standard. An absorbance of 0.627 at 280 nm for 1 mg/mL is used for the bovine serum albumin concentration standardization ***(52)***.

Fig. 2. *(continued)* followed by a second 2-μ*M* NO bolus (*bottom*). Degrees declination are determined for specific NO concentrations (i.e., 1 μ*M*, 0.5 μ*M*, and 50 n*M*) and NO metabolic rates of NOD are calculated by subtracting background rates of NO decomposition for the specific NO concentration measured under otherwise identical conditions (*see* **Subheading 3.1.** and **Note 6**). Rates (nanomol NO/min) are calculated based on a 2-μ*M* NO response height of 158 mm and are given in parentheses.

5. To prepare cell-free extracts, bacteria, yeasts, and mammalian cells are resuspended in a <1:5 volume ratio of cells to 100 m*M* sodium phosphate, pH 7.0, buffer containing 0.3 m*M* EDTA. Cells are sonicated with the microtip at a maximum power setting for two to three 20-s intervals and are kept cold with an ice-water bath. Extracts are clarified at 20,000*g* for 1 min to remove membranes, and nonlysed cells and supernatants are transferred to fresh tubes. The Y-PER®-S reagent is used to facilitate yeast lysis during sonication. To prepare tissue extracts, a PowerGen 700 is used to homogenize tissues that have been first finely minced with a scalpel or razor blade. The tissue homogenate is then sonicated at a high-power setting and debris removed by centrifugation at 20,000*g* for 30 min at 4°C. NO consumption by cell-free extracts is measured in phosphate–EDTA buffer (*see* **Subheading 2.2., item 12**) containing 200 μ*M* O_2, 100 μ*M* NAD(P)H, 1 μ*M* FAD, 0.5 mg/mL SOD, 2 μ*M* NO, and extract (*see* **Note 9**). NO metabolic activities are calculated and recorded relative to protein as nanomoles of NO per minute per milligram protein.
6. Purified NODs (flavohemoglobins) are assayed for NO metabolic activity in phosphate–EDTA buffer at 37°C as described in **Subheading 2.2.**, containing 100 μ*M* NADH, 1 μ*M* FAD, 200 μ*M* O_2, and 2 μ*M* NO (*see* **Note 9**). Maximal turnover numbers are calculated from the maximal NO metabolic rates and the enzyme (or heme cofactor) concentration.
7. Superoxide dismutase (0.5 mg/mL) is added to all aerobic reactions to determine the contribution of $O_2^{\cdot -}$ to NO decomposition rates and to limit interference by $O_2^{\cdot -}$ when required by a particular sample or assay condition (*see* **Note 10**).

3.3. NO, O_2, and NAD(P)H Dependence of NO Metabolism

1. Rates of NO metabolism are measured at various NO concentrations following injection of a NO bolus (2 μ*M*) and cells, microsomes, or protein (*see* **Subheading 3.1.** and **Fig. 2**). The apparent K_M(NO) is the concentration of NO giving 50% maximal rate under a given condition of O_2, NAD(P)H, temperature, pH, and so forth.
2. The O_2 dependence of NO consumption and apparent $K_M(O_2)$ is determined by measuring NO metabolic rates in the absence and presence of varying O_2 concentrations. O_2 is eliminated from reaction mixtures by incubating the 2-mL assay volume with 5 m*M* glucose, 4 U/mL glucose oxidase, and 260 U/mL bovine liver catalase for 5 min prior to adding 2 μ*M* NO and cells, extracts, or microsomes. Alternatively, O_2 is eliminated by scrubbing the reaction with ultrapure N_2. A rubber septum is fitted in the glass stopper port, and the assay mixture and headspace is flushed with N_2 gas at 30 mL/min for 5 min prior to placing the glass stopper (*see* **Note 11**). Effects of various O_2 concentrations on NO metabolism are tested by adding O_2 from a 1.14-m*M* saturated O_2 solution in buffer to the N_2-purged 2-mL cell containing an amount of assay mixture determined to produce the desired final concentration of O_2. O_2 concentrations produced by mixings are verified using a Yellow Springs O_2 electrode calibrated for a 200-μ*M* O_2 saturation of buffer at 37°C. The O_2 electrode is also used to measure the amount of O_2 consumed during NO metabolism by cells or isolated components.

3. The effects of NAD(P)H concentration on NO metabolism are determined by measuring initial rates of NO decomposition with varying NAD(P)H concentrations. NAD(P)H concentration is determined using a millimolar extinction coefficient of 6.22 at 340 nm for a 1-cm path cell.
4. Requirements for H_2O_2 for NO consumption activity are tested by adding catalase (500 U/mL) or H_2O_2 (<1 m*M*).

3.4. Products of O_2-Dependent NO Metabolism

1. A fresh NO stock is used to measure nitrite and nitrate formation during aerobic NO metabolism by cells, tissues, microsomes, and so forth in the sealed 2-mL cell chamber. Sufficient cells or enzyme are used to produce a high rate of NO metabolism and to limit nitrite formation via NO auto-oxidation. NO (40 nmol; 20 μL) is injected at a slow rate such that NO does not accumulate appreciably (<0.5 μ*M*) as measured by the NO electrode. Following the reaction, the 2-mL reaction volume is quickly removed and centrifuged at 20,000*g* for 10 min to separate cells (or organelles) from the assay medium. The assay medium and cell (organelle) fractions are then frozen on dry ice ethanol and stored at –80°C.
2. Nitrite and nitrate are measured spectrophotometrically using the Griess reaction and NADPH-dependent nitrate reductase essentially as previously described ***(48,49)***. Nitrite and nitrate are assayed in the assay medium. Cells (or organelles) are resuspended in a minimal volume of fresh assay medium and lysed by sonication to release nitrite and/or nitrate from intracellular stores. Cell membranes, nonlysed cells, nuclei, and other dense cell debris are then removed by centrifugation at 20,000*g* for 5 min and nitrite and nitrate are measured in the supernatant. Amounts of nitrite and nitrate produced as a result of NO metabolism by cells, microsomes, or enzymes are corrected for the amount of nitrite and nitrate introduced with the stock NO solution. For this purpose, the remaining NO stock solution is thoroughly scrubbed with ultrapure N_2 and the solution is assayed for nitrite and nitrate.
3. NAD(P)H oxidation consequent to NO metabolism by enzymes and so forth is measured by following the NO-dependent change in absorbance at 340 nm and applying the extinction coefficient of $6.22 \times 10^3\ M^{-1}\ cm^{-1}$ for the reduced cofactors.

3.5. Inhibitors of NO Metabolism and NODs

1. The effect of NO on NO metabolic rates is tested for high and low NO:O_2 ratios. NO inhibition is demonstrated when higher NO:O_2 concentration ratios produce lower rates than low NO:O_2 concentration ratios. O_2 concentration is varied (*see* **Subheading 3.3.**, **step 2**) and the effect of NO concentration on NO metabolic rate is measured (*see* **Subheading 3.3.**, **step 1**). NO consumption rates are corrected for background rates and are calculated as described in **Subheading 3.1.**
2. CO is added from a saturated CO stock (1 m*M* CO) in water. For some NODs CO is competitive with respect to O_2. In order to measure effects of micromolar CO (<50 μ*M*) on NO metabolism by cells or purified components, it is important to

use O_2 concentrations near the apparent $K_M(O_2)$ value (*see* **Subheading 3.3., step 2**). The K_i value for CO is equal to the concentration producing 50% inhibition of NO metabolism at the apparent $K_M(O_2)$.

3. Cyanide is tested at 0–250 μ*M* for effects on the NO metabolic activity. Inhibition is normally rapid for heme-dependent NODs.
4. Diphenyleneiodonium is added at 50 μ*M* or less and the effects on NO metabolic activity of cells or purified components are measured following repetitive additions of 2 μ*M* NO to the NO electrode cell (*see* **Note 12**). Controls are measured in the presence of the solvent DMSO at corresponding concentrations.
5. The role of cytochrome c oxidase in mitochondria and mammalian cells is tested with 0.5 μ*M* notenone, 0.5 μ*M* antimycin A, and 4 μ*M* myxothiazole.

4. Notes

1. Regardless of the type of electrode cell design, it is important that the cell be closed with no headspace for the escape or equilibration of gases. Specially designed multiport thermostatted NO electrode cell chambers are also currently available from World Precision Instruments Inc. (Sarasota, FL).
2. The shorter tube allows for NO or CO solution removal with a Hamilton syringe. The 1-mL water volume is optimal for rapid mixing of gas and liquid in the tube.
3. Flow rates of N_2 are typically regulated at 30 mL/min for 5 min for purging the 1-mL NO stock solutions in glass tubes or assays within the 2-mL NO chamber cell.
4. Temperature influences the NO electrode response and can delay the return to baseline. Abrupt temperature changes are avoided by incubating the electrode chamber water wash bottle at 37°C.
5. O_2 saturation of buffers is achieved by rapid mixing and equilibration at the specified assay temperature and under a normal atmosphere.
6. Rate calculations are simplified by using a protractor to determine the angle (θ) of descent of NO decomposition relative to the baseline. An equation for calculating rates of NO decomposition is derived from the NO concentration response signal and a given chart rate. The relationship is: rate (nmol NO/min) = tan θ (chart speed [mm/min]/signal response height [mm]) × total NO (nmol) in the 2 mL reaction. For example, for a 150-mm chart response (height) for 2 μ*M* NO and a chart speed of 30 mm/min, the relationship is rate (nmol NO/min) = tanθ (0.8). For a 100-mm response to 2 μ*M* NO, it is tanθ (1.2) = rate (nmol NO/min). For a 100-mm response to 1 μ*M* NO, it is tanθ (0.6) = rate (nmol NO/min).
7. A variety of factors contribute to background NO decomposition rates. These include primarily electrode oxidation and reactions of NO with O_2. $O_2^{\cdot -}$ can be an important contributor to NO decomposition rates in reactions containing trace metals, free heme, ascorbate, or any number of oxidases. Changes in electrode membrane integrity can also influence NO decomposition rates by the electrode.

8. For whole-cell and tissue NO consumption assays, it is important that the cells be metabolically active in the assay medium. Thus, other media may prove better than those suggested.
9. FAD is required for some flavohemoglobins showing NOD activity and is thus routinely included in the assay mixture.
10. SOD is added at high levels to out compete reactions of NO with $O_2^{\cdot -}$. Generally, 0.5 mg/mL (2500 U/mL; approx 16 μ*M*) SOD suffices; however, for conditions in which high $O_2^{\cdot -}$ fluxes are suspected, higher SOD levels (1 mg/mL) should be used. SOD is particularly important when using NADH as the substrate for crude cell extract assays because NADH oxidases are prevalent and more active than NADPH oxidases in most soluble cell extracts. At high levels (0.5 mg/mL), SOD shows a noncatalytic NO decomposition activity. The contribution of this NO decomposition rate can be avoided by first depleting the activity with an initial NO bolus (2 μ*M*) addition prior to assay of the sample with a fresh NO bolus.
11. N_2 purging invariably allows for a small O_2 contamination of approx 1 μ*M* as measured using the O_2 electrode. Thus, glucose oxidase/catalase is preferred for maximal O_2 elimination.
12. Inactivation of flavoenzymes by diphenyleneiodonium requires enzyme turnover. Thus, it is important to incubate with diphenyleneiodonium during extended catalysis to observe the loss of activity.

References

1. Gardner, A. M., Gessner, C. R., and Gardner, P. R. (2003) Regulation of the nitric oxide reduction operon (*norRVW*) in *Escherichia coli*. Role of NorR and σ^{54} in the nitric oxide stress response. *J. Biol. Chem.* **278,** 10,081–10,086.
2 Zumft, W. (1997) Cell biology and molecular basis of denitrification. *Microbiol. Mol. Biol. Rev.* **61,** 533–616.
3 Gardner, A. M., Helmick, R. A., and Gardner, P. R. (2002) Flavorubredoxin: an inducible catalyst for nitric oxide reduction and detoxification in *Escherichia coli*. *J. Biol. Chem.* **277,** 8172–8177.
4. Gardner, P. R., Gardner, A. M., Martin, L. A., et al. (1998) Nitric oxide dioxygenase: an enzymic function for flavohemoglobin. *Proc. Natl. Acad. Sci. USA* **95,** 10,378–10,383.
5. Gardner, P. R., Gardner, A. M., Martin, L. A., et al. (2000) Nitric oxide dioxygenase activity and function of flavohemoglobins. Sensitivity to nitric oxide and carbon monoxide inhibition. *J. Biol. Chem.* **275,** 31,581–31,587.
6. Gardner, A. M., Martin, L. A., Gardner, P. R., et al. (2000) Steady-state and transient kinetics of *Escherichia coli* nitric oxide dioxygenase (flavohemoglobin): the tyrosine B10 hydroxyl is essential for dioxygen binding and catalysis. *J. Biol. Chem.* **275,** 12,581–12,589.
7. Hausladen, A., Gow, A. J., and Stamler, J. S. (1998) Nitrosative stress: metabolic pathway involving the flavohemoglobin. *Proc. Natl. Acad. Sci. USA* **95,** 14,100–14,105.
8 Liu, L., Zeng, M., Hausladen, A., et al. (2000) Protection from nitrosative stress by yeast flavohemoglobin. *Proc. Natl. Acad. Sci. USA* **97,** 4672–4676.

9 Mills, C. E., Sedelnikova, S., Søballe, B., et al. (2001) *Escherichia coli* flavohaemoglobin (Hmp) with equistoichiometric FAD and haem contents has a low affinity for dioxygen in the absence or presence of nitric oxide. *Biochem. J.* **353,** 207–213.
10 Ouellet, H., Ouellet, Y., Richard, C., et al. (2002) Truncated hemoglobin HbN protects *Mycobacterium bovis* from nitric oxide. *Proc. Natl. Acad. Sci. USA* **99,** 5902–5907.
11 Pathania, R., Navani, N. K., Gardner, A. M., et al. (2002) Nitric oxide scavenging and detoxification by the *Mycobacterium tuberculosis* haemoglobin, HbN in *Escherichia coli*. *Mol. Microbiol.* **45,** 1303–1314.
12 Frey, A. D., Farrés, J., Bollinger, C. J. T., et al. (2002) Bacterial hemoglobins and flavohemoglobins for alleviation of nitrosative stress in *Escherichia coli*. *Appl. Environ. Microbiol.* **68,** 4835–4840.
13. Flögel, U., Merx, M. W., Gödecke, A., et al. (2001) Myoglobin: a scavenger of bioactive NO. *Proc. Natl. Acad. Sci. USA* **98,** 735–740.
14 Brunori, M. (2001) Nitric oxide moves myoglobin center stage. *Trends Biochem. Sci.* **26,** 209–210.
15 Dou, Y., Maillett, D. M., Eich, R. F., et al. (2002) Myoglobin as a model system for designing heme protein based blood substitutes. *Biophys. Chem.* **98,** 127–148.
16. Hallstrom, C. K., Gardner, A. M., and Gardner, P. R. (2003) Nitric oxide metabolism in mammalian cells: substrate and inhibitor profiles of a microsomal NO dioxygenase. *Free Radical Biol. Med.* **35,** S98 (abstract).
17 Nakahara, K., Tanimoto, T., Hatano, K.-I., et al. (1993) Cytochrome P-450 55A1 (P-450dNIR) acts as nitric oxide reductase employing NADH as the direct electron donor. *J. Biol. Chem.* **268,** 8350–8355.
18 Poock, S. R., Leach, E. R., Moir, J. W. B., et al. (2002) Respiratory detoxification of nitric oxide by the cytochrome *c* nitrite reductase of *Escherichia coli*. *J. Biol. Chem.* **277,** 23664–23669.
19 Sarti, P., Giuffré, A., Barone, M. C., et al. (2003) Nitric oxide and cytochrome oxidase. Reaction mechanisms from the enzyme to the cell. *Free Radical Biol. Med.* **34,** 509–520.
20. Borutaité, V. and Brown, G. C. (1996) Rapid reduction of nitric oxide by mitochondria, reversible inhibition of mitochondrial respiration by nitric oxide. *Biochem. J.* **315,** 295–299.
21. O'Donnell, V. B., Taylor, K. B., Parthasarathy, S., et al. (1999) 15-Lipoxygenase consumes nitric oxide and impairs activation of guanylate cyclase. *J. Biol. Chem.* **274,** 20,083–20,091.
22. O'Donnell, V. B., Coles, B., Lewis, M. J., et al. (2000) Catalytic consumption of nitric oxide by prostaglandin H synthase-1 regulates platelet function. *J. Biol. Chem.* **275,** 38,239–38,244.
23. Abu-Soud, H. M. and Hazen, S. L. (2000) Nitric oxide is a physiological substrate for mammalian peroxidases. *J. Biol. Chem.* **275,** 37,524–37,532.
24 Eiserich, J. P., Baldus, S., Brennan, M.-L., et al. (2002) Myeloperoxidase, a leukocyte-derived vascular NO oxidase. *Science* **296,** 2391–2394.

25 Pearce, L. L., Pitt, B. R., and Peterson, J. (1999) The peroxynitrite reductase activity of cytochrome *c* oxidase involves a two-electron redox reaction at the heme a_3–Cu_B site. *J. Biol. Chem.* **274,** 35,763–35,767.
26 Torres, J., Sharpe, M. A., Rosquist, A., et al. (2000) Cytochrome *c* oxidase rapidly metabolises nitric oxide to nitrite. *FEBS Lett.* **475,** 263–266.
27 Pryor, W. A. and Squadrito, G. L. (1995) The chemistry of peroxynitrite: a product from the reaction of nitric oxide with superoxide. *Am. J. Physiol.* **268,** L699–L722.
28 Liu, X., Miller, M. J. S., Joshi, M. S., et al. (1998) Accelerated reaction of nitric oxide with O_2 within the hydrophobic interior of biological membranes. *Proc. Natl. Acad. Sci. USA* **95,** 2175–2179.
29 Gardner, P. R., Martin, L. A., Hall, D., et al. (2001) Dioxygen-dependent metabolism of nitric oxide in mammalian cells. *Free Radical Biol. Med.* **31,** 191–204.
30 Liochev, S. I. and Fridovich, I. (2002) Superoxide and nitric oxide: consequences of varying rates of production and consumption: a theoretical treatment. *Free Radical Biol. Med.* **33,** 137–141.
31 Schmidt, K. and Mayer, B. (1998) Determination of NO with a Clark-type NO electrode, in *Nitric Oxide Protocols* (Titheradge, M. A., ed.), Humana, Brighton, UK, Vol. 100, pp. 101–109.
32 Zhang, X., Lin, J., Cardoso, L., et al. (2002) A novel microchip nitric oxide sensor with sub-nM detection limit. *Electroanalysis* **14,** 697–703.
33 Kelm, M. and Schrader, J. (1990) Control of coronary vascular tone by nitric oxide. *Circ. Res.* **66,** 1561–1575.
34 Clarkson, R. B., Norby, S. W., Smirnov, A., et al. (1995) Direct measurement of the accumulation and mitochondrial conversion of nitric oxide within Chinese hamster ovary cells using an intracellular electron paramagnetic resonance technique. *Biochim. Biophys. Acta* **1243,** 496–502.
35 Taha, Z., Kiechle, F., and Malinski, T. (1992) Oxidation of nitric oxide by oxygen in biological systems monitored by porphyrinic sensor. *Biochem. Biophys. Res. Commun.* **188,** 734–739.
36 Stitt, J. T., Dubois, A. B., Douglas, J. S., et al. (1997) Exhalation of gaseous nitric oxide by rats in response to endotoxin and its absorption by the lungs. *J. Appl. Physiol.* **82,** 305–316.
37 Thomas, D. D., Liu, X., Kantrow, S. P., et al. (2001) The biological lifetime of nitric oxide: implications for the perivascular dynamics of NO and O_2. *Proc. Natl. Acad. Sci. USA* **98,** 355–360.
38 Griffiths, C. and Garthwaite, J. (2001) The shaping of nitric oxide signals by a cellular sink. *J. Physiol.* **536,** 855–862.
39 Griffiths, C., Yamini, B., Hall, C., et al. (2002) Nitric oxide inactivation in brain by a novel O_2-dependent mechanism resulting in the formation of nitrate ions. *Biochem. J.* **362,** 459–464.
40 Han, T. H., Hyduke, D. R., Vaughn, M. W., et al. (2002) Nitric oxide reaction with red blood cells and hemoglobin under heterogeneous conditions. *Proc. Natl. Acad. Sci. USA* **99,** 7763–7768.

41 Aslan, M., Ryan, T. M., Adler, B., et al. (2001) Oxygen radical inhibition of nitric oxide-dependent vascular function in sickle cell disease. *Proc. Natl. Acad. Sci. USA* **98,** 15,215–15,220.
42 Coffey, M. J., Natarajan, R., Chumley, P. H., et al. (2001) Catalytic consumption of nitric oxide by 12/15-lipoxygenase: inhibition of monocyte soluble guanylate cyclase activation. *Proc. Natl. Acad. Sci. USA* **98,** 8006–8011.
43 Gardner, A. M. and Gardner, P. R. (2002) Flavohemoglobin detoxifies nitric oxide in aerobic, but not anaerobic, *Escherichia coli*: evidence for a novel inducible anaerobic nitric oxide scavenging activity. *J. Biol. Chem.* **277,** 8166–8171.
44 Gardner, P. R., Martin, L. A., and Gardner, A. M. (1999) Nitric oxide detoxification by an O_2-dependent cyanide-sensitive pathway in mammalian cells: protection of the aconitases. *Free Radical Biol. Med.* **27,** S75 (abstract).
45 Yoshida, K., Kasama, K., Kitabatake, M., et al. (1980) Metabolic fate of nitric oxide. *Int. Arch. Occup. Environ. Health* **46,** 71–77.
46 Westfelt, U. N., Benthin, G., Lundin, S., et al. (1995) Conversion of inhaled nitric oxide to nitrate in man. *Br. J. Pharmacol.* **114,** 1621–1624.
47 Gardner, P. R., Costantino, G., and Salzman, A. L. (1998) Constitutive and adaptive detoxification of nitric oxide in *Escherichia coli*. Role of nitric oxide dioxygenase in the protection of aconitase. *J. Biol. Chem.* **273,** 26,528–26,533.
48 Green, L. C., Wagner, D. A., Glogowski, J., et al. (1982) Analysis of nitrate, nitrite, and [15N]nitrate in biological fluids. *Anal. Biochem.* **126,** 131–138.
49 Titheradge, M. A. (1998) The enzymatic measurement of nitrate and nitrite, in *Nitric Oxide Protocols* (Titheradge, M. A., ed.), Humana, Brighton, UK, Vol. 100, pp. 83–91.
50 Gardner, P. R., Raineri, I., Epstein, L. B., et al. (1995) Superoxide radical and iron modulate aconitase activity in mammalian cells. *J. Biol. Chem.* **270,** 13,399–13,405.
51 Peterson, G. L. (1977) A simplification of the protein assay method of Lowry et al. which is more generally applicable. *Anal. Biochem.* **83,** 346–356.
52. Nozaki, Y. (1986) Determination of the concentration of protein by dry weight—a comparison with spectrophotometric methods. *Arch. Biochem. Biophys.* **249,** 437–446.

12

Proteomic Method for Identification of Tyrosine-Nitrated Proteins

Kulwant S. Aulak, Thomas Koeck, John W. Crabb, and Dennis J. Stuehr

Summary

Biologic nitration of protein tyrosine (to form 3-nitrotyrosine) is a recently described phenomenon that is associated with many diseases. We have devised a proteomic methodology to identify these modified proteins. This utilizes protein fractionation by two-dimensional polyacrylamide gel electrophoresis (2-D PAGE), partial transfer onto polyvinylidene difluoride (PVDF) membranes, and Western blot analysis using an antinitrotyrosine antibody to identify the proteins. Alignment of the Western blots with the partially transferred 2-D PAGE gels enables identification of immunopositive protein spots. These are then excised and trypsin digested. Proteins are then identified using either matrix-assisted laser desorption ionization–time of flight mass spectrometry or capillary liquid chromatography tandem electrospray mass spectrometry. Nonspecific crossreactivity of the antibodies is determined using reduction of protein bound 3-nitrotyrosine to 3-amino tyrosine using sodium dithionite.

Key Words: Nitric oxide; proteomics; nitroproteome; tyrosine nitration; 3-nitrotyrosine; 2-D PAGE; mass spectrometry; 3-aminotryosine.

1. Introduction

Biologic nitration of protein tyrosine (to form 3-nitrotyrosine) is a recently described phenomenon that is associated with many diseases including transplant rejection, lung infection, central nervous system (CNS) and ocular inflammation, shock, cancer, and neurological disorders (e.g., amylotrophic lateral sclerosis, Alzheimer's disease, Parkinson's disease, and stroke) ***(1,2)***. Increased levels of tyrosine nitration in these diseases have been investigated by increases in immunohistological staining, increased staining by Western blot, or increases in nitrotyrosine in samples from disease tissue upon hydrolysis. Tyrosine nitration has been shown to lead to alteration in protein function.

From: *Methods in Molecular Biology, vol. 279: Nitric Oxide Protocols: Second Edition*
Edited by: A. Hassid © Humana Press Inc., Totowa, NJ

Therefore, the identification of the nitrated proteins will enable a better understanding of its involvement in the disease process. Protein tyrosine nitration is a specific, low-abundancy posttranslational modification in which few proteins are modified in vivo and only specific tyrosine residues within these proteins are affected ***(3–6)***. Protein nitration may be unique among posttranslational modifications in its dependency on reactivity of tyrosine residues in the protein target with the site of nitration believed to be dependent on the charge environment and location of the tyrosine residue ***(5)***. Because of low abundancy and lack of a signature motif for nitration, it is impossible to predict proteins that are targets and difficult to identify proteins nitrated in vivo. Accordingly, we are developing techniques to identify and characterize nitrated proteins. The approach allows global analysis of nitrated proteins and identification by mass spectrometry.

2. Materials

2.1. Equipment

1. Protean IEF Cell (Bio-Rad, CA).
2. Criterion gel system (Bio-Rad, CA).
3. Semidry transfer apparatus (Bio-Rad, CA).
4. X-ray film processor.
5. GS-710 Calibrated imaging densitometer (Bio-Rad, CA).
6. SpeedVac system.
7. Matrix-assisted laser desorption ionization–time-of-flight mass spectrometer (MALDI-TOF; PE Biosystems Voyager DE Pro).
8. 50-μm × 5-cm Biobasic C18 column (New Objectives, Cambridge, MA).
9. Quadrupole time-of-flight mass spectrometer (Q-TOF2; Micromass, Beverly, MA).

2.2. Reagents

With the sensitivity of mass spectrometry and the number of physical manipulations associated with sample preparation, it is very important that care is taken at every point to avoid contamination. All buffers need to be prepared carefully, with the highest grades of chemicals and with the least physical contact as possible.

2.3. Two-Dimensional Gel Electrophoresis

1. Lysis buffer A: 8*M* urea, 4% 3-[(3-cholamidedopropyl)dimethylammonio]-1-propanesulfonate (CHAPS), 0.1% dithiothreitol (DTT), 2% immobilized pH gradient (IPG) ampholytes.
2. Lysis buffer B: 7*M* urea, 2*M* thiourea, 4% CHAPS, 0.5% Triton X-100, 0.1% dithiothreitol (DTT), 2% IPG ampholytes.
3. Protein assay dye (Bio-Rad, CA).
4. Ready Strips (pH gradient strips [7, 11, and 18 cm]) (Bio-Rad, CA).

5. Mineral oil (biotechnology grade).
6. Sodium dodecyl sulfate-polyacrylamide gel electrophoresis (SDS-PAGE) reducing buffer: 50 m*M* Tris-HCl, pH 8.8, 6*M* urea, 30% glycerol, 2% SDS, 1% DTT, bromophenol blue.
7. SDS-PAGE alkylating buffer: 50 m*M* Tris-HCl, pH 8.8, 6*M* urea, 30% glycerol, 2% SDS, 2% iodoacetamide, bromophenol blue.
8. SDS-PAGE running buffer: 25 m*M* Tris/191 m*M* glycine, 0.1% SDS, pH 8.8.
9. Agarose sealing solution: 1% agarose in SDS-PAGE running buffer, bromophenol blue.
10. Tyrosine-nitrated molecular-weight markers, prepared using a 100-µg marker in 50 m*M* phosphate, pH 8.0, incubated with 5 m*M* tetranitromethane for 10 min and the reaction stopped using 10 m*M* of 2-mercaptoethanol.

2.4. Western Blotting Reagents

1. Transfer buffer: 20 m*M* Tris-HCl, 96 m*M* glycine, 20% methanol, pH 8.5.
2. Sodium dithionite.
3. Pyridine.
4. TBS: 20 m*M* Tris-HCl, 150 m*M* NaCl, pH 7.5.
5. Washing buffer: TBS+ 0.2% Tween-20.
6. Blocking buffer: wash buffer + 1% bovine serum albumin (BSA).
7. Colloidal Coomassie blue (Gel Code blue; Pierce Biotech, IL).
8. Monoclonal antibody antinitrotyrosine (clone 1A6; Upstate Biotech, Lake Placid, NY).
9. Goat anti-mouse IgG–horseradish peroxidase (HRP) conjugate (Sigma, St. Louis, MO).
10. ECL-Plus (Amersham Pharmacia, NJ).
11. Hyperfilm ECL (Amersham Pharmacia, NJ).

2.5. In-Gel Digestion and Mass Spectrometry

1. *N*-Ethylmorpholine (NEM).
2. Sequencing-grade modified trypsin (Promega, Madison WI).
3. Trifluoroacetic acid.
4. C18 Zip-Tip (Millipore, NJ).
5. α-Cyano-4-hydroxy-cinnamic acid (CHCA) (further purification is typically required; *see* **Note 1**).
6. ProteoMass™ Peptide MALDI-TOF calibration kit (Sigma, St. Louis, MO).

3. Methods

Proteomics concerns the analysis of all the proteins expressed in a cell or tissue. Although a number of approaches are available for proteomic analysis, the most widely used methods involve protein fractionation by two-dimensional polyacrylamide gel electrophoresis (2-D PAGE). This technique has recently been revitalized by the development of narrow and more stable immobilized pH gradients to obtain very reproducible isoelectric focusing (IEF) results *(7)*. Although 2-D PAGE techniques present limitations for the identifi-

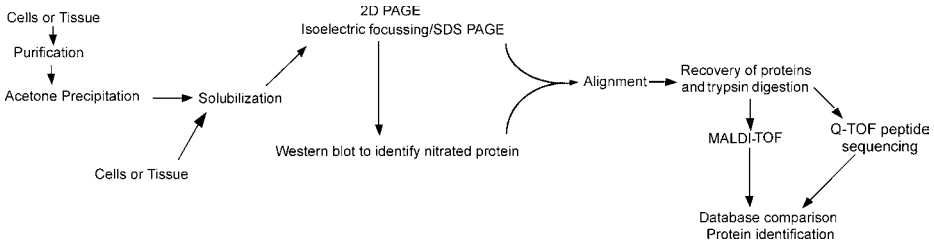

Fig. 1. Overview of the proteomic approach to analyze and identify nitrated proteins by using the high-throughput system.

cation of low-abundancy proteins, membrane proteins, and high-molecular-mass proteins, this approach combined with other methods can overcome some of these deficits ***(8–10)*** (*see* **Note 2**). An overview of the methodology we use for the identification of nitrated proteins is shown in **Fig. 1**.

3.1. Sample Preparation

For optimal 2-D separation, samples should be denatured and fully solubilized using urea, a nonionic detergent, and a reducing agent ***(11)*** (*see* **Notes 3** and **4**). Animal tissues and cultured cells are typically lysed and proteins solubilized in the IEF solvent. Selection and optimization of the IEF solvent is critically important in determining the quality of the 2-D PAGE. Sample solution containing high salt and/or SDS interfere with IEF using immobilized pH gradients. Two standard IEF solvents are lysis buffer A and lysis buffer B, and they offer a good starting point for new 2-D PAGE projects. These IEF solvents provide rapid deactivation of most enzymes, minimizing degradation and modification of samples. Samples prepared in buffers or solvents incompatible with IEF can be exchanged with other solvents by using protein precipitation in acetone (2 vol of acetone to 1 vol of sample, and centrifugation) ***(12)*** (*see* **Note 5**). Lysed samples are sonicated to break up DNA to reduce viscosity and spun down to remove any insoluble material.

3.2. Protein Concentration

Protein concentrations are calculated using a modified Bradford assay as urea, DTT, and CHAPS in the buffers can lead to inaccuracies based on other protocols ***(13)*** (*see* **Note 6**). Ovalbumin is used as the standard solution and is made up in lysis buffer to 5 mg/mL.

1. Stock ovalbumin solution is diluted to create a standard curve of 0–50 μg per 10 μL per Eppendorf tube in lysis buffer.
2. Ten microliters of 0.1*N* HCl is added first, followed by 80 μL Milli-Q water.

Table 1
Times and Voltages for the Rehydration and IEF Steps for Different-Sized Strips

Rehydration Step									
Size	7 cm			11 cm			18 cm		
	30 V, 50 μA max 14 h			30 V, 50 μA max 14 h			30 V, 50 μA max 10 h		
IEF Continues Directly from the Rehydration Step									
	Voltage (V)	Time (h)	Ramp	Voltage (V)	Time (h)	Ramp	Voltage (V)	Time (h)	Ramp
Step 1	30	0		30	0		30	0	
Step 2	250	0.01	Rapid	250	0.01	Rapid	300	0.01	Rapid
Step 3	8000	1.0	Linear	8000	2.5	Linear	3500	8.00	Linear
Step 4	8000	5	Hold	8000	10	Hold	3500	1.00	Hold
Step 5							8000	10	Hold
Stop at	20,000 V h			40,000 V h			80,000 V h		

3. Protein dye concentrate is diluted 1:3 in water and 900 μL is added into the samples and standard solutions.
4. Optical density is read at 595 nm. Protein concentrations are calculated from the standard curve.

3.3. Two-Dimensional Gel Electrophoresis

We perform 2-D PAGE using a protean IEF cell and IEF criterion gels (13-cm gels); however, equipment from many other companies may be used with equally good results ***(4,14)***. For larger gels, the iso-Dalt system can be used. Development of stable narrow-range pH gradients has allowed the increased utility of this approach. Narrow pH gradients over a single pH unit allow higher-resolution separation of proteins and increased protein loading. These pH gradients are available in 7-cm, 11-cm, 18-cm, and 24-cm strips. Focusing conditions will vary with sample composition, complexity, and pH range. The suggested values shown in **Table 1** are a good starting point and may be modified to optimize performance. The best starting point for analysis is using small gels such as 7-cm or 11-cm immobilized IEF strips with a pH 3.0–10.0 gradient, so that conditions can be quickly optimized. Longer strips, narrower pH gradients, and larger gels can be used to increase protein loading and increase resolution over regions of interest.

1. Samples are loaded into the strip holder (125 μL to 7 cm [50–200 μg]); 185 μL to 11 cm [200–400 μg]; and 350 μL to 18 cm [400–800 μg]) and the IPG strip carefully placed on top, removing any trapped air bubble.
2. Mineral oil is added to cover the strips to prevent dehydration during the run.
3. IPG strips are rehydrated and isoelectric focused as shown in **Table 1**.
4. After the run, the strips are removed and rinsed in Milli-Q water.
5. The samples on the strips are reduced using freshly prepared SDS-PAGE reducing buffer for 12 min.
6. The reducing buffer is removed and freshly prepared SDS-PAGE alkylating buffer is added for a further 12 min.
7. The strips are placed on top of a 12% acrylamide slab gels containing a 4% stacking gel. For large-format gels, Duracryl may be used as a substitute for polyacrylamide (*see* **Note 7**).
8. Adjacent to the strips, tyrosine-nitrated molecular-weight markers are run. These are prepared by mixing the nitrotyrosine-modified molecular-weight markers with SDS-PAGE-reduced loading buffer. This is then mixed with an equal volume of agarose sealing solution and soaked into filter paper squares. These serve as controls for membrane transfer, immunodetection, and aid in landmarking to enable alignment of the Western blot with the stained protein gel.
9. Agarose sealing solution is added on the top of the gel to embed the strip and molecular-weight markers.
10. The SDS-PAGE gels are run according to Laemmli at 50 V until the sample enters the body of the gel and then at 150 V until the dye front reaches the bottom of the gel.
11. After completion of the run, the acrylamide gels are soaked in transfer buffer and then partially transferred onto PVDF membrane (Millipore, MA) using a semidry transfer apparatus at 0.8 mA/cm^2 for 15 min.
12. The gels are then stained with collodial Coomassie blue (Gel Code Blue; Pierce) or silver and Western blot analysis performed on the PVDF membrane (Millipore).

The 2-D gels need to be handled with care during the protein transfer, staining, and storage and be covered at all times to eliminate the possibility of contamination.

3.4. Western Blot Analysis

1. The PVDF membranes are blocked for at least 4 h using blocking buffer.
2. Membranes are then probed overnight at 4°C with a monoclonal antibody against nitrotyrosine (1:4000; clone 1A6) in blocking buffer (*see* **Note 8**).
3. Membranes are then washed three times in washing buffer (20 min per wash).
4. Membranes are then probed with a goat anti-mouse–HRP conjugate in blocking buffer. Dilution of the secondary HRP-conjugated antibody to mouse IgG needs to be optimized for every new batch. The membranes are then washed three times in wash buffer and finally washed twice with TBS (15 min per wash).
5. Immunopositive spots are then visualized using ECL or ECL-Plus and Hyperfilm ECL (*see* **Fig. 2**).

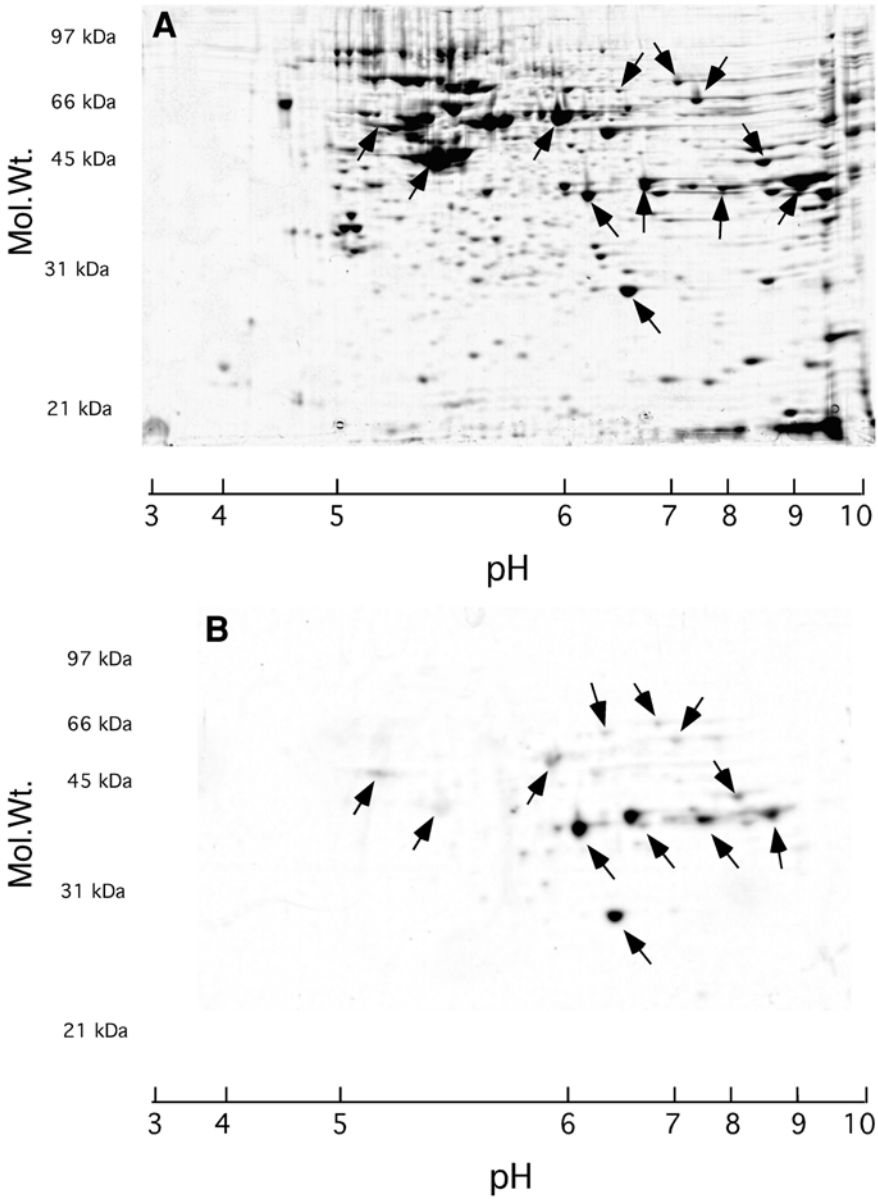

Fig. 2. Identification of tyrosine nitrated proteins in A549 cells. A549 cells were stimulated with cytokine interferon-γ (1000 U/mL), tumor necrosis factor-α (10 U/mL), and interleukin-1β (10 U/mL) for 3 d and then lysed with buffer B. The cell lysate (300 µg) was then run on 11-cm, pH 3.0–10.0; nonlinear gradient IEF strip. **(A)** Coomassie stained gel; **(B)** Western blot probed using a monoclonal antinitrotyrosine antibody. Arrows are shown to illustrate the immunopositive proteins on the stained gel and the Western blot.

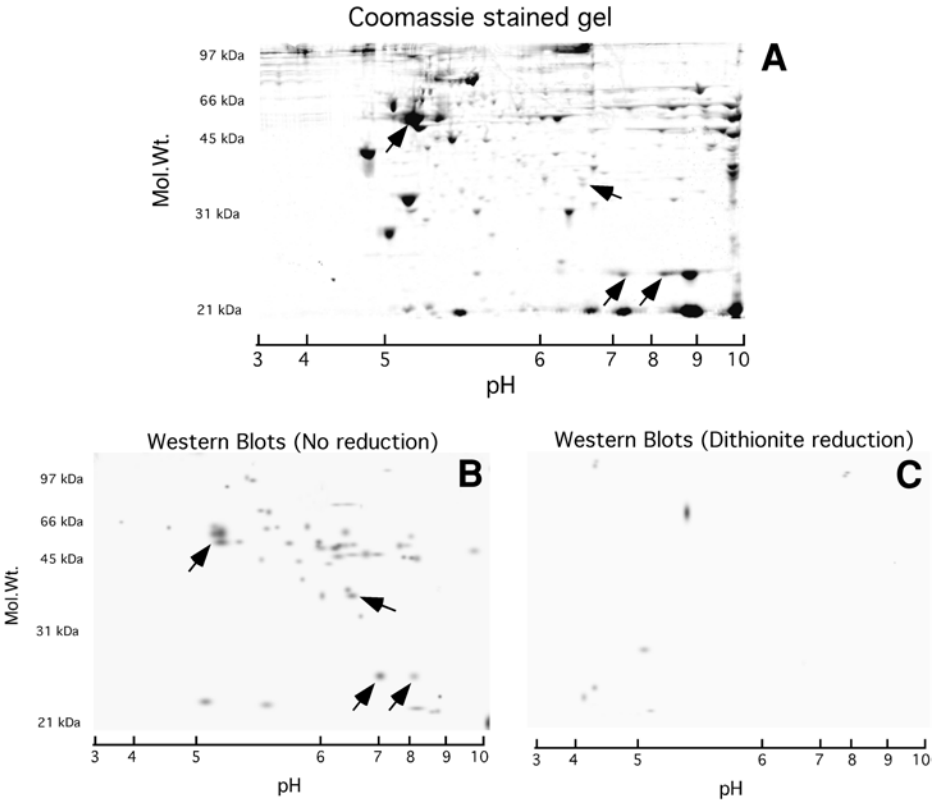

Fig. 3. Specificity of the antinitrotyrosine antibody. Mouse heart tissue was lysed in buffer B and 300 μg loaded onto duplicate 11-cm, pH 3.0–10.0; nonlinear gradient IEF strips. 2-D PAGE gels were run **(A)** (Coomassie stained) and partially transferred onto the PVDF membrane. Membranes were either probed with the monoclonal antinitrotyrosine antibody directly **(B)** or reduced using sodium dithionite before Western blot analysis. Arrows are shown to illustrate the immunopositive spots.

3.5. Elimination of False Positives

All protein nitration targets to date have been identified exclusively by antibodies directed against nitrotyrosine. However, the possibility exists that antibodies may generate some false positives. The use of a monoclonal antibody to nitrotyrosine reduces this risk. To distinguish between specific and nonspecific nitrotyrosine immunoreactivity, duplicate Western blots are performed in which the one of the PVDF membranes is reduced using freshly made 10 m*M* sodium dithionite in 50 m*M* pyridine–acetate, pH 5.0, for 1 h ***(6)*** (*see* **Note 9**). This reduces the nitrotyrosine to aminotyrosine; therefore, any remaining immunoreactivity on the membrane could be the result of nonspecific interac-

tions (*see* **Fig. 3**). After reduction, the PVDF membrane is washed with water before performing the Western blot analysis as described earlier.

3.6. Polyacrylamide/Western Blot Alignment

A critical part of this analysis is the alignment of the Coomassie-stained gel to the X-ray film. On staining the polyacrylamide gel, expansion occurs that causes a change in the size of the gel and this is more pronounced on larger-format gels. Specialized software such as PDQuest from Bio-Rad can help overcome this problem but are very expensive. When many immunopositive spots are present and using smaller gels, we find that using Adobe Photoshop can work just as well. The PAGE gels are scanned using an imaging densitometer and Photoshop is used to enlarge or reduce the size of the image to the size of the Western blot. Alternatively, Western profiles can be enlarged to the size of the 2-D gel using an office copy machine and transferred to a transparency for direct overlaying onto the stained gel ***(6)***. The immunopositive bands from the markers on either side of the gel as well as the shape and distribution of the immunopositive spots can be used to aid in the alignment. Once aligned, the corresponding immunopositive spots can be identified and cut from the gel.

3.7. Protein Identification

Once the nitrated protein spots are detected, the protein(s) contained in the spot are identified using mass spectrometry. The gel spots are first excised, the stain washed away, and then the protein digested to generate peptide fragments that can be analyzed. Numerous enzymes are available to fragment the protein; however, trypsin is most commonly used because it has a highly defined specificity, cleaves protein efficiently, and generates peptides of a size that are well suited to mass spectrometry.

3.7.1. In-Gel Trypsin Digestion

All washing is done at room temperature on a tilting table.

1. Sterile siliconized 1.5-mL Eppendorf tubes are washed three times with 500 µL of 60% acetonitrile/0.1% trifluoro acetic acid (TFA).
2. Identified immunopositive Coomassie-stained spots are cut from the gel into 1-mm^3 cubes and placed into prewashed Eppendorf tubes.
3. These pieces are then washed as follows:
   a. Twice in 250 µL of 50% acetonitrile for 15 min each wash.
   b. Once with 250 µL of 50% acetonitrile/50 m*M* ammonium bicarbonate for 30 min.
   c. Three times for 30 min each in 50% acetonitrile/30 m*M* NEM, pH 8.6.
4. The gel pieces are then completely dried on a SpeedVac.
5. Rehydrated using 15 µL of a 30-m*M* NEM solution containing 0.1 µg sequencing-grade modified trypsin.

6. After 20 min, 5–15 μL of 30 m*M* NEM is added if gels pieces are insufficiently hydrated. These samples are then incubated at 37°C overnight to allow complete trypsin digestion.

3.7.2. Extraction of Peptide

The in-gel digested peptides are extracted from the gels by incubation with 50 μL of 60% acetonitrile/0.1% TFA for 30 min on a tilting table. The wash is then collected into prewashed siliconized tubes. This extraction process is repeated two more times and then the combined washing dried on a SpeedVac for subsequent mass spectrometry. The peptides are then dissolved in 10 μL of 0.1% TFA and used directly or further purified using a C18 Zip-Tip and eluted with 75% acetonitrile containing 0.1% TFA.

3.8. Mass Spectrometry

The extracted peptides are analyzed for protein identification using two mass-spectrometric approaches: MALDI-TOF and liquid chromatography (LC) tandem mass spectrometry. MALDI-TOF mass spectrometry is highly accurate and sensitive, and allows for high-throughput analysis. Both MALDI-TOF MS and LC MS/MS can detect less than 50 fmol of protein. With LC MS/MS, we have identified tyrosine nitration sites using less than 5 fmol of protein ***(6)***. With MALDI-TOF, proteins are identified based on peptide mass mapping or peptide fingerprints (i.e., proteins digested by specific proteolysis generate peptide maps that are exclusive to that protein). Identification of four or more peptides from the protein, at high accuracy, can lend to its identification ***(15)*** (*see* **Note 10**). Major benefits of this technology are that it is rapid, relatively inexpensive, and easy to use. However, mixtures of proteins or small proteins that generate smaller numbers of peptides present difficulties for analysis by this procedure. For such samples, we prefer capillary bore LC tandem electrospray mass spectrometry (LC/MS/MS). This approach separates the peptides further by reverse-phase chromatography and then sequences select peptides following collision-induced fragmentation. This methodology is ideal for protein mixtures because only one reliable peptide sequence is needed for protein identification and it also allows localization of nitrotyrosine residues. However, this technology is more complex than MALDI-TOF MS and much more expensive.

3.8.1. MALDI-TOF Mass Spectrometry

For MALDI-TOF mass spectrometry we use a PE Biosystems Voyager DE Pro instrument equipped with a nitrogen laser (337 nm) and operated in the delayed extraction and reflector mode with a matrix of CHCA (5 mg/mL in 50% acetonitrile/0.3% TFA). Internal standards are used for calibration, such as the ProteoMass™ (*see* **Note 11**). One microliter of sample is mixed with 1 μL

of matrix and 0.5 μL of internal standard mix; then, 1.5 μL is applied to the sample plate and allowed to dry. Each spectrum is accumulated for 250 laser shots. Measured peptide masses are used to search the Swiss-Prot, TrEMBL, and NCBI sequence databases for protein identifications. Each peptide map dataset is searched using either MS-Fit (www.prospector.ucsf.edu/htmlucsf3.4/msfit) or Mascot (www.matrixscience.com). All searches are performed with a mass tolerance of 0.005% error (50 ppm) ***(4,6)***.

3.8.2. LC MS/MS

For LC MS/MS, we use a quadrupole time-of-flight mass spectrometer (QTOF). Tryptic peptides are diluted in 10 μL of 0.1% formic acid and loaded onto a 50-μm × 5-cm Biobasic C18 column at a rate of 5 μL/min. Solvent pumps are set at 8 μL/min and the flow rate is controlled with a splitter in front of the switching valve. Peptides are eluted at 250 nL/min with a gradient of 5–40% acetonitrile over 20 min. The elute is directed into the QTOF2 and immediately ionized using an electrosprayer. The mass spectrometer is operated in standard MS/MS switching mode with the three most intense ions in each survey subjected to MS/MS analysis. In identifying nitrotyrosine-containing peptides, the "include function" of the instrument operating software is used to program MS/MS analysis precursor ions of all possible nitrotyrosine-containing tryptic peptides based on the structure of the protein preidentified by MALDI-TOF MS (calculated as doubly and triply charged ions). Protein identification and MS/MS data analysis is by using micromass software protein Lynx Global Server, Mass lynx, and the Swiss-Prot, and NCBI protein sequence databases ***(6,16,17)***.

The above procedure identifies the protein that is extracted from the gel. However, the gold standard to define that a protein is tyrosine nitrated is to sequence and identify the modified amino acid in the protein sequence ***(9,18)***. However, this is a difficult procedure because the level of protein nitration is believed to be very low in vivo, and nitration is localized in specific regions of the tissue. Total tissue lysates causes mixing of the nitrated proteins with the same protein that is unmodified from other regions, thereby reducing its concentration. Procedures using protein purification and then affinity purification of the nitrated protein can lead to sufficient enrichment to be able to identify the modified tyrosine residue ***(9)***. A less stringent confirmation of a protein can be done using immunoprecitation using as protein-specific antibody, SDS-PAGE, and Western blotting and probing with the antinitrotyrosine antibody.

3.9. Summary

Protein tyrosine nitration is an important posttranslational modification implicated in many diseases; however, the pathological mechanism remains

unclear. Proteomic methods provide a means to obtain a comprehensive view of the nitroproteome. In addition to its potential for identifying novel targets of tyrosine nitration in cells and tissues, proteomic studies will provide insights regarding the consequences of nitration and the complex effect of NO on biological systems.

4. Notes

1. Most CHCA purchased commercially needs to be recrystallized to obtain high-quality data. The state of the matrix can be deduced from the color and the ability to easily dissolve into the acetonitrile/water buffer. If the matrix is orange/yellow, then recrystallization is needed. We use recrystallization using ethanol:water. Basically a saturated solution of CHCA is made in hot 95% ethanol (not boiling). This is filtered to remove undissolved matrix. Two volumes of cold Milli-Q water are then added and the sample filtered. The crystallized material is washed extensively with cold water and dried. The resultant cake is then broken up into a powder and stored in the dark at –20°C in small aliquots. The later powder dissolves instantly in the acetonitrile buffer and gives superior spectra with decrease background noise.
2. Drawbacks of 2-D PAGE are that low-abundance proteins may not be detected, membrane proteins are not solubilized efficiently, and multiple proteins can be located in a single spot. Many of these issues can be partially resolved by optimizing conditions. On a 2-D gel, 1000–2000 spots can be resolved. These are the most abundant proteins in the sample. The issue of low abundance can be overcome using enrichment procedures such as subcellular fractionation of organelle or membranes and affinity chromatography to enrich for proteins of interest or to deplete the sample from the most abundant proteins such as immunoglobulins and albumin in serum. Membrane proteins are poorly solubilized in conventional IEF buffers. New developments in specialized buffers containing dedicated zwitterionic detergents such as β-dodecyl maltoside aid in better solubilization and focusing ***(10)***. The problem of multiple proteins occupying the same spot on a gel can be partially overcome by using very narrow pH gradients on larger-format gels and also by using liquid chromatography (LC) MS/MS to identify the composition of protein spots.
3. Samples containing urea should not be heated above 37°C because this leads to protein carbamylation ***(13)***.
4. Initial sample preparation is critical to the quality of the 2-D PAGE. Protein aggregate or insoluble material can lead to poor samples and subsequent analysis. These may be the result of incorrect buffer choice or too small ratio of buffer to tissue.
5. Concentrating methods in which the sample pH fall such as trichloroacetic acid precipitation need to be avoided in the starting sample because this can lead to artificial nitration by a mechanism involving acidified nitrite ***(19)***.
6. Two-dimensional solubilization buffers use high concentrations of urea, reducing agents, nonionic detergent, and CHAPS. These are required to disrupt protein aggregates and complexes of proteins. These agents can, however, interfere with

protein estimation. For example, the Lowry, Biuret, and the BCA methods are based on reduction of Cu^{2+}. The presence of reducing agents could interfere with these assays. The Bradford agent is only slightly affected by these agents. The use of the acidified Bradford reagent improves the response over the 0- to 50-μg range ***(13)***.

7. On the large-format iso-Dalt gel system (23 cm), Duracryl (Genomic Solutions Inc., Ann Arbor, MI), an acrylamide-based matrix, can be used in the second dimension because this matrix has more strength and does not distort as much as conventional polyacrylamide ***(20)***. However, using this matrix can lead to some protein spots becoming rocket shaped compared to the round spots seen with polyacrylamide. This unusual property of this matrix can be useful to help align the Western blot to the protein gel because this spot shape provides unique landmarks on the gels.
8. The 1A6 monoclonal antinitrotyrosine antibody from Upstate Biotechnology is a well-characterized commercially available monoclonal antibody directed against nitrotyrosine and less prone to problems of nonspecific reactivity and batch variabilities of a polyclonal antibody. This antibody has indicated biological tyrosine nitration in numerous studies and was shown to recognize a variety of proteins subjected to chemical nitration, whose nitrated tyrosine residues were later confirmed by mass-spectrometric sequence analysis ***(9,18)***. However, it is not clear that this monoclonal antibody recognizes all tyrosine-nitrated proteins; therefore, the use of other antinitrotyrosine antibodies should be considered to obtain a comprehensive view of the nitroproteome.
9. Sodium dithionite is highly reactive and needs to be added to the buffer seconds before it is added to the membrane ***(6)***. Efficiency of reduction is dramatically reduced if the membrane is preblocked with protein; therefore, this method cannot be used to reprobe a previously used membrane.
10. MALDI-TOF mass spectrometry measures the precise size of the peptide. Algorithms are then used to compare the fragmentation patterns of known proteins in the sequence databases. Identifications can only be made against known proteins, unless they are highly conserved and similar proteins from other species are known. Small proteins (<15 kDa) generate small numbers of tryptic fragments and so may be difficult to match to the protein because the number of matches may be low (two or three fragments). In some samples, multiple proteins may be present, and although the software may be able to deconvolute mixtures of two or three proteins, more complex mixtures can be difficult. In the case of complex mixtures, or with small proteins, or when the signals from the Western blot suggest that the protein spot identified may be contaminated with adjacent proteins, it is better to determine the composition of the protein spot using capillary liquid chromatography tandem mass spectrometry. Identifying the nitrotyrosine-modified residue is essential to determine the identity of the nitrated protein in a mixture of proteins.
11. Any internal standards can be used as long as they give clean signals for the MALDI-TOF. We have purchased or produced our own peptides for this purpose. Best standards are combinations of two peptides with masses at approx 1000 and 2400 Da.

Acknowledgments

This work was supported by the National Institutes of Health (grants CA53914, GM51491, and NS41644) and the American Heart Association (grant AHA 01601598).

References

1 Beckman, J. S. and Koppenol, W. H. (1996) Nitric oxide, superoxide, and peroxynitrite: the good, the bad, and ugly. *Am. J. Physiol.* **271,** C1424–C1437.
2 Ischiropoulos, H. (1998) Biological tyrosine nitration: a pathophysiological function of nitric oxide and reactive oxygen species. *Arch. Biochem. Biophys.* **356,** 1–11.
3 MacPherson, J. C., Comhair, S. A., Erzurum, S. C., et al. (2001) Eosinophils are a major source of nitric oxide-derived oxidants in severe asthma: characterization of pathways available to eosinophils for generating reactive nitrogen species. *J. Immunol.* **166,** 5763–5772.
4 Aulak, K. S., Miyagi, M., Yan, L., et al. (2001) Proteomic method identifies proteins nitrated in vivo during inflammatory challenge. *Proc. Natl. Acad. Sci. USA* **98,** 12,056–12,061.
5 Souza, J. M., Daikhin, E., Yudkoff, M., et al. (1999) Factors determining the selectivity of protein tyrosine nitration. *Arch Biochem. Biophys.* **371,** 169–178.
6 Miyagi, M., Sakaguchi, H., Darrow, R. M., et al. (2002) Evidence that light modulates protein nitration in rat retina. *Mol. Cell. Proteomics* **1,** 293–303.
7 Rabilloud, T. (2002) Two-dimensional gel electrophoresis in proteomics: old, old fashioned, but it still climbs up the mountains. *Proteomics* **2,** 3–10.
8 Lescuyer, P., Strub, J. M., Luche, S., et al. (2003) Progress in the definition of a reference human mitochondrial proteome. *Proteomics* **3,** 157–167.
9 Aslan, M., Ryan, T. M., Townes, T. M., et al. (2003) Nitric oxide-dependent generation of reactive species in sickle cell disease. Actin tyrosine induces defective cytoskeletal polymerization. *J. Biol. Chem.* **278,** 4194–4204.
10 Luche, S., Santoni, V., and Rabilloud, T. (2003) Evaluation of nonionic and zwitterionic detergents as membrane protein solubilizers in two-dimensional electrophoresis. *Proteomics* **3,** 249–253.
11 Rabilloud, T. (1999) Solubilization of proteins in 2-D electrophoresis. An outline. *Methods Mol. Biol.* **112,** 9–19.
12. Crabb, J. W., West, K. A., Dodson, W. S., et al. (1997) Amino acid analysis, in *Current Protocols in Protein Science* (Coligan, J. E., Ploegh, H. L., Smith, J. A., et al., eds.), Wiley, New York, pp. 11.9.1–11.9.42. Unit 11.9 suppl. 7.
13 Ramagli, L. S. (1999) Quantifying protein in 2-D PAGE solubilization buffers. *Methods Mol. Biol.* **112,** 99–103.
14 West, K. A., Yan, L., Miyagi, M., et al. (2001) Proteome survey of proliferating and differentiating rat RPE-J cells. *Exp. Eye Res.* **73,** 479–491.
15 Jensen, O. N., Wilm, M., Shevchenko, A., et al. (1999) Sample preparation methods for mass spectrometric peptide mapping directly from 2-DE gels. *Methods Mol. Biol.* **112,** 513–530.

16 Crabb, J. W., Miyagi, M., Gu, X., et al. (2002) Drusen proteome analysis: an approach to the etiology of age-related macular degeneration. *Proc. Natl. Acad. Sci. USA* **99,** 14,682–14,687.
17 West, K. A., Yan, L., Shadrach, K., et al. (2003) Protein database, human retinal pigment epithelium. *Mol. Cell. Proteomics* **2,** 37–49.
18 Haqqani, A. S., Kelly, J. F., and Birnboim, H. C. (2002) Selective nitration of histone tyrosine residues in vivo in mutatect tumors. *J. Biol. Chem.* **277,** 3614–3621.
19 van der Vliet, A., Eiserich, J. P., O'Neill, C. A., et al. (1995) Tyrosine modification by reactive nitrogen species: a closer look. *Arch. Biochem. Biophys.* **319,** 341–349.
20. Patton, W. F., Lopez, M. F., Barry, P., et al. (1991) A mechanically strong matrix for protein electrophoresis with enhanced silver staining properties. *Biotechniques* **12,** 580–585.

13

Immunohistochemical Detection of *S*-Nitrosylated Proteins

Andrew J. Gow, Christiana W. Davis, David Munson, and Harry Ischiropoulos

Summary

Accumulating evidence shows that *S*-nitrosothiols, formed by the addition of nitric oxide (NO) to a cysteine thiol, *S*-nitrosylation, are involved in basal cellular regulation. It has been proposed that SNO formation/removal may be disrupted in a variety of pathophysiological conditions. Two types of methodology are presently available to identify specific *S*-nitrosylated proteins: (1) derivatization and (2) post-purification chemical detection. Neither of these techniques allows for *in situ* visualization of SNOs. Recently, we demonstrated that an antibody generated to the SNO moiety could be used to detect SNO formation from each of three isoforms of NOS by immunohistochemistry. This chapter details the immunohistochemical methodology used to detect SNOs *in situ*, offering a potentially powerful alternative for detection of SNO within tissue sections.

Key Words: *S*-Nitrosothiols; immunohistochemistry; nitric oxide synthase; nitrosylation.

1. Introduction

In the increasingly complex biology of NO-related signaling, the formation of *S*-nitrosothiols (SNOs) is recognized as one potential pathway for NO-based cellular regulation ***(1)***. A number of proteins with diverse functions have been identified as *S*-nitrosylated in vivo including the NMDA receptor ***(2)***, $p21^{ras3}$, OxyR ***(4)***, necrosis factor (NF-κB) ***(5)***, caspase-3 ***(6)***. At present, there are two types of methodology available to identify specific *S*-nitrosylated proteins, namely isolation and chemical analysis ***(7)*** or derivatization followed by electrophoretic separation ***(8)***. The identification of specific protein *S*-nitrosylation *in situ* has been difficult to achieve largely because of a variety of technical difficulties. Moreover, it has been difficult to demonstrate that SNO-adduct formation was associated with in vivo activation of nitric oxide synthase (NOS) isoforms. Recently, it has been demonstrated that an antibody generated against conjugated SNO can be used for detection of SNO proteins by enzyme-linked

From: *Methods in Molecular Biology, vol. 279: Nitric Oxide Protocols: Second Edition*
Edited by: A. Hassid © Humana Press Inc., Totowa, NJ

immunosorbent assay (ELISA), electrophoresis, and immunohistochemistry ***(9)***. Furthermore, these studies showed that each isoform of NOS is capable of generating SNO upon stimulation. There now exists a challenge to utilize this immunological approach to examine the production of SNO in a variety of pathophysiological states in which NOS function is altered. Here, we present an immunohistochemical method, utilizing anti-SNO antibodies to examine SNO production in tissue sections.

Three pathways for the production of SNO within biological systems have been proposed, namely nitrosation via the formation of N_2O_3 ***(10)***, metal catalysis ***(11,12)***, and direct reaction followed by electron abstraction ***(13)***. The first of these operates through the formation of the nitrosonium cation (NO^+), which reacts readily with nucleophilic targets, such as thiol. There is some debate as to the possibility of nitrosonium formation under physiological conditions, although under conditions of combined oxidative and nitrosative stress, such reactions will become more likely. The precise mechanisms involved in these reactions are unclear, either there is a concerted electron abstraction and thiol reaction as appears to operate in cerulo plasmin ***(11)*** or they may proceed through a radical intermediate (*R*-*S*-$NOH^{\cdot}$). SNO formation within hemoglobin has been shown to be associated with the formation of a novel radical intermediate ***(14)***.

The nitrosonium chemistry can be capitalized upon to make SNO-positive controls. By mixing equimolar quantities of acid and nitrite, one can generate nitrosonium intermediates. The addition of these intermediates to tissue sections (**Subheading 3.2., step 4**) results in the generation of SNO adducts within these tissues. In addition, this chemistry can be utilized to generate SNO equivalents within solution. Routinely, we synthesize *S*-nitrosoglutathione (GSNO) by mixing acidified glutathione with nitrite in equimolar quantities (*see* **Note 1**). Importantly, just as metals can be involved in SNO synthesis, they are readily able to catalyze the breakdown of the SNO bond. In particular, copper and mercury ions are known to operate in this regard. Indeed, these reactions have been utilized to construct chemical assays for SNO (the Saville and copper/cysteine assays ***[15]***). Mercury is unique in its reaction with SNO among metals; rather than merely catalyzing the cleavage of the bond, mercury forms a covalent bond with the sulfur (a mercaptan). This is critically important for the use of mercury as a negative control within SNO immunohistochemistry, as it means that once an SNO moiety has reacted with the mercury compound, the thiol is captured in the form of the mercaptan.

2. Materials

1. Phosphate-buffered saline (PBS): 2.88 g Na_2HPO_4, 16.0 g NaCl, 0.4 g KCl, and 0.48 g KH_2PO_4 in 2000 mL of water, pH to 7.2.

2. PBS/Triton: 3 mL of Triton X-100 in 1 L of PBS to make a 0.3% Triton–PBS mixtures.
3. Blocking buffer: 100% goat serum.
4. Borohydride: 0.1 g of $NaBH_4$ in 100 mL PBS (*see* **Note 2**).
5. Antigen retrieval solution: 0.28 g of EDTA and 0.41 g of Tris base in 750 mL of water (pH to anywhere within the range 6.0–9.0; as is appropriate for the tissue with which one is working).
6. Nitrosation solution: 0.34 g $NaNO_2$ in 2 mL of 0.1*M* HCl (*see* **Note 3**).
7. Organic mercury: 0.019 g *p*-hydroxymercuricbenzoatesulfone (pHMB) in 15 mL PBS (*see* **Note 4**).
8. Primary antibody: Antinitrosocysteine monoclonal antibody (in addition a rabbit polyclonal is available and this has also been used in this protocol) obtained from A. G. Scientific (www.agscientific.com; product no. N-1078). Supplied as a lyophilized powder, from PBS, and can be reconstituted with 150 µL distilled water, aliquoted and frozen at –20°C. Aliquots can be frozen and thawed up to five times.
9. Secondary antibody: Anti-mouse $F(ab)_2$ fragments conjugated with fluorescein isothiocyanate (FITC) for immunofluorescence or horseradish peroxidase (HRP) for 3,3'-diaminobenzidine (DAB) staining (Sigma). 1:100 dilution in 100% goat serum is optimal for both fluorescent and DAB staining.
10. Hydrogen peroxide: 5 mL of H_2O_2 in 25 mL methanol.
11. Primary antibody solution: Add 10 µL of reconstituted primary antibody to the blocking buffer (100% goat serum) to produce a 1:100 dilution that is optimal for immunohistochemistry (*see* **Note 5**).
12. PBS/BSA: 0.1g of bovine serum albumin (BSA) (fatty-acid-free fraction V) in 100 mL PBS (store at 4°C).
13. DAB solution: 5 mg DAB in 10 mL of PBS containing 0.1% BSA (fatty-acid-free fraction V). This solution should be filtered prior to use.

3. Methods

3.1. Immunofluorescent Detection of Tissue SNO

1. Both frozen and paraffinized tissue sections can be used for analysis. As both negative and positive controls are critical to the assessment of the degree of staining, it is preferable to have three serial sections mounted per slide.
2. Paraffinized tissue must be deparaffinized by placing slides within Coplin jars for 3 min in a succession of solutions, namely 2X xylene, 100% ethanol, 70% ethanol, 30% ethanol, and then distilled water.
3. Following deparaffinization or defrosting, slides are washed two times in PBS/Triton for 5 min each.
4. Slides are placed in antigen retrieval solution for 5 min. After incubation, the slides are microwaved twice for 5 min with a 1-min interval at full power. If necessary, more antigen retrieval solution can be added (*see* **Note 6**).
5. Wash slides for 5 min in distilled water and then 5 min in PBS/Triton.
6. After washing, encircle sections with a hydrophobic pen.

7. At this point, the slides are ready for staining and positive and negative controls can be created (*see* **Subheading 3.2.**).
8. Wash slides twice for 5 min in PBS/Triton.
9. Slides are immersed for 2 min three times in freshly prepared borohydride to remove background fluorescence (*see* **Note 7**).
10. Incubate slides for 30 min in blocking buffer (*see* **Note 8**).
11. Incubate slides overnight in the dark at 4°C in primary antibody (*see* **Note 9**).
12. Wash slides twice for 5 min in PBS/Triton.
13. Incubate slides with secondary antibody solution at room temperature in the dark for 2 h.
14. Wash slides twice for 5 min in PBS/Triton.
15. Wash slides twice for 5 min in PBS.
16. Wash in distilled water for 2 min.
17. Allow to air-dry in the dark.
18. Place a cover slip over the sections. Mounting solutions can be used, although it is preferred to use none and examine the slides immediately.

3.2. Immunohistochemistry Controls

1. *Tissue staining with antigen-competed primary antibody*. One potential negative control to gage the specificity of the staining achieved is to utilize antigen competition. For this control, 0.5 m*M* of GSNO is added to the primary antibody solution (*see* **Note 1**). The primary antibody solution is incubated for 2 h at room temperature prior to incubation with the slides.
2. *Conversion of SNO to a mercaptan with mercury solution*. As stated previously, the *S*-nitroso bond can be specifically broken by the reaction of sulfur with mercury to form a mercaptan. This can be achieved using either inorganic mercury, namely $HgCl_2$, or an organically linked mercurial such as pHMB. In our experience, although chemically inorganic mercury is more effective at SNO cleavage, pHMB works best in staining. Therefore, for a negative control, we utilize a 30-min incubation with organic mercury (**Subheading 3.1.**, **step 7**). The advantage of this step is that it controls directly for the specificity of the interaction of the antibody with SNO. Its disadvantage is that one cannot be certain of the degree of SNO cleavage that has been achieved with the use of the mercurial compound.
3. *Tissue staining with nonspecific purified mouse IgG*. An alternative negative control can be used of replacing the primary antibody with a similar titer of nonspecific mouse IgG.
4. *Generation of positive slides by acidified nitrite treatment*. It is beneficial to perform positive controls in order to check the quality of the stain. Positive controls are generated by placing fresh nitrosation solution on the tissue section and incubating for 30 min at room temperature at (*see* **Subheading 3.1.**, **step 7**).

3.3. DAB Staining for SNO

Adaptations of the protocol to conduct nonfluorescent staining for SNO utilizing DAB.

1. At **step 9** of **Subheading 3.1.**, replace immersion in borohydride with a 20-min incubation with hydrogen peroxide.
2. Wash two times for 5 min in PBS/BSA.
3. Incubate with HRP-linked $F(ab)_2$ secondary for 1 h
4. Wash twice with PBS/BSA for 5 min.
5. Add 10 μL of 30% H_2O_2 solution to DAB solution (mix well) and apply to the tissue sections.
6. Wait until the sections start to turn brown (pay particular attention to the positive controls).
7. Stop the reaction by rinsing the slides with PBS and then distilled water.
8. For counterstaining, follow steps in succession: 3X in xylene, 3 min each; 3X in 100% ethanol for 3 min; 2X in 95% ethanol for 2 min; several dips in water; 1 min in hematoxylin; several dips in water; 10 s in bluing agent; several dips in water; 3X in 95% ethanol for 2 min; 3X in 100% ethanol for 3 min; 3X in xylene for 3 min (*see* **Note 10**).
9. Air-dry in dark.
10. Mount with xylene base media and cover slip.

4. Notes

1. *S*-Nitrosoglutathione can be synthesized by mixing 0.5*M* glutathione dissolved in 0.5*M* HCl containing 0.1 μ*M* diethylenetriamine pentaacetic acid (DTPA) with 0.5*M* $NaNO_2$ dissolved in water containing DTPA. This makes a 0.25*M* GSNO solution that can be diluted to 0.05*M* in antibody solution and then further diluted in the primary antibody solution.
2. The borohydride solution should be made up fresh and immediately before use.
3. Upon mixing the nitrite and HCl nitrosonium, ions are formed immediately. If left on the bench for any period of time, these ions are lost and nitrogen equivalents are lost to the gas phase in the form of NO and NO_2. Therefore, these two reactants are mixed immediately prior to application to the tissues.
4. This solution should be stored in the dark.
5. The antibody dilution listed is optimal for most tissues. However, in any individual case, the optimal signal to background staining should be determined by serial dilution.
6. Frozen sections are considerably more fragile than paraffin embedded. Therefore, considerable care should be taken in their handling. The antigen retrieval step should only be used for paraffin sections, as it damages frozen ones and does not appear to improve staining in these sections.
7. Routinely with paraffin sections, slides are immersed in the borohydride solution, with each change of solution being made up immediately before use. Agitation of the sections during the washes has resulted in more efficient background reduction. When using frozen sections, we have found that this sort of treatment can cause damage to the tissues. Therefore, we spot apply and tap off fresh borohydride rather than immerse the whole slide.
8. Glycine can be added to the blocking step in order to block reactive aldehydes if background fluorescence persists.

9. All incubations of slides are performed in humidified boxes.
10. All alcohols used in counterstaining must be changed after each use. Using the same solution twice affects the degree of staining. Do not use the same alcohol solutions used for deparaffinizing.

References

1 Stamler, J. S., Lamas, S., and Fang, F. C. (2001) Nitrosylation. the prototypic redox-based signaling mechanism. *Cell* **106,** 675–683.

2 Choi, Y. B., Tenneti, L., Le, D. A., et al. (2000) Molecular basis of NMDA receptor-coupled ion channel modulation by *S*-nitrosylation. *Nature Neurosci.* **3,** 15–21.

3 Lander, H. M., Ogiste, J. S., Pearce, S. F., et al. (1995) Nitric oxide-stimulated guanine nucleotide exchange on p21ras. *J. Biol. Chem.* **270,** 7017–7020.

4 Kim, S. O., Merchant, K., Nudelman, R., et al. (2002) OxyR: a molecular code for redox-related signaling. *Cell* **109,** 383–396.

5 Marshall, H. E. and Stamler, J. S. (2001) Inhibition of NF-kappa B by *S*-nitrosylation. *Biochemistry* **40,** 1688–1693.

6 Mannick, J. B., Schonhoff, C., Papeta, N., et al. (2001) *S*-Nitrosylation of mitochondrial caspases. *J. Cell Biol.* **154,** 1111–1116.

7 Mannick, J. B., Hausladen, A., Liu, L., et al. (1999) Fas-induced caspase denitrosylation. *Science* **284,** 651–654.

8 Jaffrey, S. R., Erdjument-Bromage, H., Ferris, C. D., et al. (2001) Protein *S*-nitrosylation: a physiological signal for neuronal nitric oxide. *Nature Cell Biol.* **3,** 193–197.

9 Gow, A. J., Chen, Q., Hess, D. T., et al. (2002) Basal and stimulated protein s-nitrosylation in multiple cell types and tissues. *J. Biol. Chem.* **277,** 9637–9640.

10. Kharitonov, V. G., Sundquist, A. R., and Sharma, V. S. (1995) Kinetics of nitrosation of thiols by nitric oxide in the presence of oxygen. *J. Biol. Chem.* **270,** 28,158–28,164.

11. Inoue, K., Akaike, T., Miyamoto, Y., et al. (1999) Nitrosothiol formation catalyzed by ceruloplasmin. Implication for cytoprotective mechanism in vivo. *J. Biol. Chem.* **274,** 27,069–27,075.

12 Gow, A. J. and Stamler, J. S. (1998) Reactions between nitric oxide and haemoglobin under physiological conditions. *Nature* **391,** 169–173.

13 Gow, A. J., Buerk, D. G., and Ischiropoulos, H. (1997) A novel reaction mechanism for the formation of *S*-nitrosothiol in vivo. *J. Biol. Chem.* **272,** 2841–2845.

14 McMahon, T. J., Moon, R. E., Luschinger, B. P., et al. (2002) Nitric oxide in the human respiratory cycle. *Nature Med.* **8,** 711–717.

15. Fang, K., Ragsdale, N. V., Carey, R. M., et al. (1998) Reductive assays for *S*-nitrosothiols: implications for measurements in biological systems. *Biochem. Biophys. Res. Commun.* **252,** 535–540.

14

Gene Therapy Techniques for the Delivery of Endothelial Nitric Oxide Synthase to the Corpora Cavernosa for Erectile Dysfunction

Trinity J. Bivalacqua, Weiwen Deng, Hunter C. Champion, Wayne J. G. Hellstrom, and Philip J. Kadowitz

Summary

Erectile dysfunction (ED) is defined as the consistent inability to obtain or maintain an erection for satisfactory sexual intercourse. In the last decade, significant advancements in the pathophysiology of male ED have occurred. Basic science research on erectile physiology has been devoted to investigating the pathogenesis of ED and has led to the conclusion that ED is predominately a disease of vascular origin. Nitric oxide (NO) is the principal mediator of penile erection. NO is synthesized by endothelial nitric oxide synthase (eNOS) and neuronal NOS (nNOS) in the penis. Loss of the functional integrity of the endothelium and subsequent endothelial dysfunction plays an integral role in the occurrence of ED. This chapter reviews the use of two gene transfer techniques: adenoviral gene transfer of eNOS and eNOS gene-modified rat marrow stromal cells (rMSCs) to the penis of aged rats for the potential application of gene therapy for the treatment of ED.

Key Words: Erectile dysfunction; gene therapy; nitric oxide synthase; eNOS; stem cells; adenovirus.

1. Introduction

Penile erection is a complex neurovascular phenomenon that requires an increase in penile arterial inflow, relaxation of cavernosal smooth muscle, and restriction of venous outflow. Erectile capacity is dependent on the vascular tone, and relaxation of corporal smooth muscle is essential for normal erectile function. Recent evidence indicates that neuronal- and endothelial-derived nitric oxide (NO) is the principal mediator of cavernosal smooth muscle relaxation and penile erection ***(1,2)***. NO released by the endothelium that lines the corpus cavernosum and arteries that supply the penis and NO from nonadrenergic,

From: *Methods in Molecular Biology, vol. 279: Nitric Oxide Protocols: Second Edition*
Edited by: A. Hassid © Humana Press Inc., Totowa, NJ

noncholinergic (NANC) nerves bind to the soluble form of guanylyl cyclase to activate the enzyme and increase cavernosal intracellular levels of cyclic GMP (cGMP). The enzyme that catalyzes this reaction in the endothelium and NANC neurons is endothelial nitric oxide synthase (eNOS) and neuronal NOS (nNOS), respectively.

Adenoviral vectors are frequently used for gene transfer because of their high cellular transduction efficiency in a wide variety of cell types and tissues in vivo ***(3)***. Adenoviral vectors can be produced at very high titers, thereby allowing efficient gene transfer to a specific tissue with small volumes of virus, and accommodate a cDNA insert up to approx 8 kb. The greatest disadvantage of first-generation adenoviral vectors is the expression of viral proteins in infected cells, which can trigger a host-immune and inflammatory response that precludes repeated administration of this vector, as well as long-term and transient expression of the desired gene. However, there has been great interest in the development of replication-deficient second-generation or helper-dependent ("gutless") adenoviral vectors in which all viral genes are deleted and, thus, reduce host-inflammatory responses ***(4)***.

One of the most important recent discoveries in biomedical research is that stem cells are found in many tissues of the adult that can provide new cells for normal tissue turnover and can regenerate damaged and diseased tissue ***(5,6)***. Marrow stromal cells (MSCs), also known as mesenchymal stem cells, are adult stem cells from bone marrow that have multilineage differentiation potential and contribute to the regeneration of mesenchymal tissue, such as bone, cartilage, fat, and muscle ***(7–13)***. Because MSCs are relatively easy to isolate, expand ex vivo, and gene engineer, genetically modified MSCs have recently been used for gene delivery and tissue regeneration in the treatment of a variety of diseases with little to no host-immune response ***(14–20)***. In this chapter, we describe a method for using adenoviral gene transfer of eNOS and eNOS gene-modified rat marrow stromal cells (rMSCs) to the penis of aged rats for the potential application of gene therapy for the treatment of erectile dysfunction. This chapter will focus on the gene transfer technique for delivery of vectors to the corpus cavernosum of the penis.

2. Materials

1. Ad5RSVlacZ or Ad5RSVeNOS, replication-deficient recombinant adenoviruses carrying nuclear-targeted β-galactosidase (lacZ) or the bovine eNOS gene under the control of the rous sarcoma virus (RSV) promoter.
2. HEK 293 cells, COS-1 cells.
3. pAdRSV4.
4. Dulbecco's modified medium (DMEM), 100 μg/mL penicillin, 100 U/mL streptomycin, and 5% fetal bovine serum (FBS).

5. Culture medium for rMSCs: α-MEM, 20% FBS, 100 units/mL penicillin, 100 μg/mL streptomycin, 25 ng/mL amphotericin B, and 2 m*M* L-glutamine.
6. Six-week-old male brown Norway rats and 25-mo-old male brown Norway rats (Harlan, San Diego, CA).
7. Scalpel, scissors, forceps, syringe, needle, cell strainer with 70-μm Nylon mesh (BD Bioscience, Bedford, MA), T75 tissue culture flask, phosphate-buffered saline (PBS), and 0.25% trypsin/1 m*M* EDTA.
8. Sodium pentobarbital (Sigma, St. Louis, MO).
9. PE-50 tubing, 25-gage needles, pressure transducers.
10. Data acquisition system (Biopac Systems, Santa Barbara, CA).
11. Mouse Immunocruz Staining System (Santa Cruz Biotechnology, Santa Cruz, CA).
12. Mouse anti-eNOS monoclonal antibody (BD Transduction Laboratories, San Diego, CA).
13. Protease inhibitor (P.I.) buffer: 50 m*M* Tris-HCl, pH 7.4, 1 m*M* EDTA, containing protease arrest (Genotech).
14. Nitrocellulose membrane (Hybond-ECL, Amersham Life Sciences, Ghent, Belgium).
15. Blotto-Tween: 5% nonfat dry milk, 0.1% Tween-20.

3. Methods

The methods described outline (1) generation of replication-deficient recombinant adenoviruses, (2) isolation and ex vivo expansion of rMSCs, (3) adenoviral gene transfer of eNOS into rMSCs, (4) intracavernosal injection of adenoviruses encoding eNOS and eNOS gene modified rMSCs, and (5) functional analysis of erectile response.

3.1. Generation of Replication-Deficient Recombinant Adenoviruses

3.1.1. Preparation of Adenoviral Vectors

Replication-deficient recombinant adenoviruses encoding the reporter gene for nuclear-targeted β-galactosidase (lacZ; AdlacZ) and bovine endothelial nitric oxide synthase (AdeNOS), driven by the Rous sarcoma virus (RSV) promoters were generated by standard methods of the University of Iowa Gene Transfer Vector Core Laboratory ***(21–23)***.

1. Briefly, the cDNA for bovine eNOS was subcloned into the shuttle plasmid, derived from pAdRSV4. This plasmid contains serotype 5 human adenoviral sequences from 0–1 and 9–16 map units in addition to pBR322 backbone sequences. This plasmid also contains a long terminal repeat for RSV as a promoter, a simian virus 40 polyadenylation signal, and multiple signal sites.
2. The recombinant adenoviral vectors was generated by homologous recombination between the shuttle plasmid and genomic DNA from human adenovirus serotype 5 derivative sub360, which is partially deleted in the E3 region ***(22,23)***.
3. The shuttle vector that carried bovine eNOS or genes of interest was linearized and contransfected with *Xba* I/*Cla*I-digested sub360 DNA into human embry-

onic kidney (HEK) 293 cells. Because the recombinant adenovirus was deleted of E1, the ability of the virus to replicate was impaired and, thus, grown in HEK293 cells.
4. Infectious virus was identified by plaque isolation and screening for eNOS by polymerase chain reaction (PCR) using a 5' primer (sequence) anchored in the pCDNA3 sequence upstream of the RSVeNOS cassette, and a 3' primer (sequence) in eNOS.
5. Recombinant clones were expanded and triple plaque purified to assure that viral suspensions used for in vivo experiments were free of wild-type virus.
6. Virus titer was determined by plaque assay on HEK293 cells. After purification, the virus was suspended in PBS with 3% sucrose and was kept at –70°C until used.

3.1.2. In Vitro Test of cDNA Constructs

1. To verify the proper expression of eNOS from adenoviral constructs, COS-1 cells that have low levels of endogenous NOS activity were transfected with Ad5RSVeNOS. COS-1 cells were prepared with 10^6 cells (70% confluence) in 35-mm dishes containing DMEM with 100 μg/mL penicillin, 100 U/mL streptomycin, and 5% FBS.
2. Cells were rinsed twice with warm PBS. Dulbecco's medium (1 mL) with and without virus (1 or 10 plaque-forming units [PFU]/cell) was applied to the cells. Cells were rinsed with PBS and 2 mL of DMEM (with 100 μg/mL penicillin, 100 U/mL streptomycin, and 5% FBS) 1 h later.
3. After 2 d, cells were harvested and analyzed for constitutive NOS activity using the conversion of L-[^{3}H]arginine to L-[^{3}H]citrulline ***(22,24,25)*** (*see* **Note 1***)*. Non-infected cells were used as controls.

3.2. Isolation and Ex Vivo Expansion of rMSCs

Rat MSCs were isolated by their adherence to tissue culture plastic (*see* **Note 2**).

1. Briefly, 6-wk-old male brown Norway rats were euthanized with CO_2.
2. Under sterile conditions, femur and tibias were removed and placed in culture medium for rMSCs.
3. Both ends of femur and tibias were removed and the bone marrow was flushed out with a 21-gage needle attached to a 10-mL syringe.
4. The bone marrow cells were filtered through a cell strainer with 70-μm Nylon mesh and then cultured in a T75 flask at 37°C with 5% humidified CO_2.
5. Fresh culture medium for rMSCs was added and replaced every 2–3 d to remove nonadherent cells.
6. The adherent rMSCs were grown to confluency over about 7 d. These confluent rMSCs were harvested with 0.25% trypsin/1 m*M* EDTA, diluted 1:3 per passage, replated in T75 flasks, again grown to confluency for further ex vivo expansion (*see* **Fig. 1**).

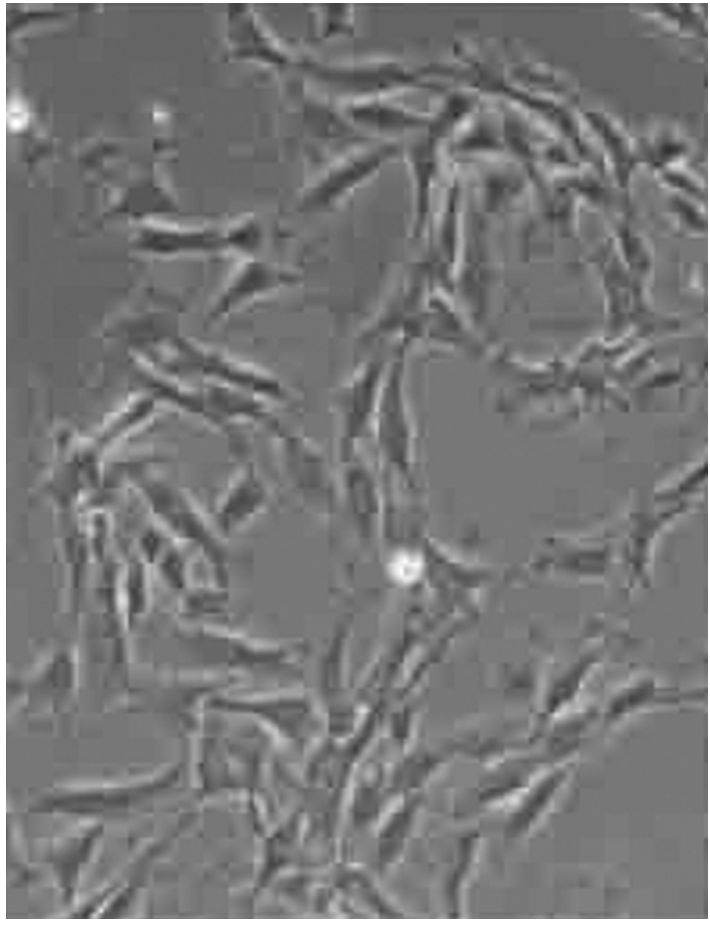

Fig. 1. Phase-contrast microscopy of rMSCs at log phase (magnification ×250; reduced from original magnification).

3.3. Adenoviral Gene Transfer of eNOS Into rMSCs

1. Rat MSCs were plated at a density of 10,000 cells/cm^2 in a T75 flask and cultured overnight (*see* **Note 3**).
2. The cells were then exposed to fresh culture medium containing Ad5RSVlacZ or Ad5RSVeNOS at 300 multiplicity of infection (MOI, defined as PFUs per cell) for 48 h and the virus-containing supernatant was removed (*see* **Note 4** and **Fig. 2**).
3. The cells were washed three times with PBS, harvested with 0.25% trypsin/1 m*M* EDTA, washed again with PBS, and a cell suspension at a concentration of 12,500 cells/μL was prepared in PBS.
4. These eNOS gene-modified rMSCs cells were then kept on ice until they were implanted, usually within 30 min.

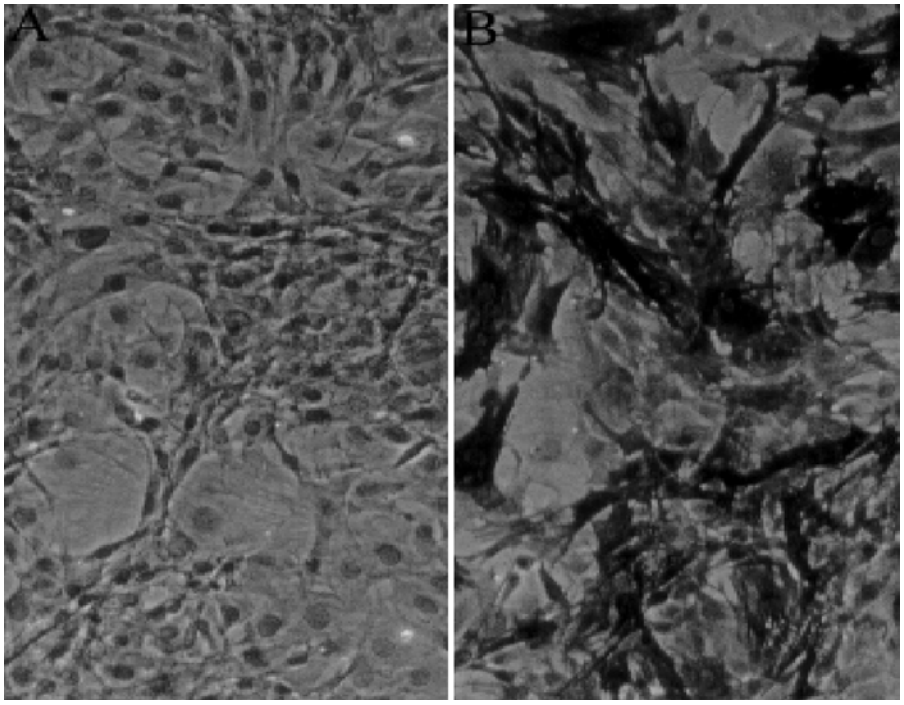

Fig. 2. Photomicrograph showing eNOS gene-modified rMSCs. rMSCs were transduced with Ad5RSVeNOS at MOI 300 for 48 h and the cells were immunostained for eNOS transgene expression. **(A)** Control rMSCs; **(B)** rMSCs transduced with Ad5RSVeNOS at MOI 300 (magnification ×250; reduced from original magnification).

3.4. In Vivo Gene Transfer of AdeNOS and eNOS Gene-Modified rMSCs

3.4.1. AdeNOS Intracavernous Gene Transfer to the Penis

The in vivo gene transfer of adenoviruses is based on the technique developed by Christ et al. ***(26)***. The effectiveness of AdeNOS in augmenting erectile responses was studied in 25-mo-old male brown Norway rats.

1. The rats are anesthetized with sodium pentobarbital (30 mg/kg intraperitoneally) and placed in a supine position on a thermoregulated surgical table. Body temperature is maintained at 37°C with a water-jacketed heating blanket.
2. Using sterile technique, the penis is exposed. Using a 30-gage needle attached to a microliter syringe, 20 μL of vehicle (3% sucrose in PBS), Ad5RSVlacZ (1×10^8 parts/mL) or AdRSVeNOS (1×10^8 parts/mL), is injected into the corpus cavernosum ***(24,25,27–31)*** (*see* **Note 5**).
3. Immediately before instillation, blood drainage via the dorsal veins is halted by circumferential compression at the base of the penis with an elastic band. Com-

pression is released 1 min after injection of 20 μL of the vehicle/virus. After time periods ranging from 5 to 21 d following intracavernosal injection of the adenoviral vector, erectile responses are measured in the aged rats.

3.4.2. AdeNOS rMSCs Intracavernous Gene Transfer to the Penis

The effectiveness of treatment with eNOS gene-modified rMSCs in augmenting erectile responses was studied in 25-mo-old male brown Norway rats.

1. The rats were anesthetized with sodium pentobarbital (30 mg/kg intraperitoneally) and placed on a thermoregulated surgical table.
2. The penis was exposed and a volume of 40 μL of cell suspension containing 500,000 lacZ or eNOS gene-modified rMSCs was slowly injected into the corpus cavernosum with a 25-gage needle attached to a microtiter syringe.
3. Immediately before rMSC injection, blood drainage via the dorsal vein was halted by circumferential compression of the penis at the base with an elastic band. The compression was released 1 min after the injection. Erectile responses were measured after periods ranging from 2 to 21 d following intracavernosal injection of the modified rMSCs.

3.4.3. Western Blot Analysis of eNOS in Corpus Cavernosum From the Aged Rat

In order to determine if adenoviral gene transfer of eNOS results in eNOS overexpression in the corpus cavernosum of the aged rat, Western blot analysis is performed at various times after transfection.

1. Cavernosal tissue was homogenized (Polytron; Brinkmann Instruments, Westbury, NY) in ice-cold protease inhibitor (P.I.) buffer and centrifuged at 48,000*g* for 1 h at 4°C ***(25,32)*** (*see* **Note 6**). The cytosolic supernatant liquid was removed; this cellular fraction contains approx 90% nNOS ***(33)***.
2. The particulate fraction was resuspended and rehomogenized in P.I. buffer containing 1*M* KCl and then centrifuged at 48,000*g* for 1 h at 4°C. The particulate was again suspended and homogenized in P.I. buffer. Next, 10% (v/v) of 200 m*M* CHAPS solution was added to the homogenate and vigorously mixed for 30 min at room temperature, followed by centrifugation at 48,000*g*. This detergent-extracted membrane fraction contained approx 80% eNOS ***(33)***.
3. The membrane fraction supernatant for eNOS was mixed with an equal volume of 2% sodium dodecyl sulfate (SDS)/1% β-mercaptoethanol and fractionated using 8% SDS-PAGE (polyacrylamide gel electrophoresis) (70 μg/lane).
4. Proteins were transferred to a nitrocellulose membrane, blocked for 1 h with blotto-Tween and incubated with a primary polyclonal rabbit anti-eNOS IgG (1:250) (Transduction Laboratories, Lexington, KY).
5. Bound antibody was detected with labeled goat anti-rabbit IgG secondary antibody conjugated to horseradish peroxidase and visualized using enhanced chemiluminescence (*see* **Fig. 3**) (*see* **Note 7**).

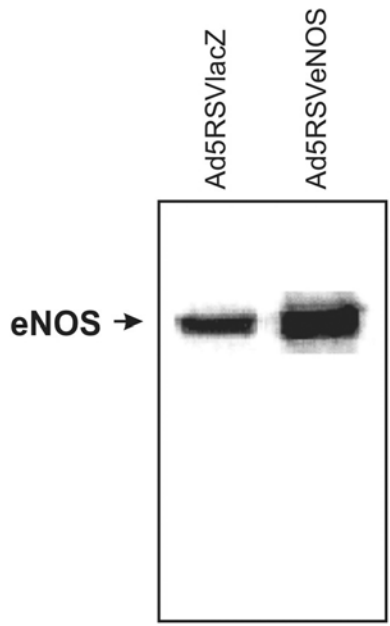

Fig. 3. Western blot analysis of cytosolic eNOS protein expression (135 kDa) in aged rats 7 d posttransfection with Ad5RSVlacZ and Ad5RSVeNOS. There was significantly more cytosolic eNOS protein in aged rats transfected with Ad5RSVeNOS when compared to aged rats transfected with the reporter gene (from **ref.** ***27*** with permission).

3.5. In Vivo Measurement of Erectile Response

In order to determine the effect of overexpression of eNOS in the corpus cavernosum of aged rats, erectile function in young (2 mo) and aged (25 mo) brown Norway rats 7 d after adenovirus or AdeNOS rMSCs administration was determined.

1. Animals were anesthetized with sodium pentobarbital (30 mg/kg intraperitoneally) and placed on a thermoregulated surgical table. The trachea was cannulated (PE-240 polyethylene tubing) to maintain a patent airway, and the animals breathed room air enriched with 95% O_2/5% CO_2.
2. A carotid artery was cannulated (PE-50 tubing) for the measurement of mean systemic arterial pressure (MAP). Systemic arterial pressure was measured with a Viggo-Spectramed transducer (Viggo Spectramed, Oxnard, CA), which was attached to a data acquisition system (Biopac Systems, Santa Barbara, CA) and connected to a computer simultaneously recording MAP.
3. The left jugular vein was cannulated (PE-50 tubing) for the administration of fluids and supplemental anesthesia (15 mg/kg intravenously). The shaft of the

penis was freed of skin and fascia, and by removing part of the overlying ischiocavernous muscle, exposure of the right crus was performed.

4. A 25-gage needle filled with 250 U/mL of heparin and connected to PE-50 tubing was inserted into the right crura and connected to a pressure transducer to permit continuous measurement of intracavernosal pressure (ICP).
5. The bladder and prostate were exposed through a midline abdominal incision. The right major pelvic ganglion and cavernosal nerve were identified posterolateral to the prostate on one side, and an electrical stimulator with a stainless-steel bipolar hook was placed around the cavernosal nerve ***(24–30)***. MAP and ICP were measured with a pressure transducer connected to a data acquisition system (Biopac Systems, Santa Barbara, CA) for continuous measurement of MAP and ICP pressures.
6. The cavernosal nerve was stimulated with a square-wave stimulator (Grass Instruments, Quincy, MA). Each rat underwent cavernosal nerve stimulation (CNS) at a frequency of 15 Hz and pulse width of 30 s. The application of 2.5, 5, and 7.5 V is used to achieve significant and consistent erectile responses. The duration of stimulation is 1 min, with rest periods of 2–3 min between subsequent stimulations (*see* **Note 8**).
7. Total erectile response or total ICP was determined by the area under the erectile curve (AUC; mm Hg/s) from the beginning of cavernosal nerve stimulation until the ICP pressure returned to baseline or prestimulation pressure. The ratio between the maximal ICP and MAP obtained at the peak of erectile response was calculated and used to express erectile function (*see* **Fig. 4**) (*see* **Note 9**).

4. Notes

1. COS-1 cells were homogenized and suspended in 1 mL of ice-cold 50 mmol/L Tris-HCl buffer (pH 7.4) containing 0.1 mmol/L EDTA, 0.1 mmol/L ethylene glycol-bis(β-aminoethyl ether)-*N*,*N*,*N*',*N*'-tetraacetic acid (EGTA), 2 nmol/L leupeptin, 1 nmol/L pepstatin A, 2 nmol/L bestatin, and 1 mmol/L phenylmethylsulfonyl fluoride (PMSF). The cell suspension was centrifuged at 10,000*g* for 45 min. The pellet was incubated in 50 mmol/L Tris-HCl, 0.1 mmol/L EDTA, 0.1 mmol/L EGTA, 1 mmol/L NADPH, 3 μmol/L (6*R*)-5,6,7,8-tetrahydrobiopterin, 100 nmol/L calmodulin, 1 μmol/L flavin mononucleotide, 1 μmol/L flavin adenine dinucleotide, 2.5 mmol/L $CaCl_2$, and L-[^{3}H]arginine (0.2 mCi, specific activity 55 Ci/mmol) for 45 min at 37°C. After a 45-min incubation, the reaction was quenched by the addition of 1 mL of 20 m*M* of *N*-2-hydroxyethylpiperazine-*N*'-2-ethanesulfonic acid buffer, pH 5.5, containing 2.5 mmol/L EDTA and 2.5 mmol/L EGTA. The reaction mixture was then passed over a 1-mL column containing Dowex AG 5OWX-8 (Na^+ form) resin, washed with 1 mL of water, and collected directly into a 20-mL liquid scintillation vial containing scintillation mixture. To characterize overexpressed enzyme, we tested calcium dependency by depletion of calcium and addition of 2.5 mmol/L of EGTA in the reaction mixture. Specificity of converted L-citrulline was confirmed by using thin-layer chromatography.

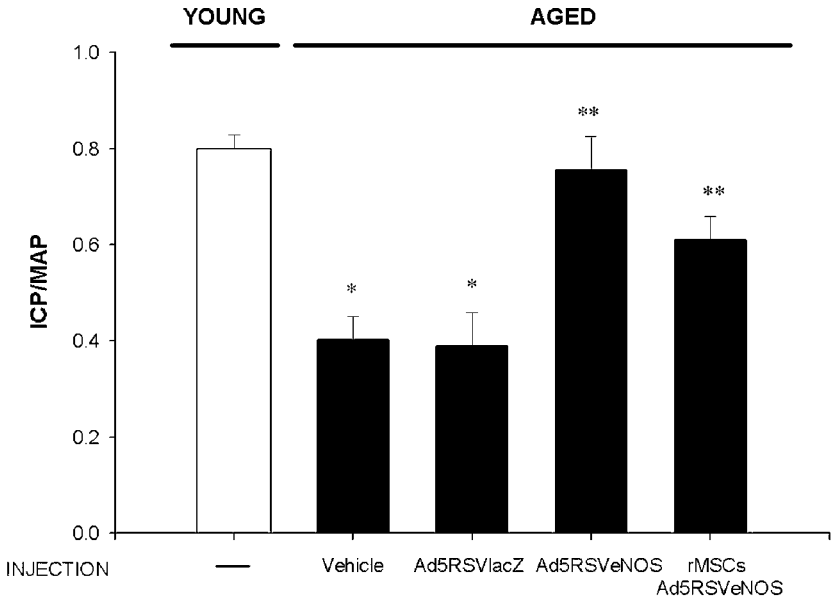

Fig. 4. Bar graph showing an increase in intracavernosal pressure in response to cavernosal nerve stimulation (5 V) as measured by the ratio of ICP/MAP in young rats and aged rats transfected with vehicle (3% sucrose in PBS), Ad5RSVβgal, Ad5RSVeNOS, or rMSCs treated with Ad5RSVeNOS. In vivo erection experiments were conducted 7 d after transfection with adenoviruses and rMSCs. $n = 8–12$; $*p < 0.05$, response significantly different compared to young rats; $**p < 0.05$, response significantly different compared to aged rats transfected with vehicle or Ad5RSVβgal. Aged rats transfected with either Ad5RSVeNOS or rMSCs treated with Ad5RSVeNOS had significant improvements in erectile responses to cavernosal nerve stimulation to values similar to young rats.

2. Postnatal bone marrow contains two types of stem cell: hematopoietic stem cells and MSCs. Hematopoietic stem cells are suspension cells that give rise to red cells, monocytes, platelets, granulocytes, and lymphocytes. MSCs are adherent cells that are capable of differentiating into osteoblasts, chondrocytes, adipocytes, and myocytes. After bone marrow cells are plated in a tissue culture flask, MSCs rapidly adhere to plastic and can be easily separated from the nonadherent hematopoietic stem cells by repeated changing the cell culture medium.
3. At a density of 10,000 cells/cm^2, rMSCs are at log phase and the cell condition is excellent.
4. At MOI 300, the transduction efficiency of Ad5RSVeNOS is greater than 60% and the viral cytopathic effect on rMSCs is the minimum. Transduction efficiency was determined by immunocytochemical analysis for eNOS transgene expression using the mouse Immunocruz Staining System. Briefly, rMSCs were trans-

duced with Ad5RSVeNOS for 48 h, fixed with ice-cold methanol for 5 min, and treated with serum block for 20 min. The cells were then incubated in mouse anti-eNOS monoclonal antibody (1:100 dilution) at 4°C overnight followed by biotinylated secondary antibody for 30 min. The cells were incubated in the HRP–streptavidin complex for 30 min, treated with HRP substrate for 15 min, and rinsed with distilled water (dH_2O). The cells were then counterstained with hematoxylin. Expression of eNOS transgene in rMSCs was evaluated *in situ* by light microscopy scoring of cells expressing eNOS. The eNOS-positive brown cells found in three representative microscopic fields were counted and expressed as a percentage of the total number of cells in those fields.

5. Each intracavernosal injection should be performed in the midshaft of the penis and when the needle is removed from the corpus cavernosum, blood should escape from the corpora. This ensures that the injection was in the corpus cavernosum. Additionally, higher titers of adenoviruses only cause more inflammation, not increased gene and protein expression of your particular gene of interest.
6. The paired corpus cavernosum are isolated from the urethra from the shaft of the penis. Care should be taken to include only the cavernosal tissue rich in smooth muscle and endothelium from the penis posttransfection.
7. When analyzing eNOS protein expression in the corpus cavernosum, it is important to isolate the membrane-bound fraction that contains the majority of the functional eNOS in the cell. Recently, it has been shown that there is a difference in cytosolic vs. membrane-bound fraction of eNOS in pathophysiological conditions associated with erectile dysfunction in particular diabetic cavernosal tissue ***(25,32)***.
8. Rest periods after cavernosal nerve stimulation must be performed in the erectile protocol so that neuropraxia does not occur.
9. The ratio ICP/MAP is used to express erectile function in order to normalize for variations in systemic blood pressure between different groups of animals. Gene therapy with both Ad5RSVeNOS and rMSCs expressing eNOS improved erectile response to cavernosal nerve stimulation in the aged rat (*see* **Fig. 4**).

Acknowledgments

The authors would like to thank Janice Ignarro for her help in the preparation of the manuscript and Dr. Beverley Davidson and Dr. Donald D. Heistad and the University of Iowa Vector Core Laboratory for preparation of the adenoviral vectors. This work was supported in part by NIH grant HL62000.

References

1 Burnett, A. L., Lowenstein, C. J., Bredt, D. S., et al. (1992) Nitric oxide: physiologic mediator of penile erection. *Science* **257,** 401–403.

2 Rajfer, J., Aronson, W. J., Bush, P. A., et al. (1992) Nitric oxide as a mediator of relaxation of the corpus cavernosum in response to nonadrenergic, noncholinergic neurotransmission. *N. Engl. J. Med.* **326,** 90–94.

3 Nabel, E. G., Pompil, V. J., Plantz, G. E., et al. (1994) Gene transfer and vascular disease. *Cardiovasc. Res.* **28,** 445–455.
4 Morral, N., O'Neal, W., Rice, K., et al. (1999) Administration of helper-dependent adenoviral vectors and sequential delivery of different vector serotype for long-term liver-directed gene transfer in baboons. *Proc. Natl. Acad. Sci. USA* **96,** 12,816–12,821.
5. Gerlach, J. C. and Zeilinger, K. (2002) Adult stem cell technology—prospects for cell based therapy in regenerative medicine. *Int. J. Artif. Organs* **25,** 83–90.
6 Poulsom, R., Alison, M. R., Forbes, S. J., et al. (2002) Adult stem cell plasticity. *J. Pathol.* **197,** 441–456.
7 Gronthos, S. and Simmons, P. J. (1996) The biology and application of human bone marrow stromal cell precursors. *J. Hematother.* **5,** 15–23.
8 Pittenger, M. F., Mackay, A. M., Beck, S. C., et al. (1999) Multilineage potential of adult human mesenchymal stem cells. *Science* **284,** 143–147.
9 Bianco, P., Riminucci, M., Gronthos, S., et al. (2001) Bone marrow stromal stem cells: nature, biology, and potential applications. *Stem Cells* **19,** 180–192.
10 Ferrari, G., Cusella-De Angelis, G., Coletta, M., et al. (1998) Muscle regeneration by bone marrow-derived myogenic progenitors. *Science* **279,** 1528–1530.
11 Liechty, K. W., MacKenzie, T. C., Shaaban, A. F., et al. (2000) Human mesenchymal stem cells engraft and demonstrate site-specific differentiation after *in utero* transplantation in sheep. *Nature Med.* **6,** 1282–1286.
12 Toma, C., Pittenger, M. F., Cahill, K. S., et al. (2002) Human mesenchymal stem cells differentiate to a cardiomyocyte phenotype in the adult murine heart. *Circulation* **105,** 93–98.
13 Shake, J. G., Gruber, P. J., Baumgartner, W. A., et al. (2002) Mesenchymal stem cell implantation in a swine myocardial infarct model: engraftment and functional effects. *Ann. Thorac. Surg.* **73,** 1919–1925.
14 Cherington, V., Chiang, G. G., McGrath, C. A., et al. (1998) Retroviral vector-modified bone marrow stromal cells secrete biologically active factor IX *in vitro* and transiently deliver therapeutic levels of human factor IX to the plasma of dogs after reinfusion. *Hum. Gene Ther.* **9,** 1397–1407.
15 Riew, K. D., Wright, N. M., Cheng, S., et al. (1998) Induction of bone formation using a recombinant adenoviral vector carrying the human BMP-2 gene in a rabbit spinal fusion model. *Calcif. Tissue Int.* **63,** 357–360.
16 Schwarz, E. J., Alexander, G. M., Prockop, D. J., et al. (1999) Multipotential marrow stromal cells transduced to produce L-DOPA: engraftment in a rat model of Parkinson disease. *Hum. Gene Ther.* **10,** 2539–2549.
17 Chuah, M. K., Van Damme, A., Zwinnen, H., et al. (2000) Long-term persistence of human bone marrow stromal cells transduced with factor VIII-retroviral vectors and transient production of therapeutic levels of human factor VIII in nonmyeloablated immunodeficient mice. *Hum. Gene Ther.* **11,** 729–738.
18 Niyibizi, C., Smith, P., Mi, Z., et al. (2001) Transfer of proalpha2(I) cDNA into cells of a murine model of human Osteogenesis Imperfecta restores synthesis of type I collagen comprised of alpha1(I) and alpha2(I) heterotrimers *in vitro* and *in vivo*. *J. Cell Biochem.* **83,** 84–91.

19 Weber, M., Steinert, A., Jork, A., et al. (2002) Formation of cartilage matrix proteins by BMP-transfected murine mesenchymal stem cells encapsulated in a novel class of alginates. *Biomaterials* **23,** 2003–2013.
20 Van Damme, A., Vanden Driessche, T., Collen, D., et al. (2002) Bone marrow stromal cells as targets for gene therapy. *Curr. Gene Ther.* **2,** 195–209.
21 Nishida, K., Harrison, D. G., Navas, J. P., et al. (1992) Molecular cloning and characterization of the constitutive bovine aortic endothelial cell nitric oxide synthase. *J. Clin. Invest.* **90,** 2092–2096.
22 Ooboshi, H., Chu, Y., Rios, C. D., et al. (1997) Altered vascular function after adenovirus-mediated overexpression of endothelial nitric oxide synthase. *Am. J. Physiol.* **273,** H265–H270.
23 Davidson, B. L., Allen, E. D., Kozarsky, K. F., et al. (1993) A model system for in vivo gene transfer into the central nervous system using an adenoviral vector. *Nature Genet.* **3,** 219–223.
24 Champion, H. C., Bivalacqua, T. J., Hyman, A. L., et al. (1999) Gene transfer of endothelial nitric oxide synthase to the penis augments erectile responses in the aged rat. *Proc. Natl. Acad. Sci. USA* **96,** 11,648–11,652.
25 Bivalacqua, T. J., Usta, M. F., Champion, H. C., et al. (2003) Gene transfer of endothelial nitric oxide synthase partially restores nitric oxide synthesis and erectile function in streptozotocin diabetic rats. *J. Urol.* **169,** 1911–1917.
26 Christ, G. J., Rehman, J., Day, N., et al. (1998) Intracorporal injection of hSlo cDNA in rats produces physiologically relevant alterations in penile function. *Am. J. Physiol.* **275,** H600–H608.
27 Bivalacqua, T. J., Champion, H. C., Mehta, Y. S., et al. (2000) Adenoviral gene transfer of endothelial nitric oxide synthase (eNOS) to the penis improves age-related erectile dysfunction in the rat. *Int. J. Impotence Res.* **12,** S1–S10.
28 Bivalacqua, T. J., Champion, H. C., Abdel-Mageed, A. B., et al. (2001) Gene transfer of prepro-calcitonin gene related peptide restores erectile function in the aged rat. *Biol. Reprod.* **65,** 1371–1377.
29 Bivalacqua, T. J. and Hellstrom, W. J. (2001) Potential application of gene therapy for the treatment of erectile dysfunction. *J. Androl.* **22,** 183–190.
30 Bivalacqua, T. J., Armstrong, J. S., Biggerstaff, J., et al. (2003) Gene transfer of extracellular SOD to the penis reduces superoxide anion and improves erectile function in aged rats. *Am. J. Physiol. Heart Circ. Physiol.* **284,** H1408–H1421.
31. Bivalacqua, T. J., Champion, H. C., Hellstrom, W. J., et al. (2000) Pharmacotherapy for erectile dysfunction. *Trends Pharmacol. Sci.* **21,** 484–489.
32 Akingba, A. G. and Burnett, A. L. (2001) Endothelial nitric oxide synthase protein expression, localization, and activity in the penis of the alloxan-induced diabetic rat. *Mol. Urol.* **5,** 189–197.
33. Pollock, J. S., Forstermann, U., Mitchell, J. A., et al. (1991) Purification and characterization of particulate endothelium-derived relaxing factor synthase from cultured and native bovine aortic endothelial cells. *Proc. Natl. Acad. Sci. USA* **88,** 10,480–10,484.

15

Adenovirus-Mediated Nitric Oxide Synthase Gene Transfer Into the Nucleus Tractus Solitarius in Conscious Rats

Yoshitaka Hirooka and Koji Sakai

Summary

The nucleus tractus solitarius (NTS) of the brainstem is an important site for the regulation of sympathetic nerve activity. In the brain, nitric oxide (NO) has been shown to reduce blood pressure by inhibiting sympathetic nerve activity. However, most studies were performed in an acute state of anesthesia. Therefore, we developed a technique to increase the local production of NO in vivo by the transfer of endothelial NO synthase (eNOS) gene into the NTS. Adenovirus vectors encoding either the β-galactosidase gene (Adβgal) or the eNOS gene (AdeNOS) were infected into the NTS. In the Adβgal-infected rats, the local expression of β-galactosidase was confirmed by X-Gal staining, and β-galactosidase activity was quantified using a colorimetric assay. In the AdeNOS-infected rats, the local expression of eNOS was confirmed by immunohistochemistry and Western blot analysis. Production of NO was measured by in vivo microdialysis. Blood pressure and heart rate were monitored by a radiotelemetry system in a conscious state. In the AdeNOS-infected rats, blood pressure and heart rate significantly decreased from d 5 to d 10, and then gradually recovered over time. These methods should be useful in examining the local effect on cardiovascular function of a particular substance produced by a specific gene in the brain.

Key Words: Blood pressure; heart rate; sympathetic nervous system; gene expression, brain.

1. Introduction

In the brainstem, nitric oxide (NO) plays an important role in cardiovascular regulation ***(1–4)***. The nucleus tractus solitarius (NTS) is the site of termination of primary afferent fibers arising from many cardiovascular receptors ***(5–8)***. Previous studies examined mainly the effects of microinjection of NO synthase (NOS) inhibitors, such as N^G-monomethyl-L-arginine (L-NMMA) into the NTS or the rostral ventrolateral medulla in the brainstem on blood pressure, heart rate, and/or sympathetic nerve activity in anesthetized animals ***(3,4)***.

From: *Methods in Molecular Biology, vol. 279: Nitric Oxide Protocols: Second Edition*
Edited by: A. Hassid © Humana Press Inc., Totowa, NJ

Thus, most previous studies examined acute effects of NO or NOS inhibitors. Therefore, it is important to examine the role of NO in a particular nucleus in the brainstem on cardiovascular responses in the conscious state. To address this, we developed a technique for the transfer of the endothelial NOS (eNOS) gene into the NTS of rats in vivo ***(9–12)***. This was achieved by infection of adenovirus encoding the cDNA of eNOS into the NTS. This technique allows us to examine for a longer time the local effects of an increase in NO on blood pressure, heart rate, and sympathetic nerve activity, in vivo.

2. Materials

1. Phosphate-buffered saline (PBS) containing recombinant adenovirus (1×10^8 plaque forming units (PFU)/mL; the Gene Transfer Vector Core Laboratory at the University of Iowa, IA).
2. Purified β-galactosidase (Roche Applied Science).
3. Vibratome (DTK-1000, Dosaka EM Co. Ltd, Tokyo, Japan).
4. *Ortho*-nitrophenyl-β-D-galactophyranosidase (ONPG, Boehringer Mannheim, Biochemica, Mannheim, Germany).
5. Phenylmethanesulfonyl fluoride (PMSF).
6. Brain lysis buffer: 40 m*M* HEPES; 1% Triton X-100; 10% glycerol, and 1 m*M* PMSF.
7. Artificial cerebrospinal fluid (ACSF): 123 m*M* NaCl, 0.86 m*M* $CaCl_2$, 3.0 m*M* KCl, 0.89 m*M* $MgCl_2$, 25 m*M* $NaHCO_3$, 0.5 m*M* NaH_2PO_4, and 0.25 m*M* Na_2HPO_4, pH 7.4
8. NTS lysis buffer: 40 m*M* HEPES, 1% Triton X-100, 10% glycerol, 1 m*M* PMSF, pH 7.4.
9. Mouse IgG1 monoclonal antibody to human eNOS (Transduction Laboratories, Lexington, KY) diluted in 1% bovine serum albumin (BSA) and 0.05% NaN_3 in PBS for immunohistochemistry
10. TBS: 6 m*M* Tris-HCL + 4 m*M* Tris-base, 150 m*M* NaCl/distilled water (ddH_2O + 800 μL/L of Tween-20 for Western blot analysis.
11. Biotinylated horse anti-mouse IgG (Vector Laboratories, Burlingame, CA) diluted in 1% BSA + 0.05% NaN_3/PBS.
12. Streptavidin-conjugated fluorescein isothiocyanate (Vector Laboratories).
13. Propidium iodide (final concentration: 10 μg/mL) (PI, Sigma-Aldrich).
14. Vectashield (Vector Laboratories).
15. BCA protein assay kit (Pierce, Rockford, IL).
16. Immunobilon-P membrane (Millipore, Bedford, MA).
17. "ECS Plus" Western blotting detection kit (Amersham Pharmacia Biotechnology, Tokyo, Japan).
18. Rat stereotaxic frame (SR-5, Narishige, Tokyo, Japan).
19. Hamilton microsyringe.
20. Microdialysis probe (A-I-12-01; 1 mm length) (Eicom, Kyoto, Japan).
21. β-Galactosidase assay buffer: 80 m*M* PBS, 102 m*M* of 2-mercaptoethanol, 9 m*M* $MgCl_2$, 8 m*M* ONPG, pH 7.3.

22. Ringer's solution: 140 m*M* NaCl, 4 m*M* KCl, 1.26 m*M* $CaCl_2$, 1.15 m*M* $MgCl_2$, pH 7.4.
23. Automated NO detector high-performance liquid chromatography (HPLC) system (ENO-10; Eicom).
24. *N*-Methyl-D-aspartic acid (NMDA; Sigma–Aldrich).
25. L-Arginine (L-Arg; Wako Chemicals, Osaka, Japan).
26. L-*N*-Monomethyl arginine (Sigma–Aldrich).
27. Ventilator, model SN-480-6 (Shinano, Tokyo, Japan).
28. Radiotelemetry system (UA-10; Data Science International, St. Paul, MN).
29. Transmitter (radiofrequency transducer model; TA11PA-C40 or TL11M2-C50-PXT), receiver panel, consolidation matrix.
30. MacLab System (AD Instruments, Milford, MA).

3. Methods

The methods described outline (1) construction and purification of recombinant adenovirus, (2) in vivo gene transfer, (3) histochemical analysis of gene expression for β-galactosidase, (4) immunohistochemistry for eNOS, (5) Western blot analysis for eNOS, (6) microdialysis and measurement of NO metabolites, (7) radiotelemetry monitoring of blood pressure and heart rate, and (8) measurement of urinary norepinephrine excretion.

3.1. Construction and Purification of Recombinant Adenovirus

We used adenoviral vectors encoding either bacterial β-galactosidase gene or bovine eNOS gene. These adenoviral vectors were constructed in the Gene Transfer Vector Core Laboratory at the University of Iowa ***(13–15)***. A replication-deficient recombinant adenovirus, adenovirus serotype 2/cytomegalovirus–β-galactosidase (Ad2/CMV-βgal) was used as a reporter virus. The vector DNA construct comprised a full-length copy of the adenovirus genome of approx 37.5 kb, in which the early region 1 (E1) genes were deleted and replaced with cDNA encoding the bacterial β-galactosidase gene preceded by the simian virus 40 (SV40) nuclear localization signal in Ad2/CMV-βGal. A replication-deficient recombinant adenovirus, Ad2/CMV-eNOS (AdeNOS) was also constructed as follows. The cDNA encoding the bovine eNOS was subcloned into one of the unique cloning sites of the shuttle plasmid. The recombinant virus was grown in human embryonic kidney (293) cells that complement the E1 early viral promoters. The viral particles were suspended in PBS with 20% sucrose and kept at –80°C until use.

3.2. In Vivo Gene Transfer

All animals were treated according to the protocols approved by Kyushu University Animal Care Committee of the Center's Animal Care Facility. Adult male Wistar–Kyoto rats (16–20 wk old) were used for in vivo gene trans-

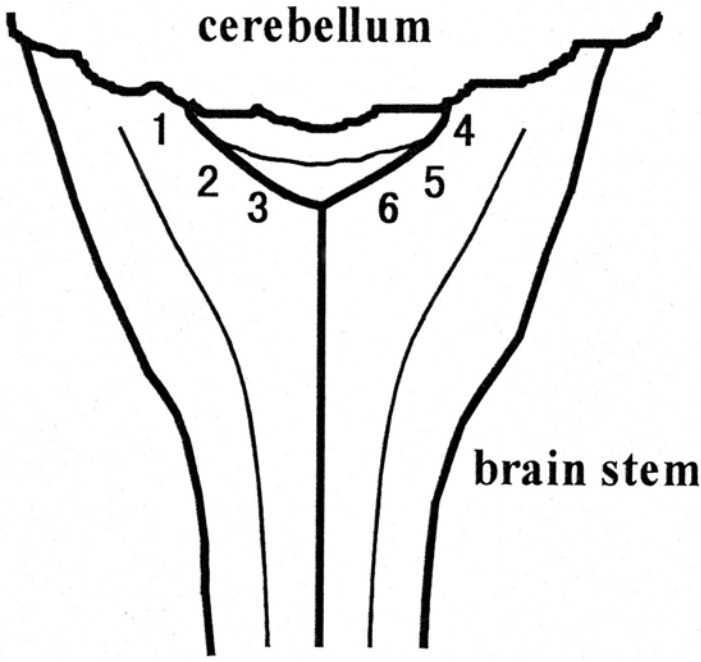

Fig. 1. Schematic outline of the dorsal surface of the medulla. Positions 1–6 represent sites of injections in the NTS. (Reproduced with permission from **ref. *10***.)

fer. Some rats were used for in vivo gene transfer after the implantation of the transmitter of the telemetry system.

1. For in vivo gene transfer, rats were anesthetized with sodium pentobarbital (50 mg/kg, intraperitoneally) and secured on a rat stereotaxic frame. An incision was made on the skin at the midline of the head, and muscles were dissected to expose the cisterna magna. The atlanto-occipital membrane was cut, and the dorsal surface of the medulla was visualized.
2. A glass micropipet (5 μm outer diameter) was filled with artificial cerebrospinal fluid (aCSF) or a suspension of AdCMV-βgal or AdCMVeNOS. The pipet was placed in a micromanipulator and positioned in the injection sites. Microinjection was performed at three sites at each side of the NTS (*see* **Fig. 1**).
3. A polyvinyl tube, connected to the microinjection pipet, was led to a Hamilton microsyringe (100 μL), and aCSF or adenovirus vector was microinjected bilaterally into the NTS using the Hamilton microsyringe. The sites of microinjections were defined according to a rat brain atlas ***(16)***, with reference to the midline, the dorsal surface of the medulla, and the rostral border of the calamus scriptorius. A total of 5 μL of each adenoviral suspension containing 1×10^8 PFU/mL (*see* **Note 1** and **2**) or ACSF was injected at the injection site of the bilateral NTS for 30 min (injection rate: approx 0.2 μL/min). Special care was taken to inject

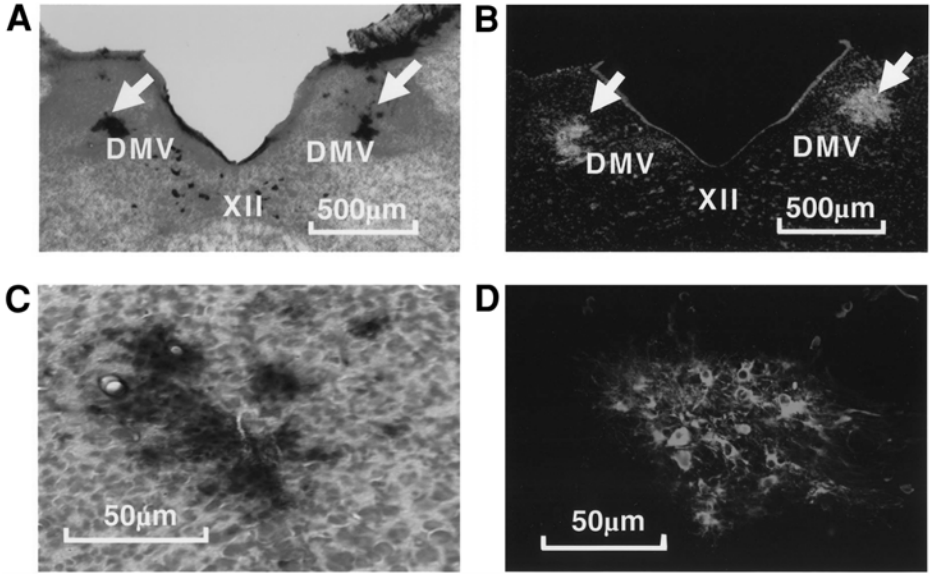

Fig. 2. Photomicrographs showing expression of β-galacotosidase by X-Gal staining **(A, B)** and expression of eNOS protein detected by immunohistochemistry **(C, D)** in the NTS. XII, hypoglossal nucleus. (Reproduced with permission from **ref. *10***.)

slowly to avoid tissue damage and spread of the solution into other portions of the NTS (*see* **Note 1** and **3**).

4. The pipet was removed and the incision was closed. After the injection, all rats recovered from anesthesia and were allowed to move freely within their cage.

3.3. Histochemical Analysis of Gene Expression for β-Galactosidase and Quantification of β-Galactosidase Activity

1. On d 7 after gene transfer, animals were deeply anesthetized with an overdose of pentobarbital and perfused transcardially with PBS, followed by 4% paraformaldehyde in PBS (*see* **Note 4**).
2. The brain was removed and the coronal sections of the medulla were cut serially with a vibratome. Sections of the medulla (50 μm) were evaluated for β-galactosidase expression by X-Gal staining ***(17)***, as shown in **Fig. 2A**,**B**.
3. We quantified β-galacotosidase activity in the rats infected with Adβgal by a colorimetric assay using *o*-nitrophenyl-β-D-galactophyranosidase (ONPG) as described previously ***(17–19)***, with some modification. The β-galactosidase activity was assayed before and at 7, 14, and 21 d after the gene transfer (*see* **Fig. 3**).
4. The rats were deeply anesthetized with sodium pentobarbital and perfused transcardially with PBS, followed by 4% paraformaldehyde in PBS.
5. The brain was removed and a coronal block of the brain, weighing 0.2 g, was excised and placed in ice-cold PBS containing 1 m*M* PMSF.

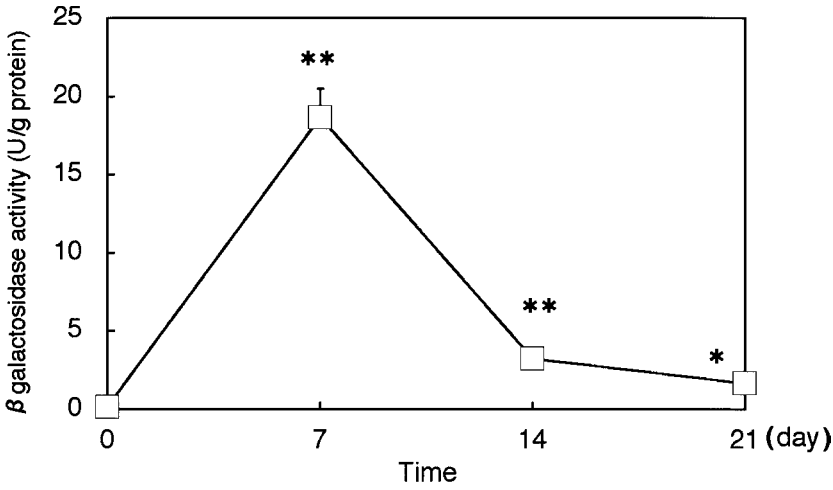

Fig. 3. β-Galactosidase activity in the NTS of rats transfected with Adβgal ($n = 5$ at each point, $*p < 0.05$, $**p < 0.01$ compared with values at d 0). (Reproduced with permission from **ref. *11***.)

6. The brain blocks were homogenized for 60 s in 3 mL lysis buffer. Thirty microliters of each lysate was assayed in a 270-μL reaction mixture containing β-galactosidase assay buffer and the color produced by the reaction was measured using a spectrophotometer. Purified bacterial β-galactosidase was used to generate a standard curve for quantitative analysis. Ten microliters of purified β-galacotosidase was diluted 10,000 times (concentration: 30 U/g protein). By definition, 1 unit is the amount of enzyme that hydrolyzes 1 μmol of ONPG/min at 37°C for 30 min. The computer is set up using a software (Soft max Pro). Absorbance for ONPG is 405 nm. The β-galactosidase activity was normalized with respect to the protein content as determined by a dye-binding assay ***(19)***. The time-course of changes of β-galactosidase should also determined before and after transfection (*see* **Note 5**).

3.4. Immunohistochemistry for eNOS

1. For immunohistochemical analysis of eNOS, we used mouse immunoglobulin G1 (IgG1) monoclonal antibody to human eNOS. At 7 d postinjection, rats were fixed by transcardiac perfusion with 4% paraformaldehyde in PBS under anesthesia of sodium pentobarbital (50 mg/kg, intraperitoneally) (*see* **Note 4**).
2. Whole brains were removed and postfixed with the same fixatives. After postfixation, brains were rinsed in PBS three times and 2- to 3-mm-thick coronal slices of medulla were cut.
3. Fifty-micrometer-thick coronal sections of medulla were cut serially on a vibratome, collected in vials, and rinsed for 30 min in PBS. After incubation overnight in 1% BSA in PBS, sections were incubated in mouse IgG1 monoclonal antibody to human eNOS ***(15,20,21)*** (1:200) at room temperature for 1 wk and rinsed three times in PBS.

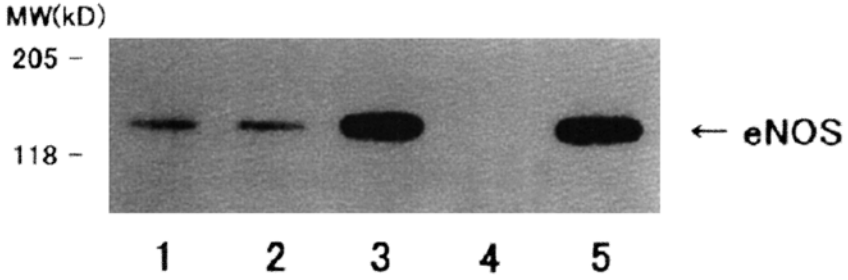

Fig. 4. Western blot analysis for eNOS. Lane 1, untreated rat; lane 2, Adβgal-treated rat; lane 3, AdeNOS-treated rat; lane 4, negative control; lane 5, homogenate of cultured bovine endothelial cells. (Reproduced with permission from **ref. *10***.)

4. After incubation in biotinylated horse anti-mouse IgG (1:1000) overnight, sections were rinsed three times in PBS and incubated in a mixture of streptavidin-conjugated fluorescein isothiocyanate (1:100) and propidium iodide (PI, 10 μg/mL). After rinsing three times in PBS, sections were mounted in Vectashield. BSA (1%) and Triton X-100 (0.3%) were included in each dilution buffer of the primary and secondary antibodies.
5. Double-stained sections with eNOS antibody and PI were photographed with a confocal laser scanning microscope using laser beams of 488 and 568 nm for excitation with appropriate filter sets.
6. Confocal images were transferred to a personal computer and analyzed using the Quantitative Image Analysis software NIH Image (*see* **Fig. 2C**,**D**), as described ***(22)***. The other parts of the brain also should be examined (*see* **Note 6**).

3.5. Western Blot Analysis for eNOS

1. At d 7 after gene transfer, coronal blocks (2 mm thickness) of the brain containing the injected sites of the NTS were obtained.
2. The NTS tissues (approx 500 mg) were homogenized in 2 mL NTS lysis buffer. The tissue lysates were centrifuged at 6000 rpm (approx 4000*g*) for 5 min at 4°C with a microcentrifuge.
3. The lysates were collected, and the protein concentrations determined with a BCA protein assay kit.
4. An aliquot of 20 μg of protein from each sample was resolved by electrophoresis on a 12% sodium dodecyl sulfate (SDS)-polyacrylamide gel and the proteins were subsequently transferred onto a polyvinylidene difluoride membrane (Immunobilon-P membrane) at 4°C.
5. Membranes were incubated for 2 h with mouse IgG1 monoclonal antibody to eNOS (1:2500), washed and incubated with horseradish peroxidase-conjugated horse anti-mouse IgG antibody (1:10000) for 40 min.
6. Immunoreactivity was detected by enhanced chemiluminesence autoradiography (ECS Plus Western blotting detection kit; Amersham) (*see* **Fig. 4** and **Note 7**).

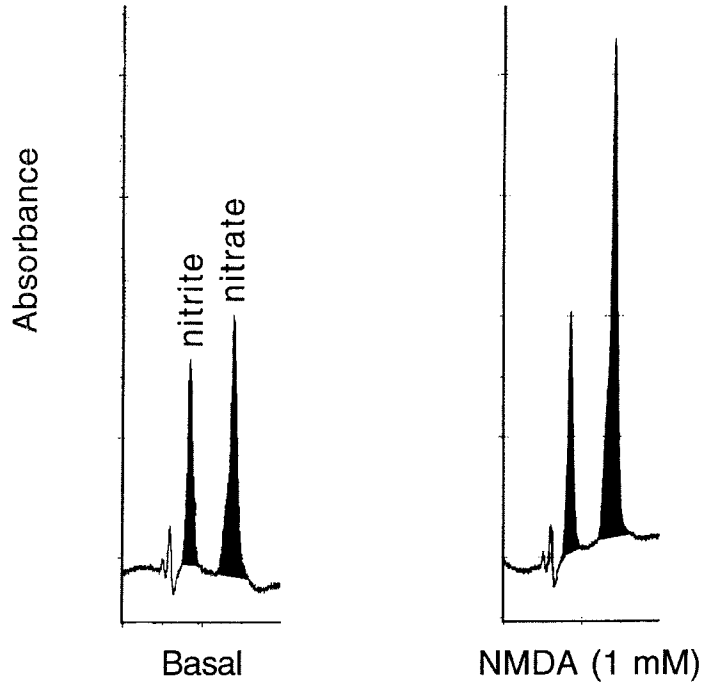

Fig. 5. Sample chromatograms showing the effect of infusion of NMDA in the NTS on the levels of nitrite and nitrate in dialysate. (Reproduced with permission from **ref. *24***.)

The time-course of expression levels was determined by Western blot analysis (*see* **Note 5**).

3.6. Microdialysis and Measurement of NO Metabolites

1. We measured the production of NO in the NTS as nitrite and nitrate (NO_x) by an in vivo microdialysis method ***(23,24)*** before and after gene transfer (*see* **Fig. 5**) (*see* **Note 8**).
2. Rats were anesthetized with pentobarbital (50 mg/kg, intraperitoneally) and mechanically ventilated through endotracheal tubing with room air supplemented with oxygen.
3. A femoral vein was canulated with PE-50 tubing and supplemental doses of pentobarbital (20 mg/kg, intravenously) and pancronium bromide (4 mg/kg, intravenously) were given hourly.
4. The rats were placed in a stereotaxic frame with the head inclined downward at an angle of 45°. An incision was made on the skin of the head, and the muscles were dissected to expose the cisterna magna.
5. The dorsal surface of the medulla was visualized. A microdialysis probe was inserted into the NTS and perfusion with Ringer's solution was carried out at a constant flow rate of 2 μL/min. The perfused dialysates were collected every

10 min in the sample loop of an automated sample injector connected to an automated NO detecter HPLC system (ENO-10), which is based on the Griess reaction. The test agents were administered after three consecutive stable samples had been collected (basal levels). The basal NO_x levels were measured by averaging the three consecutive stable dialysate samples, which were obtained at intervals of 1–2 h after starting the brain perfusion.

6. We used two types of stimulus administered locally via the microdialysis probes. The first stimulus consisted of a 1-m*M* pulse of NMDA, and the second stimulus consisted of a 100-μ*M* pulse of L-Arg. Each drug was dissolved in Ringer's solution and the pH was adjusted to 7.4. L-Arg or NMDA was infused for 10 min into the NTS through a dialysis probe after three consecutive stable samples were obtained (basal sample) with perfusion of normal Ringer's solution.
7. After the pulse of L-Arg or NMDA, the microdialysis probe was perfused again with Ringer's solution. We injected L-NMMA intracisternally to confirm that increased NO level is indeed mediated by NOS overexpression (*see* **Note 8**).
8. At the end of the experiments, the microdialysed site was evaluated histologically. Under anesthesia, brains were removed and serial sections (50 μm) were cut on a vibratome for histological confirmation of the location.

3.7. Radiotelemetry Monitoring of Blood Pressure and Heart Rate

Arterial pressure recordings were acquired on a multichannel amplifier and converted to a digital signals for analysis (MacLab System). A telemetry system was used for measurement of systolic arterial pressure, mean arterial pressure, and heart rate (*see* **Fig. 6**) ***(25,26)***.

1. Before the telemetry device was implanted, it was calibrated to verify accuracy to within ±3 mm Hg. Rats (16–20 wk old) were anesthetized with pentobarbital (50 mg/kg, intraperitoneally).
2. The abdominal wall was cut by scissors from the sternum to the hypogastric region in the midline to reach the abdominal aorta.
3. A hole was made in the abdominal aorta by a 23G needle and the tip of the flexible catheter of the transmitter was inserted into the aorta and affixed with Vetbont (3M Animal Care Products).
4. The tip of the flexible catheter in the abdominal aorta was placed just below the renal arteries and pointing upstream (against the flow).
5. The transmitter was sutured to the abdominal wall. Rats were housed in individual cages after the operation. Each cage was placed over the receiver panel that was connected to a personal computer for data acquisition. The rats were unrestrained and free to move within their cages.
6. All hemodynamic data were sampled continuously for 10 min/d between 10 AM and 11 AM. Previous studies showed that arterial pressure and heart rate took up to 7 d to stabilize postoperatively. Therefore, each microinjection of aCSF or adenovirus vector into the NTS was performed 7 d after surgery and telemetry data were collected for 14 d or more.

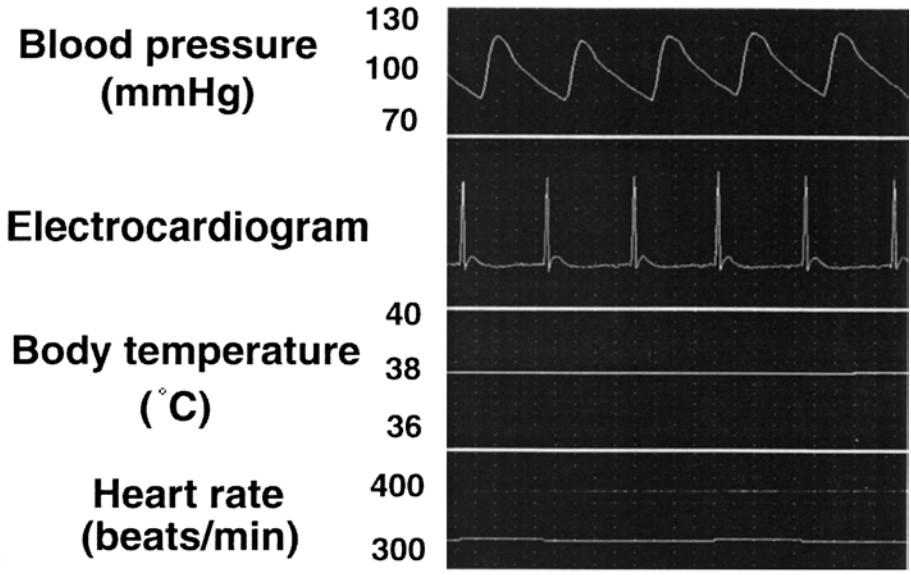

Fig. 6. Examples of original recordings of blood pressure, an electrocardiogram, body temperature, and heart rate using the radiotelemetry system. (Reproduced with permission from **ref. *11***.)

7. To confirm that changes in blood pressure and heart rate were induced by AdeNOS transfection, intracisternal injection of L-NMMA was performed at d 7 after the gene transfer. This approach and the dose of L-NMMA were chosen on the basis of a previous study ***(27)***. It is preferable to examine the effect of microinjection of L-NMMA into the NTS, although it was difficult to cover the transfected areas in the NTS.

3.8. Measurement of Urinary Norepinephrine Excretion

Urine was collected for 24 h by means of a metabolic cage. We measured urinary norepinephrine concentration before and 7 d after the gene transfer by HPLC and calculated the urinary norpenephrine excretion.

4. Notes

1. Inflammatory responses in the brain caused by adenovirus gene transfer must be taken into account when planning experiments and interpreting the results obtained using these vectors ***(28)***. It is helpful to examine the extent of ED-1-positive cell infiltration, a marker of inflammation ***(29)***. It is also important to perform a careful control experiment using Adβgal and to confirm that this does not cause blood pressure changes, and so forth. In addition, it is important to be cognizant of the titer used. The absolute value of a titer is given as PFU/mL.

However, this measurement varies among laboratories according to the criteria used.

2. As long as adenoviral vectors are used, all cell types are infected, including neurons, glia, and vasculature ***(13)*** because it is not possible to transfect the virus into a specific cell type. However, the size of the cell (surface area for viral uptake) may be a factor that influences the effectiveness of transfection.
3. The NTS is a relatively large nucleus that contains not only areas relating to cardiovascular function but also other autonomic function. It is technically impossible to infect adenovirus into only the area concerned with cardiovascular function. However, we determined the infected area by prior injection of a small amount of L-glutamate, which caused a depressor response.
4. The brain needs to be perfused carefully to remove as much blood as possible. The tissue should be rinsed with PBS (cooled by ice) three times. BSA should be dissolved slowly (1 h) in approx 20 mL of PBS, because it foams. The pH of BSA solution is easily changed, so it is advisable to wait until the temperature of the solution goes down. To avoid high background, long incubation times should be avoided (less than 4 h).
5. The time-course of the expression of the transferred gene should be confirmed in each experiment. In the case of infection into the brain of an adenovirus with a cytomegalovirus (CMV) promoter, the expression of the gene peaked at d 7 and then gradually declined over time ***(10,11)***. Therefore, the efficacy of the results (including physiological response) of the transduced gene should be examined in each case. Intracebroventrical, intracisternal, or intrathecal transfection does not last longer than intraparechymal transfection ***(30)***. It was reported that it peaked at d 1–3 after infection and was undetectable by d 7 ***(30)***. Rous sarcoma virus (RSV) as a promotor may last much longer ***(30)***. Feline immunodeficiency virus (FIV) infection lasts for longer periods and is more neuron-specific ***(31)***. However, the efficiency of the delivery of the gene is not as good as adenovirus ***(32)***. Adeno-associated virus was suggested to be more neuron-specific in its mode of transfection ***(32)***.
6. Retrograde transfer of replication-deficient recombinant adenovirus vector in the brain should be taken into account ***(33,34)***. Therefore, other areas that have connections with the NTS must be examined. As far as we could ascertain, we did not see any detectable eNOS expression in the ventrolateral medulla or the hypothalamus.
7. For Western blot analysis, total protein should be quantified by spectrophotometer using Soft max Pro. For eNOS, electrophoresis for 1 h at 150 V was found to be a suitable approach.
8. In the case of NO, it diffuses beyond the transfected cells because it is a small soluble molecule. This needs to be taken into account for interpreting the results.
9. We were not able to perfuse the NTS with L-NMMA from the dialysis probe because this procedure interfered with the measurement of NO_x ***(24)***. This technical difficulty was also described by others ***(23)***.
10. This approach (described in this chapter) was also applied into the rostral ventrolateral medulla, where the cardiovascular center is located ***(35)***.

Acknowledgments

This work was supported by a Grant-in Aid for Encouragement of Young Scientists (09770489) and the Grant-in-Aid for Scientific Research (C11670689, C13670721, C15590757) from the Ministry of Education, Science, Sports, and Culture and the Japan Society for the Promotion of Science. We thank Dr. Akira Takeshita, Dr. Hiroaki Shimokawa, Dr. Takuya Kishi, Dr. Isamu Matsuo, Dr. Kenichi Eshima, and Dr. Hideaki Shigematsu of this Institute for valuable advice and discussion, and Dr. Donald D. Heistad, Dr. Beverly L. Davidson, and Dr. Richard D. Anderson (The University of Iowa Gene Transfer Vector Core, supported by National Institute of Health Grants and the Carver Foundation) for the preparation of the vectors. We also thank Dr. Toshio Kosaka for his advice in the immunohistochemical analysis for eNOS and the use of his facility for microscopic analysis.

References

1. Patel, K. P., Li, Y.-F., and Hirooka, Y. (2001) Role of nitric oxide in central sympathetic outflow. *Exp. Biol. Med.* **226,** 814–824.
2 Harada, S., Tokunaga, S., Momohara, M., et al. (1993) Inhibition of nitric oxide formation in the nucleus tractus solitarius increases renal sympathetic nerve activity in rabbits. *Circ. Res.* **72,** 511–516.
3 Zanzinger, J., Czachurski, J., and Seller, H. (1997) Neuronal nitric oxide reduces sympathetic excitability by modulation of central glutamate effects in pigs. *Circ. Res.* **80,** 565–571.
4 Tseng, C.-J., Liu, H.-Y., Lin, H.-C., et al. (1996) Cardiovascular effects of nitric oxide in the brain stem nuclei of rats. *Hypertension* **27,** 36–42.
5 Dampney, R. A. L. (1994) Functional organization of central pathways regulating the cardiovascular system. *Physiol. Rev.* **74,** 323–364.
6 van Giersbergen, P. L. M., Palkovits, M., and de Jong, W. (1992) Involvement of neurotransmitters in the nucleus tractus solitarii in cardiovascular regulation. *Physiol. Rev.* **72,** 789–824.
7 Andresen, M. C. (1994) Nucleus tractus solitarius: gateway to neural circulatory control. *Annu. Rev. Physiol.* **56,** 93–116.
8 Shihara, M., Hirooka, Y., Eshima, K., et al. (2001) Stimulatory effect of endothelin-1 on neurons in the nucleus tractus solitarii is mediated by non-*N*-methyl-D-aspartate receptors. *Hypertens. Res.* **24,** 137–142.
9 Hirooka, Y., Kishi, T., Sakai, K., et al. (2003) Effect of overproduction of nitric oxide in the brain stem on the cardiovascular response in conscious rats. *J. Cardiovasc. Pharmacol.* **41(Suppl. 1),** S119–S126.
10 Sakai, K., Hirooka, Y., Matsuo, I., et al. (2000) Overexpression of eNOS in NTS causes hypotension and bradycardia in vivo. *Hypertension* **36,** 1023–1028.
11 Hirooka, Y., Sakai, K., Kishi, T., et al. (2001) Adenovirus-mediated gene transfer into the NTS in conscious rats: a new approach to examining the central control of cardiovascular regulation. *Ann. NY Acad. Sci.* **940,** 197–205.

12 Hirooka, Y., Sakai, K., Ito, K., et al. (2003) Enhanced depressor response to endothelial nitric oxide synthase gene transfer into the nucleus tractus solitarii of spontaneously hypertensive rats. *Hypertens. Res.* **26,** 325–331.
13 Davidson, B. L., Allen, E. D., Kozarsky, K. F., et al. (1993) A model system for in vivo gene transfer into the central nervous system using an adenoviral vector. *Nature Genet.* **3,** 219–223.
14 Ooboshi, H., Welsh, M. J., Rios, C. D., et al. (1995) Adenovirus-mediated gene transfer in vivo to cerebral blood vessels and perivascular tissue. *Circ. Res.* **77,** 7–13.
15 Ooboshi, H., Chu, Y., Rios, C. D., et al. (1997) Altered vascular function after adenovirus-mediated overexpression of endothelial nitric oxide synthase. *Am. J. Physiol.* **273,** H265–H270.
16. Paxinos, G. and Watoson, C. (1998) The rat brain in stereotaxic coordinates, in *The Rat Brain in Stereotaxic Coordinates*, Academic, New York.
17. Ueno, H., Li, J.-J., Tomita, H., et al. (1995) Quantitative analysis of repeat adenovirus-mediated gene transfer into injured canine femoral arteries. *Arteriosclerosis Thromb. Vasc. Biol.* **15,** 2246–2253.
18 Eustice, D. C., Feldman, P. A., Colberg-Poley, A. M., et al. (1991) A sensitive method for the detection of β-galactosidase in transfected mammalian cells. *BioTechniques* **11,** 739–741.
19 Bradford, M. M. (1976) A rapid and sensitive method for the quantitation of microgram quantities of protein utilizing the principle of protein-dye binding. *Anal. Biochem.* **72,** 248–254.
20 Chen, A. F. Y., O'Brien, T., Tsutsui, M., et al. (1997) Expression and function of recombinant endothelial nitric oxide synthase gene in canine basilar artery. *Circ. Res.* **80,** 327–335.
21 Cable, D. G., O'Brian, T., Kullo, I. J., et al. (1997) Expression and function of a recombinant endothelial nitric oxide synthase gene in porcine coronary arteries. *Cardiovasc. Res.* **35,** 553–559.
22 Kosaka, K., Toida, K., Margolis, F. L., et al. (1997) Chemically defined neuron groups and their subpopulations in the glomerular layer of the rat main olfactory bulb, II: prominent differences in the intraglomerular dendritic arborization and their relationship to olfactory nerve terminals. *Neuroscience* **76,** 775–786.
23 Yamada, K. and Nabeshima, T. (1997) Simultaneous measurement of nitrite and nitrate levels as indices of nitric oxide release in the cerebellum of conscious rats. *J. Neurochem.* **68,** 1234–1243.
24 Matsuo, I., Hirooka, Y., Hironaga, K., et al. (2001) Glutamate release via NO production evoked by NMDA in the NTS enhances hypotension and bradycardia in vivo. *Am. J. Physiol. Regul. Integr. Comp. Physiol.* **280,** R1285–R1291.
25 Anderson, N. H., Devlin, A. M., Graham, D., et al. (1999) Telemetry for cardiovascular monitoring in a pharmacological study: new approaches to data analysis. *Hypertension* **33,** 248–255.
26 van den Buuse, M. (1994) Circadian rhythm of blood pressure, heart rate, and locomotor activity in spontaneously hypertensive rats as measured with radiotelemetry. *Physiol. Behav.* **55,** 783–787.

27 Hironaga, K., Hirooka, Y., Matsuo, I., et al. (1998) Role of endogenous nitric oxide in the brain stem on the rapid adaptation of baroreflex. *Hypertension* **31,** 27–31.
28 Byrnes, A. P., Rusby, J. E., Wood, M. J. A., et al. (1995) Adenovirus gene transfer causes inflammation in the brain. *Neuroscience* **66,** 1015–1024.
29. Tomita, H., Egashira, K., Kubo-Inoue, M., et al. (1998) Inhibition of NO synthesis induces inflammatory changes and monocyte chemoattractant protein-1 expression in rat hearts and vessels. *Arteriosclerosis Thromb. Vasc. Biol.* **18,** 1456–1464.
30 Mannes, A. J., Caudle, R. M., O'Connell, B. C., et al. (1998) Adenoviral gene transfer to spinal-cord neurons: intrathecal vs intraparechymal administration. *Brain Res.* **793,** 1–6.
31 Sinnayah, P., Lindley, T. E., Staber, P. D., et al. (2002) Selective gene transfer to key cardiovascular regions of the brain: comparison of two viral vector systems. *Hypertension* **39,** 603–608.
32 Okada, T., Nomoto, T., Shimazaki, K., et al. (2002) Adeno-associated virus vectors for gene transfer to the brain. *Methods* **28,** 237–247.
33 Kuo, H., Ingram, D. K., Crystal, R. G., et al. (1995) Retrograde transfer of replicant deficient recombinant adenovirus vector in the central nervous system for tracing. *Brain Res.* **705,** 31–38.
34 Vasquez, E. C., Beltz, T. G., Meyrelles, S. S., et al. (1999) Adenovirus-mediated gene delivery to hypothalamic magnocellular neurons in mice. *Hypertension* **34,** 756–761.
35. Kishi, T., Hirooka, Y., Sakai, K., et al. (2001) Overexpression of eNOS in the RVLM causes hypotension and bradycardia via GABA release. *Hypertension* **38,** 896–901.

16

Gene Therapy in Cancer Via Use of a Retrovector Having a Tumor Specificity and Expressing Inducible Nitric Oxide Synthase

Masahide Kuroki

Summary

The generation of retrovectors (retroviral vectors) with tumor specificity is a promising and effective approach to targeted gene therapy of cancer. Carcinoembryonic antigen (CEA), overexpressed by various tumor cells, provides a specific tool for tumor-specific targeting by retrovectors. The conventional suicidal gene delivery systems need additional drugs other than their gene products. The inducible nitric oxide synthase (iNOS) gene product yields nitric oxide (NO), which directly induces autocytotoxicity and cytolysis of bystander cells. A novel method is described here that explains how to prepare a novel recombinant retrovector that displays a chimeric envelope protein containing a single-chain fragment variable (scFv) antibody to CEA and carries the *iNOS* gene in the genome. The resultant bifunctional retrovector showed a specific delivery of the *iNOS* gene to human CEA-expressing carcinoma cells, resulting in the direct and efficient killing of CEA-expressing carcinoma cells by induction of apoptosis. This approach may offer a one-step procedure for effective gene therapy of CEA-expressing tumors and also be applied to other tumor antigens expressed on cancer cells.

Key Words: Apoptosis; carcinoembryonic antigen (CEA); Chinese hamster ovary (CHO) cells; gene therapy; inducible nitric oxide synthase (iNOS); nitric oxide (NO); nitric oxide synthase (NOS); *N*-methyl-L-arginine (NMA); polymerase chain reaction (PCR); retrovectors (retroviral vectors); reverse transcription-PCR (RT-PCR); single-chain fragment variable (scFv) antibody; tumor specificity.

1. Introduction

Retroviruses have evolved the mechanism to insert their genetic materials into the target cells. The majority of clinical trials to date have used the Moloney murine leukemia virus-based retrovectors for gene transfer. Mammalian retroviruses are commonly of two types depending on their host range, as either ecotropic, which infects only murine cells, or amphotropic, which infects

From: *Methods in Molecular Biology, vol. 279: Nitric Oxide Protocols: Second Edition*
Edited by: A. Hassid © Humana Press Inc., Totowa, NJ

both the murine and nonmurine cells. Host range depends on the properties of viral envelope glycoproteins. Recently, it has been possible to change the tropism of an ecotropic retroviral receptor-binding domain with an scFv antibody that recognizes a human tumor-specific cell surface antigen ***(1,2)***.

Carcinoembryonic antigen (CEA) is a cell surface antigen with a molecular mass of 180 kDa and is widely overexpressed on the tumor cell surface of various human malignancies. We have previously prepared a novel monoclonal antibody clone F11-39, which shows a high affinity to CEA and discriminates CEA in tumor tissues from the other CEA gene family proteins in the normal tissues ***(3)***. Thus, the scFv form of this antibody seems to be applicable to targeting of retrovectors to CEA-expressing tumor cells by expression in the envelope proteins of the virus particles that contain a certain killing or suicidal gene.

The second important issue in this approach is the selection of gene used for cell killing. Nitric oxide (NO), one of the smallest biologically active molecules, is a potential toxin for immunological self-defense. The formation of NO from L-arginine in mammalian cells is catalyzed by nitric oxide synthases (NOSs) including inducible NOS (iNOS), endothelial NOS, and brain NOS ***(4)***. Under physiological conditions, iNOS is absent from mammalian cells, but when cells are activated, it is induced and causes a long-lasting generation of NO, which is associated with a cytotoxic reaction against pathogens and tumor cells ***(4)***. Previous studies have shown that *iNOS* transfected into mouse melanoma cells suppressed their tumorigenicity ***(5)*** and also lysed bystander murine cells under in vitro and in vivo conditions, which suggested that NO-mediated cell killing does not require the transfection of every cell ***(6)***.

This chapter deals with methods for preparation of a bifunctional Moloney murine leukemia virus-based retrovector that displays a chimeric envelope protein, including an anti-CEA scFv antibody derived from F11-39 and carries the *iNOS* gene in the genome (*see* **Fig. 1**) ***(7)***. The recombinant retrovirus showed a specific delivery of the *iNOS* gene to human CEA-expressing carcinoma cells and directly killed the infected cells by induction of apoptosis without any additional drugs ***(8)***.

2. Materials

2.1. Plasmid Construction

2.1.1. The Recombinant Envelope Expression Vector

1. Mouse Ig-Primer Set (Novagen, Madison, WI).
2. pT7 blue vector (Novagen).
3. Polymerase chain reaction (PCR) primers for an anti-CEA scFv: sense primer 5'-TCTCGAGGACATCCAGATGACTCAGTCT-3' and antisense primer 5'-TGGTGACCTCAGCAGAGACAG TGACCAGA-3'. These primers include

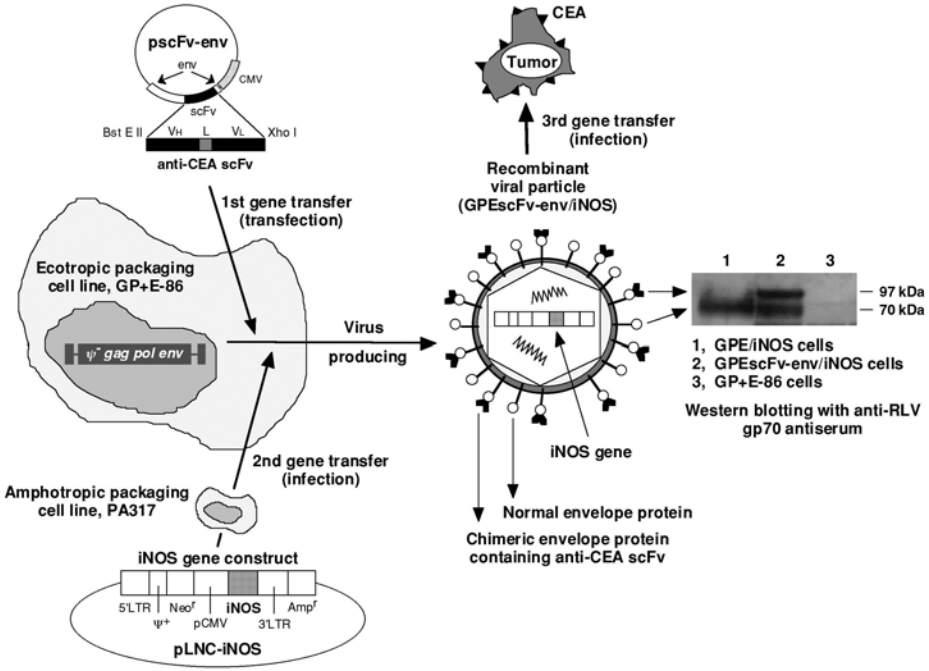

Fig. 1. Specific targeting strategy of iNOS gene to CEA-expressing tumor cells using a recombinant retrovector displaying an anti-CEA scFv-envelope chimeric protein. Expression of anti-CEA scFv chimeric envelope protein in recombinant retrovirus is also shown. (Adapted with permission from **ref. *7***.)

the unique sequences to introduce the *Xho*I and *BstE*II sites, respectively (underlined).

4. Envelope expression vector pEnv 20.22 (kindly gifted by Dr. N. V. Somia, Salk Institute, USA)

2.1.2. The iNOS Expression Vector

1. piNOSL8 construct (Oxford Biomedical Research Inc., Rochester Hills, MI).
2. pLNCX retrovector with the cytomegalovirus promoter and a neomycin-resistance gene (Clontech, Palo Alto, CA).

2.2. Reconstruction of Packaging Cells

1. GP+E-86 ecotropic retroviral packaging cells derived the mouse fibroblast cell line NIH3T3 (American Type Culture Collection, Rockville, MD).
2. PA317 amphotropic retroviral packaging cells (American Type Culture Collection).
3. Hygromycin-B phosphotransferase expression vector pcDNA3.1/Hygro(+) (Invitrogen, Carlsbad, CA).

4. Hygromycin B (Wako Pure Chemical, Osaka, Japan).
5. Biotinylated CEA ***(9)***.
6. Fluorescein isothiocyanate (FITC)-conjugated avidin (Vector Laboratories, Burlingame, CA).

2.3. Production of Viruses

1. Polybrene (Sigma Chemical Co., St. Louis, MO).
2. Specific iNOS inhibitor NMA (Sigma).
3. G418 (Calbiochem-Novabiochem, San Diego, CA).
4. 0.45-μm-pore filter (Millipore Corp., Milford, MA).

2.4. Immunoblotting

1. Sodium dodecyl sulfate–polyacrylamide gel electrophoresis (SDS-PAGE) sample buffer: 25 m*M* Tris, 192 m*M* glycine, 0.1% SDS.
2. Nitrocellulose membrane (Amersham Pharmacia Biotech, Buckinghamshire, UK).
3. Goat Anti-RLV gp70 anti-serum (anti-Rouscher leukemia murine envelope gp69/71; Quality Biotech, Camden, NJ).
4. Biotinylated anti-goat IgG and horseradish peroxidase (HRP)-conjugated avidin (Vector).
5. Hyperfilm-ECL (Amersham).

2.5. NO Analysis

1. Griess reagent: 1% sulfanilamide, 0.1% naphthylethylene diamine dihydrochloride, and 2.5% phosphoric acid (Wako).
2. Sodium nitrite (Wako).

2.6. Virus Infection and Reverse Transcription-PCR

1. Target cells: three human gastric carcinoma cell lines MKN-45 (CEA-expressing), KATO-III (CEA-expressing) and MKN-74 (CEA-nonexpressing) (The Japanese Cancer Research Resources, Tokyo, Japan); Chinese hamster ovary (CHO) cells; and a CEA-expressing CHO (CHO-CEA) cell line obtained as described previously ***(10)***.
2. Dulbecco's modified Eagle's medium (Nissui, Tokyo).
3. Fetal bovine serum (FBS) (Bio-Whittaker, Walkersvilli, MD).
4. Penicillin (Banyu Pharmaceutical Co., Tokyo).
5. Streptomycin (Meiji Seika Kaisha, Tokyo).
6. α-Minimum essential medium (Gibco-BRL, Gaithersburg, MD).
7. Six-well plates (Becton-Dickinson, Franklin Lakes, NJ).
8. Polybrene (4 μg/mL) High Pure RNA Isolation Kit (Boehringer Mannheim, Indianapolis, IN).
9. High Pure RNA Isolation Kit (Boehringer Mannheim, Indianapolis, IN).
10. Superscript Preamplification System (Life Technologies, Rockville, MD).
11. AmpliTaq Gold DNA polymerase (Perkin-Elmer, NJ).
12. The primers synthesized from published sequences: sense primer 5'-CTGCAA GAGAACGGAGAACGT-3' and antisense primer 5'-GATCCTCACATACTG

TGGACG-3' for iNOS; 5'-TCAGCGCAGGGGCGCCCGGTTCTTT-3' and 5'-ATCGACAAGACCGGCTTCCATCCGA-3' for neomycin; 5'-GTGGGC CGCTCTAGGCACCAA-3' and 5'-CTCTTTGATGTCACGCACGATTTC-3' for mouse β-actin; 5'-TCCTGACCGAGCGTGGCTACAGC-3' and 5'-CTCCTG GAAGGTGGA CAGTGAGG-3' for hamster β-actin; 5'-GGGAATTCGAGC AAGAGATG-3' and 5'-GGGAATTCATAGTCCGCCTAGAA-3' for human β-actin; and the above-mentioned primers for anti-CEA scFv.

2.7. In Vitro Cytotoxicity Assay

1. 96-Well black plates (Labsystems, Helsinki, Finland).
2. Fluorescent dye H33342 (25 μg/mL) (Calbiochem-Novabiochem).

2.8. Analysis of DNA Fragmentation

1. Apop Ladder Ex Kit (Takara Biomedicals, Tokyo).
2. Ethidium bromide (Sigma).

3. Methods

3.1. Plasmid Construction

3.1.1. The Recombinant Envelope Expression Vector

1. The F11-39 V_H and V_κ cDNA genes were specifically amplified by PCR using the Mouse Ig-Primer Set, and joined into the *scFv* gene by the overlap extension PCR method.
2. The PCR products were cloned into the pT7 blue vector. This *scFv* cDNA was modified at its 5' and 3' ends with the above-mentioned primers introducing the unique *Xho*I and *BstE*II sites, respectively (*see* **Subheading 2.1.1., step 3**).
3. The modified *scFv* cDNA (728 bp) was inserted into the *Xho*I and *BstE*II restriction sites of the envelope expression vector pEnv 20.22, which contains a strong cytomegalovirus immediate–early promoter, yielding the plastid pscFv-env (*see* **Fig. 1** and **Note 1**).

3.1.2. The iNOS Expression Vector

1. An adapter containing a *Hinc*II and an *Ssp*I site was inserted into the multiple cloning site of the pLNCX retrovector.
2. The piNOSL8 construct was digested with *Hinc*II and *Ssp*I, and the resulting 3.9-kb *iNOS* fragment was cloned into the *Hinc*II/*Ssp*I site of pLNCX, yielding the plasmid pLNC-iNOS (*see* **Fig. 1**).

3.2. Reconstruction of Packaging Cells

1. To establish a permanent clone of ecotropic packaging cells for expression of the chimeric envelope displaying anti-CEA scFv antibody, 5×10^5 GP+E-86 cells were cotransfected with 12 μg of the plasmid pscFv-env (**Fig. 1**, 1st gene transfer) and 2 μg of the pcDNA3.1/Hygro (+) vector by the calcium phosphate method.

2. Clones were selected in the presence of hygromycin B (200 μg/mL) for 10–12 d. The positive clones were screened by RT-PCR using the primers for *anti-CEA scFv* (*see* **Subheading 2.1.1.**, **step 3**) and by an EPICS flow cytometer (Coulter, Miami, FL) using biotinylated CEA and FITC-conjugated avidin.
3. The highest positive permanent packaging cell clone thus obtained was named GPEscFv-env.
4. For control, the GP+E-86 cells were transfected only with the *hygromycin-B phosphotransferase* gene, selected and designated GPE-hgB.

3.3. Virus Production by Reconstructed Packaging Cells

1. Retrovirus carrying the *iNOS* gene was obtained by transfection of the PA317 packaging cells with pLNC-iNOS using the calcium phosphate method (*see* **Fig. 1**).
2. After 48 h, the GPEscFv-env or GPE-hgB packaging cells were infected with the culture supernatant of the transfected PA317 cells in the presence of Polybrene (4 μg/mL) by spin infection at 700*g* for 2 h at 32°C (*see* **Fig. 1**, 2nd gene transfer).
3. After washing, cells successfully infected with *iNOS* were selected for 14 d in medium containing 2 m*M* of specific iNOS inhibitor NMA and 600 μg/mL of G418.
4. For virus production, medium was harvested from confluent monolayers of the virus-producing cells 18–20 h after a medium change.
5. The supernatant was filtered through a 0.45-μm-pore filter and used immediately for infection or stored at –80°C.
6. The resultant recombinant retrovirus displaying anti-CEA scFv and carrying the *iNOS* gene was termed GPEscFv-env/iNOS (*see* **Fig. 1**) and the retrovirus only carrying the *iNOS* gene was termed GPE/iNOS.
7. To increase the virus titer, the viral supernatants were concentrated by centrifugation at 4000*g* for 18 h at 4°C.

3.4. Immunoblotting

1. For detection of envelope proteins, 6 mL of viral supernatants were centrifuged as described above (*see* **Subheading 3.7.**) and the pellet was dissolved in 100 μL of the SDS-PAGE sample buffer.
2. Proteins were then separated by SDS-PAGE on 8% gel and electroblotted onto nitrocellulose membranes.
3. After blocking, the membrane was reacted successively with anti-RLV gp70 antiserum and biotinylated anti-goat IgG and HRP-conjugated avidin.
4. Proteins on the membranes were visualized by using the ECL system (Amersham) and Hyperfilm-ECL according to the manufacturer's instructions. The GPE/iNOS retrovirus contained only the normal envelope protein of about 70 kDa, whereas the GPEscFv-env/iNOS retrovirus contained the chimeric envelope protein of about 97 kDa as well as the normal envelope protein (*see* **Fig. 1**), confirming the expected size of scFv to be about 27 kDa (*see* **Note 2**).

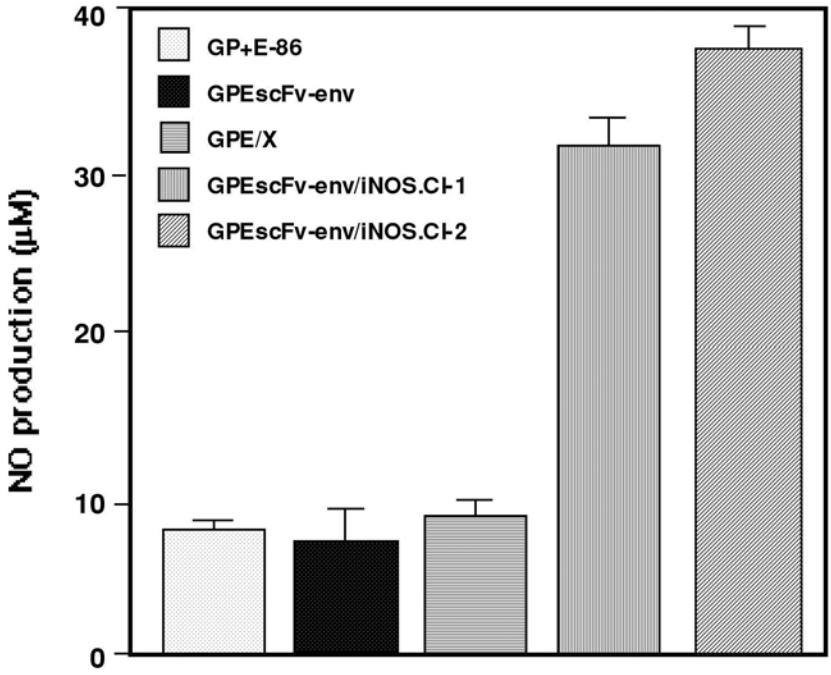

Fig. 2. Production of NO by reconstructed packaging cells. The cells tested were the GP+E-86 cells, the reconstructed GPEscFv-env cells, the iNOS negative GPE/X cells, and two different GPEscFv-env/iNOS retrovirus producing clones Cl-1 and Cl-2. Bars represent the standard deviation. High levels of NO were observed in the Cl-1 and Cl-2 clones, and the GP+E-86, GPEscFv-env, and GPE/X cells produced much lower levels of NO in the absence of NMA. (Adapted with permission from **ref. *8***.)

3.5. Production of NO by Reconstructed Packaging Cells

1. One hundred microliters of supernatant cultured in the absence of NMA was mixed with 100 μL of the Griess reagent at room temperature for 10 min in the dark.
2. The absorbance at 540 nm was monitored by a microplate reader (Benchmark; Bio-Rad, Hercules, CA), and NO concentration was determined using sodium nitrite as the standard (*see* **Fig. 2**).

3.6. Virus Infection and RT-PCR

1. Three target cells, MKN-45, KATO-III and MKN-74, were cultured in Dulbecco's modified Eagle's medium supplemented with 10% heat-inactivated FBS, 100 units/mL penicillin, and 100 μg/mL streptomycin. The CHO and CHO-CEA cells were cultured in α-minimum essential medium supplemented with 10% heat-inactivated FBS, 2 m*M* glutamine, and the antibiotics. The cell cultures were maintained at 37°C in a humidified atmosphere with 5% CO_2.

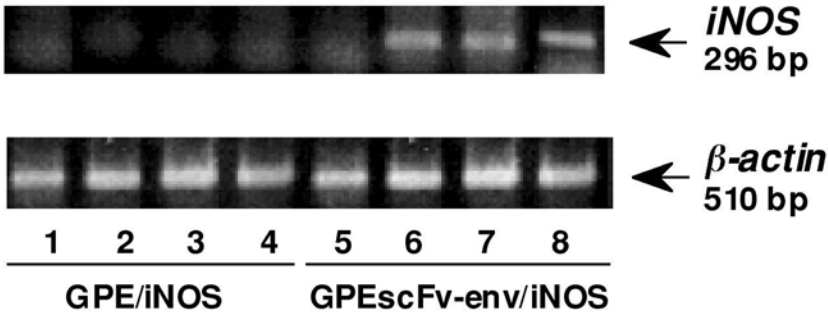

Fig. 3. Detection of iNOS transcripts in CEA-expressing cells infected with the GPEscFv-env/iNOS retrovirus. Total RNA was isolated from MKN-74 (*lanes 1* and *5*), MKN-45 (*lanes 2* and *6*), CHO-CEA (*lanes 3* and *7*) and KATO-III (*lanes 4* and *8*) cells infected with the GPEscFv-env/iNOS retrovirus (*lanes 5–8*) and the GPE/iNOS retrovirus (*lanes 1–4*) in the presence of NMA. Only the GPEscFv-env/iNOS retrovirus-infected CEA-expressing cells showed the specific band of iNOS (*lanes 6–8*), whereas no band was observed in the GPEscFv-env/iNOS retrovirus-infected CEA-nonexpressing cells (*lane 5*) or the GPE/iNOS retrovirus-infected cells (*lanes 1–4*). (Adapted with permission from **ref. *8***.)

2. Target cells were seeded at 1×10^5 cells/well in six-well plates.
3. After 24 h, the target cells were infected with the GPEscFv-env/iNOS or GPE/iNOS retrovirus in the presence of Polybrene by spin infection at 700*g* for 2 h at 32°C (*see* **Fig. 1**, *3rd gene transfer*).
4. Total RNA was isolated from the infected target cells using the High Pure RNA Isolation Kit according to the manufacturer's instructions.
5. Isolated RNA (5 μg) was reverse transcribed by using the Superscript Pre-amplification System.
6. PCR amplification was performed using the AmpliTaq Gold DNA polymerase and the above-mentioned primers (*see* **Subheading 2.6.**, **step 12**).
7. PCR products were subjected to electrophoresis on 1.5% agarose gel and stained with ethidium bromide (*see* **Fig. 3**).

3.7. In Vitro Cytotoxicity Assay

1. Target cells were infected as described above (*see* **Subheading 3.6.**, **step 3**). The multiplicity of infection used was adjusted to 0.1 (*see* **Note 4**).
2. After washing, the cells were cultured for 7 d at 37°C in the absence of NMA. Noninfected control target cells were incubated for the same days in the plain medium.
3. The remaining cells were collected in 96-well black plates, centrifuged, and incubated with the fluorescent dye H33342 for 1 h at 37°C.
4. Cells were washed and suspended in 100 μL of PBS and their fluorescence intensity was measured at an excitation wavelength of 355 nm and an emis-

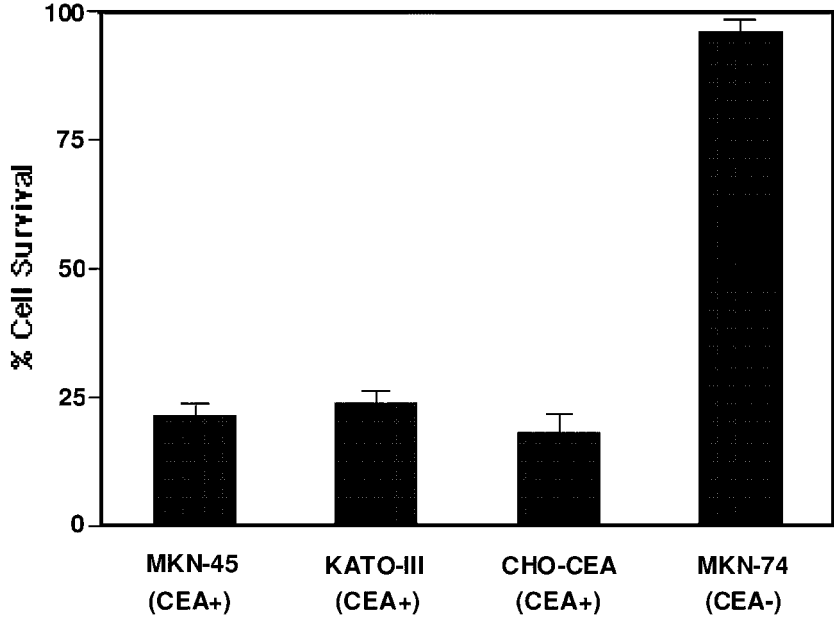

Fig. 4. In vitro cytotoxicity assay of the GPEscFv-env/iNOS retrovirus. Cells were infected with the GPEscFv-env/iNOS retrovirus for 2 h and cultured for 7 d without NMA. The results were expressed as percent survival, which was obtained by the following formula: [(mean test – mean blank/mean control – mean blank)] × 100. Bars represent standard deviations. (Adapted with permission from **ref. *8***.)

sion wavelength of 460 nm by using a Fluoroskan II fluorometer (Labsystems) (*see* **Fig. 4**).

3.8. Analysis of DNA Fragmentation

1. Target cells were infected with the GPEscFv-env/iNOS or GPE/iNOS retrovirus as described in **Subheading 3.6.**
2. After 7 d culture in the absence of NMA, the low-molecular-mass DNA was extracted from the infected cells using the Apop Ladder Ex Kit according to the manufacturer's instructions.
3. Samples were subjected to electrophoresis together with molecular-weight markers on 2% agarose gel. DNA was visualized by ethidium bromide staining. Significant DNA fragmentation occurred in CEA-expressing cells infected with the GPEscFv-env/iNOS retrovirus but did not in CEA-expressing cells infected with the GPE/iNOS retrovirus (data not shown) ***(8)***.

3.9. Discussion

Our specifically targeted killing approach has several features that make it attractive for clinical gene delivery. First, the recombinant retrovirus obtained

specifically bound to CEA-expressing cells. This prevents the uptake of virus by nontarget cells or CEA-nonexpressing cells, resulting in lesser side effects. Second, the targeted cells were directly killed by the biological product of the therapeutic gene, which is very convenient for practical retroviral targeted delivery, because the established suicidal gene therapy systems using such as herpes simplex virus–thymidine kinase and cytosine deaminase need the additional drug treatments. Furthermore, the "bystander effect" of NO may overcome the limitation of retrovector gene transfer efficiency.

4. Notes

1. The generation of retrovectors incorporating a chimeric envelope protein with an scFv antibody should use fusion close to the amino terminus of ecotropic Moloney envelope protein. Our anti-CEA scFv antibody was inserted between the sixth and seventh amino acid residue from the amino terminal of the ecotropic envelope protein.
2. The ratio of normal envelope to chimeric envelope protein in the viral membrane appears to determine the efficiency of infection. Our final GPEscFv-env/iNOS retroviral particles codisplayed the chimeric envelope and normal envelope proteins, and their ratio was almost the same (*see* **Fig. 1**).
3. The recombinant GPEscFv-env/iNOS retroviral particles (*see* **Fig. 2**) specifically transfected the iNOS gene into CEA-expressing cells (*see* **Fig. 3**). However, endogeneous iNOS expression in human carcinoma cells is very diverse. The expression of endogenous iNOS in the human carcinoma and hamster cell lines used in the present study was undetectable even by RT-PCR (data not shown). The expression of endogenous iNOS of each cell line used in this kind of experiment should be tested in advance.
4. The recombinant GPEscFv-env/iNOS retrovirus also revealed significant cytotoxicity against CEA-expressing cells (*see* **Fig. 4**). Cell death was directly correlated with the amount of NO produced, suggesting that NO-mediated cytotoxicity is directly related to the production of NO in culture supernatants. A higher multiplicity of infection of recombinant retrovirus may lead to higher number of cells infected and killed.

Acknowledgments

This work was supported in part by Grant-in-Aids for High-technology Research Center and for Scientific Research (C) from the Ministry of Education, Culture, Sports, Science and Technology, Japan. The author is indebted to Dr. Pranay D. Khare, who has been a part of the development of many of the techniques described in this chapter. I also acknowledge the journals *Anticancer Research* and *Cancer Research* for their permission to reproduce Figs. 1–4 as the original sources of the materials.

References

1 Russell, S. J., Hawkins, R. E., and Winter, G. (1993) Retroviral vectors displaying functional antibody fragments. *Nucleic Acids Res.* **21,** 1081–1085.

2 Somia, N. V., Zoppe, M., and Verma, I. M. (1995) Generation of targeted retroviral vectors by using single-chain variable fragment: an approach to in vivo gene delivery. *Proc. Natl. Acad. Sci. USA* **92,** 7570–7574.

3 Kuroki, Ma., Arakawa, F., Haruno, M., et al. (1992) Biochemical characterization of 25 distinct carcinoembryonic antigen (CEA) epitopes recognized by 57 monoclonal antibodies and categorized into seven groups in terms of domain structure of the CEA molecule. *Hybridoma* **11,** 391–407.

4 Nathan, C. (1992) Nitric oxide as a secretory product of mammalian cells. *FASEB J.* **6,** 3051–3064.

5 Xie, K., Huang, S., Dong, Z., et al. (1995) Transfection with the inducible nitric oxide synthase gene suppresses tumorigenicity and abrogates metastasis by K-1735 murine melanoma cells. *J. Exp. Med.* **181,** 1333–1343.

6 Xie, K., Huang, S., Dong, Z., et al. (1997) Destruction of bystander cells by tumor cells transfected with inducible nitric oxide (NO) synthase gene. *J. Natl. Cancer Inst.* **89,** 421–427.

7 Kuroki, Ma., Arakawa, F., Khare, P. D., et al. (2000) Specific targeting strategies of cancer gene therapy using a single-chain variable fragment (scFv) with a high affinity for CEA. *Anticancer Res.* **20,** 4067–4071.

8 Khare, P. D., Liao, S., Kuroki, Mo., et al. (2001) Specifically targeted killing carcinoembryonic antigen (CEA)-expressing cells by a retroviral vector displaying single chain variable fragmented (scFv) antibody to CEA and carrying the gene for inducible nitric oxide synthase (iNOS). *Cancer Res.* **61,** 370–375.

9 Kuroki, Ma. (1996) A simple solid-phase competition assay with labeled antigen, in *Methods in Molecular Biology*, *Vol. 66. Epitope Mapping Protocols* (Morris, G.E., ed.), Humana, Totowa, NJ, pp. 47–53.

10. Kuroki, Mo., Arakawa, F., Matsuo, Y., et al. (1991) Molecular cloning of nonspecific cross-reacting antigens in human granulocytes. *J. Biol. Chem.* **266,** 11,810–11,817.

17

Gene Transfer of Nitric Oxide Synthase Via the Use of Adeno-Associated Virus Vectors

Yoshikazu Maeda, Kazuyuki Shimada, and Uichi Ikeda

Summary

Adeno-associated virus (AAV) is a replication-defective dependovirus and is not known to cause disease in humans. AAV vectors have a broad host range and can transduce both dividing and nondividing cells. Five primate AAV serotypes have been characterized in the literature and are designated as AAV types 1–5 (AAV1–5). There is divergence in homology and tropism for various AAV serotypes. AAV vectors can be produced by triple plasmids transfection system (adenovirus-free system) and purified by ultracentrifugation using CsCl gradient. The titer of AAV vectors is determined by dot-blot analysis. We have produced the AAV type 2 vectors encoding endothelial NOS (eNOS) gene and transduced rat aortic segments.

Key Words: AAV vectors; transfection; calcium phosphate; cesium chloride gradient; dot-blot analysis; endothelial NOS (eNOS).

1. Introduction

There are many gene transfer vehicles, including adenovirus, retrovirus, and liposomes. Although adenoviral vectors have been shown to transduce cells with high efficiency, gene expression is transient as a result of an episomal feature ***(1–9)***. In addition, adenoviral vectors may have some direct cytopathic effects and induce immunological responses in transduced cells, because leaky expression of adenoviral genes cannot be completely eliminated. These features are limitations for clinical applications. Retroviral vector transduces cells less efficiently. Moreover, this vector cannot transduce nondividing cells ***(10)***.

Adeno-associated virus (AAV) is a dependovirus (parvovirus) with a single-strand liner DNA genome (length = 4680 nt; *see* **Fig. 1**). The genome contains ITR (inverted terminal repeat, which is required in *cis* for vector replication), *Cap*, and *Rep* (nonstructural protein, which are required for vector replication) sequences. AAV is replication defective and not known to cause disease in

From: *Methods in Molecular Biology, vol. 279: Nitric Oxide Protocols: Second Edition*
Edited by: A. Hassid © Humana Press Inc., Totowa, NJ

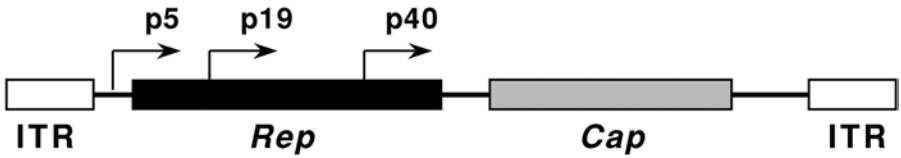

Fig. 1. Structure of wild-type AAV genome. Filled boxes indicate cording sequences. ITR: inverted terminal repeat. Arrows indicate transcription start sites (p5, p19, and p40).

Table 1
Characteristics of Primate AAV Serotypes

Serotype	Host	Homology with AAV2 Cap	Heparin affinity	Receptor	Major tissue tropism
1	Monkey	High (83%)	–	Unknown	Skeletal muscle
2	Human	100%	+	Heparin sulfate	Neuron
3	Human	High (87%)	+	Unknown	Neuron
4	Monkey	Low (62%)	–	Sialic acid (α2–3)	Ependymal cell
5	Human	Low (58%)	–	Sialic acid (α2–3, α2–6)	Neuron, astrocyte retina, airway, liver

humans. Five primate AAV serotypes have been characterized in the literature and are designated as AAV types 1–5. (AAV1–5). There is divergence in homology and tropism for various AAV serotypes (*see* **Table 1**). AAV vectors have been shown to have a broad host range (murine, rabbit, monkey, and human). It is known that lung epithelial cells ***(11)***, neuronal cells ***(12)***, and skeletal muscle cells (*see* **Fig. 2**) ***(13,14)*** are efficiently transduced with AAV vectors.

The AAV life cycle is unique in that AAV infection of a cell might result in either a lytic infection or persistence of the viral DNA in the infected cell following integration into host chromosomal DNA (latent infection). The AAV requires replication functions from coinfecting helper virus (adenovirus or herpesvirus) to proceed through AAV replication and a lytic infection.

The wild-type AAV is known to integrate predominantly in a site-specific chromosomal location in the host genome (i.e., at the human chromosome 19q 13.3-qter [AAVS1]). This feature raised hopes that AAV-mediated gene transfer would provide persistent transgene expression because of site-specific integration. However, recent studies revealed that this site-specific integration occurs via a Rep-dependent mechanism. Therefore, the site-specific integra-

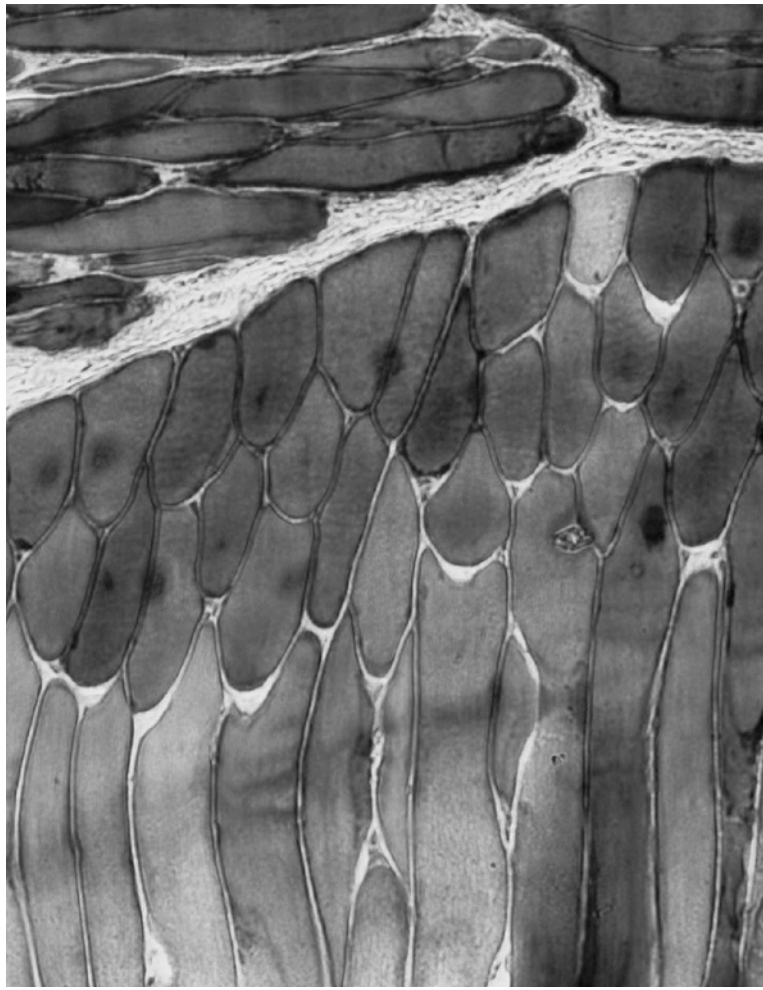

Fig. 2. X-gal staining of AAV-lacZ transduced mice anterior tibial muscle. 2.5×10^{12} particle unit (PU). AAV-lacZ vectors are injected. Two weeks after injection, the muscle is resected and stained. Almost all muscle cells are positively stained.

tion of the interest gene is indeterminate using AAV vectors because they lack a *Rep* protein.

Table 2 indicates the advantage and disadvantage of the AAV vectors. The long-term gene expression is one of the advantages of the AAV vectors (compared with adenovirus vectors) and the abilities of gene transfer into nondividing cells is another feature of these vectors (compared with retrovirus vectors).

Table 2
Characteristics of AAV Vectors

Advantages
- Parent virus: nonpathogenic
- Transduce nondividing cells: muscles, neurons, hepatocytes, etc.
- Long-term stable expression in nondividing cells
- Efficient cotransduction with multiple vectors
- Absence of viral genes
- Stable vector particles

Disadvantages
- Hard to make GMP-grade vectors in large quantities
- Inefficient second-strand synthesis: need a large amount of vectors per target cell
- Small capacity for gene insertion
- Inefficient and random integration

2. Materials

1. Sterile ultracentrifugation tube (Ultrabottle, cat. no. 3430-3870; Nalge Nunc, Rochester, NY).
2. Sterile acrodisc syringe filter (Pall Gelman Laboratory, Ann Arbor, MI).
3. SW 40 rotor (Beckman Instruments, Palo Alto, CA).
4. VTi 65.2 rotor (Beckman Instruments, Palo Alto, CA).
5. Slide-A-Lyzer dialysis cassette (Pierce, Rockford, IL).
6. Ultrafree-4 centrifugation filter (Millipore, Bedford, MA).
7. 2X HBS: 290 m*M* NaCl, 50 m*M* HEPES buffer, 1.5 m*M* Na_2HPO_4, pH 7.1.
8. 300 m*M* $CaCl_2$.
9. HEK293 cells.
10. DME/F12 culture medium, 10% fetal calf serum (FCS).
11. Phosphate-buffered saline (PBS).
12. 1*M* HEPES buffer, pH 7.4.
13. TBS: 100 m*M* Tris-HCl, pH 8.0, 150 m*M* NaCl.
14. 0.5*M* EDTA, pH 8.0.
15. 40% Sucrose, 0.01% bovine serum albumin (BSA) in TBS.
16. DNAse I (Boehringer Mannheim).
17. DNAse buffer I: 50 m*M* HEPES, pH 7.6, 0.15 *M* NaCl, 10 m*M* $MgCl_2$.
18. DNAse buffer II: 10 m*M* Tris-HCl, pH 7.5, 5 m*M* $MgCl_2$.
19. Proteinase K digestion buffer: 10 m*M* Tris-HCl, pH 8.0, 10 m*M* EDTA, pH 8.0.
20. Proteinase K (Boehringer Mannheim).
21. HNE: 50 m*M* HEPES, pH 7.4, 0.15*M* NaCl, 25 m*M* EDTA.
22. CsCl in HNE (1.25 g/mL).
23. CsCl in HNE (1.50 g/mL).
24. Helper plasmid DNA (*pHelper* and *pAAV-RC*).

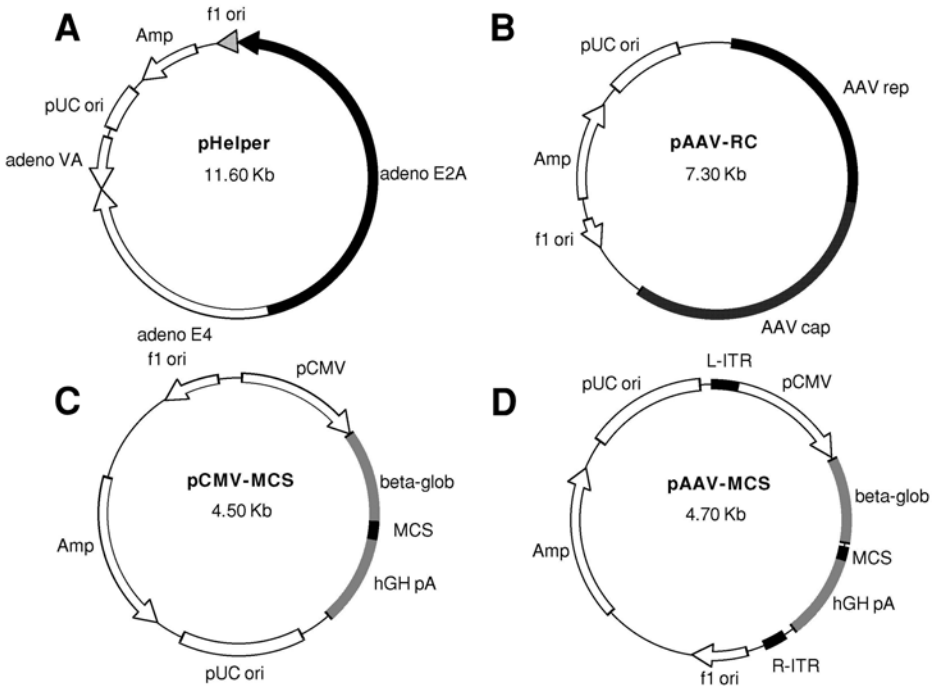

Fig. 3. Schematic of helper **(A,B)** and vector **(C,D)** plasmids adapted from Stratagene.

25. Vector plasmid harboring gene of interest flanked with and without ITRs (*pAAV-MCS*, *pCMV-MCS*). These plasmids are included in AAV Helper-free System™ (*see* **Fig. 3**).
26. *pAAV-NOS*.
27. The full-length bovine endothelial constitutive NOS (ecNOS) cDNA, a kind gift from D.G. Harrison (Emory University School of Medicine), was isolated from Bluescript SK+ vector (*pBS-NOS*) by restriction enzyme digest with *Sal*I (4096 bp). To generate *pCMV-NOS*, this *Sal*I-digested fragment was ligated into the *Sal*I cloning site of the pCMV expression plasmid (4050 bp). The *pCMV-MCS* vectors were engineered by introducing cytomegalovirus (CMV) immediate–early promotor, and human growth hormone first intron into pUC 18 vectors. The *pCMV-NOS* plasmids were digested with *BstB*I in order to delete the human growth hormone first intron (269 bp) and then self-ligated to generate *pCMV-NOS* (7877 bp). To construct *pAAV-NOS*, *pCMV-NOS* plasmids were digested with *Not*I, and the resulting *Not*I–*Not*I expression cassette (5146 bp) was inserted between the ITRs of a pUC-based plasmid containing both AAV inverted terminal repeats (*pAAV-MCS*).

28. 3,3-Diaminobenzidine tetrahydrochloride (DAB; Sigma Chemical Co.) in 0.1*M* Tris-buffer, pH 7.2, containing 0.01% H_2O_2.
29. Hybond N+ Nylon membrane (Amersham).
30. Dot-blot manifold (Schleicher & Schuell).

3. Methods

3.1. Principle of Triple Plasmid Transfection System

Adeno-associated virus is naturally replication-deficient and normally requires coinfection with an unrelated helper virus, such as adenovirus, to generate AAV virions. This novel system uses a vector containing the necessary genes from adenovirus to induce the lytic phase of AAV, producing recombinant, replication-defective AAV virions ready to deliver a gene of interest to target cells. The minimum sets of regions in helper adenovirus that mediate AAV vector replication are the E1, E2A, E4, and VA. A human embryonic kidney cell line 293 encodes the E1 region of the Ad5 genome. When the helper plasmid assembling E2A, E4, and VA regions (*pHelper*) are cotransfected into the 293 cells, along with plasmids encoding the AAV vector genome (*pAAV-MCS*) as well as *rep* and *cap* genes (*pAAV-RC*), the AAV vector is produced as efficiently as when using adenovirus infection as a helper virus. Elimination of the heat inactivation for contaminating adenovirus can improve yield of the virus. Furthermore, contamination of most adenovirus proteins can be avoided in the AAV vector stock made by this helper virus-free method. Stratagene provides the helper-free AAV vector production kit (AAV Helper-free System™).

3.2. Transfection and Viral Extraction

This protocol is for the transfection of one 225 cm^2 flask. For additional flasks or different size of capacity, increase volumes on a proportional basis.

1. Trypsinize 293 cells and plate 5×10^6 cells per 225-cm^2 flask to achieve a monolayer confluency of 20–40% when cells initially attach to the surface of the flask. The volume of medium per flask is 40 mL. Try to avoid plating clumps of cells and make sure that cells are distributed evenly across the plate. An even cell density in all areas of the plate is essential for high yield and can be attained by moving the plates of newly plated cells gently in a cross pattern before the cells attach. Transfer plates to a 5% CO_2 incubator and grow to a confluency of 80% over the next 24–48 h (*see* **Note 1**).
2. At 1 h before the transfection, exchange half of medium in tissue culture flasks with fresh DME/F12 culture medium containing 10% FCS.
3. Add 23 μg each of vector and helper plasmids to 4 mL of 300 m*M* $CaCl_2$. Gently add this solution to 4 mL of 2X HBS and immediately mix by gentle inversion three times. Immediately pipet this mixture into a 225-cm^2 flask of 293 cells containing 40 mL of DME/F12 medium plus 10% FCS and swirl to produce a homogeneous solution.

4. Immediately transfer plates to a 5% CO_2 incubator and incubate at 37°C for 4–6 h. Do not disturb plates during this period.
5. At the end of the incubation, replace medium with prewarmed DME/F12 culture medium containing 2% FCS (*see* **Note 2**).
6. Three days after transfection, add 1 mL of 0.5*M* EDTA to each flask and incubate for 3 min at room temperature.
7. Collect cell suspension and centrifuge at 300*g* for 10 min. Remove supernatant and resuspend cell pellet in 2 mL of TBS.
8. Freeze/thaw cells suspended in TBS three times by placing them alternately in a dry ice/ethanol bath until completely frozen and in a 37°C water bath until completely thawed. Immediately transfer sample back to ice bath when completely thawed (*see* **Note 3**).
9. Remove tissue debris by centrifuging at 10,000*g* for 10 min and collect supernatant.

3.3. AAV Vector Purification (see Note 4)

1. For the material obtained from 24 flasks, add 11 mL of 40% sucrose/0.01% BSA in TBS to a sterile ultracentrifugation tube.
2. Carefully overlay 48 mL of the freeze/thaw supernatant on the solution.
3. Pellet the crude virus particles by centrifuging at 100,000*g* for 16 h at 4°C.
4. Resuspend the pellet vigorously in 5 mL DNase buffer I. Add 1000 units of DNase I and incubate for 1 h at 37°C.
5. Add 250 μL of 0.5*M* EDTA and then remove debris by centrifuging at 10,000*g* for 2 min followed by filtration with a low-protein-binding 5-μm syringe filter.
6. Load the material onto a two-tier CsCl gradient (1.25 and 1.50 g/mL) in HNE buffer.
7. Spin the gradient at 220,000*g* for 2 h at 16°C in an SW 40 rotor.
8. Collect the virus-rich fraction by measuring the refractive index (RI; 1.371–1.380) and load again onto a two-tier CsCl gradient (1.25 and 1.50 g/mL) in HNE buffer.
9. Spin the gradient at 416,000*g* for 2 h at 16°C in a VTi 65.2 rotor.
10. Collect 0.5 mL each of fraction and select the virus-rich fraction by measuring RI (1.371–1.380), semiquantitative polymerase chain reaction (PCR) analysis, Western blotting analysis for Cap, or quantitative DNA dot-blot hybridization.
11. By using a dialysis cassette, desalt the virus-rich fraction by three cycles of dilution with 300 mL of HNE buffer.
12. Concentrate the material to 50 μL with an Ultrafree-4 centrifugation filter.
13. The final titer is usually (1–5) × 10^{13} particles from 5 × 10^8 293 cells as determined by quantitative DNA dot-blot hybridization or Southern blotting. In the case of AAV vector expressing lacZ, vector production can be functionally assessed by titration using 293 cells. The transduced cultures are incubated for 24 h at 37°C before fixation and X-gal staining. The stained cells are counted under light microscopy. The genome particle-to-functional ratio is determined as the level of total genome divided by that of functional units (lacZ staining) to verify infectivity.

3.4. Particle Titer Determination (Dot-Blot Analysis)

The vector particle titer was determined by measuring encapsulated vector genomes resistant to DNase I treatment.

1. Fifty milliliters of vector solution was incubated with 5 U DNase I in DNAse buffer II at 37°C for 1 h to digest plasmid DNA that contaminated the vector solution.
2. DNase-resistant viral DNA was extracted after proteinase K digestion (37.5 μg/mL) at 37°C for 1 h in proteinase K digestion buffer.
3. Serial dilutions of virion DNA were applied on a Nylon membrane using a dot-blot manifold. Serial dilutions of *pBS-NOS* fragment digested with *Eco*NI (1248 bp) were used as standards (*see* **Note 5**).
4. Membranes were subjected to ultraviolet (UV) crosslinking and hybridized with ^{32}P-labeled *pBS-NOS* fragment digested with *Eco*NI (1248 bp).
5. The hybridization signals were quantified by an image analyzer (BAS image analyzer system, Fujix). Particle titers were calculated by comparison to the standards and expressed as the number of vector particles per milliliter.

3.5. Gene Transfer of NOS Via the Use of AAV Vectors

Transduction efficiency using AAV vectors is lower than that using adenovirus vectors. We have reported that AAV vectors need several hours to get maximum transduction efficiency in cultured rat vascular smooth-muscle cells and cardiomyocytes (*see* **Fig. 4**) ***(15,16)***. Therefore, it is essential to consider how long AAV vectors are incubated with target cells.

We have investigated AAV-NOS mediated gene transfer into dissected aortic segments ***(17)***.

1. The segments were incubated in medium DMEM/F12 plus 10% FBS, 1% penicillin/streptomycin, and 1% glutamate, at 37°C under 5% CO_2 with viral solution (2×10^{12} P.U./mL).
2. After 24-h incubation, the aortic segments were fixed with a mixture of 2% paraformaldehyde and 0.2% glutaraldehyde in PBS for 5 min at 4°C, rinsed in PBS, and then frozen in liquid nitrogen.
3. Cryostat-sections (10 μm thick) were cut with a Reichert–Jung Frigocut 2800E. An immunohistochemical stain for ecNOS expression was carried. Ten micrometer cryostat sections were mounted on slides, washed twice with TBS, and blocked with normal rabbit serum, diluted 1:5 in TBS for 45 min.
4. The sections were incubated overnight with the anti-ecNOS antibody (2 mg/mL), then for 1 h with a rabbit anti-mouse IgG peroxidase conjugate (dilution 1:50; preabsorbed overnight at 4°C with 10% preimmune rat serum and 3% BSA).
5. Antibody binding was visualized with 0.5 mg/mL DAB. Control experiments consisted of omission of the vector from the 24-h incubation medium.

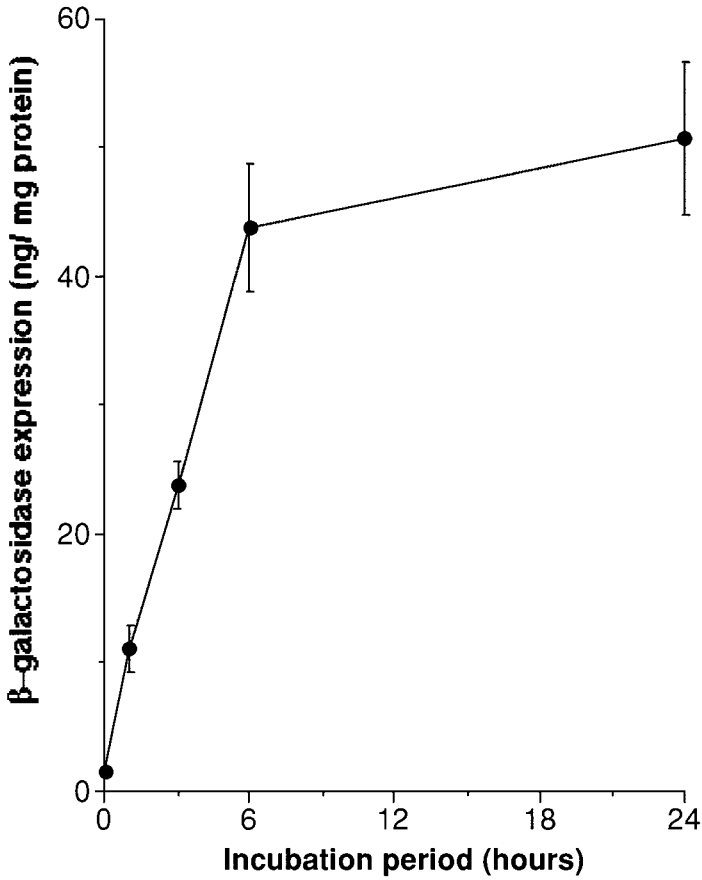

Fig. 4. Graph showing incubation time–response curve of AAV-mediated gene transfer into cultured rat cardiac myocytes. Cardiac myocytes were exposed for increasing incubation periods to AAV-lacZ at a multiplicity of infection of 1×10^6. Twenty-four hours after infection, β-galactosidase expression was measured in cell lysates using a colorimetric enzyme immunoassay.

Figure 5 demonstrates immunohistochemical staining for ecNOS protein. In AAV-NOS transduced aortic segments, adventitial cells were stained strongly positive.

4. Notes

1. You must not use cells with too high a density (>120% confluency), because this may cause reduction of transfection efficiency and a the lower yield of recombinant AAV (rAAV). Try to avoid plating clumps of cells and make sure that cells are distributed evenly across the plate.

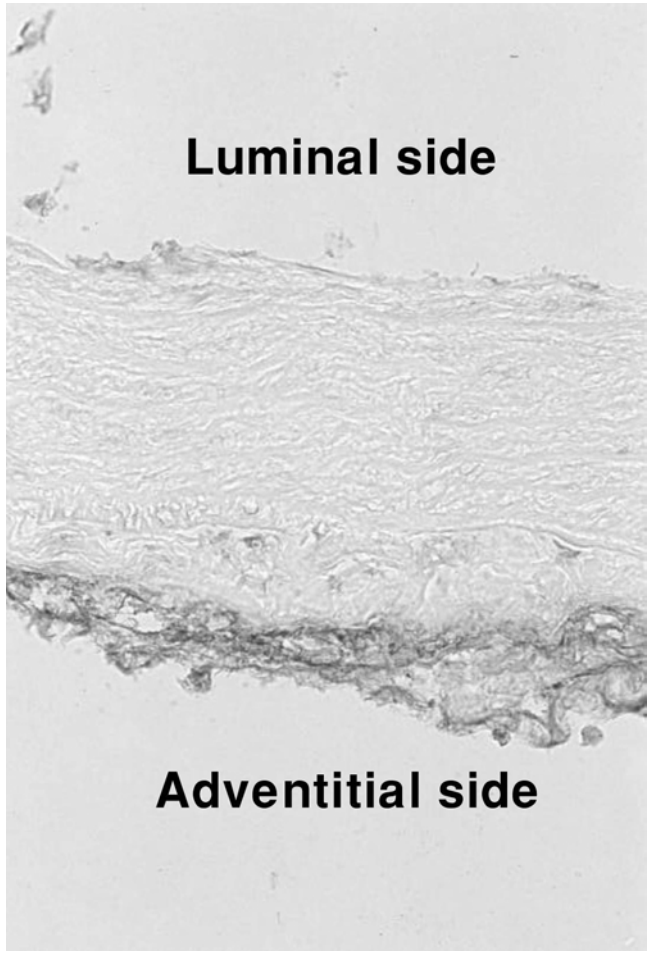

Fig. 5. Immunohistochemical staining for ecNOS in rat aortic segments at 24 h after incubation with the vector-containing medium. The endothelium was denuded by swabbing. A marked increase in immunoreactivity was seen in the adventitia of ecNOS-transduced vessels.

An even cell density in all areas of the plate is essential for high yield and can be attained by moving the flasks of newly plated cells gently in a cross pattern before the cells attach.

2. Transfection is a most important step for making rAAV vectors. If you leave the DNA solution in 2X HBS for more than several minutes, the precipitate of the DNA–calcium complex becomes too large and the transfection may not succeed. After 2 or 3 h incubation, you should verify that the precipitate of the DNA–calcium complex covers the surface of the flask evenly. If you fail to notice the

precipitate, the transfection may fail. If you have difficulty with transfection, the most probable cause would be nonoptimal pH of HBS (even passing through a filter may alter the pH of HBS). We recommend that you prepare slightly different pH HBS (around pH 7.1) and try to evaluate transfection efficiency using a marker gene (such as *lacZ*), before making rAAV vectors.

3. To avoid the aggregation of cell debris, you should vortex and shake the solution vigorously every time after thawing.
4. Once you start the purification, you should not stop the protocol until the dialysis step. You can omit the sucrose ultracentrifugation in **Subheading 3.3.**, **steps 1–4**.
5. Before assembling the apparatus, the membrane and filter paper should be wetted with distilled water. Filter paper should cover all the wells of the apparatus. Samples cannot be vacuumed if there is an air leak from the side of the apparatus.

   a. When you use the plasmid (double strand DNA) as standard, rAAV (single strand DNA) titer should be doubled.
   b. 2.7 μg of 5000 bp plasmid is nearly equivalent to 5×10^{11} copies.
   c. Prepare 5×10^{11} copies of plasmid in 1 ml of TE. Then make a serial dilution. You can change the amount of plasmid according to the length of base pairs. 5×10^{11} copies of plasmid are calculated as 1×10^{12} copies of rAAV.

References

1 Barr, E., Carroll, J., Kalynych, A. M., et al. (1994) Efficient catheter-mediated gene transfer into the heart using replication-defective adenovirus. *Gene Ther*. **1,** 51–58.
2 French, B. A., Mazur, W., Geske, R. S., et al. (1994) Direct in vivo gene transfer into porcine myocardium using replication-deficient adenoviral vectors. *Circulation* **90,** 2414–2424.
3 Gilgenkrantz, H., Duboc, D., Juillard, V., et al. (1995) Transient expression of genes transferred in vivo into heart using first-generation adenoviral vectors: role of the immune response. *Hum. Gene Ther*. **6,** 1265–1274.
4 Guzman, R. J., Lemarchand, P., Crystal, R. G., et al. (1993) Efficient gene transfer into myocardium by direct injection of adenovirus vectors. *Circ. Res*. **73,** 1202–1207.
5. Kass, E. A., Falck, P. E., Alvira, M., et al. (1993) Quantitative determination of adenovirus-mediated gene delivery to rat cardiac myocytes in vitro and in vivo. *Proc. Natl. Acad. Sci. USA* **90,** 11,498–11,502.
6 Kirshenbaum, L. A., MacLellan, W. R., Mazur, W., et al. (1993) Highly efficient gene transfer into adult ventricular myocytes by recombinant adenovirus. *J. Clin. Invest*. **92,** 381–387.
7 Li, J. J., Ueno, H., Pan, Y., et al. (1995) Percutaneous transluminal gene transfer into canine myocardium in vivo by replication-defective adenovirus. *Cardiovasc. Res*. **30,** 97–105.
8 Magovern, C. J., Mack, C. A., Zhang, J., et al. (1996) Direct in vivo gene transfer to canine myocardium using a replication-deficient adenovirus vector. *Ann. Thorac. Surg*. **62,** 425–433.

9 Muhlhauser, J., Jones, M., Yamada, I., et al. (1996) Safety and efficacy of in vivo gene transfer into the porcine heart with replication–deficient, recombinant adenovirus vectors. *Gene Ther*. **3,** 145–153.
10 Sanes, J. R., Rubenstein, J. L. R., and Nicolas, J. F. (1986) Use of recombinant retrovirus to study post-implantation cell lineage in mouse embryos. *EMBO J*. **5,** 3133–3142.
11. Flotte, T. R., Afione, S. A., Conrad, C., et al. (1993) Stable in vivo expression of the cystic fibrosis transmembrane conductance regulator with an adeno-associated virus vector. *Proc. Natl. Acad. Sci. USA* **90,** 10,613–10,617.
12 Kaplitt, M. G., Leone, P., Samulski, R. J., et al. (1994) Long-term gene expression and phenotypic correction using adeno-associated virus vectors in the mammalian brain. *Nature Genet*. **8,** 148–154.
13 Fisher, K. J., Jooss, K., Alston, J., et al. (1997) Recombinant adeno-associated virus for muscle directed gene therapy. *Nature Med*. 3, 306–312.
14. Kessler, P. D., Podsakoff, G. M., Chen, X., et al. (1996) Gene delivery to skeletal muscle results in sustained expression and systemic delivery of a therapeutic protein. *Proc. Natl. Acad. Sci. USA* **93,** 14,082–14,087.
15 Maeda, Y., Ikeda, U., Ogasawara, Y., et al. (1997) Gene transfer into vascular cells using adeno-associated virus (AAV) vectors. *Cardiovasc. Res*. **35,** 514–521.
16 Maeda, Y., Ikeda, U., Shimpo, M., et al. (1998) Efficient gene transfer into cardiac myocytes using adeno-associated virus (AAV) vectors. *J. Mol. Cell. Cardiol.* **30,** 1341–1348.
17. Maeda, Y., Ikeda, U., Shimpo, M., et al. (2001) Adeno-associated virus-mediated transfer of endothelial nitric oxide synthase gene reduces vasoconstrictive response. *Exp. Clin. Cardiol*. **6,** 50–55.

18

Adenovirus-Mediated Nitric Oxide Synthase Gene Transfer

Kathleen G. Raman, Richard A. Shapiro, Edith Tzeng, and Melina R. Kibbe

Summary

The varied biological effects of nitric oxide (NO) have led to intense research into its diverse physiologic and pathophysiologic roles in multiple disease processes. It has been implicated in the development of altered vasomotor tone, intimal hyperplasia, atherosclerosis, impotence, host defense, and wound healing. Using the modern technologies of recombinant DNA and gene transfer using adenoviral vectors, the effects of NO derived from various NO synthase (NOS) enzymes can be studied in a variety of tissues and the therapeutic applications of NOS is possible. Such uses of NOS gene transfer have been investigated extensively in the vasculature where NO is critical to regulating vascular homeostasis. NOS gene therapy has the theoretical advantage of allowing NO delivery to be localized, thereby limiting potential adverse effects of NO. The benefits of adenoviral vectors in gene transfer include relatively high transduction efficiencies, both replicating and nonreplicating cells may be infected, and the high titers of adenovirus that can be produced. The methods described in this chapter include the cloning of the iNOS cDNA into a recombinant adenoviral vector, large-scale production of that vector AdiNOS preparation, and the use of the vector to transduce tissue in vitro and in vivo.

Key Words: AdiNOS; nitric oxide synthase; gene transfer.

1. Introduction

The varied biological effects of nitric oxide (NO) have led to intense research into its diverse physiologic and pathophysiologic roles in multiple disease processes. Nitric oxide has been implicated in the development of altered vasomotor tone, intimal hyperplasia, atherosclerosis, impotence, host defense, and wound healing. Using the modern technologies of recombinant DNA and gene transfer using adenoviral vectors, the effects of NO derived from various NO synthase (NOS) enzymes can be studied in a variety of tissues, and therapeutic applications of NOS are emerging. The therapeutic uses of NOS gene transfer have been investigated extensively in the vasculature, where NO is critical to regulating vascular homeostasis.

From: *Methods in Molecular Biology, vol. 279: Nitric Oxide Protocols: Second Edition*
Edited by: A. Hassid © Humana Press Inc., Totowa, NJ

The most commonly used method of delivering NO to target organs and tissues is the systemic administration of NO donor compounds. Early experiments involved simple dietary arginine supplementation as a means of augmenting local or systemic NO synthesis in rodent models of vascular injury. Dietary arginine significantly reduced intimal hyperplasia in a model of arterial injury ***(1)*** and this protective effect was reversed by the administration of NOS inhibitors, suggesting that dietary arginine elicited these biological actions by augmenting NO synthesis. Direct delivery of NO using an inhalational route inhibited neointimal formation in animal models of arterial injury by 55% ***(2)***. Studies utilizing NO donors compounds in similar rodent models of arterial injury demonstrated a 50–80% reduction in injury-induced intimal hyperplasia ***(3,4)***. However, potential shortcomings of systemic NO delivery include the risk of vascular collapse resulting from hypotension as well as the uncertain toxicity in sensitive tissues and cell types. Given this, NOS gene therapies have the theoretical advantage of allowing NO delivery to be fairly localized, thereby limiting the potential adverse effects of NO.

Nitric oxide biosynthesis begins with a family of NOS enzymes that catalyzes the conversion of L-arginine and molecular oxygen to yield NO and L-citrulline. Heme, tetrahydrobiopterin (BH_4), nicotinamide adenine dinucleotide phosphate (NADPH), calmodulin (CaM), flavin mononucleotide (FMN), and flavin adenine nucleotide (FAD) are all essential cofactors ***(5)***. Three distinct NOS isoforms have been identified in many species and in humans. The endothelial NOS (eNOS), neuronal NOS (nNOS), and inducible NOS (iNOS) have all been cloned, and further characterization of these enzymes revealed that they are truly distinct proteins that originate from three separate genes. The availability of cDNAs for these different NOS enzymes has allowed the development of NOS gene transfer strategies that optimally harnesses the unique characteristics of each isoform, including enzymatic specific activity, cofactor requirement, and posttranslational modification.

The adenovirus is a DNA virus characterized by a complex, nonenveloped, icosahedral outer protein capsid ***(6)***. It enters the cell via specific receptor interactions and, following infection, the adenoviral DNA enters the nucleus, where it remains episomal, thus avoiding the possibility of insertional mutagenesis ***(7)***. The viral genome is organized into four distinct early regions, termed E1–E4, and five alternatively spliced late regions, L1–L5. Adenoviral vectors lacking the E1 and E3 regions are referred to as first-generation, or Av1, vectors. The benefits of adenoviral vectors in gene transfer include relatively high transduction efficiencies, both replicating and nonreplicating cells may be infected, and the high titers of adenovirus that can be produced, as high as 10^{13} plaque-forming units (PFU)/mL. The methods described in this chapter include the cloning of the iNOS cDNA into a recombinant adenoviral vector,

large-scale production of that vector AdiNOS preparation, and the use of the vector to transducer tissue in vitro and in vivo.

2. Materials

2.1. Isolation of iNOS cDNA Fragment

1. pBluescript-iNOS plasmid.
2. Restriction enzymes *Eco*RI, *Hin*dIII, *Eco*RV, *Not*I, *Afl*II, *Nco*I (New England Biolabs, Beverly, MA).
3. Polymerase chain reaction (PCR) primers (Invitrogen Corporation, Carlsbad, CA):
   5' aag cca tag cca tgg cct gtc 3' (forward);
   5' gtg gga ttt cga aga gct cag g 3' (reverse).
4. Klenow (Roche, Indianapolis, IN).

2.2. Creation of Recombinant AdiNOS

1. pAdlox (GenBank U62024).
2. ψ5 viral DNA.
3. L-N^5-(1-iminoethyl)-ornithine dihydrochloride (L-NIO) (Alexis Biochemicals, San Diego, CA).
4. GTG agarose (BioWhittaker, Rockland, ME).
5. 293 cells, CRE8 cells (ATCC, Manassas, VA).
6. Dulbecco's modified Eagle's medium (DMEM) (BioWhittaker, Rockland, ME).
7. Griess reaction reagents (Sigma, St. Louis, MO).
8. Neutral red (Sigma, St. Louis, MO).

2.3. Large-Scale AdiNOS Preparation

1. Tris saline: 50 m*M* Tris-HCl, pH 7.5, 200 m*M* NaCl.
2. CsCl solutions:
   a. d = 1.4 mg/mL CsCl (53 g CsCl, 0.87 mL of 1*M* Tris-HCl, pH 8.0, 86.13 mL double-distilled water [ddH_2O]).
   b. d = 1.2 mg/mL CsCl (26.8 g CsCl, 0.92 mL of 1*M* Tris-HCl, pH 8.0, 91.08 mL ddH_2O).
3. Adenovirus preservation buffer: 20 m*M* Tris-HCl, pH 7.8, 75 m*M* NaCl, 2 m*M* $MgCl_2$, 5% Trehalose, 0.0025% Tween-80 in 1 L ddH_2O: filter-sterilized.
4. Trehalose (Fisher Scientific, Somerville, NJ).

2.4. In Vitro iNOS Gene Transfer

1. DMEM (low glucose) (Invitrogen Corporation, Carlsbad, CA).
2. Ham's F12 medium (Invitrogen Corporation, Carlsbad, CA).
3. Optimem I ((Invitrogen Corporation, Carlsbad, CA).
4. Hanks' balanced salt solution (HBSS) (Invitrogen Corporation, Carlsbad, CA).
5. Tetrahydrobiopterin (BH_4) (Alexis Biochemicals, San Diego, CA).

2.5. Ex Vivo and In Vivo iNOS Gene Transfer

1. Polyethylene tubing (PE 10) (VWR International, Bridgeport, NJ).
2. Poloxamer 407 NF (BASF, Mount Olive, NJ).
3. 2-Fr, 3-Fr Fogarty embolectomy catheters (Edwards Life Sciences, Memphis, TN).
4. Phosphate buffer, pH 7.0: 0.015*M* Na_2HPO_4, 0.05*M* NaH_2PO_4; store at 4°C until use.
5. Adenoviral gel: Add 750 mg poloxamer to 2.3 mL phosphate buffer and place in a beaker at 4°C overnight.

3. Methods

3.1. Isolation of iNOS cDNA Used in Adenoviral Construction

1. The human iNOS cDNA originally cloned from cytokine-stimulated human hepatocytes ***(8)*** was cloned into the pBluescript plasmid ***(9)***. The sequence of the cDNA may be obtained from GenBank accession number L09210.
2. Prepare an iNOS expression plasmid containing the entire 5' untranslated region (UTR) and minimal 3' UTR. Linearize the iNOS pBluescript plasmid with *Afl*II at bp 3705. Fill in the created overhang with Klenow to generate a blunt end. Remove the cDNA at the 5' end using *Hin*dIII in the multicloning site of pBluescript. Subclone this fragment into the *Hin*dIII and *Eco*RV sites of pcDNA3.
3. To create an adenoviral vector carrying as little of the untranslated regions of the iNOS cDNA as possible, create an *Nco*I site by PCR at the ATG translational start site (bp 207) using the pBluescript–iNOS plasmid as a template. This will create an 850-bp fragment from the *Nco*I site to the *Eco*RI site at bp 1059.
4. Prepare an intermediate iNOS expression plasmid. Remove the *Eco*RI to *Afl*II fragment (2646 bp) from iNOS pcDNA3 by digesting with *Eco*RI and the *Not*I that is in the multicloning site 3' of the *Eco*RV site. Ligate this fragment and the blunted *Nco*I to *Eco*RI PCR fragment (*see* **step 3**) together at the *Eco*RI site and into the *Eco*RV (a blunt end) and *Not*I sites of pcDNA3.
5. To subclone the iNOS coding sequence into pAdlox, excise the iNOS cDNA from the pcDNA3-iNOS plasmid with *Hin*dIII at the 5' end and *Not*I at the 3' end and then ligate this fragment into pAdlox using these same restriction sites. In this construct, the iNOS cDNA is placed downstream of a constitutively active human CMV early enhancer/promoter and upstream of a SV40 polyadenylation signal (*see* **Note 1**).

3.2. Creation of Recombinant AdiNOS

1. Linearize pAdlox–iNOS with *Sfi*I.
2. Cotransfect linearized pAdlox–iNOS and the ψ5 helper virus DNA into the adenoviral packaging cell line CRE8.
3. Maintain the cells in medium containing L-NIO (100 m*M*) to block iNOS activity and NO synthesis, which can be toxic to the transfected cells and decrease viral production.
4. Ten days after transfection, isolate bulk viral lysate by collecting the CRE8 cells and lysing them. Spin out the cellular debris and save the supernatant.

5. Plate 293 cells in duplicate and infect with bulk viral lysate. Assay for NO production 24–48 h later using the Griess reaction to detect nitrite accumulation in the absence of L-NIO ***(10)***. If nitrite production is detected, continue to plaque purification. Nitrite production indicates that successful recombination occurred within the CRE8 cell line and that infectious AdiNOS was generated.

3.3. Plaque Purification

1. Plate 293 cells in 12-well plates and infect the cells with the bulk viral lysate at dilutions ranging from 10^{-5} to 10^{-10} and overlay with GTG agarose.
2. Ten days later, stain plaques with neutral red (they will appear white in a red background of cells).
3. Select plaques for further purification by picking the plaques and resuspending each plaque in 300 μL of medium.
4. Infect plated 293 cells with 100 μL of each suspension to see if AdiNOS has been produced in the plaque and if functional iNOS is expressed.
5. After 72 h, assay culture supernatants for nitrite production using the Griess reaction to confirm iNOS expression and NO production. Select the plaque with highest nitrite production for another round of plaque purification.
6. Infect 293 cells with the plaque suspension from the plaque that yielded the highest level of NO production and select plaques as detailed in **steps 1–4**. Infect 293 cells as detailed in **step 5** and assay for nitrite production using the Griess reaction.
7. Identify plaques with the highest level of nitrite production.
8. Resuspend the plaques from **step 7** in 1 mL of medium and infect 293 cells with the plaque suspension. Monitor cells for the cytopathic effect; cells will become rounded and detach from the cell culture plate. Once observed, lyse the cells and centrifuge to remove cellular debris. The remaining supernatant is the crude viral lysate from which large-scale AdiNOS preparation is performed.

3.4. Large-Scale AdiNOS Preparation

Day 1

1. Plate ten 15-cm plates of 293 cells at 90–99% confluency at time of infection.
2. Remove media from cells and add 1.0 mL lysate with 4 mL DMEM (no serum) per plate. Let sit 60–90 min, rocking plates every 15 min.
3. After 60–90 min, add 20 mL DMEM with 10% serum per plate and incubate at 37°C.
4. Examine daily for cytopathic effect; move media twice daily until cytopathic effect is seen.

Day 3

1. When cells are rounded but not detached, harvest by scraping cells off the plates directly into the culture media. Combine cell harvests into 50-mL Falcon tubes.
2. Spin cells at 225*g* for 10 min and discard medium.

3. Resuspend cell pellet in remaining medium and combine pellets in 15-mL Falcon tube.
4. Add 5 mL Tris saline to combined pellets.
5. In dry ice–EtOH bath, freeze–thaw the cell suspension three to five times and vortex. This lyses the cells and releases the recombinant adenovirus being propagated within the cells.
6. Centrifuge the lysate at 800*g* for 10 min to pellet the cell debris and keep the supernatant that contains the adenoviral particles.
7. Add 3.5 mL of 1.4 CsCl lower, then 3.5 mL 1.2 CsCl upper to an ultracentrifuge tube. Layer the adenoviral supernatant to the top of the CsCl in the tube.
8. Centrifuge in SW41 rotor for 1 h at 15,000*g* at 4°C.
9. Collect the lower band, which contains the adenovirus, with a 22-gage ½-in. needle attached to a 3-cm^3 syringe.
10. Resuspend virus in 5 mL Tris saline and repeat CsCl gradient centrifugation.
11. Isolate the lower viral band as in **step 9**.
12. Dialyze viral solution using dialysis membrane in 500 mL adenovirus preservation buffer overnight to remove the CsCl from the viral preparation.

Day 4

1. Change adenovirus preservation buffer and dialyze 5 h.
2. Remove virus and store at –80°C in desired aliquots.
3. The titer (in particles) of the adenoviral solution is determined by checking the fluorescence at OD_{260}. 1 OD_{260} × dilution/9.09 × 10^{-13} = particles/mL. The biological activity of the virus should be verified by infecting cells and measuring NO production by the Griess reaction (*see* **Subheading 3.5.**).

3.5. In Vitro iNOS Gene Transfer

1. Rodent aortic smooth-muscle cells: Plate cells onto 12-well plates in DMEM/Ham's F12 (1:1 [v:v]) supplemented with 10% fetal bovine serum (FBS), 100 μg/mL streptomycin, 100 U/mL penicillin, and 4 mmol/L L-glutamine and maintain in a 37°C, 95% air/5% CO_2 incubator. When cells reach approx 50% confluence, they are ready to be infected.
2. Thaw the frozen viral stock on ice and dilute the virus to the desired multiplicity of infection (MOI) in serum-free medium or Optimem I to allow approx 100–200 μL of viral solution/well. For rat aortic smooth-muscle cells, an MOI of 1000 particles/cell is appropriate. Remove the medium from the plated cells and rinse with serum-free medium or HBSS. Place the viral solution in the wells and incubate with the cells for 4 h at 37°C; rotate plates every 30 min to ensure complete coverage of the cells and to prevent cell dessication. The infection is performed in a minimal volume to increase viral concentration and cell contact (*see* **Note 2**).
3. Following infection, remove virus and wash once with HBSS. Replace with serum-free media or Optimem I for 24 h. In the absence of serum, there will be

minimal NO production following iNOS expression because smooth-muscle cells are deficient BH_4 synthesis. To assay for NO production, replace the serum-free medium with medium supplemented with BH4 (10 μ*M* final concentration).
4. Assay for nitrite production with the Griess reaction after 24 h (*see* **Note 3**).
5. To study the effect of iNOS gene transfer on smooth-muscle cell proliferation, the cells should be placed into serum-free medium 24 h prior to infection to promote growth arrest and cell cycle synchronization. After infection, the cells are maintained in serum-free medium to minimize NO production so that relative numbers of cells in different wells are kept similar. The effect of iNOS gene transfer can then be studied when the cells are stimulated to proliferate with the addition of serum and BH_4.

3.6. Ex Vivo iNOS Gene Transfer

Ex vivo iNOS gene transfer using adenoviral vectors has been used in models of transplantation ***(11,12)*** and vein bypass grafts ***(13)***.

1. Aortic transplantation. Following excision of the descending thoracic aorta from donor rats, immerse the aortic segments in 2 mL of Optimem I or serum-free medium containing AdiNOS or a control vector carrying a marker gene such as β-galactosidase (AdlacZ). Viral concentrations are 10^9 particles/mL and the tissues are incubated for a period of 60 min at 27°C. Following viral infection, rinse the aortic grafts and transplant the organs into recipient animals into a heterotopic position below the renal arteries and above the aortic bifurcation as previously described by Mennander and colleagues ***(14)***.
2. Heart transplantation: Infuse cold heparinized saline into the inferior vena cava of an anesthetized mouse to arrest the donor heart. Ligate the ascending aorta proximal to the origin of the innominate artery. Infuse viral solution at a concentration of 10^{11} particles/mL combined with 10^{-7} *M* acetylcholine into the proximal aorta with a 27-gage needle with enough volume to fill the organ. The acetylcholine facilitates permeabilization of the endothelium. The aorta, main pulmonary artery, and three systemic veins are then transected distal to ligatures. The donor heart is preserved in 4°C saline solution for 30 min and then the ascending aorta is anastomosed to the recipient abdominal aorta and the donor pulmonary artery anastomosed to the recipient vena cava.
3. Vein bypass: Expose bilateral internal jugular veins in pigs through a midline neck incision. Harvest approx 5–6 cm of vein. Excise the vein and rinse it with serum-free medium. Incubate the vein in 1 mL of serum-free medium containing 10^{11} particles/mL of either AdiNOS or AdlacZ for 30 min at room temperature. Rinse the vein in serum-free medium and then interpose it into the arterial circulation. Excise a similar length of target artery prior to implanting the vein graft to avoid kinking. To quantitate iNOS expression and NO production, remove a small segment of the transduced vein graft prior to implantation. Culture the small segment of vein with growth medium supplemented with BH_4. The medium is analyzed for nitrite production using the Griess reaction in 24–48 h.

3.7. In Vivo iNOS Gene Transfer

In vivo iNOS gene transfer using an adenoviral vector has been used in models of arterial injury ***(15)*** and wound healing ***(16)***.

1. Rat carotid injury with intraluminal gene transfer: Expose the common carotid arteries (CCA) of rats through a midline neck incision and obtain proximal and distal vascular control with noncrushing vascular clamps. Insert a 2 Fr arterial embolectomy balloon catheter into the CCA via an arteriotomy in the external carotid artery. Inflate the balloon to 5 atm of pressure for 5 min. Instill AdiNOS or AdlacZ viral solution (1×10^7 PFU/mL diluted in Optimem I, 200 μL/rat) through the external carotid artery via a 1-cm^3 syringe with a 30-gage needle attached to PE 10 tubing. Incubate the viral solution in the artery for 30 min; the artery should remain distended with the viral solution. After the incubation period, evacuate the viral solution, ligate the external carotid artery, and re-establish blood flow through the internal carotid artery.
2. Rat carotid injury with adventitial gene transfer: Once the arterial injury has been created as detailed in **step 1**, ligate the external carotid artery and re-establish blood flow through the internal carotid artery. The adenoviral gel solution made with Poloxamer 407 and phosphate buffer must be prepared 24 h in advance and stored at 4°C. This gel is a liquid at 4°C but becomes a gel at room temperature. Add adenoviral vector to the gel in a ratio of 3:1. Apply the gel to the adventitial surface of the common carotid artery, where the balloon injury was created. Close the neck incision once the gel has polymerized with the adenoviral gel in place.
3. Combined intraluminal and adventitial gene transfer: After intraluminal adenoviral delivery has been performed as detailed in **step 2**, ligate the external carotid artery and apply the adenoviral gel to the adventitial surface of the common carotid artery.
4. Pig iliac artery injury: Expose bilateral iliac arteries through a low-midline laparotomy incision. Obtain vascular control of the iliac arteries proximally and distally with noncrushing vascular clamps. Insert a 3 Fr embolectomy catheter through a side branch and inflate the balloon to 2 atm of pressure for 5 min. Instill the adenoviral vector (AdiNOS or AdlacZ) (1×10^9 PFU/mL diluted in Optimem I, 500–750 μL/iliac artery) into the common iliac artery through the same side branch using an 18-gage angiocatheter. The viral solution is maintained in the artery for 30 min. After the incubation period, evacuate the adenovirus solution, ligate the side branch, and re-establish blood flow.
5. Excisional wound model: After animals are anesthetized, shave the back of the mouse and prep the skin with povidine–iodine. Create a full-thickness wound (1.5×1.5 cm) and measure the surface area of the wound after the skin edges have retracted. Adenovirus-mediated gene transfer is performed either by direct application of viral solution on the wound for 30 min or by the use of adenoviral gel made by adding viral solution to the poloxamer mixture (poloxamer:gel ratio 3:1) and applying this mixture directly to the wound. After 30 min, wash the solution or gel off the wound and cover with a bio-occlusive dressing to maintain

sterility. Wound closure rates may be determined by serially tracing the wound area on acetate sheets, digitizing tracings, and calculating the area of the traced region.

4. Notes

1. The ligation of the blunted *Nco*I and *Eco*RV creates a Kozak consensus sequence.
2. Virus should be diluted in the least possible volume to cover the bottom of the well.
3. BH4 does not need to be added subsequent to infection. BH_4 is a necessary cofactor for the dimerization and, thus, activation, of all iNOS protein ***(17)***.

References

1 McNamara, D. B., Bedi, B., Aurora, H., et al. (1993) L-arginine inhibits balloon catheter-induced intimal hyperplasia. *Biochem. Biophys. Res. Commun.* **193,** 291–296.

2 Lee, J. S., Adrie, C., Jacob, H. J., et al. (1996) Chronic inhalation of nitric oxide inhibits neointimal formation after balloon-induced arterial injury. *Circ. Res.* **78,** 337–342.

3 Groves, P. H., Banning, A. P., Penny, W. J., et al. (1995) The effects of exogenous nitric oxide on smooth muscle cell proliferation following porcine carotid angioplasty. *Cardiovasc. Res.* **30,** 87–96.

4 Marks, D. S., Vita, J. A., Folts, J. D., et al. (1995) Inhibition of neointimal proliferation in rabbits after vascular injury by a single treatment with a protein adduct of nitric oxide. *J. Clin. Invest.* **96,** 2630–2638.

5 Moncada, S., Palmer, R. M., and Higgs, E. A. (1991) Nitric oxide: physiology, pathophysiology, and pharmacology. *Pharmacol. Rev.* **43,** 109–142.

6. Stratford-Perricaudet, L. D. and Perricaudet, M. (1994). Gene therapy: the advent of adenovirus, in Gene Therapeutics: Methods and Applications of Direct Gene Transfer (Wolff, J. A., ed.), Birkhaeuser, Boston, pp. 344–362.

7. Horwitz, M. (1990) The adenoviruses, in *Virology* (Fields, B. N. and Knipe, D. M., eds.), Raven, New York, p. 1723.

8 Dorko, K., Freeswick, P. D., Bartoli, F., et al. (1994) A new technique for isolating and culturing human hepatocytes from whole or split livers not used for transplantation. *Cell Transplant* **3,** 387–395.

9 Geller, D. A., Lowenstein, C. J., Shapiro, R. A., et al. (1993) Molecular cloning and expression of inducible nitric oxide synthase from human hepatocytes. *Proc. Natl. Acad. Sci. USA* **90,** 3491–3495.

10 Geller, D. A., Nussler, A. K., Di Silvio, M., et al. (1993) Cytokines, endotoxin, and glucocorticoids regulate the expression of inducible nitric oxide synthase in hepatocytes. *Proc. Natl. Acad. Sci. USA* **90,** 522–526.

11 Shears, L. L., Kawaharada, N., Tzeng, E., et al. (1997) Inducible nitric oxide synthase suppresses the development of allograft arteriosclerosis. *J. Clin. Invest.* **100,** 2035–2042.

12 Nykanen, A. I., Krebs, R., Saaristo, A., et al. (2003) Angiopoietin-1 protects against the development of cardiac allograft arteriosclerosis. *Circulation* **107,** 1308–1314.

13 Kibbe, M. R., Tzeng, E., Gleixner, S. L., et al. (2001) Adenovirus-mediated gene transfer of human inducible nitric oxide synthase in porcine vein grafts inhibits intimal hyperplasia. *J. Vasc. Surg.* **34,** 156–165.
14 Hayry, P., Mennander, A., Tiisala, S., et al. (1991) Rat aortic allografts: an experimental model for chronic transplant arteriosclerosis. *Transplant Proc.* **23,** 611–612.
15 Shears, L. L., Kibbe, M. R., Murdock, A. D., et al. (1998) Efficient inhibition of intimal hyperplasia by adenovirus-mediated inducible nitric oxide synthase gene transfer to rats and pigs in vivo. *J. Am. Coll. Surg.* **187,** 295–306.
16 Yamasaki, K., Edington, H. D., McClosky, C., et al. (1998) Reversal of impaired wound repair in iNOS-deficient mice by topical adenoviral-mediated iNOS gene transfer. *J. Clin. Invest.* **101,** 967–971.
17. Tzeng, E., Billiar, T. R., Robbins, P. D., et al. (1995) Expression of human inducible nitric oxide synthase in a tetrahydrobiopterin (H4B)-deficient cell line: H4B promotes assembly of enzyme subunits into an active dimer. *Proc. Natl. Acad. Sci. USA* **92,** 11,771–11,775.